Microfluidic engineering of artificial stem cell niches

THÈSE N° 6528 (2015)

PRÉSENTÉE LE 20 FÉVRIER 2015
À LA FACULTÉ DES SCIENCES DE LA VIE
UNITÉ DU PROF. LUTOLF
PROGRAMME DOCTORAL EN BIOTECHNOLOGIE ET GÉNIE BIOLOGIQUE

ÉCOLE POLYTECHNIQUE FÉDÉRALE DE LAUSANNE

POUR L'OBTENTION DU GRADE DE DOCTEUR ÈS SCIENCES

PAR

Simone ALLAZETTA

acceptée sur proposition du jury:

Prof. S. Maerkl, président du jury
Prof. M. Lütolf, directeur de thèse
Prof. E. Amstad, rapporteuse
Prof. A. DeMello, rapporteur
Dr M. Ehrbar, rapporteur

EPFL

ÉCOLE POLYTECHNIQUE
FÉDÉRALE DE LAUSANNE

Suisse
2015

To my special angel…

Acknowledgements

I would like to address my acknowledgements to all the people without whom this thesis would not have been possible and who contributed to my personal and professional growth, during this journey:

My first big thanks goes to Professor Matthias Lutolf who gave me the opportunity to, first, conclude my master project, and, later, to carry out a challenging and fascinating research project, joining his multidisciplinary laboratory where I could interact with many great scientists from the biological and the engineering universes. Thanks also for giving me the unique opportunity to collaborate for a couple of years with a company, experience through which I could express and cultivate my passion for developing new products.

Second thanks goes to all the members of my committee, Professor Andrew deMello, Professor Martin Ehrbar, Professor Esther Amstad and Professor Sebastian Maerkl, for the great scientific discussion we had during my private defense and thanks, also, for reading my one-hundred-and-ninety-pages thesis!

I am very grateful to all the LSCB colleagues with whom, in addition to spend my daily time in the laboratory, I also spent great moments in the mountains and, finally, also in my hometown. Thanks to Laura for her countless questions about beads, microfluidics and clean room, as well as for being my favorite Mother Theresa; thanks to Nikolche for being a great neighbor colleague making me laugh all the time, as well as for proof-reading this thesis; thanks to Yuya for his unforgettable Japanese lessons and great scientific suggestions; thanks to Vincent for always being so nice with me, to Massi for listening to me and giving me useful advices, to Nath for her super-funny accent and to Sylke for her cakes!! Thanks to Marta who first introduced me to the cell culture world and to Nicola for giving me the opportunity to spend a great time in his hometown!! And still, a thanks goes also to all the remaining colleagues, Stefan, Mukul, Yoji, Marlen, Aline, Andrea, Lilia, Adrian, Michael, Vasco and Josefine, who contributed to render the lab atmosphere great.

Furthermore, I would thank all the people who have been working in the various EPFL facilities without whom this Ph.D. would not have been completed. Therefore, thanks to Jean-Baptiste Bureau for helping me solving issues in the clean room, to Thierry Laroche and José Artacho for their constant support on microscopes and to Miguel Garcia for his help with flow cytometry.

I would like also to address a big thanks to the entire Laboratory of Cell Biophysics, in particular, to Dr Benoit Vianay and Dr Chiara Gabella, who introduced me to the fascinating world of the atomic force microscopy.

During my PhD, I also had the opportunity to interact with many master and semester students, who all differently contributed, to a certain extent, to my professional and personal growth.

<div align="right">Simone</div>

Summary

Stem cells play a key role in a wide range of biological processes, in large part due to their ability to self-renew or differentiate into specialized cell types in response to various biological cues. *In vivo*, stem cells reside in a complex microenvironment, termed niche, that regulates cell fate through intricate combinations of biophysical and biochemical factors. To recapitulate some of these crucial interactions *ex vivo* and to facilitate a quicker transition to clinical and pharmaceutical applications of stem cells, numerous technologies have been developed in recent years to better control and manipulate the cellular microenvironment. In particular, combining synthetic hydrogels having controllable mechanical and biochemical signaling with microfluidic technologies that can automatically and precisely handle fluids results in unprecedented control over *in vitro* microenvironmental conditions. In this thesis, novel microfluidic approaches were developed to engineer stem cell niches presenting defined and modular cell-instructive physico-chemical cues.

In a first approach, a novel platform based on computer-controlled hydrodynamic flow focusing was developed in order to tether steady-state gradients of tagged proteins, using Fc or biotin tags, onto the surface of poly(ethylene glycol) (PEG)-based hydrogels displaying selective capturing proteins (ProteinA or NeutrAvidin). This versatile patterning strategy permitted the generation of complex biomolecule gradients, with fine control over the patterning resolution and shape. Furthermore, the chosen binding schemes enabled parallel and orthogonal gradients of multiple proteins to be formed. As a proof-of-principle, we employed this technology to assess the influence of immobilized leukemia inhibitor factor (LIF) concentration on mouse embryonic stem cell self-renewal.

While this technology allowed biomolecule dose effect on stem cell behavior to be investigated, it was limited in its ability to modulate multiple microenvironmental factors simultaneously. To address this limitation, droplet-based microfluidic technology was adopted which allows perturbing microenvironmental conditions in a combinatorial fashion and with nearly unmatched precision and throughput. To this end, microfluidic chips were fabricated for the generation of PEG-based microgels with precisely controlled dimensions and physico-chemical properties. First, we developed a versatile biofunctionalization technique for tethering biomolecules of interest to the reactive PEG microgels. Then, selective peptide- and protein-modified formulations were tested for their ability to promote adhesion and proliferation of various stem cell types in a bioreactor-based suspension culture.

Next, programmable modulation of the flows was adopted to generate microgels with varying elasticity, biochemical ligands or both. The different microgel properties were encoded with specific fluorescent markers such that the microenvironment properties could be readily identified via microscopy or flow cytometry. Controlling syringe pumps through computer programming allowed us to generate up to 100 populations of microgels with different elasticities and bioactive ligand concentrations in a single experiment. Thousands of compositionally distinct microgels

were then analyzed by the intensity levels of two fluorescent moieties incorporated in the hydrogel network. As a proof-of-principle, we demonstrated that this technology can be adopted to assess the effects of biophysical and biochemical cues on cell proliferation, as well as on epithelial-to-mesenchymal transition (EMT).

The ease in manipulation and the large throughput and precision in their generation make the microgels ideal candidates for high-throughput screening and discovery of artificial stem cell niches. Therefore, the microgel technology was interfaced with flow cytometric analysis for rapid screening purposes.

Since a three-dimensional (3D) approach to cell biology has been suggested to mimic the physiology of native cellular microenvironments more accurately, we have applied the above microgel technology to the encapsulation of cells. The versatile droplet-based microfluidic system was successfully exploited to generate cell-laden microcapsules with defined biophysical and biochemical properties. Multiple mammalian cells were encapsulated, demonstrating the potential of this technology to elucidate cell behavior in controllable 3D microenvironments.

Taken together, this thesis presents several innovative and unique microfluidic platforms able to reconstruct and modulate multiple niche signaling cues *in vitro*. Particularly, the combinatorial microgel platform presented could facilitate the discovery of novel extracellular matrix compositions and provide insight into the effect of biophysical and biochemical signals on cell behavior in both 2D and 3D settings.

Keywords: stem cell, niche, self-renewal, differentiation, microfluidics, hydrodynamic flow focusing, hydrogel, poly(ethylene) glycol (PEG), patterning, gradient, microgel, combinatorial, stiffness, microscopy, high-throughput technology

Sommario

Le cellule staminali possiedono la capacità unica di auto-rigenerarsi e di differenziarsi in diverse cellule specializzate, contribuendo pertanto all'omeostasi dell'organismo e alla rigenerazione dei tessuti. *In vivo*, le cellule staminali risiedono all'interno di un complesso microambiente in cui molteplici fattori fisico-chimici agiscono sinergicamente al fine di influenzare il loro comportamento. Per meglio comprendere alcune di queste interazioni *ex vivo* e facilitare un più rapido utilizzo delle cellule staminali in campo clinico e farmaceutico, alcune tecnologie alla micro-scala sono state recentemente sviluppate per manipolare il microambiente cellulare. In particolare, idrogeli sintetici, caratterizzati da modulari proprietà meccaniche e dalla capacità di mostrare specifici segnali biochimici, e tecnologie microfluidiche, atte a manipolare e controllare precisamente piccole quantità di liquidi, rappresentano validi strumenti per controllare *in vitro* le condizioni microambientali delle cellule staminali. In questa tesi, sono state sviluppate delle innovative tecnologie microfluidiche, capaci di ingegnerizzare il microambiente delle cellule staminali con proprietà fisico-chimiche modulari.

Per prima cosa, viene presentato un nuovo approccio microfluidico per immobilizzare gradienti di biomolecole sulla superficie di idrogeli sintetici. La presenza di proteine di riconoscimento all'interno del gel, quali la Proteina A o la Neutravidina, permette di legare selettivamente biomolecole che presentano, rispettivamente, il fattore Fc o la biotina. Attraverso l'ausilio di un computer, le soluzioni di proteine possono essere idrodinamicamente focalizzate, permettendo un preciso controllo della quantità e del profilo delle biomolecole immobilizzate. Con tale tecnologia, è stato investigato l'effetto di un morfogeno, il fattore d'inibizione leucemico (LIF), sulla capacità di cellule embrionali staminali murine di auto-rigenerarsi.

Sebbene tale tecnologia abbia permesso di investigare l'effetto di concentrazioni di biomolecole sul comportamento delle cellule staminali, essa è limitata nella capacità di modulare simultaneamente diversi fattori microambientali. Pertanto, una nuova tecnologia microfluidica, basata sulla formazione di microsfere di gel è stata adottata per modulare in modo combinatoriale diverse condizioni cellulari microambientali. A tale scopo, chip microfluidici sono stati generati al fine di sintetizzare microgeli di polietilene glicole (PEG), con un preciso controllo delle loro dimensioni e proprietà fisico-chimiche. Diverse microsfere funzionalizzate con peptidi o proteine d'interesse sono state validate per la loro capacità di promuovere l'adesione e la proliferazione di diversi tipi di cellule staminali.

In seguito, una modulazione programmata dei flussi è stata adottata al fine di sintetizzare microsfere di gel con elasticità modulare, diverse concentrazioni di bioligandi, o entrambe. Le proprietà di ogni microsfera di gel sono state codificate per mezzo di marker fluorescenti, al fine di permettere una loro analisi, attraverso la microscopia o la citometria a flusso. Il controllo dei flussi, per mezzo dell'ausilio di un computer, ha permesso di sintetizzare 100 popolazioni di microsfere di gel con diverse elasticità e, contemporaneamente, diverse concentrazioni di bioligandi, in un singolo esperimento. Pertanto, migliaia di tali microsfere composizionalmente distinte sono state analizzate per mezzo del loro livello d'intensità. Come prova di principio,

abbiamo dimostrato come tale tecnologia possa essere usata per investigare la proliferazione e la transizione epitelio-mesenchimale (EMT) di cellule coltivate su microsfere di gel con differenti proprietà fisico-chimiche.

La possibilità di dispensare tali microsfere, la facilità nel maneggiarle e l'estrema rapidità nel generarle, attraverso la microfluidica, ha reso questa tecnologia particolarmente adatta a testare simultaneamente l'enorme diversità di microambienti cellulari. Pertanto, in questa tesi, viene mostrato come integrare tale tecnologia con metodi di screening ad alta resa, come la citometria a flusso.

Poiché le cellule risiedono in un microambiente tridimensionale, mimare le interazioni cellulari in 3D rappresenta sicuramente un approccio biologico più fisiologico. Pertanto, abbiamo utilizzato la tecnologia sviluppata precedentemente per l'incapsulazione di cellule all'interno di microcapsule, con proprietà fisico-chimiche modulari. Diversi tipi di cellule sono stati incapsulati, dimostrando la potenzialità della tecnologia nell'investigare il comportamento cellulare in microambienti tridimensionali.

Pertanto, questa tesi presenta delle innovative ed uniche tecnologie microfluidiche capaci di ricostruire e modulare *in vitro* alcuni tra i molteplici segnali fisico-chimici presenti nel microambiente cellulare. In particolare, la generazione di microsfere con proprietà combinatoriali potrebbe facilitare la scoperta di nuove composizioni di matrice extracellulare (MEC), facendo luce su nuovi meccanismi biologici alla base del comportamento cellulare in 2D o in 3D.

Parole chiave: cellule staminali, microambiente, auto-rigenerazione, differenziamento, microfluidica, focalizzazione dei flussi idrodinamica, microfluidica per la formazione di emulsioni, idrogelo, polietilene glicole (PEG), patterning, gradienti, microtrasportatore, microgel, combinatoriale, rigidità, microscopia, tecnologia ad alta resa.

Résumé

Les cellules souches jouent un rôle clé dans de multiples processus biologiques dû à leur capacité d'auto-renouvellement et de différentiation en types cellulaires spécialisés en réponse à différents signaux biologiques. *In vivo*, ces cellules souches résident dans un micro-environnement complexe, appelé « niche », qui régule leur destin par une combinaison spécifique de facteurs biophysiques et biochimiques. Afin de récapituler certaines de ces importantes interactions *ex vivo* et de permettre l'application des cellules souches en clinique plus rapidement, de nombreuses technologies ont été récemment développées pour mieux contrôler et manipuler le micro-environnement de ces cellules. En particulier, la combinaison d'hydrogels synthétiques ayant des propriétés mécaniques et biochimiques contrôlables avec les technologies microfluidiques qui peuvent automatiser et manipuler précisément les flux offre une plateforme idéale pour un mimétisme strict des conditions micro-environnementales trouvées *in vivo*. Dans ce travail de doctorat, une nouvelle plateforme microfluidique a été développée pour ingénieurer des niches présentant des signaux physico-chimiques modulaire et définis pour la culture des cellules souches.

Premièrement, une plateforme innovatrice, basée sur un flux hydrodynamique focalisé contrôlé par ordinateur, a été développée pour attacher de manière covalente un gradient stable de protéines taguées, utilisant des tags Fc ou biotin, sur une surface d'hydrogel à base de poly(éthylène glycol) (PEG) contenant des protéines sélectives pour ces tags (proteinA ou NeutrAvidin). Cette stratégie versatile de patterning sélectif permet la génération de gradients complexes de biomolécules avec un contrôle fin sur leur résolution et leur forme. En plus, la chimie choisie pour attacher ces protéines offre la possibilité de fabriquer des gradients parallèles et/ou orthogonaux de protéines multiples. Comme preuve de concept, nous avons utilisé cette méthode pour étudier l'influence d'un gradient de concentration de facteur inhibiteur de la *leucémie*, ou LIF, immobilisé sur l'auto-renouvellement de cellules souches embryonnaires de souris.

Bien que cette technologie permette d'investiguer l'effet de différentes doses de protéines spécifiques sur le comportement de cellules souches, elle est limitée par son incapacité à moduler simultanément différents types de facteurs micro-environnementaux. Afin de résoudre ce problème, la technologie de fabrication de gouttelettes à l'aide de canaux microfluidiques a été utilisée. Cette technologie permet la manipulation des conditions micro-environnementales de manière combinatoire avec une haute précision et un haut débit. Pour réaliser ce concept, des systèmes microfluidiques ont été fabriqués pour permettre la génération de micro-gels à base de PEG ayant des dimensions et des propriétés physico-chimiques ultra-précises. Dans un premier temps, nous avons développé une technique versatile de biofonctionnalisation pour attacher les molécules d'intérêts sur les micro-gels en PEG. En utilisant cette technique, des formulations spécifiques de peptides ou de protéines modifiées ont été testées pour leur capacité à promouvoir l'adhésion et la prolifération de multiples types de cellules souches en culture dans un bioréacteur.

Ensuite, une modulation programmable des flux a été utilisée pour générer des micro-gels variant en élasticité et ayant différentes concentrations de ligands biochimiques. Les micro-gels ayant des propriétés différentes sont encodés avec des marqueurs fluorescents spécifiques pour permettre leur identification en les imageant ou en utilisant des cytomètres en flux. Le contrôle des seringues par ordinateur a permit la génération de plus de 100 populations de micro-gels différentes ayant des propriétés physico-chimiques différentes en une seule étape de production. Ces populations ont ensuite été analysées en mesurant l'intensité des deux molécules fluorescentes, représentant, comme expliqué ci-dessus, les propriétés des populations de micro-gels. Comme preuve de concept, nous montrons, dans ce travail, que cette technologie peut être utilisée pour étudier l'effet des propriétés physico-chimiques sur la prolifération cellulaire ainsi que sur la *transition* épithélio-mésenchymateuse (TEM) de types cellulaires spécifiques.

De plus, étant donné qu'un environnement en trois-dimension (3D), a été suggéré de représenter plus fidèlement le micro-environnement cellulaire natif, nous avons utilisé la technologie de génération de micro-gels décrite ci-dessus, pour encapsuler les cellules à l'intérieur de ces micro-gels. Cette technologie microfluidique versatile de production de gouttelettes fut utilisée avec succès pour générer des microcapsules contenant des cellules et ayant des propriétés physico-chimiques définies. Plusieurs types cellulaires de mammifères furent encapsulées, démontrant ainsi le potentiel de cette technologie pour la compréhension du comportement cellulaire dans un micro-environnement contrôlable.

La facilité de manipulation ainsi que le haut-débit et la haute précision dans la génération de ces micro-gels, les positionnent comme candidats idéaux pour les screening pharmaceutiques à haut-débit et le développement de nouvelles niches artificielles pour les cellules souches. C'est pourquoi, dans le dernier chapitre de ce travail, ces micro-gels ont été interfacés avec une analyse utilisant les cytomètres en flux pour des screening ultra-rapides.

Ce travail de doctorat présente plusieurs plateformes microfluidiques innovatrices et uniques capables de reconstruire et de moduler de multiples signaux de la niche *in vitro*. En particulier, la plateforme de micro-gels combinatoires montre un potentiel certain pour la découverte de nouvelles compositions de matrices extracellulaire et offre la possibilité d'analyser l'effet des signaux biochimiques ainsi que les signaux biomécaniques sur le comportement cellulaire en deux-dimensions et en trois-dimensions.

Mots clés : cellules souches, niche, auto-renouvellement, différentiation, microfluidique, focalisation hydrodynamique de flux, hydrogel, poly(éthylène glycol) (PEG), patterning, gradient, micro-gel, combinatoire, élasticité, microscopie, technologie à haut-débit

Zusammenfassung

Stammzellen spielen eine Schlüsselrolle in einer Vielzahl von biologischen Prozessen hauptsächlich wegen ihrer Fähigkeit sich selbst zu erneuern und als Antwort auf zahlreiche biologische Signale zu spezialisierten Zelltypen zu differenzieren. *In vivo* befinden sich Stammzellen in einer komplexen Mikroumgebung, genannt Nische, die das Zellschicksal durch ein komplexes Zusammenspiel aus biophysikalischen und biochemischen Faktoren reguliert. Um einige dieser wesentlichen Interaktionen e*x vivo* zu rekapitulieren und einen schnelleren Übergang zu klinischen und pharmazeutischen Anwendungen von Stammzellen zu erleichtern, wurden zahlreiche Technologien in den letzten Jahren entwickelt, um die Zellmikroumgebung besser zu kontrollieren und zu manipulieren. Insbesondere die Kombination von synthetischen Hydrogelen mit kontrollierbaren mechanischen und biochemischen Signalen mit Mikrofluidiktechnologien, die Flüssigkeiten automatisch und präzise handhaben können, führt zu beispielloser Präzision über die *in vivo* Bedingungen der Mikroumgebungen. In dieser Doktorarbeit wurden neue mikrofluidische Methoden entwickelt, um Stammzellnischen mit definierten und modularen zellinstruktiven physikalisch-chemischen Signalen zu konstruieren.

In einem ersten Ansatz wurde eine neue Plattform basierend auf einer computerkontrollierten hydrodynamischen Durchfluss-Fokussierung entwickelt, um einen stationären Gradienten von getaggten Proteinen, versehen mit einem Fc- oder einen Biotin-Tag, herzustellen. Sie werden auf der Oberfläche von Polyethylenglycol (PEG)-basierten Hydrogelen mithilfe von selektiven Bindeproteine (in diesem Fall ProteinA oder NeutrAvidin) immobilisiert. Diese vielseitige Oberflächenstrukturierungsstrategie erlaubte die Herstellung von komplexen Biomolekülgradienten mit einer Feinkontrolle über die Strukturierungsauflösung und –form. Außerdem ermöglichte das ausgewählte Bindeschema die Ausbildung von parallelen und orthogonalen Gradienten von mehreren Proteinen. Als prinzipiellen Beweis wurde die Technologie angewendet, um den Einfluss der Konzentration vom immobilisierten Leukämiehemmfaktor (LIF) auf die Selbsterneuerung von embryonalen Stammzellen zu studieren.

Während diese Technologie die Erforschung von Dosierungseffekten von Biomolekülen auf das Stammzellverhalten gestattete, ist sie in ihrer Fähigkeit limitiert mehrere Mikroumgebungsfaktoren simultan zu modulieren. Um dieses Problem anzugehen wurde eine Tröpfchen-basierte Mikrofluidiktechnologie genutzt, die ermöglicht, die Mikroumgebungsbedingungen auf eine kombinatorische Weise und mit nahezu unvergleichlicher Präzision und Durchsatz zu verändern. Zu diesem Zweck wurden mikrofluidische Chips für die Erzeugung von PEG-basierten Mikrogelen mit präzise kontrollierten Dimensionen und physikalisch-chemischen Eigenschaften hergestellt. Zuerst entwickelten wir eine vielseitige Biofunktionalisierungstechnik, um bestimmte Biomoleküle gezielt an reaktive PEG Mikrogele zu binden. Anschließend wurden selektive Peptid- und Protein-modifizierte Rezepturen auf ihre Fähigkeit, Adhäsion und Vermehrung von verschiedenen Stammzelltypen in Bioreaktor-basierten Suspensionskulturen zu unterstützen, getestet.

Daraufhin wurde eine programmierbare Regulierung der Durchflüsse verwendet, um Mikrogele mit unterschiedlicher Elastizität, biochemischen Liganden oder beides zu erzeugen. Die variierenden Mikrogeleigenschaften wurden mit spezifischen fluoreszenten Markern enkodiert, sodass die Eigenschaften der Mikroumgebung leicht via Mikroskop oder Durchflusszytometrie identifiziert werden können. Die Kontrolle über die Spritzenpumpen durch Computerprogrammierung ermöglichte uns über 100 Mikrogelpopulationen mit unterschiedlichen Elastizitäten und bioaktiven Ligandenkonzentrationen in einem einzigen Experiment herzustellen. Tausende Mikrogele, die sich in ihrer Zusammensetzung unterscheiden, wurden anschließend anhand des Intensitätslevel von zwei fluoreszenten Bestandteilen, die in das Hydrogelnetzwerk inkorporiert wurden, analysiert. Als prinzipieller Beweis demonstrierten wir, dass diese Technologie genutzt werden kann, um die Effekte von biophysikalischen und biochemischen Signalen sowohl auf die Zellproliferation als auch auf die Epithelial-zu-Mesenchymal Transition (EMT) zu studieren.

Die Leichtigkeit in Handhabung und hoher Durchsatz sowie Präzision in ihrer Erzeugung macht Mikrogele zu idealen Kandidaten für ein Hochdurchsatz-Screening und Entdeckung von künstlichen Stammzellnischen. Daher wurde im Kapitel 6 der Doktorarbeit die Mikrogeltechnologie mit der Durchflusszytometrie verbunden, um schnelle Screening-Anwendungen zu ermöglichen.

Da generell angenommen wird, dass ein dreidimensionaler (3D) Ansatz in der Zellbiologie die Physiologie der natürlichen Zellmikroumgebung getreuer wiedergeben kann, wendeten wir die genannte Mikrogeltechnologie für die Verkapselung von Zellen an. Das vielseitige Tröpfchen-basierte mikrofluidische System wurde erfolgreich genutzt, um zellbeladene Mikrokapseln mit definierten biophysikalischen und biochemischen Eigenschaften herzustellen. Mehrere Säugerzellen wurden verkapselt, was das Potential dieser Technologie, das Zellverhalten in kontrollierten 3D Mikroumgebungen aufdecken zu können, unterstreicht.

Zusammengenommen präsentiert diese Doktorarbeit verschiedene innovative und einzigartige Mikrofluidikplattformen, die die *in vitro* Rekonstruktion und Modulation von mehreren Nischsignale emöglichen. Insbesondere die kombinatorische Mikrogelplattform könnte die Entdeckung von neuen extrazellulären Matrixkompositionen erleichtern und Einsicht in die Rolle von biophysikalischen und biochemischen Signalen auf das Zellverhalten sowohl in 2D als auch 3D Milieus liefern

Schlüsselwörter: Stammzelle, Nische, Selbsterneuerung, Differenzierung, Mikrofluidik, hydrodynamische Durchfluss-Fokussierung, Hydrogel, Polyethyleneglycol (PEG), Strukturierung, Gradient, Mikrogel, kombinatorisch, Steifigkeit, Mikroskop, Hochdurchsatztechnologie

Table of contents

Motivation and objectives

Stem cells play a crucial role in the development of an organism and, later on in life, in the maintenance and regeneration of tissues. Their unique dual properties to renew themselves over a long period of time and to give rise to specialized cell types makes these rare cells very attractive for many biomedical and pharmaceutical applications.[1-3]

In vivo, stem cell behavior is critically dependent on interactions with a complex microenvironment, termed niche, which is composed of a wide variety of chemical and physical signaling cues.[4-6] Despite very extensive efforts in the past decade, many stem cells and their niches remain poorly defined, and little is known about how multiple niche signals act in concert to regulate stem cell self-renewal and lineage commitment. As a result, there are also major challenges in growing stem cells outside of their native habitats to make them useful for various applications.

In order to shed light on the biology of stem cells and their niches and, ultimately, facilitate stem cell-based applications, novel technologies are needed that allow reliably manipulating stem cells in culture. To this end, model systems designed to recapitulate some of the critical stem cell-niche interactions in a cell culture setting are particularly promising as they could pave the way to better understand microenvironmental regulation of stem cell behavior.[7-9]

Synthetic bioactive hydrogels have emerged as promising niche-mimicking biomaterials. Hydrogels possess multiple characteristics that make them ideal candidates for modeling stem cell niches. For example, hydrogels have physico-chemical properties that are reminiscent of native stem cell niches. They are often inert but can be readily modified with desired cell-signaling cues and many gel systems have very well defined compositions and can be modulated nearly on-demand, depending on a particular application.[10-12] However, a major difficulty in emulating stem cell niches via hydrogel engineering is that the specific gel composition to control a desired stem cell fate and type is a priori not known. In the absence of efficient screening methodologies, hydrogel formulations can currently only be found using time-consuming and expensive approaches based on trial-and-error. Therefore, novel approaches to rapidly assemble the different gel building blocks in a high-throughput manner are urgently needed.

Recently, microfluidic technology has offered the unique possibility to precisely handle and control small amounts of fluids in order to efficiently process multiple samples, thereby dramatically reducing the analysis times.[13-15] Taking advantage of the power of microfluidics for high-throughput multiplexing, the overall goal of this thesis is the development of novel paradigms to recapitulate *in vitro* some of the intricate combinatorial signaling environments that regulate stem cell behavior in our body. The platforms should allow for a versatile modulation of key regulatory factors, for cell culture applications in two and three dimensions. Moreover, these technologies can be interfaced with high-throughput screening technologies.

Chapter 1 of this thesis provides a general background on stem cell niches and provides the impetus for engineering artificial niche models, displaying modular biophysical and biochemical cues. Moreover, an overview is given about some of the existing microtechnologies, particularly focusing on microfluidic gradient generators and droplet microfluidics, as powerful techniques to recapitulate *in vitro* some of the stem cell niche environmental cues.

Due to the active role of the temporal and spatial display of morphogens in many biological processes, in **Chapter 2** and **3** a first microfluidic approach is presented that allows generating tethered biomolecule gradients on the surface of soft synthetic hydrogels. Specifically, a versatile computer-controlled hydrodynamic flow focusing platform is utilized to generate any user-defined gradient shape. In **Chapter 3**, the capability and resolution of the above biomolecule hydrogel patterning approach is further improved by the generation of overlapped gradients of morphogens whose activity on embryonic stem cells self-renewal was explored.

Although these examples already demonstrate the possibility to engineer *in vitro* key signaling aspects of a stem cell microenvironment, the described technology is limited in its capability of simultaneously modulating multiple microenvironmental factors. To address this issue, in **Chapter 4**, a droplet-based microfluidic technology was employed for the generation of poly(ethylene glycol) (PEG)-based microgels with precisely controlled dimensions and physico-chemical properties. Furthermore, a versatile chemical scheme was used to render the microgels cell-type-specific by tuning their bioactive properties for the manipulation of various stem cell types. Based on these achievements, in **Chapter 5** this strategy was expanded to rapidly synthesize, process and screen a continuous 'landscape' of microgels with fluorescently encoded physical and chemical compositions. This unique platform should facilitate the discovery of artificial niches for various stem cell types and provide novel insights into the effect of biophysical and biochemical microenvironmental perturbations on cell behavior.

The ease in manipulation and distribution and the fast microfluidic generation make microgels ideal candidates for high-throughput experimentation. **Chapter 6** demonstrates the possibility to process the microgels and to interface them with high-throughput analysis, such as flow cytometry analysis, for rapid screening purposes.

Since 3D microenvironments provide more physiological mimics of native cellular microenvironments, in **Chapter 7** of this thesis droplet microfluidics was tested for the encapsulation of cells within enzymatically cross-linked PEG microgels. Cell-laden microcapsules were generated with various biophysical and biochemical properties. This approach enables the investigation of cell behavior upon modulation of their 3D environment.

Finally, the last part of this thesis provides a summary of this work and discusses current limitations of this technology as well as ways for overcoming them. Future perspectives for its application as a powerful tool to study fundamental stem cell biology are also discussed.

References:

1   Passier, R., van Laake, L. W. & Mummery, C. L. Stem-cell-based therapy and lessons from the heart. *Nature* **453**, 322-329 (2008).
2   Deasy, B. M., Yong, L. I. & Huard, J. Tissue engineering with muscle-derived stem cells. *Curr Opin Biotech* **15**, 419-423 (2004).
3   Daley, G. Q. & Scadden, D. T. Prospects for stem cell-based therapy. *Cell* **132**, 544-548 (2008).
4   Scadden, D. T. The stem-cell niche as an entity of action. *Nature* **441**, 1075-1079 (2006).
5   Lane, S. W., Williams, D. A. & Watt, F. M. Modulating the stem cell niche for tissue regeneration. *Nat Biotechnol* **32**, 795-803 (2014).
6   Walker, M. R., Patel, K. K. & Stappenbeck, T. S. The stem cell niche. *The Journal of pathology* **217**, 169-180 (2009).
7   Vazin, T. & Schaffer, D. V. Engineering strategies to emulate the stem cell niche. *Trends Biotechnol* **28**, 117-124 (2010).
8   Lutolf, M. P., Gilbert, P. M. & Blau, H. M. Designing materials to direct stem-cell fate. *Nature* **462**, 433-441, doi:Doi 10.1038/Nature08602 (2009).
9   Lutolf, M. P. & Blau, H. M. Artificial Stem Cell Niches. *Adv Mater* **21**, 3255-3268 (2009).
10   Lutolf, M. P. & Hubbell, J. A. Synthetic biomaterials as instructive extracellular microenvironments for morphogenesis in tissue engineering. *Nat Biotechnol* **23**, 47-55 (2005).
11   Seliktar, D. Designing Cell-Compatible Hydrogels for Biomedical Applications. *Science* **336**, 1124-1128 (2012).
12   DeForest, C. A. & Anseth, K. S. Advances in Bioactive Hydrogels to Probe and Direct Cell Fate. *Annu Rev Chem Biomol* **3**, 421-444 (2012).
13   Elvira, K. S., Solvas, X. C. I., Wootton, R. C. R. & deMello, A. J. The past, present and potential for microfluidic reactor technology in chemical synthesis. *Nat Chem* **5**, 905-915 (2013).
14   Sackmann, E. K., Fulton, A. L. & Beebe, D. J. The present and future role of microfluidics in biomedical research. *Nature* **507**, 181-189 (2014).
15   Khademhosseini, A., Langer, R., Borenstein, J. & Vacanti, J. P. Microscale technologies for tissue engineering and biology. *P Natl Acad Sci USA* **103**, 2480-2487 (2006).

Chapter 1

Introduction

The stem cell niche

Apart from all other cells, stem cells have the unique dual ability to self-renew over a long period of time and to differentiate into functionally mature cells. Therefore, they are responsible for the development of an organism and the tissue homeostasis and regeneration later in life.[1-3] *In vivo*, stem cells reside in a complex, heterotypic and highly dynamic microenvironment, termed niche, where the cells are exposed to intricate combinations of signaling cues.[4-6] The bidirectional interaction between stem cells and their niche strongly regulates viability, renewal and differentiation potential.[7]

In 1978, Schofield was the first to propose the existence of a microenvironment that regulates stem cell function in the hematopoietic compartment.[8] Later, studies conducted by the Spradling group showed the importance of the microenvironment in shifting the balance between self-renewal and differentiation of germline stem cells in *Drosophila*.[9,10] Today, the niche is considered to be crucial in controlling the function of various stem cell types, such as hematopoietic [11-13], intestinal [14-16], neural [17,18], epithelial [19], mesenchymal [20] and skeletal muscle cells [21,22].

Within the niche, many factors affect stem cells: niche stiffness, topography, chemical composition, shear stresses, temperature and oxygen gradients, interactions with the extracellular matrix (ECM) and biochemical cues including gradients of soluble and tethered growth factors, cytokines and metabolic signals (Figure 1.1).
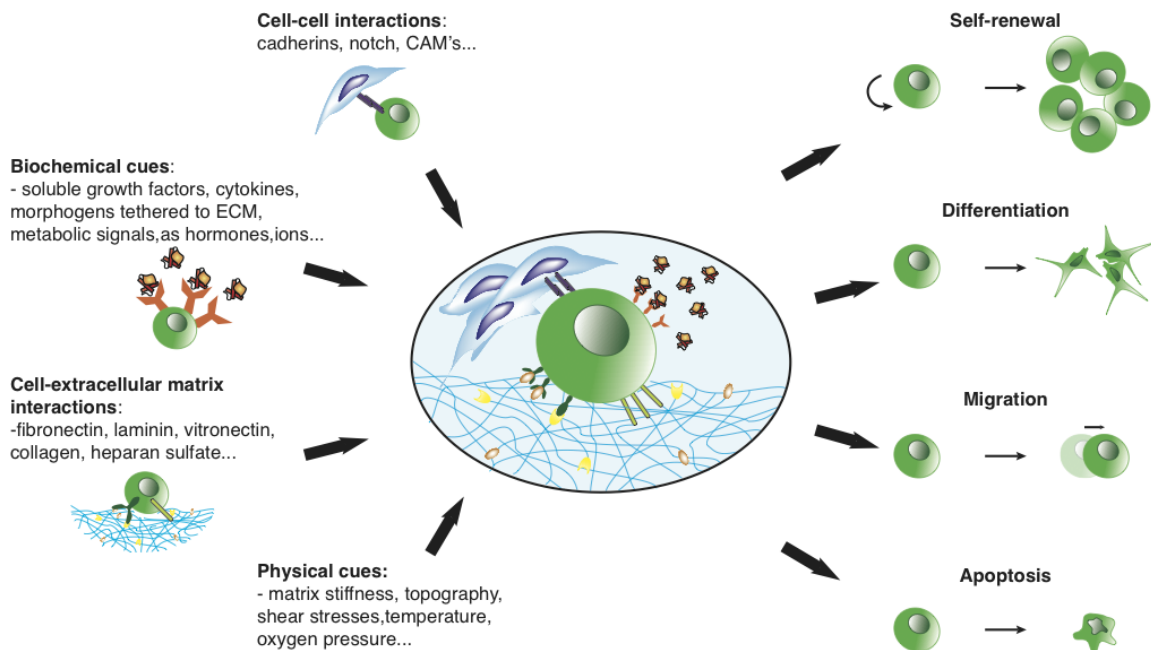
Figure 1.1 – The stem cell niche. Scheme depicting the complexity of stem cell niche *in vivo*, where multiple microenvironmental signals affect cell behavior. Biophysical and biochemical cues, as well as metabolic signals all regulate stem cell self-renewal and differentiation potential. Furthermore, stem cells interact with other niche cells through cadherins or the notch signaling pathway and with the extracellular matrix, through proteins, such as fibronectin, laminin and collagen or polysaccharides, such as heparan, sulfate and hyaluronic acid. The various signal transduction pathways of a stem cell lead to different fates, such as self-renewal, differentiation, migration and apoptosis.

In many adult tissues, the stem cell niche contains different cell types with distinct functions that communicate with the stem cell in addition to physicochemical cues. One example is the hematopoietic stem cell (HSC) niche where megakaryocytes, macrophages, and osteoblastic, vascular, neural and immune cells all interact with the stem cells and regulate their function.[23-25] Also, in the small intestine, Paneth cells support intestinal stem cells through secretion of WNT3A and epidermal growth factors.[15,26] Therefore, interactions with other niche cells through membrane protein-mediated direct cell-cell contact or through secretion of paracrine growth factors have been shown to be crucial regulators of stem cell fate. Epithelial stem cells [27] and HSCs [28] are just two examples. These signaling cues come together to form an intricate network of factors that strongly affects the stem cell fate in terms of self-renewal, differentiation, migration, proliferation or apoptosis.[29,30]
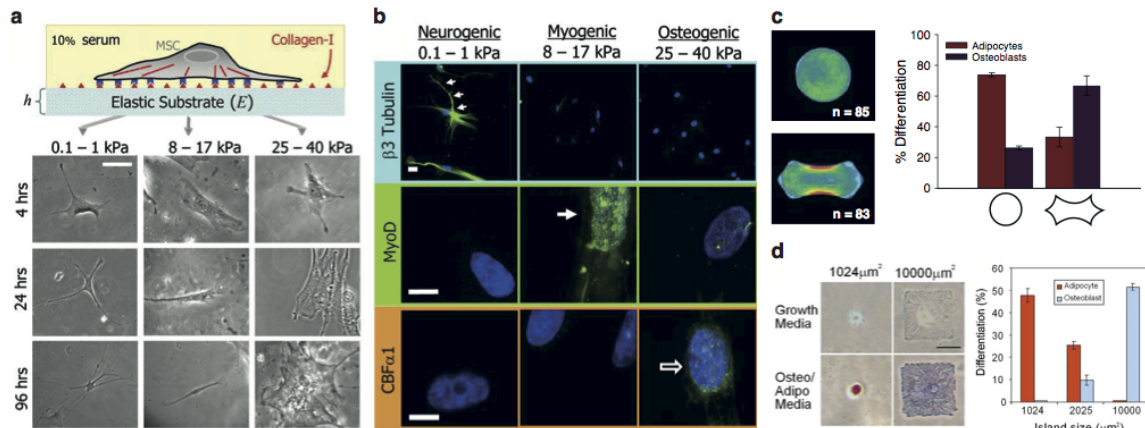
Biophysical niche regulators

The ECM is a key component of the niche due to its dual role of physically anchoring the stem cells and directing their fate. The ECM is a hydrated environment, mainly composed of major structural proteins, such as collagen, fibronectin, vitronectin and laminin, yet containing also proteoglycans, including perlacan and heparan sulfate, and polysaccharides, such as hyaluronic acid. Stem cells interact with the ECM growth factors, morphogens and adhesion proteins through specific membrane receptors called integrins. Through these interactions, forces and signaling cues are transmitted from the outside of a cell into the cytoplasm and then converged in the nucleus to regulate gene expression and, ultimately, cell phenotype.[29]

Regulation of stem cell behavior is orchestrated through the physical and chemical properties of the ECM, such as stiffness, topography and composition. Substrate elasticity is one of the key physical regulators of stem cell behavior. Pioneers in this field, Engler and Discher showed a stiffness-mediated mesenchymal stem cell (MSC) differentiation on polyacrylamide gels with different elasticities in the absence of specific biochemical cues.[31] Cells committed to different lineages when cultured on substrates with a stiffness resembling that of native tissues. Therefore, MSCs differentiated into the neural lineage when cultured on soft gels (elastic modulus between 0.1-1 kPa), muscle cells when cultured on gels with intermediate stiffness (elastic modulus between 8-17 kPa) and osteoblasts when cultured on stiff gels (elastic modulus between 25-40 kPa), as clearly shown by different cell morphologies and gene expression (Figure 1.2 a,b). Other important examples about stiffness-mediated stem cell differentiation have also been demonstrated for muscle cells [22] and mammary epithelial cells [32].

Substrate topography, shape and dimension have also been highlighted as important physical parameters directing stem cell lineage commitment. To examine substrate shape, researchers micro-patterned cell-adhesive islands with different shapes and dimensions to control the degree of spreading of single cells (Figure 1.2 c,d). With this method, the differentiation of MSCs into the adipogenic or osteogenic lineages occurs based on the shape and the dimension of fibronectin-patterned micro-islands.[33,34] Other work has revealed a terminal differentiation of human epidermal stem cells when cells are confined on small circular substrates.[35] Therefore, modifying the shape and dimensions of the substrate adhesion sites affects the degree of integrin engagement and the remodeling of the actin cytoskeleton that initiates intracellular signaling cascades and affects gene expression.

Hence, the interplay of matrix stiffness, topography, porosity and protein tethering contributes to the regulation of stem cell differentiation in a complex and intricate manner.[32,36,37] In addition to these biophysical cues, other factors, such as temperature, oxygen gradients and shear stresses, influence stem cell fate and contribute, for instance, to HSCs survival and maintenance.[38,39] These examples highlight the complexity of the niche and how the combinatorial interaction of multiple factors strongly impacts stem cell differentiation.

Figure 1.2 – Biophysical niche regulators. a, Collagen-coated polyacrylamide gels can be cast with different cross-linking rates to achieve different substrates elasticities. Naïve MSCs, cultured on gel with varying elasticity in the absence of biochemical cues, showed different morphologies. The cells were branch-shaped on soft gels, spindle-shaped on intermediate stiffness gels and polygonal-shaped on stiff gels. **b**, Stainings showing different lineage commitment of MSCs on matrices with different elasticities. The neuronal cytoskeletal marker ß3-tubulin is expressed in branches only on soft gels. The muscle transcription factor MYOD1 is up-regulated and localized in the nuclei of cells only when cultured on myogenic substrates. The osteoblast transcription factor CBFα1 is expressed on cells grown on osteogenic gels. Adapted from ref. [31] with permission of Elsevier. **c**, The shape of the substrate influences human MSCs (hMSCs) lineage commitment. Cells presented different localization and expression of myosin IIa when they were cultured on circles or holy leaves-shaped fibronectin islands. Circles favoured adipogenic differentiation, whereas the holy leaves shape induced osteogenic commitment. Adapted from ref. [33] with permission from NAS. **d**, Micrographs showing hMSCs cultured on fibronectin islands with different dimensions. Lipid were stained in red in the adipocytes; alkaline phosphatase was stained in blue in the osteoblasts. The substrate topography influences the cell shape that drives hMSC commitment. Cells cultured on small islands tend to differentiate into adipogenic lineage, whereas cells on big islands differentiate into osteogenic lineage. Adapted from ref. [34] with permission from Elsevier.

Biochemical niche regulators

Biochemical cues also act as important regulators of stem cell behavior, very often strictly interconnected to the biophysical ones. Cells respond to biomolecules through surface receptors that activate specific intracellular signaling pathways by either enhancing the pathways generated by physical interactions or suppressing them. An example is represented by hMSCs commitment towards the osteogenic lineage achieved by culturing cells on myogenic substrates while exposing them to the bone morphogenic factor, BMP-2. This biomolecule activates the BMP-Smad

pathway and induces the formation of osteoblasts, showing how substrate elasticity effects can be achieved by exposing the cells to soluble chemical cues alone.[40]

Within the stem cell niche, ECM proteins, growth factors, morphogens or cytokines can all act as biochemical cues, which can be present in a soluble or tethered form. This form dictates the way signals are transduced into the nucleus and thus results in a distinct cell response.[41] In addition to exerting forces to the cells, the ECM protein composition also provides biochemical cues by displaying tethered biomolecular gradients, therefore exposing the stem cells to local concentrations of agonists.[42] Research has shown a different bioactivity of growth factors when bound to artificial substrates. For example, tethered BMP induced better adhesion and spreading of C2C12 myoblasts[43], and matrix-bound VEGF showed improved growth of endothelial cells[44]. Another example is the leukemic inhibitor factor (LIF), a cytokine that, in its soluble form, is critical in promoting embryonic stem cell self-renewal through STAT3 activation. Recently, we generated gradients of LIF tethered on the surface of soft biomimetic hydrogels and identified a specific threshold of 85 ng/cm^2, below which stem cells become unable to retain their pluripotency by expression of the Rex1/Zfp42 marker.[45] Therefore, the form in which biomolecules are displayed to cells and the variable concentration given by gradients play a vital role in developmental decision-making of cells. In fact, during many biological processes the biochemical signaling cues are expressed in the form of biomolecular gradients. For example, morphogen gradients are involved in the differentiation of cells during development, inflammation and cell migration mechanisms including cancer metastasis.[46]

Another example is the differentiation of embryonic stem (ES) cells during development. Morphogen gradients regulate this process and thus determine the arrangement and fate of the responding cells by the morphogen concentration.[47] The mammalian pituitary gland development relies on the presence of overlapping gradients of various morphogens, such as BMPs, fibroblasts growth factors (FGFs), WNT and sonic hedgehog (SHH).[48] Xu et al. recently showed that the stimulation of uncommitted cells in the blastula animal pole with opposing gradients of BMP and NODAL is sufficient to reorganize the cells into a well-developed embryo, compared to the un-stimulated cells (Figure 1.3).[49]
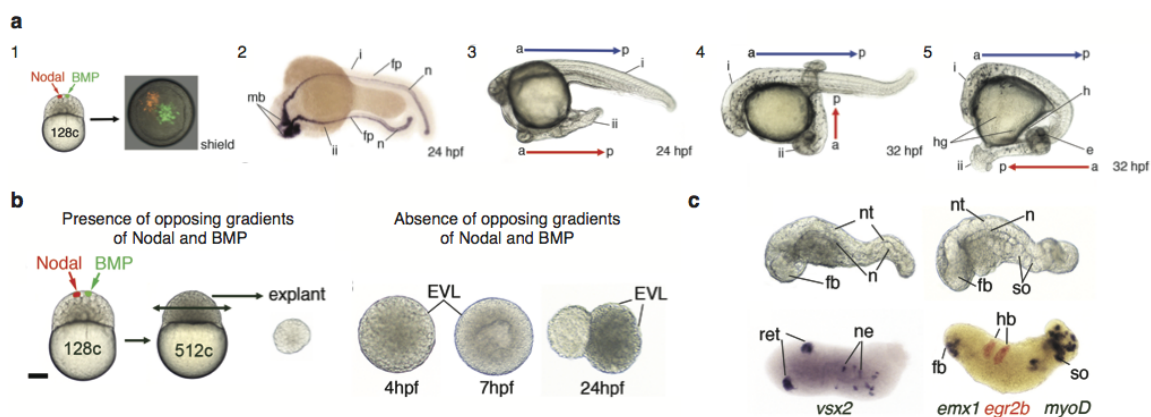
Figure 1.3 – The importance of morphogen gradients during embryonic development. a, Injection of engineered opposing gradients of BMP and Nodal into the zebrafish blastula animal pole (1) led to the formation of a secondary embryonic axis expressing sonic hedgehog (ii) from the midbrain to the tip of the tail (2). The different orientations, parallel (3), perpendicular (4) and antiparallel (5) to antero-posterior (a-p) one, show the formation of different organs, such as eye, heart, midbrain and hatching gland. **b**, Animal

pole injection and explantation (left panel) in contrast with the uninjected explants (right panel) in which no differentiation of any embryonic tissues or organs was observed. **c**, In the presence of opposing gradients of the two morphogens, explants differentiated into embryos with distinct morphological structures, such as the forebrain, neural tube, notochord and somites. Adapted from ref. [49] with permission from AAAS.

During cancer progression, cells must escape the primary tissue. To do so, they invade a new tissue and then recruit endothelial cells to create new vessels (process called angiogenesis). This cascade of biological processes is governed by gradients of biomolecules, such as TGF-ß, which induces an epithelial-to-mesenchymal transition (EMT) and ultimately allows cells to escape from the primary tissue, and cytokines that attract endothelial cells during the tumor-induced angiogenesis. Thus, in addition to biophysical interactions, the spatial and temporal arrangement of various biomolecules in soluble or tethered form, and potentially in a gradient, influences cell behavior in many biological processes.

## Biomaterials as artificial stem cell niches

Biomaterials have emerged as powerful and versatile tools to better mimic the physiological complexity of the natural cellular microenvironment.[29,50-52] Although traditional cell culture performed on 2D tissue culture plastic contributed to the understanding of some important biological processes, it intrinsically lacks the capability of mimicking the physiological aspects of the natural cell environment. Due to the complexity of the niche, faithful artificial reconstruction requires a modular tool with high degrees of versatility and modularity and that can display defined and tunable physicochemical properties.

Hydrogels are soft and highly hydrated materials that have been employed for the generation of artificial extracellular matrices through a mild cross-linking strategy. Importantly, hydrogels do not form cytotoxic side products, and they allow well-controlled tethering of biomolecules and reproducible mechanical properties. Due to their ability to provide specific biophysical and biochemical cues, they showed promise in a number of biomedical applications, such as regenerative medicine, drug and cell delivery, acting as versatile 2D substrates as well as 3D matrices.[53] Three types of hydrogels have been primarily used: natural, synthetic and hybrid systems, i.e. a blend of different gels. Natural gels are derived from different natural sources and, therefore, are biocompatible and bioactive. They intrinsically contain adhesion sites and signaling peptides that promote cell attachment, viability, migration, proliferation and differentiation.[53] Generally, natural hydrogels are either ECM components, such as collagen (or its denaturated version, gelatin), fibrin, hyaluronic acid, Matrigel, or materials derived from other biological sources, such as agarose, alginate and chitosan. Although natural gels have been extensively used for cell culture applications in 2D and 3D, they have several disadvantages. Biochemical modification usually lacks specificity and relies on poorly controllable adsorption. Also, current methods have poor control and reproducibility over the mechanical properties due to the intrinsic batch-to-batch variability, which hinders a reliable cell behavior observation.

On the other hand, synthetic bioactive hydrogels, such as polyglycerol, self-assembling peptides and poly(ethylene) glycol (PEG), have been extensively proven as cell-instructive materials, due to their defined and reproducible composition, modular mechanical properties and

capability to precisely display biochemical signals.[29,52,54] In particular, PEG-based hydrogels offer the unique advantage of displaying an inert polymer backbone which prevents non-specific protein adsorption yet gives the possibility to reliably tune the mechanical and biochemical properties. In fact, the gels show an elastic behavior, and the gel mass and elastic modulus exhibit a linear relationship that can be exploited simply by changing the mass content of the precursors. Furthermore, well-established chemical modification strategies can be applied to tether different biomolecules in a highly controlled fashion.[55] Therefore, the hydrogel system allows for strict and independent control over both biophysical and biochemical properties.

In this thesis, we primarily utilized two types of PEG hydrogels, which differed in the cross-linking reactions: Michael-type addition gels, used for 2D applications, and enzyme-mediated cross-linking gels, for 3D applications (Figure 1.4). Michael-type addition gels are based on the covalent bond between a vinylsulfone (VS)-terminated PEG macromer and thiolated gel building blocks, which are either peptides or PEG macromers. Thiols react efficiently with unsaturated carbonyls to form stable thioether linkages, without requiring any initiator or catalyst. On the other hand, enzyme-mediated cross-linked PEG gels rely on the capability of the enzyme to catalyze reactions in aqueous solutions at low temperature, neutral pH and with very high affinity for their substrates. We adopted a transglutaminase (TG)-mediated hydrogelation, in which the enzyme FactorXIIIa catalyzes the formation of N-ε-(γ-glutamyl) lysine isopeptide bond.[56,57]
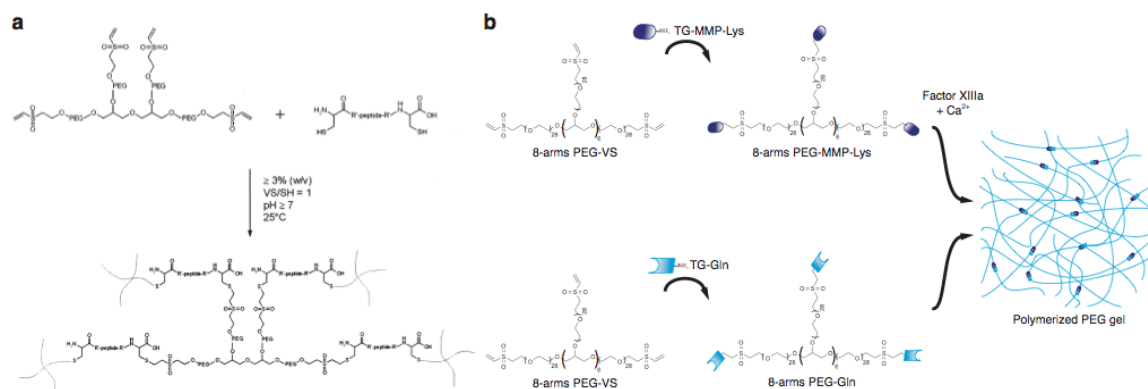
Figure 1.4 – Chemical structures of PEG-based hydrogels. a, Chemical scheme for the stepwise co-polymerization of thiols-containing biomolecules with vinylsulfone-functionalized PEG macromers. The reaction occurs at basic pH at room temperature. Adapted from Ref. [55] with permission of ACS. **b**, Synthesis scheme for the formation of an enzyme-mediated cross-linked hydrogel: unsaturated multibranch PEG-VS macromers were chemically link to a lysine and glutamine donor peptides. FactorXIIIa enzyme catalyzes a transglutaminase-mediated reaction between the two chemically modified PEG macromers, in presence of calcium. Scheme modified from [56].

Microtechnologies to engineer stem cell niches

Due to the complexity of the stem cell microenvironment, there is a undeniable necessity to artificially build novel *in vitro* systems to unveil and recapitulate the critical physicochemical cues within the niche.[58] Newly engineered platforms would help researchers to understand the mechanisms and principles governing the microenvironmental regulation of stem cell fate and,

therefore, ultimately promote a faster implementation of stem cells for therapeutic and clinical applications. The importance of recreating an artificial niche is highlighted by some approved clinical trials that aim at controlling the function of stem cells through stem cell niche modification. For instance, bone marrow failure treatment may consist of anti-thymocyte globulin, which targets immune cells in the niche [59], and for skin damage, platelet-derived growth factors-loaded gels have been used to target the ECM and growth factors in the epithelial niche.[60] Therefore, *in vitro* stem cell niche models could lead to new niche-directed therapies that target the microenvironment to support endogenous repair and therefore represent valuable alternatives to cell transplantation or *in vivo* stem cell manipulation.[7] To this end, new generations of cell culture platforms based on microfabrication techniques combined with advanced biomaterials have come about, and the development and application of the platforms have been developed at a rapid pace. In the next paragraphs, some of them will be discussed to demonstrate their potential in biology, even though the section is not intended to be an extensive dissertation about all the microtechnologies developed in literature.

Micro-scale technologies for displaying niche signals

Microtechnologies have been widely used for many biological applications due to the small transport distances and volumes of sample, the capability to introduce and measure fast dynamic changes in cellular responses and their high-throughput potential.[61] In fact, the microscale size is naturally suited for studying samples at the same scale, such as cellular phenomena. Furthermore, these technologies also permit screening of the huge diversity of potentially relevant microenvironmental conditions by controlling several properties independently from each other, which allows for a decoupled observation of cellular phenomena in a combinatorial fashion.

Microfabrication techniques and robotic spotting have made it possible to generate multifunctional microarrays for studying the effect of biochemical and biophysical cues on stem cells. For instance, Bathia and colleagues developed a microarray system to screen for the combinatorial effects of ECM molecules on the differentiation of mouse embryonic stem cells.[62] Combinations of such technology with hydrogels have led to the creation of functional microwells to screen multiple microenvironmental cellular conditions.[63,64] Our group recently engineered a PEG-based microwell array with modular stiffness and combinatorially spotted proteins to investigate microenvironmental perturbations on proliferation and differentiation of human mesenchymal stem cells (Figure 1.5a,b,c).[63] The platform was also used to investigate artificial niches to support self-renewal of neural stem cells. However, microarray approaches usually require the use of expensive robotic handling, do not allow precise control of the protein concentration being incorporated within the gel, and demand an image-based analysis approach that is rarely compatible with high-throughput screening.

Recently, microfluidics offered the unique possibility to rapidly assemble the different gel building blocks in a high-throughput manner in addition to precisely handling and controlling small amounts of fluid. In microfluidic systems, the only mixing through diffusion of molecules across the fluid interface occurs; the fluids do not mix convectively. These systems are generally characterized by low values of Reynolds number (Re), defined as the ratio between the inertial and viscous forces. Therefore, in this flow regime, the flows are dominated by viscous forces and are also laminar. Microfluidics allows for miniaturization and, as a result, parallelization and

automation of experiments, which reduces the waste of expensive reagents and shortens the analysis times.[65] For these reasons, it has been used to precisely display biochemical niche signals for the spatial and temporal perturbation of the cell microenvironment for analysis at the single cell level.

Microfluidic gradient generators were proposed by Whitesides [66] and consisted of a serial flow dilution in multiple micro-branches of a serpentine channel; however, a much simpler design was proposed by Georgescu[67]: three microchannels were adopted to generate accurate and reproducible protein gradients. Dynamic computer control allowed hydrodynamic flow focusing to modulate the stream widths of each flow by selectively controlling the amount of deposited proteins. Linear, exponential and overlapping gradients of multiple proteins were generated with high control (Figure 1.5d). Hydrodynamic patterning was also used to recapitulate the polarized niche structure of embryos in microfluidic channels.[68] Although these approaches provide powerful models to study the role of biomolecules and matrix elasticity in controlling stem cell behavior, they omit the third dimension as another important fate determinant. Carrion and colleagues, combining a microfluidic approach to hydrogels, patterned endothelial cells adjacent to stromal cells within 3D gel fibrin structures, inducing morphogenesis in a capillary network with hollow lumens (Figure 1.5e,f,g).[69]

The complexity of tissue model microfabrication through a combination of microfluidics and biomaterials has increased with the generation of organs-on-a-chip, such as lung [70], gut [71] and liver [72]. Interestingly, Torisawa and colleagues recently also reported a functional hematopoietic niche *in vitro* by first engineering new bone *in vivo*.

A sub-category of microfluidics is the droplet-based technology, which is widely used to compartmentalize chemical reactions or biological samples with the opportunity to recreate a library of unique environments to study the stem cell behavior in a 3D setting. In the next section, different applications of this technology will be reported, focusing on the generation of versatile microgels for displaying mechanical and biochemical niche signals.
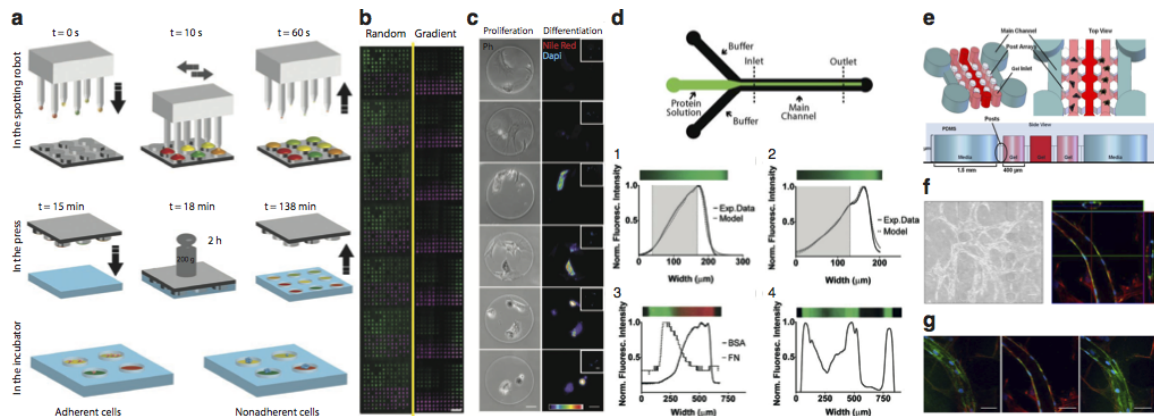
Figure 1.5 – Microscale technologies for displaying niche signaling. a, Microfabrication of an artificial niche microarray: a robotic spotter was used to print different protein solutions on micropillars of a silicon stamp. The latter was pressed against a partially cross-linked layer of PEG hydrogel. Upon release, the microwells were used to culture different types of stem cells. **b**, Examples of microarrays printed with fluorescent proteins in a random or gradient fashion. **c**, Mesenchymal stem cells cultured in combinatorial microwells. Phase contrast micrographs (left) showing the different proliferation trends. Differentiation in

the adipogenic lineage was shown by Nile Red staining (pseudocolored). Cell nuclei and actin filaments were stained with DAPI and green Phalloidin, respectively. Adapted from Ref. [63] with permission of NPG. **d**, Microfluidic channels used to generate user-defined gradients: by modulating the stream widths of the flows, it was possible to pattern surfaces with linear (1), exponential (2), overlapping (3) and complex-shaped (4) gradients. Adapted from Ref. [67] with permission of Royal Chemical Society. **e**, Microfluidic set-up used to form capillary-like networks in 3D fibrin gels. Medium and nutrients are provided from the main channels, and cell-containing gel is injected through inlets. **f**, Phase contrast (left) and confocal image (right) of HUVEC cells in presence of stromal fibroblasts. F-actin is stained with red phalloidin, CD31 in green and nuclei with DAPI. **g**, Confocal images showing the formation of a hollow lumen from different sections, bottom, center and top. Adapted from Ref. [69] with permission of Wiley Periodicals.

Droplet-based microfluidic technology

Droplet-based microfluidics is a technology that allows the formation of sub-droplets, relying on the emulsification of an aqueous solution, called the discontinuous phase, into an immiscible nonpolar solution, such as oil, named the continuous phase. Microdroplet formation is strictly regulated by the physical equilibrium between the shear forces and the surface tension at the liquid-liquid interface, expressed by the capillary number, *Ca*. First, an interface is generated between two immiscible liquids; then a droplet starts to grow, and a pressure gradient causes the deformation of the dispersed phase until it breaks off into a bead.[73] The surface-induced instability can be generated using different device geometries depending on the required droplet frequency and dimensions. Typically, the most common designs to generate microdroplets are the flow focusing and the T-junction in a planar chip format or the co-flow in a capillary format.[74] Droplet-based microfluidics allows for tight control over the droplet dimensions and shape that can be tuned by changing the channel dimensions and by modulating the flow parameters, particularly the ratio between the flow rate of the continuous phase and the discontinuous phase. Additionally, the automation and precise liquid handling, dictated by the laminar flow regime, enable the formation of multicomponent beads in high-throughput with frequencies higher than 10 kHz.[75]

Compartmentalization in microdroplets, with a volume between 0.5 pl and 4 nl, has been widely used for many chemical and biological applications. Droplets were used as micro-reactors to miniaturize chemical reactions with consequent efficient mixing of small reagent volumes, reduced cross-contamination risk and the possibility to parallelize and scale out the production.[76] Furthermore, due to the high surface-to-volume ratio, heat and mass transfer phenomena are enhanced, the diffusion distances are shorter and, consequently, the reaction times much lower. Parallelization, automation and manipulation of the beads through splitting, merging, storing and transporting them rendered this technology very attractive for the possibility to interface it with high-throughput analysis technologies for screening purposes, such as flow cytometry or mass spectrometry.[77,78] Because of these advantages, this technology has been extensively employed for drug discovery and delivery [79-81], cell encapsulation [82-84], precise microparticle synthesis [85-87] and to perform chemical and biochemical reactions [78,88,89] (Figure 1.6).
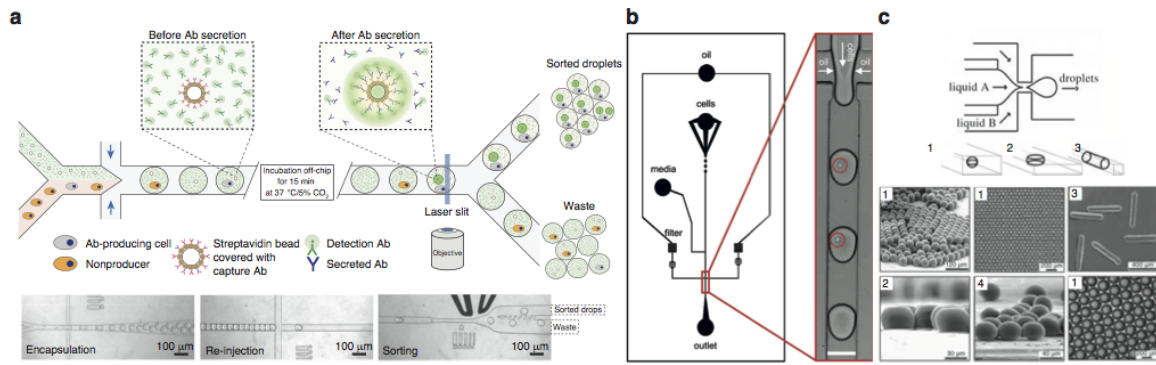
Figure 1.6 – Applications of the droplet-based microfluidics in biology and chemistry. a, Example of droplet-based microfluidics used for miniaturization of cell-mediated chemical reactions. Microfluidic encapsulation of antibody-producing cells together with streptavidin beads covered with capture antibody and detection antibodies. After antibody secretion, streptavidin beads become fluorescent. The cell-laden microbeads are re-injected into a second microfluidic chip and droplets containing the fluorescent beads are sorted using a droplet-sorter incorporated in the device. On the bottom row, micrographs showing the different microfluidic steps of the process are reported. Adapted from Ref. [78] with permission from NPG. **b,** Schematic of a flow focusing microfluidic chip for the encapsulation of mammalian cells. Adapted from Ref. [84] with permission from Elsevier. **c**, Generation of microparticles with controlled size, morphology and composition. By modifying the microfluidic channel aspect ratio, microparticles with different shapes can be generated, such as microspheres (1), disks (2), rods (3) and ellipsoids (4), as represented in the optical images. Adapted from Ref. [85] with permission from John Wiley and Sons.

Microgels-based technology

The precision and reliability offered by droplet-based microfluidics combined with the versatility of the hydrogel-based chemistry have been successfully adopted in microgel-based technology. It enabled the *in vitro* reconstruction of the stem cell niche by manipulating and assembling cells with different gel components into a microgel artificial stem cell niche. This technology has also generated bioactive cell microcarriers and three-dimensional (3D) matrices that enhance *in vitro* tissue models (Figure 1.7).
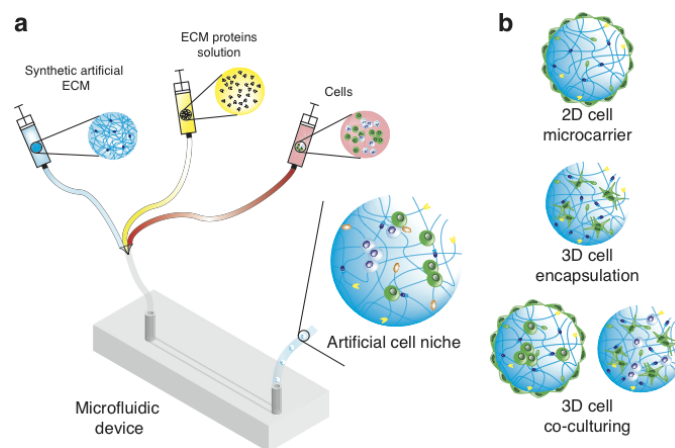
Figure 1.7 – Reconstruction of the stem cell niche by using the microgel-based technology. a, Stem cell niche reconstruction *in vitro* can be performed by using the droplet-based microfluidic technology:

each gel building block, such as an artificial ECM, bioactive proteins and multiple cell types, can be manipulated within a microfluidic device, resulting in the formation of a microgel that acts as an artificial stem cell niche. **b,** Microgel-based technology has been used for the generation of bioactive 2D microcarriers to expand stem cells, as well as producing 3D matrixes for cell encapsulation. Moreover, microgels can be adopted for co-culturing different cell types, generating various type of 3D cell co-culturing models.

Microgels, used as microcarriers, combined with bioreactor technologies have been a valuable alternative for large-scale cell production in suspension under more specific conditions, such as enhanced exposure to oxygen and nutrients, and have the potential to employ stem cells for therapeutic purposes.[90-92] Microcarriers generated with different shapes from various materials, such as polystyrene, glass, cellulose, alginate or dextran, have been classically used in biotechnology industry to grow adherent cell populations for large-scale production of proteins or viruses.[93,94] Microgels were successfully implemented for the expansion and differentiation of several types of stem cells, including mouse and human embryonic stem cells [95-100], human mesenchymal stem cells [101-103] and pancreatic progenitor cells.[104] Even so, conventional microgels are limited in the extent to which they can mimic key aspects of physiological stem cell niches. PEG-based microgels were microfluidically generated with an imbalanced stoichiometric ratio of reactive groups, which enabled a versatile chemical functionalization to tailor the microcarrier physicochemical properties to a specific cell type and cell function (Figure 1.8 a,b).[87]

Microgel-based technology also offers the unique opportunity to compartmentalize cells into monodisperse and physico-chemically defined matrices, which allows accurate and controlled investigation of cell behavior in response to the microenvironment. Controlling and modulating the mechanical and biochemical gel properties is of the utmost importance to create reliable and biologically faithful *in vitro* 3D platforms to study cell behavior. To this end, many types of synthetic and natural hydrogels have been specifically selected for use based on their different properties. For instance, PEG [105,106], polyglycerol [107,108] and self-assembling peptides (SAP) [109] have been used in combination with microfluidics to encapsulate cells into microcapsules with modular biophysical and biochemical properties (Figure 1.8 c).

Another valuable alternative to synthetic hydrogels are natural biopolymers that provide superior cell binding and biodegradability. Collagen [110,111], agarose [86,112], alginate [113] and hyaluronic acid [114] microgels have been successfully adopted for generating 3D cell microniches (Figure 1.8 d). Droplet-based microfluidic technology was also elegantly applied to develop a reliable in vitro 3D cell co-culture models.[112,115] Kumacheva's group showed that microfluidics could be applied to modulate the ratio between the concentrations of two cell types within a microgel, by simply playing with the flow rate ratio between two cell streams. Encapsulation of differently labeled mouse embryonic stem cells within agarose microgels resulted into a reliable 3D cell co-culture model (Figure 1.8 e). Flow cytometry analysis was then carried out to confirm the presence of different cell concentration ratios within the microgels (Figure 1.8f), as well as to study the proliferation and survival of co-cultured cell populations. Another interesting approach to build 3D cell co-culture models was developed by Sakai and colleagues who microfluidically generated cell-laden unmodified microgels to fabricate artificial tissue constructs by co-culturing another cell type on gelatin-enclosing microgels (Figure 1.8g).[115]

The ease in manipulation and high-throughput generation through droplet-based microfluidics make the microgels ideal candidates for investigating the enormous diversity of stem cell microenvironments. Combining the microgel-based technology with high-throughput analysis techniques, either *off chip* or integrated *on chip*, would have a large and significant impact on the approach to screenings. For instance, Mazutis and colleagues presented a powerful droplet-based antibody detection screening method by integrating microfluidic cell encapsulation with droplet sorting *on chip* (Figure 1.6a). Antibody-secreting cells were first encapsulated with detection antibodies, and streptavidin beads coated with capture antibody, which permitted a sandwich assay to be performed. Then, microdroplets were re-injected into a second microfluidic device containing a fluorescence-activated droplet sorter. Only the microbeads in which cell-secreted antibodies were captured on the streptavidin beads became fluorescent and, therefore, were sorted. The authors showed a very high droplet-sorting efficiency, which was demonstrated by the high percentage of fluorescent-containing cell droplets compared to the non-sorted condition.[78] *On chip*-integrated fluorescent detection was also used to screen enzymatic reactions [116] and molecule cytotoxicity [83,89] in droplets.

Microgels were also successfully interfaced with high-throughput approaches *off chip* by Kumacheva's group, who analyzed cell-laden microgels through flow cytometry to efficiently investigate biological processes.[112] Recently, Huck and colleagues reliably generated and performed flow cytometry analysis on monodisperse w/o/w double emulsion droplet bearing different concentrations of a fluorescent marker.[117]

Although more technological optimization is required, these examples interestingly show the great potential of microgel-based technology when integrated with high-throughput analysis methods, such as flow cytometry, for screening different cell types, as well as biochemical reactions in beads, with a strong influence on cell biology. Overall, we can envision that combinatorial microgel generation integrated with flow or mass cytometry analysis will significantly impact basic and applied stem cell biology.
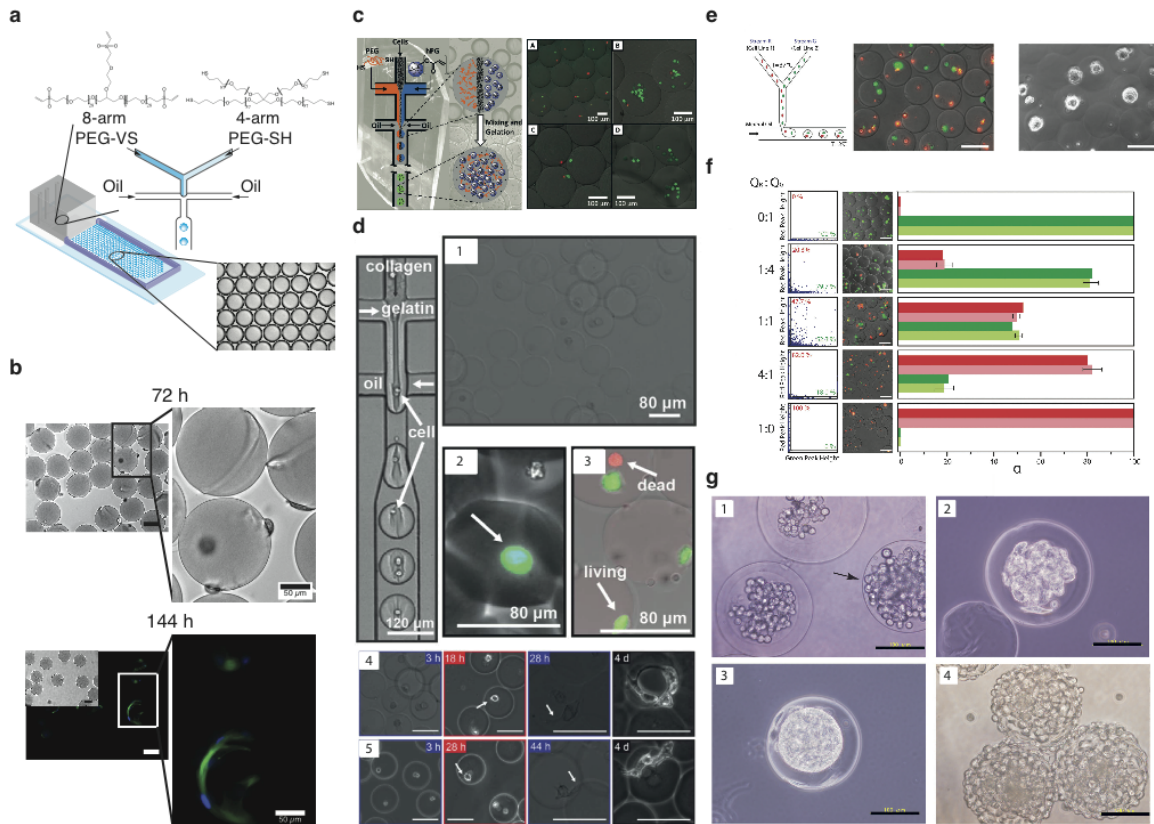
Figure 1.8 – Microgel-based technology for generation of microbeads for stem cell technology. a, Schematic displaying the microfluidic chip used for the generation of engineered poly(ethylene glycol)-based microgels: the two PEG macromer precursors are injected into the microfluidic channels, and they lead to the formation of microgels bearing a molar excess of one of the two reactive groups, either vinyl sulfone (VS-) or thiols (SH-). **b**, Human mesenchymal stem cell adhesion and growth on cell-type specific PEG microgels in bioreactor culture, after 72 and 144 hours: stem cells were expanded on microgels functionalized with fibronectin via affinity binding scheme (first functionalization step with maleimide-activated ProteinA and second functionalization step with biotin-activated fibronectin). Actin filaments were stained with green phalloidin and nuclei with DAPI. Adapted from Ref. [87] with permission of American Chemical Society. **c**, Schematic of the flow focusing microfluidic device used for the generation of microgels by co-polymerization of hyperbranched polyglycerol and polyethylene glycol. The platform was used to successfully encapsulate lymphoblasts and fibroblasts. Adapted from Ref. [107] with permission of American Chemical Society. **d**, Microfluidic encapsulation of cells into collagen-gelatin microbeads with different elasticities and biodegradability. Micrographs show cell-laden microbeads, and the arrows indicate live and dead fibroblasts. Authors show fibroblasts encapsulated for up to 4 days in microbeads with different gelatin concentration and degree of cross-linking. Adapted from Ref. [110] with permission of Royal Society of Chemistry. **e**, Schematic of the T-junction design used to co-encapsulate multiple cell types into agarose microgels: changing the flow rates of the two streams resulted into microbeads bearing different concentration ratios of the two encapsulated cell types. The micrographs show encapsulated mouse embryonic stem cells, stained with two different color trackers. **f**, Flow cytometry analysis was performed on microgels to show different concentration ratios of the two cell types at different flow rate ratios. Adapted from Ref. [112] with permission of Royal Society of Chemistry. **g**, Micrographs of rat adipose-derived cells encapsulated in unmodified gelatin microbeads, after encapsulation (1) and after 4 days (2). Co-culturing of L929 cells on cell-enclosing gelatin microbeads after 1 day (3) and 4 days (4). Adapted from Ref. [115] with permission of American Institute of Physics.

37

References

1   Deasy, B. M., Yong, L. I. & Huard, J. Tissue engineering with muscle-derived stem cells. *Curr Opin Biotech* **15**, 419-423 (2004).

2   Passier, R., van Laake, L. W. & Mummery, C. L. Stem-cell-based therapy and lessons from the heart. *Nature* **453**, 322-329 (2008).

3   Daley, G. Q. & Scadden, D. T. Prospects for stem cell-based therapy. *Cell* **132**, 544-548 (2008).

4   Wagers, A. J. The Stem Cell Niche in Regenerative Medicine. *Cell Stem Cell* **10**, 362-369 (2012).

5   Scadden, D. T. The stem-cell niche as an entity of action. *Nature* **441**, 1075-1079 (2006).

6   Lutolf, M. P. & Blau, H. M. Artificial Stem Cell Niches. *Adv Mater* **21**, 3255-3268 (2009).

7   Lane, S. W., Williams, D. A. & Watt, F. M. Modulating the stem cell niche for tissue regeneration. *Nature biotechnology* **32**, 795-803 (2014).

8   Schofield, R. The relationship between the spleen colony-forming cell and the haemopoietic stem cell. *Blood cells* **4**, 7-25 (1978).

9   Kai, T. S. & Spradling, A. An empty Drosophila stem cell niche reactivates the proliferation of ectopic cells. *P Natl Acad Sci USA* **100**, 4633-4638 (2003).

10   Fuller, M. T. & Spradling, A. C. Male and female Drosophila germline stem cells: Two versions of immortality. *Science* **316**, 402-404 (2007).

11   Calvi, L. M. *et al.* Osteoblastic cells regulate the haematopoietic stem cell niche. *Nature* **425**, 841-846 (2003).

12   Ehninger, A. & Trumpp, A. The bone marrow stem cell niche grows up: mesenchymal stem cells and macrophages move in. *J Exp Med* **208**, 421-428 (2011).

13   Mendelson, A. & Frenette, P. S. Hematopoietic stem cell niche maintenance during homeostasis and regeneration. *Nat Med* **20**, 833-846 (2014).

14   Clevers, H. Stem Cells a Unifying Theory for the Crypt. *Nature* **495**, 53-54 (2013).

15   Barker, N. Adult intestinal stem cells: critical drivers of epithelial homeostasis and regeneration. *Nat Rev Mol Cell Bio* **15**, 19-33 (2014).

16   Crosnier, C., Stamataki, D. & Lewis, J. Organizing cell renewal in the intestine: stem cells, signals and combinatorial control. *Nat Rev Genet* **7**, 349-359 (2006).

17   Conover, J. C. & Notti, R. Q. The neural stem cell niche. *Cell Tissue Res* **331**, 211-224 (2008).

18   Gilbertson, R. J. & Rich, J. N. Making a tumour's bed: glioblastoma stem cells and the vascular niche. *Nat Rev Cancer* **7**, 733-736 (2007).

19   Fuchs, E. Finding One's Niche in the Skin. *Cell Stem Cell* **4**, 499-502 (2009).

20   Mazhari, R. & Hare, J. M. Mechanisms of action of mesenchymal stem cells in cardiac repair: potential influences on the cardiac stem cell niche. *Nature clinical practice. Cardiovascular medicine* **4 Suppl 1**, S21-26 (2007).

21   Collins, C. A. *et al.* Stem cell function, self-renewal, and behavioral heterogeneity of cells from the adult muscle satellite cell niche. *Cell* **122**, 289-301 (2005).

22   Gilbert, P. M. *et al.* Substrate elasticity regulates skeletal muscle stem cell self-renewal in culture. *Science* **329**, 1078-1081 (2010).

23   Kunisaki, Y. *et al.* Arteriolar niches maintain haematopoietic stem cell quiescence. *Nature* **502**, 637-+ (2013).

24   Lo Celso, C. *et al.* Live-animal tracking of individual haematopoietic stem/progenitor cells in their niche. *Nature* **457**, 92-U96 (2009).

25   Fujisaki, J. *et al.* In vivo imaging of T-reg cells providing immune privilege to the haematopoietic stem-cell niche. *Nature* **474**, 216-U256 (2011).

26   Sato, T. *et al.* Paneth cells constitute the niche for Lgr5 stem cells in intestinal crypts. *Nature* **469**, 415-+ (2011).

27   Ambler, C. A. & Watt, F. M. Adult epidermal Notch activity induces dermal accumulation of T cells and neural crest derivatives through upregulation of jagged 1. *Development* **137**, 3569-3579 (2010).

28   Butler, J. M. *et al.* Endothelial Cells Are Essential for the Self-Renewal and Repopulation of Notch-Dependent Hematopoietic Stem Cells. *Cell Stem Cell* **6**, 251-264 (2010).

29   Lutolf, M. P. & Hubbell, J. A. Synthetic biomaterials as instructive extracellular microenvironments for morphogenesis in tissue engineering. *Nature biotechnology* **23**, 47-55 (2005).

30   Burdick, J. A. & Vunjak-Novakovic, G. Engineered Microenvironments for Controlled Stem Cell Differentiation. *Tissue Eng Pt A* **15**, 205-219 (2009).

31   Engler, A. J., Sen, S., Sweeney, H. L. & Discher, D. E. Matrix elasticity directs stem cell lineage specification. *Cell* **126**, 677-689 (2006).

32   Chaudhuri, O. *et al.* Extracellular matrix stiffness and composition jointly regulate the induction of malignant phenotypes in mammary epithelium. *Nat Mater* **13**, 970-978 (2014).

33   Kilian, K. A., Bugarija, B., Lahn, B. T. & Mrksich, M. Geometric cues for directing the differentiation of mesenchymal stem cells. *P Natl Acad Sci USA* **107**, 4872-4877 (2010).

34   McBeath, R., Pirone, D. M., Nelson, C. M., Bhadriraju, K. & Chen, C. S. Cell shape, cytoskeletal tension, and RhoA regulate stem cell lineage commitment. *Dev Cell* **6**, 483-495 (2004).

35   Connelly, J. T. *et al.* Actin and serum response factor transduce physical cues from the microenvironment to regulate epidermal stem cell fate decisions. *Nature cell biology* **12**, 711-718 (2010).

36   Wen, J. H. *et al.* Interplay of matrix stiffness and protein tethering in stem cell differentiation. *Nat Mater* **13**, 979-987 (2014).

37   Trappmann, B. *et al.* Extracellular-matrix tethering regulates stem-cell fate. *Nat Mater* **11**, 642-649 (2012).

38   Kimura, W. & Sadek, H. A. The cardiac hypoxic niche: emerging role of hypoxic microenvironment in cardiac progenitors. *Cardiovascular diagnosis and therapy* **2**, 278-289 (2012).

39   North, T. E. *et al.* Hematopoietic Stem Cell Development Is Dependent on Blood Flow. *Cell* **137**, 736-748 (2009).

40   Zouani, O. F., Kalisky, J., Ibarboure, E. & Durrieu, M. C. Effect of BMP-2 from matrices of different stiffnesses for the modulation of stem cell fate. *Biomaterials* **34**, 2157-2166 (2013).

41   Kuhl, P. R. & GriffithCima, L. G. Tethered epidermal growth factor as a paradigm for growth factor-induced stimulation from the solid phase. *Nat Med* **2**, 1022-1027 (1996).

42   Watt, F. M. & Huck, W. T. S. Role of the extracellular matrix in regulating stem cell fate. *Nat Rev Mol Cell Bio* **14**, 467-473 (2013).

43   Crouzier, T., Fourel, L., Boudou, T., Albiges-Rizo, C. & Picart, C. Presentation of BMP-2 from a Soft Biopolymeric Film Unveils its Activity on Cell Adhesion and Migration. *Adv Mater* **23**, H111-H118 (2011).

44   Chen, T. T. *et al.* Anchorage of VEGF to the extracellular matrix conveys differential signaling responses to endothelial cells. *J Cell Biol* **188**, 595-609 (2010).

45   Cosson, S., Allazetta, S. & Lutolf, M. P. Patterning of cell-instructive hydrogels by hydrodynamic flow focusing. *Lab Chip* **13**, 2099-2105 (2013).

46   Keenan, T. M. & Folch, A. Biomolecular gradients in cell culture systems. *Lab Chip* **8**, 34-57 (2008).

47   Gurdon, J. B. & Bourillot, P. Y. Morphogen gradient interpretation. *Nature* **413**, 797-803 (2001).

48   Scully, K. M. & Rosenfeld, M. G. Development - Pituitary development: Regulatory codes in mammalian organogenesis. *Science* **295**, 2231-2235 (2002).

49   Xu, P. F., Houssin, N., Ferri-Lagneau, K. F., Thisse, B. & Thisse, C. Construction of a Vertebrate Embryo from Two Opposing Morphogen Gradients. *Science* **344**, 87-89 (2014).

50   Lutolf, M. P. Spotlight on hydrogels. *Nat Mater* **8**, 451-453 (2009).

51   Elisseeff, J. Hydrogels - Structure starts to gel. *Nat Mater* **7**, 271-273 (2008).

52   DeForest, C. A. & Anseth, K. S. Advances in Bioactive Hydrogels to Probe and Direct Cell Fate. *Annu Rev Chem Biomol* **3**, 421-444 (2012).

53   Tibbitt, M. W. & Anseth, K. S. Hydrogels as Extracellular Matrix Mimics for 3D Cell Culture. *Biotechnol Bioeng* **103**, 655-663 (2009).

54   Seliktar, D. Designing Cell-Compatible Hydrogels for Biomedical Applications. *Science* **336**, 1124-1128 (2012).

55   Lutolf, M. P. & Hubbell, J. A. Synthesis and physicochemical characterization of end-linked poly(ethylene glycol)-co-peptide hydrogels formed by Michael-type addition. *Biomacromolecules* **4**, 713-722 (2003).

56   Ehrbar, M. *et al.* Enzymatic formation of modular cell-instructive fibrin analogs for tissue engineering. *Biomaterials* **28**, 3856-3866 (2007).

57   Ehrbar, M. *et al.* Biomolecular hydrogels formed and degraded via site-specific enzymatic reactions. *Biomacromolecules* **8**, 3000-3007 (2007).

58   Lutolf, M. P., Gilbert, P. M. & Blau, H. M. Designing materials to direct stem-cell fate. *Nature* **462**, 433-441 (2009).

59   Rosenfeld, S. J., Kimball, J., Vining, D. & Young, N. S. Intensive Immunosuppression with Antithymocyte Globulin and Cyclosporine as Treatment for Severe Acquired Aplastic-Anemia. *Blood* **85**, 3058-3065 (1995).

60   Wieman, T. J., Smiell, J. M. & Su, Y. C. Efficacy and safety of a topical gel formulation of recombinant human platelet-derived growth factor-BB (becaplermin) in patients with chronic neuropathic diabetic ulcers - A phase III randomized placebo-controlled double-blind study. *Diabetes Care* **21**, 822-827 (1998).

61   Cimetta, E. & Vunjak-Novakovic, G. Microscale technologies for regulating human stem cell differentiation. *Exp Biol Med* **239**, 1255-1263 (2014).

62   Flaim, C. J., Chien, S. & Bhatia, S. N. An extracellular matrix microarray for probing cellular differentiation. *Nat Methods* **2**, 119-125 (2005).

63   Gobaa, S. *et al.* Artificial niche microarrays for probing single stem cell fate in high throughput. *Nat Methods* **8**, 949-955 (2011).

64   Gupta, N. *et al.* A versatile approach to high-throughput microarrays using thiol-ene chemistry. *Nat Chem* **2**, 138-145 (2010).

65   Maerkl, S. J. Integration column: Microfluidic high-throughput screening. *Integr Biol* **1**, 19-29 (2009).

66   Jeon, N. L. *et al.* Generation of solution and surface gradients using microfluidic systems. *Langmuir* **16**, 8311-8316 (2000).

67   Georgescu, W. *et al.* Model-controlled hydrodynamic focusing to generate multiple overlapping gradients of surface-immobilized proteins in microfluidic devices. *Lab Chip* **8**, 238-244 (2008).

68   Lucchetta, E. M., Lee, J. H., Fu, L. A., Patel, N. H. & Ismagilov, R. F. Dynamics of Drosophila embryonic patterning network perturbed in space and time using microfluidics. *Nature* **434**, 1134-1138 (2005).

69   Carrion, B. *et al.* Recreating the Perivascular Niche Ex Vivo Using a Microfluidic Approach. *Biotechnol Bioeng* **107**, 1020-1028 (2010).

70   Huh, D. *et al.* Reconstituting organ-level lung functions on a chip. *Science* **328**, 1662-1668 (2010).

71   Kim, H. J. & Ingber, D. E. Gut-on-a-Chip microenvironment induces human intestinal cells to undergo villus differentiation. *Integrative biology : quantitative biosciences from nano to macro* **5**, 1130-1140 (2013).

72   Khetani, S. R. & Bhatia, S. N. Microscale culture of human liver cells for drug development. *Nature biotechnology* **26**, 120-126 (2008).

73   Seemann, R., Brinkmann, M., Pfohl, T. & Herminghaus, S. Droplet based microfluidics. *Rep Prog Phys* **75**, 016601 (2012).

74   Solvas, X. C. I. & deMello, A. Droplet microfluidics: recent developments and future applications. *Chem Commun* **47**, 1936-1942 (2011).

75   Yobas, L., Martens, S., Ong, W. L. & Ranganathan, N. High-performance flow-focusing geometry for spontaneous generation of monodispersed droplets. *Lab Chip* **6**, 1073-1079 (2006).

76   Weibel, D. B. & Whitesides, G. M. Applications of microfluidics in chemical biology. *Curr Opin Chem Biol* **10**, 584-591 (2006).

77   Niu, X. Z., Gielen, F., Edel, J. B. & deMello, A. J. A microdroplet dilutor for high-throughput screening. *Nat Chem* **3**, 437-442 (2011).

78   Mazutis, L. *et al.* Single-cell analysis and sorting using droplet-based microfluidics. *Nat Protoc* **8**, 870-891 (2013).

79   Li, L. *et al.* Nanoliter microfluidic hybrid method for simultaneous screening and optimization validated with crystallization of membrane proteins. *P Natl Acad Sci USA* **103**, 19243-19248 (2006).

80   Lau, B. T. C., Baitz, C. A., Dong, X. P. & Hansen, C. L. A complete microfluidic screening platform for rational protein crystallization. *J Am Chem Soc* **129**, 454-455 (2007).

81   Suzuki, D., Sakai, T. & Yoshida, R. Self-flocculating/Self-dispersing oscillation of microgels. *Angew Chem Int Edit* **47**, 917-920 (2008).

82   Chabert, M. & Viovy, J. L. Microfluidic high-throughput encapsulation and hydrodynamic self-sorting of single cells. *P Natl Acad Sci USA* **105**, 3191-3196 (2008).

83   Brouzes, E. *et al.* Droplet microfluidic technology for single-cell high-throughput screening. *P Natl Acad Sci USA* **106**, 14195-14200 (2009).

84   Clausell-Tormos, J. *et al.* Droplet-based microfluidic platforms for the encapsulation and screening of mammalian cells and multicellular organisms (vol 15, pg 427, 2008). *Chem Biol* **15**, 875-875 (2008).

85   Xu, S. *et al.* Generation of monodisperse particles by using microfluidics: Control over size, shape, and composition (vol 44, pg 724, 2005). *Angew Chem Int Edit* **44**, 3799-3799, doi:Doi 10.1002/Anie.200462226 (2005).

86   Kumachev, A. *et al.* High-throughput generation of hydrogel microbeads with varying elasticity for cell encapsulation. *Biomaterials* **32**, 1477-1483 (2011).

87   Allazetta, S., Hausherr, T. C. & Lutolf, M. P. Microfluidic Synthesis of Cell-Type-Specific Artificial Extracellular Matrix Hydrogels. *Biomacromolecules* **14**, 1122-1131 (2013).

88   Burns, J. R. & Ramshaw, C. The intensification of rapid reactions in multiphase systems using slug flow in capillaries. *Lab Chip* **1**, 10-15 (2001).

89   Cho, S. *et al.* Droplet-Based Microfluidic Platform for High-Throughput, Multi-Parameter Screening of Photosensitizer Activity. *Anal Chem* **85**, 8866-8872 (2013).

90   Serra, M. *et al.* Process engineering of human embryonic stem cells for clinical application. *Hum Gene Ther* **22**, A56-A56 (2011).

91   Chu, L. & Robinson, D. K. Industrial choices for protein production by large-scale cell culture. *Curr Opin Biotech* **12**, 180-187 (2001).

92   King, J. A. & Miller, W. M. Bioreactor development for stem cell expansion and controlled differentiation. *Curr Opin Chem Biol* **11**, 394-398 (2007).

93   Vanwezel, A. L. Growth of Cell-Strains and Primary Cells on Micro-Carriers in Homogeneous Culture. *Nature* **216**, 64-& (1967).

94   Alfred, R. *et al.* Efficient Suspension Bioreactor Expansion of Murine Embryonic Stem Cells on Microcarriers in Serum-Free Medium. *Biotechnol Progr* **27**, 811-823 (2011).

95   Fok, E. Y. L. & Zandstra, P. W. Shear-controlled single-step mouse embryonic stem cell expansion and embryoid body-based differentiation. *Stem Cells* **23**, 1333-1342 (2005).

96   Abranches, E., Bekman, E., Henrique, D. & Cabral, J. M. S. Expansion of mouse embryonic stem cells on microcarriers. *Biotechnol Bioeng* **96**, 1211-1221 (2007).

97   Fernandes, A. M. *et al.* Mouse embryonic stem cell expansion in a microcarrier-based stirred culture system. *J Biotechnol* **132**, 227-236, doi:Doi 10.1016/J.Jbiotec.2007.05.031 (2007).

98   Oh, S. K. W. *et al.* Long-term microcarrier suspension cultures of human embryonic stem cells. *Stem Cell Res* **2**, 219-230 (2009).

99   Chen, A. K. L., Chen, X. L., Choo, A. B. H., Reuveny, S. & Oh, S. K. W. Critical microcarrier properties affecting the expansion of undifferentiated human embryonic stem cells. *Stem Cell Res* **7**, 97-111 (2011).

100   Nie, Y., Bergendahl, V., Hei, D. J., Jones, J. M. & Palecek, S. P. Scalable Culture and Cryopreservation of Human Embryonic Stem Cells on Microcarriers. *Biotechnol Progr* **25**, 20-31 (2009).

101   Eibes, G. *et al.* Maximizing the ex vivo expansion of human mesenchymal stem cells using a microcarrier-based stirred culture system. *J Biotechnol* **146**, 194-197 (2010).

102   Yang, Y., Rossi, F. M. V. & Putnins, E. E. Ex vivo expansion of rat bone marrow mesenchymal stromal cells on microcarrier beads in spin culture. *Biomaterials* **28**, 3110-3120 (2007).

103   Schop, D. *et al.* Expansion of human mesenchymal stromal cells on microcarriers: growth and metabolism. *J Tissue Eng Regen M* **4**, 131-140 (2010).

104   Serra, M. *et al.* Stirred bioreactors for the expansion of adult pancreatic stem cells. *Ann Anat* **191**, 104-115 (2009).

105   Li, C. Y., Wood, D. K., Huang, J. H. & Bhatia, S. N. Flow-based pipeline for systematic modulation and analysis of 3D tumor microenvironments. *Lab Chip* **13**, 1969-1978 (2013).

106   Headen, D. M., Aubry, G., Lu, H. & Garcia, A. J. Microfluidic-based generation of size-controlled, biofunctionalized synthetic polymer microgels for cell encapsulation. *Adv Mater* **26**, 3003-3008 (2014).

107   Rossow, T. *et al.* Controlled Synthesis of Cell-Laden Microgels by Radical-Free Gelation in Droplet Microfluidics. *J Am Chem Soc* **134**, 4983-4989 (2012).

108   Steinhilber, D. *et al.* Hyperbranched polyglycerols on the nanometer and micrometer scale. *Biomaterials* **32**, 1311-1316 (2011).

109   Tsuda, Y., Morimoto, Y. & Takeuchi, S. Monodisperse Cell-Encapsulating Peptide Microgel Beads for 3D Cell Culture. *Langmuir* **26**, 2645-2649 (2010).

110   Ma, S. H. *et al.* Monodisperse collagen-gelatin beads as potential platforms for 3D cell culturing. *J Mater Chem B* **1**, 5128-5136 (2013).

111   Matsunaga, Y. T., Morimoto, Y. & Takeuchi, S. Molding Cell Beads for Rapid Construction of Macroscopic 3D Tissue Architecture. *Adv Mater* **23**, H90-H94 (2011).

112   Tumarkin, E. *et al.* High-throughput combinatorial cell co-culture using microfluidics. *Integr Biol* **3**, 653-662 (2011).

113   Morimoto, Y., Tan, W. H., Tsuda, Y. & Takeuchi, S. Monodisperse semi-permeable microcapsules for continuous observation of cells. *Lab Chip* **9**, 2217-2223 (2009).

114   Jia, X. Q. *et al.* Hyaluronic acid-based microgels and microgel networks for vocal fold regeneration. *Biomacromolecules* **7**, 3336-3344 (2006).

115   Sakai, S. *et al.* Cell-enclosing gelatin-based microcapsule production for tissue engineering using a microfluidic flow-focusing system. *Biomicrofluidics* **5** (2011).

116   Chang, C. *et al.* Droplet-based microfluidic platform for heterogeneous enzymatic assays. *Lab Chip* **13**, 1817-1822 (2013).

117   Yan, J. *et al.* Monodisperse Water-in-Oil-in-Water (W/O/W) Double Emulsion Droplets as Uniform Compartments for High-Throughput Analysis via Flow Cytometry. *Micromachines-Basel* **4**, 402-413 (2013).

Chapter 2

Programmable Microfluidic Patterning of

Protein Gradients on Hydrogels
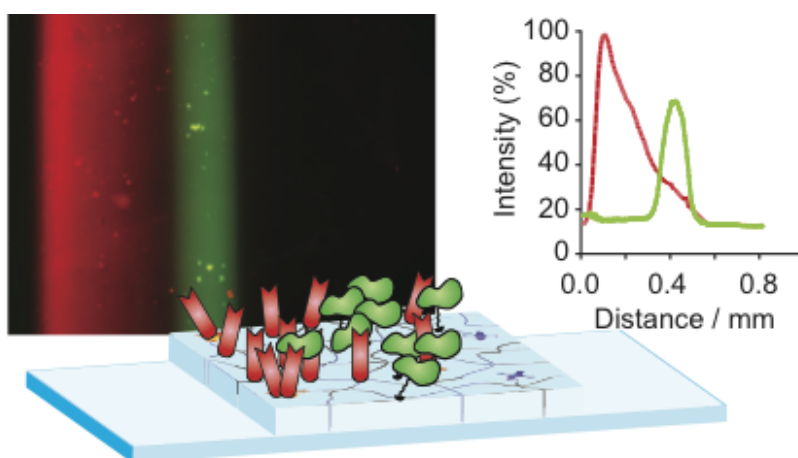
Programmable Microfluidic Patterning of Protein Gradients on Hydrogels[1]

Simone Allazetta, Steffen Cosson and Matthias P. Lutolf

Computer-controlled hydrodynamic flow focusing was utilized to generate tethered protein gradients of any user-defined shape on the surface of soft synthetic hydrogels.

Introduction

Graded signaling cues govern cell behavior in many essential biological processes.[1] Cells of a developing embryo, for example, interpret the concentration-dependent signaling information of proteins termed "morphogens" to generate the precise patterns of specialized cell types that ultimately make up a functional tissue. The importance of biomolecule gradients in biology has spurred the intense development and application of *in vitro* model systems conceived to replicate the temporally and spatially controlled display of signals just like in an *in vivo* context. Traditionally, the focus has been on reproducing gradients of soluble signals such as chemokines by using, for instance, macroscopic chambers or micropipette-based approaches.[2] However, the lack of precise gradient control in these set-ups has stimulated the development of microfluidic approaches to generate gradients of tiny amounts of soluble or surface-absorbed biomolecules with excellent spatial resolution and even temporally changing characteristics.[3] Microfluidic gradients thus allow to approach the spatiotemporal complexity of graded signaling microenvironments found in vivo, but the type of substrate on which they are commonly generated is far from physiological. Since it is increasingly appreciated that cells are sensitive to the biophysical characteristics of their substrate,[4] the mere use of rigid (for instance glass or plastic) cell culture dishes could compromise the validity of an experiment. Therefore, there is an unmet need for in vitro gradient model systems that are built on materials mimicking the biophysical characteristics of the natural, soft and hydrated extracellular milieu.[5-7]

To address this technology gap, we have reported a microfluidic method to pattern protein gradients on biomimetic poly(ethylene) glycol (PEG)-based hydrogels.[8] This system proved useful to form tethered gradients of one or more (overlapping) proteins on gel surfaces, but gradient shapes were relatively poorly controlled and limited to simple linear gradients, while *in vivo* gradients can often have a very complex shapes.[1] Consequently, here we present a scheme to form, in an automated fashion, gel-immobilized protein patterns with virtually *any* type of shape.

Results and discussion

The generation of graded protein patterns on hydrogels was performed exploring the versatile concept of "hydrodynamic flow focusing".[9,10] A microfluidic poly (dimethylsiloxane) (PDMS) chip was fabricated consisting of a channel system with three inlets, each of which was independently controllable by a pump (Figure 2.1A). Software-controlled adjustment of the flow rates of the individual liquid streams thus should allow to dynamically control the position and width of the protein stream.[10]

To capture Biotin- or Fc-labeled biomolecules from solution by affinity we generated low-swelling PEG hydrogel substrates displaying covalently bound NeutrAvidin and/or ProteinA (Figure 2.1B). Michael-type addition was used to form polymer networks by stepwise copolymerization of vinyl sulfone (VS)-terminated 8arm-PEG macromers and thiol (SH)-terminated 4arm-PEG macromers at equimolar amounts of functional groups.[11] In the same reaction step, the gels were bioconjugated with NeutrAvidin and/or ProteinA using a heterofunctional NHS-PEG-maleimide linker. Thin hydrogel films (concentration: 5% w/v) were

cast on macroscopic glass slides that were modified with 3-mercaptopropyl-trimethoxylsilane to expose free thiol groups. The gel films were equilibrated in PBS overnight prior to protein patterning.
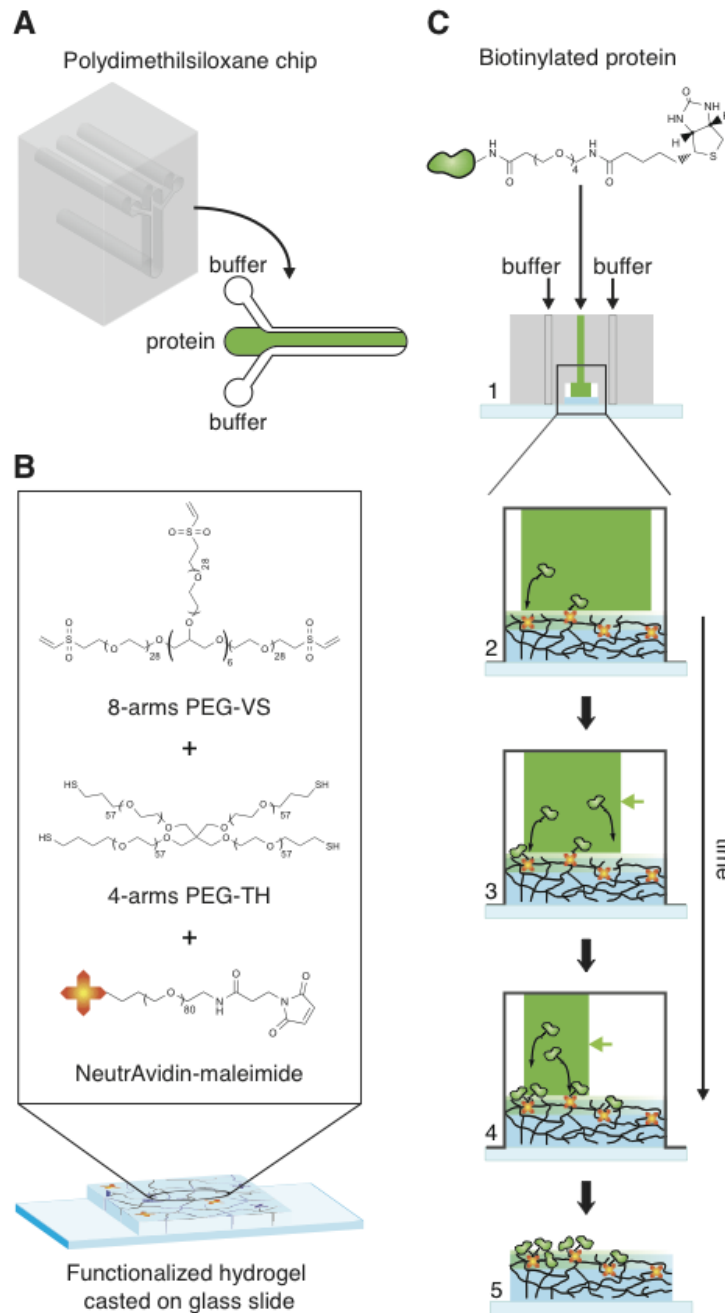
Figure 2.1 - Schematic representation of the microfluidic patterning of functionalized PEG hydrogels. **A** Microfluidic chip for hydrodynamic flow focusing. **B** Formation of NeutrAvidin-conjugated hydrogels from aqueous precursor solutions containing multi-arm PEG macromers and "PEGylated" NeutrAvidin. **C** Patterning of gels using hydrodynamic flow focusing. Step 1: the PDMS chip is pressed onto a glass slide bearing a thin hydrogel coating. Steps 2-4: gradient patterning by flow focusing. Step 5: the PDMS chips is removed for cell culture experiments.

To generate predictable gradients of various shapes by automated flow focusing, we first determined the capture kinetics of Biotin-tagged proteins on NeutrAvidin-modified PEG gels. Substrates were exposed for variable period of time to a constant, focused stream of fluorescein- and Biotin-labelled bovine serum albumin (FITC-BSA-Biotin) model protein. Fluorescence intensities were plotted as a function of the exposure time to obtain the capture kinetics at a particular flow rate, BSA and NeutrAvidin concentration (data not shown here). These curves served as a basis to generate a desired gradient type by step-wise flow focusing (Figure 2.2, left column): we first defined a gradient of interest by a mathematical equation of the intensity as a function of the discrete steps n (typically $n_{max}=10$) performed by the syringe pumps during gradient patterning. Utilizing the experimentally determined immobilization curves, the intensity value of each step was converted into a specific exposure time of the protein to the gel surface. Finally, the flow rates were calculated imposing a constant velocity of the protein stream form one step to the following one, allowing to program the syringe pumps for all the steps.

Graded protein patterns were generated by dynamic flow focusing and simultaneous protein capture from the central protein stream (Figure 2.1C). Starting from an almost completely filled channel (Figure 2.1C, step 1), the width of the protein stream was decreased in a step-wise fashion by increasing the buffer flow rates on one or both sides (Figure 2.1C, step 3 and 4). Finally, the PDMS chip was removed from the patterned gel for further cell culture experiments. (Figure 2.1C, step 5).

As instructive examples, we programmed the syringe pumps to obtain liner, exponential and Gaussian gradients (Figure 2.2a-c). Indeed, fluorescent microscopy and subsequent image analysis showed reproducible patterning for all three gradients along the entire length of the hydrogel (9 mm). Notably, we also overlapped two different protein gradients by sequential flow focusing on PEG gels functionalized with both NeutrAvidin and Protein A. An example of dual, overlapping gradient is shown in Figure 2.3.
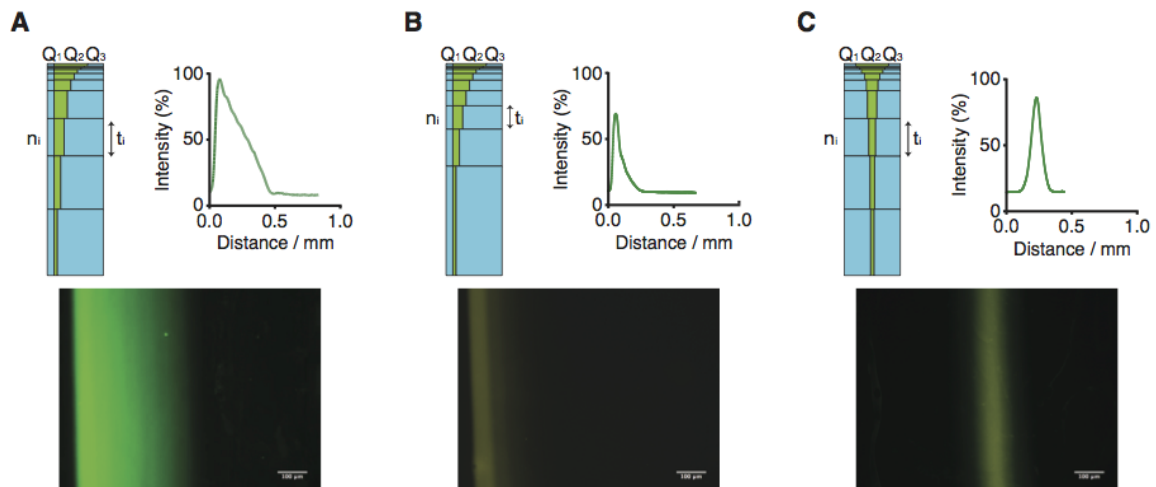
Figure 2.2 - Generation of three types of model gradients by hydrodynamic flow focusing of FITC-BSA-Biotin on NeutrAvidin-conjugated PEG gels. Fluorescent micrographs and graphical representations obtained by image analysis of a linear (**A**), exponential (**B**) and Gaussian (**C**) gradients (scale bar=100 μm). Schemes on the left of each gradient depict the step-wise flow focusing process with the two buffer streams (Q_1 and Q_3) flanking the protein stream Q_2. Flow rates were maintained constant for a time t_i for each step n_i.
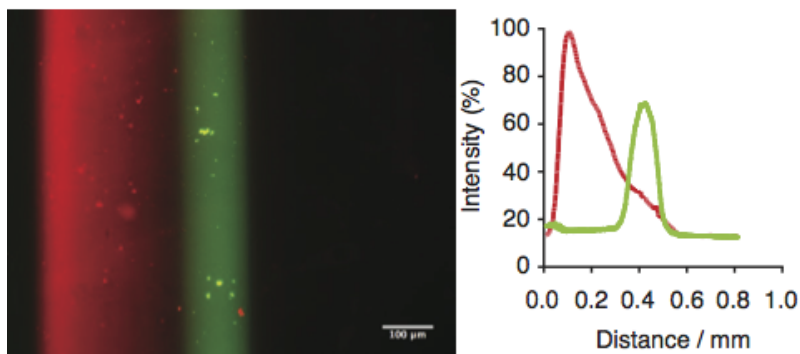
Figure 2.3 - Generation of gel-immobilized overlapping gradients by sequential hydrodynamic flow focusing. Fluorescence micrograph and measured fluorescence intensities showing a linear gradient of tethered DsRed-BSA-Biotin combined with a Gaussian gradient of FITC-labelled IgG. Scale bar = 100 μm.

Conclusions

In summary, here we demonstrated the generation of user-defined graded protein patterns on biofunctionalized hydrogels. Quantification of the capture kinetics of tagged biomolecules on these gels allows us to generate, by automated hydrodynamic flow focusing, nearly any type of protein profile with a simple microfluidic channel system. Indeed, the types of gradients and gradient combinations that can be generated are only limited by the imagination of the user. Since the microfluidic chip can be removed after patterning, the presented technique should be of interest for multiple cell-based assays.

References

1   Ashe, H. L. & Briscoe, J. The interpretation of morphogen gradients. *Development* **133**, 385-394 (2006).

2   Keenan, T. M. & Folch, A. Biomolecular gradients in cell culture systems. *Lab Chip* **8**, 34-57 (2008).

3   Velve-Casquillas, G., Le Berre, M., Piel, M. & Tran, P. T. Microfluidic tools for cell biological research. *Nano Today* **5**, 28-47 (2010).

4   Discher, D. E., Janmey, P. & Wang, Y. L. Tissue cells feel and respond to the stiffness of their substrate. *Science* **310**, 1139-1143 (2005).

5   Genzer, J. & Bhat, R. R. Surface-bound soft matter gradients. *Langmuir* **24**, 2294-2317 (2008).

6   Burdick, J. A., Khademhosseini, A. & Langer, R. Fabrication of gradient hydrogels using a microfluidics/photopolymerization process. *Langmuir* **20**, 5153-5156 (2004).

7   DeLong, S. A., Moon, J. J. & West, J. L. Covalently immobilized gradients of bFGF on hydrogel scaffolds for directed cell migration. *Biomaterials* **26**, 3227-3234 (2005).

8   Cosson, S., Kobel, S. A. & Lutolf, M. P. Capturing Complex Protein Gradients on Biomimetic Hydrogels for Cell-Based Assays. *Adv Funct Mater* **19**, 3411-3419 (2009).

9   Knight, J. B., Vishwanath, A., Brody, J. P. & Austin, R. H. Hydrodynamic focusing on a silicon chip: Mixing nanoliters in microseconds. *Phys Rev Lett* **80**, 3863-3866 (1998).

10   Georgescu, W. *et al.* Model-controlled hydrodynamic focusing to generate multiple overlapping gradients of surface-immobilized proteins in microfluidic devices. *Lab Chip* **8**, 238-244 (2008).

11   Lutolf, M. P. & Hubbell, J. A. Synthesis and physicochemical characterization of end-linked poly(ethylene glycol)-co-peptide hydrogels formed by Michael-type addition. *Biomacromolecules* **4**, 713-722 (2003).

Chapter 3

Patterning of Cell-instructive Hydrogel By Hydrodynamic Flow Focusing

Patterning of Cell-instructive Hydrogels by Hydrodynamic Flow Focusing[2]

Steffen Cosson[+], Simone Allazetta[+] and Matthias P. Lutolf

Microfluidic gradient systems offer a very precise means to probe the response of cells to graded biomolecular signals in vitro, for example to model how morphogen proteins affect cell fate during developmental processes. However, existing gradient makers are designed for non-physiological plastic or glass cell culture substrates that are often limited in maintaining the phenotype and function of difficult-to-culture mammalian cell types such as stem cells. To address this bottleneck, we combine hydrogel engineering and microfluidics to generate tethered protein gradients on the surface of biomimetic poly(ethylene glycol) (PEG) hydrogels. Here we used software-assisted hydrodynamic flow focusing for exposing and rapidly capturing tagged-proteins to gels in a step-wise fashion, resulting in immobilized gradients of virtually any desired shape and composition. To render our strategy amenable for high-throughput screening of multifactorial artificial cellular microenvironments, a dedicated microfluidic chip was devised for parallelization and multiplexing, yielding arrays of orthogonally overlapping gradients of up to 4x4 proteins. To illustrate the power of the platform for stem cell biology, we assessed how gradients of tethered leukemia inhibitory factor (LIF) influence embryonic stem cell (ESC) behavior. ESC responded to LIF gradients in binary manner, maintaining the pluripotency marker Rex1/Zfp42 and forming self-renewing colonies above a threshold concentration of 85 ng cm^{-2}. Our concept should be broadly applicable to probe how complex signaling microenvironments influence stem cell fate in culture.
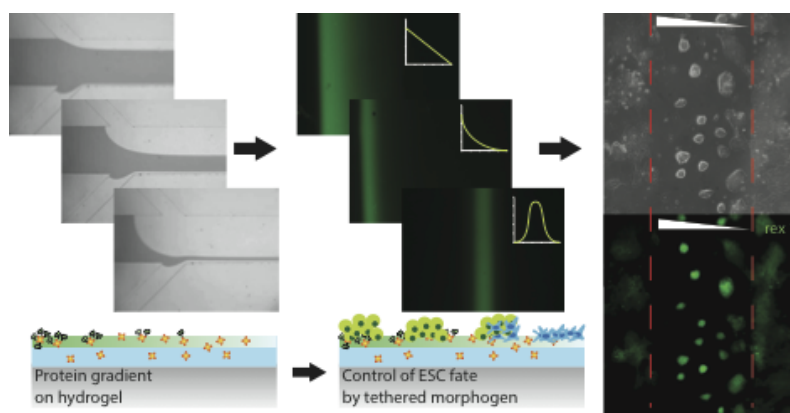
Introduction

Protein-mediated signaling is of upmost importance in governing cellular behavior, for example in the patterning of the developing embryo by morphogen proteins,[1] such as Activin and Nodal directing left/right asymmetry,[2] or the differentiation into mesodermal/endodermal lineages.[3] Notably, morphogens are often displayed in a combinatorial and graded fashion,[4] and they are frequently tethered to the extracellular matrix (ECM).[5]

Microtechnologies offer unprecedented means to generate precise gradients of soluble and surface-tethered biomolecules, opening up exciting applications in (stem) cell biology.[6-8] For instance, microfluidic systems have been used to establish cytokine gradients to control human neural progenitor cell differentiation,[9] or to investigate the role of autocrine and paracrine signaling in regulating ESC self-renewal.[10]

However, despite these exciting early examples, microfluidic gradient systems have not been widely used to address pertinent questions in stem cell biology. We postulate that this is due to some shortcomings of microfluidic cell culture platforms: First, these systems are built on non-physiological plastic or glass cell culture substrates that may negatively impact cell fate. Secondly, microfluidic systems are not well suited for long-term stem cell culture due to the limited space available for cell growth and the difficulties to manipulate cells in microchannels.[11-13] Thirdly, the continuous perfusion of microfluidic systems may expose cultured cells to aberrant shear stresses.[11] Finally, microfluid gradient sytems may have a relatively limited throughput compared to other approaches, such as protein microarrays used for cell phenotypic screenings.[14,15]

To address these issues, we have been developing microfluidic approaches to pattern gradients on the surface of soft and biomimetic PEG hydrogels.[16,17] We recently reported proof-of-principle experiments on the protein gradient patterning of gels using software-controlled hydrodynamic flow focusing (HFF).[17] Here we aimed at fully characterizing this versatile method, as well as expanding its usefulness towards high-throughput screening experiments. We performed a parametric analysis of the effect of several HFF parameters and hydrogel properties, generating high-resolution protein gradients of virtually any shape. Furthermore, we designed a microfluidic device to parallelize gradient pattering, producing arrays of overlapping gradients as a mean to rationally screen stem cell culture microenvironments. Finally, we validated this system by probing the effect of tethered LIF gradients on the behavior of mouse ESC, identifying a threshold concentration of immobilized LIF that is necessary for the maintenance of pluripotency on soft hydrogel substrates.

Results and discussion

Engineering hydrogel substrates for protein capture

Our method of gradient making by HFF relies on a succession of discrete patterning steps where, for a given flow rate, the duration of each step is predetermined by the immobilization kinetics of a tagged protein on the PEG gel substrate (Figure 3.1). Consequently, we first determined the binding kinetics of the two fluorescent model proteins FITC-BSA-biotin and Alexa488-hIgG. To this end, thin NeutrAvidin- or ProteinA-functionalized hydrogels (Figure 3.1a) were exposed for

variable durations to a focused protein stream (Figure 3.1b). Identical assay were performed for three different flow rates of the protein stream to assess its effect on the patterning process. To avoid a significant widening of the focused protein stream along the entire length of the microchannels, a range of flow rates was chosen that resulted in minimal lateral biomolecule diffusion (not shown). Indeed, the cross-sectional profile of the protein pattern is indistinguishable from the channel beginning to its end, that is, over *ca.* one centimeter (Appendix A, Figure S1). The intensities of the resulting protein patterns (Figure 3.1b) were plotted against time to yield immobilization kinetics for both binding schemes (Figure 3.1c,d). In all cases, increasing protein amounts are captured with increasing exposure times until saturation was obtained. This indicates that a rather large concentration (max. 200 ng cm^{-2} for both model proteins)[16] can be immobilized on these PEG hydrogels.
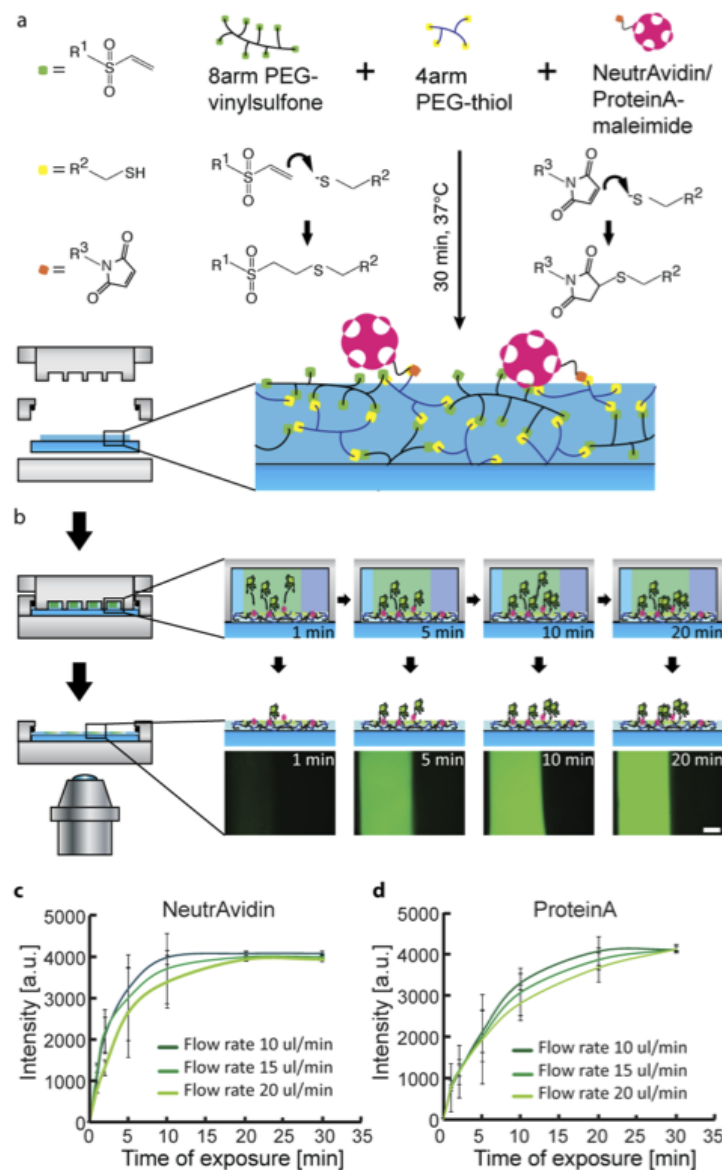
Figure 3.1 - Hydrogel engineering and protein capture by flow focusing. a, A schematic representation of hydrogel formation and bioconjugation NeutrAvidin and/or ProteinA. **b,** Determination of protein

immobilization kinetics for Alexa488-BSA-biotin captured on gel-displaying NeutrAvidin. Fluorescent micrographs of the resulting patterned protein stripes after various exposure times are shown (scale bar = 100 µm). **c**, BSA-biotin immobilization curves for variable flow rates. **d**, hIgG immobilization curves for variable flow rates.

Biomolecule gradient patterning of gels by HFF

We next utilized the knowledge on biomolecule immobilization kinetics to pattern protein gradients by HFF (Figure 3.2a,b). Patterns were generated at variable flow rates using an increasing number of steps (Figure 3.2c, programming parameters are listed in Appendix A, Table S1-2), resulting in a transition from a step-wise to a smooth gradient profile (Figure 3.2c). Statistical analysis by Matlab (*polyfit* and *polyval* functions setting the grade to one) of the comparison between the angular coefficient of the theoretical and the interpolated line of the pattern intensity profile demonstrated a decreasing error percentage with increasing number of steps (Table 3.1). Furthermore, in accordance with our calculations, variations of the flow rates resulted in a widening of linear gradients (Figure 3.2d). Further statistical analysis demonstrated an optimal equivalence between the model and the resulting pattern profile widths using an intermediate flow rate (Table 3.1). Overall, these data show that highly controlled gradient patterning can be achieved using optimized HFF parameters.

Step number	Angular coefficient interpolated curve	Angular coefficient theoretical curve	Error [%]
5	-7.9*10e3	-6.66*10e3	15.55
10	-6.96*10e3	-7.44*10e3	6.97
20	-4.19*10e3	-4.19*10e3	1.73
Flow rate [µL min^{-1}]	Pattern width theoretical [µm]	Pattern width Measured [µm]	Error [%]
10	360	320.7	10.91
15	540	513.9	4.83
20	720	638.9	28.62

Table 3.1 - Statistical analysis of the patterning resolution optimization

Programmable patterning of more complex gradient shapes

Next, we sought to use HFF for patterning of gradients with fully user-defined profiles. To demonstrate this, we chose to pattern exponential and Gaussian gradients using NeutrAvidin/Biotin and ProteinA/Fc affinity binding strategies (Appendix A, Table S3-4). The resulting patterns showed a very good agreement with the programmed intensity profiles (Figure 3.3a,b). Moreover, a measurement of fluorescent intensity profiles every three millimeters along the entire gradient length showed very good cross-sectional profile stability of the patterns (Figure 3.3 and Appendix A, Figure S2). Finally, we used HFF to pattern gradients of molecules having a biological function. To this end, we successfully patterned biotinylated recombinant fibronectin fragment III9-10 and Fc-chimeric leukemia inhibitory factor (FcLIF) as linear

gradients (Figure 3.3c,d), other examples of complex patterns these biologically relevant proteins can be seen in Appendix A, Figure S2.
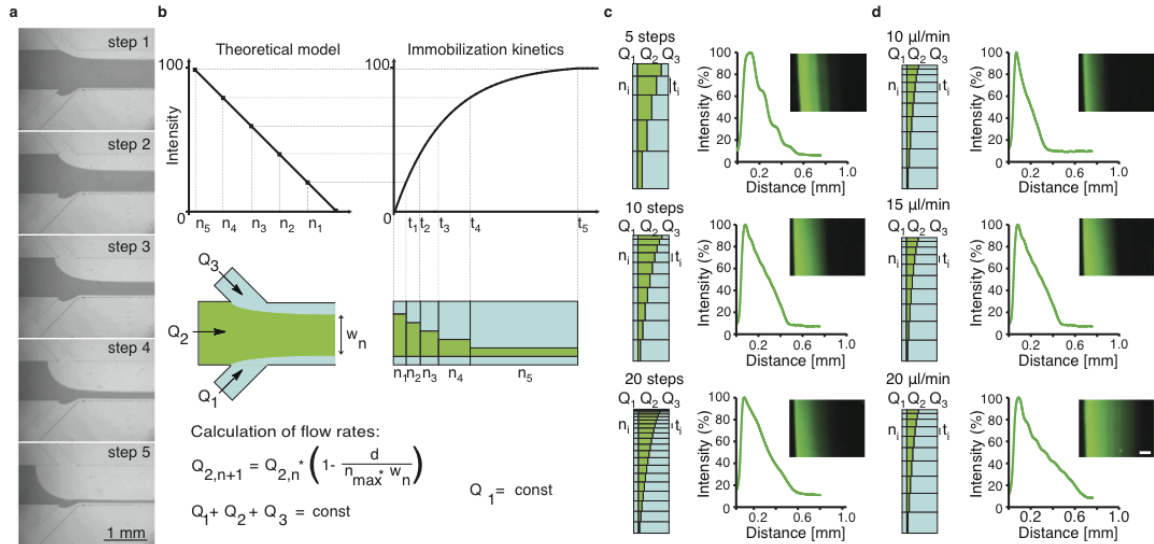
Figure 3.2 - Protein gradient patterning on hydrogels by HFF; example of a linear gradient. a, Selected micrographs from a time series of HFF patterning. At each step, the central stream (in grey) is narrowed (Scale bar = 1 mm). **b**, Implementation of the correlation between theoretical model and empiric data to yield a linear gradient pattern. Buffer and protein solution flow rate (Q_1, Q_3 and Q_2) are calculated to sequentially narrow the protein stream (green, w_n), where d is the width of the main channel (*ca.* 900 µm). Note that for all experiment, the total flow rate was maintained at 25 µL min^{-1}. Determination of the duration of each step (t_n) is obtained by correlating the mathematical model, here a straight line, to the measured immobilization kinetic curve. **c**, Micrographs and intensity plots of linear gradient obtained with variable step number. **d**, Micrographs and intensity plots of linear gradient obtained with variable flow rate. (Scale bar = 100 µm).

Patterning of protein gradient arrays

We next sought to employ HFF to generate arrayed protein gradients that might be powerful tools for high-throughput screening of multifactorial artificial stem cell microenvironments. A dedicated microfluidic PDMS chip was designed consisting of a channel system with four parallel flow-focusing units (1200 µm x 900 µm x 100 µm) (Appendix A, Figure S3a). To minimize the number of inlets and outlets for patterning of multiple gradients in one step, the buffer inlets of each unit are coupled together, while each unit has individual inlets for protein solutions. The width of connecting microchannels is 200 µm at the flow focusing regions with an intersection angle of 45°. The width from inlet to the intersection was calculated to yield equal fluidic resistance. As a result, software-controlled adjustment of the flow rates of individual liquid streams allows dynamic control of the width of the protein streams simultaneously in each of the flow-focusing units.

This device was used to pattern four parallel linear gradients of Alexa488-hIgG on ProteinA-modified PEG gels (Figure 3.4). The resulting patterns on hydrogels obtained after device disassembly and washing are shown in Figure 3.4a. Quantification of the intensities across

the four parallel gradients showed a highly similar linear profile, demonstrating that simultaneous patterning by flow focusing is possible over long distances (Figure 3.4b).
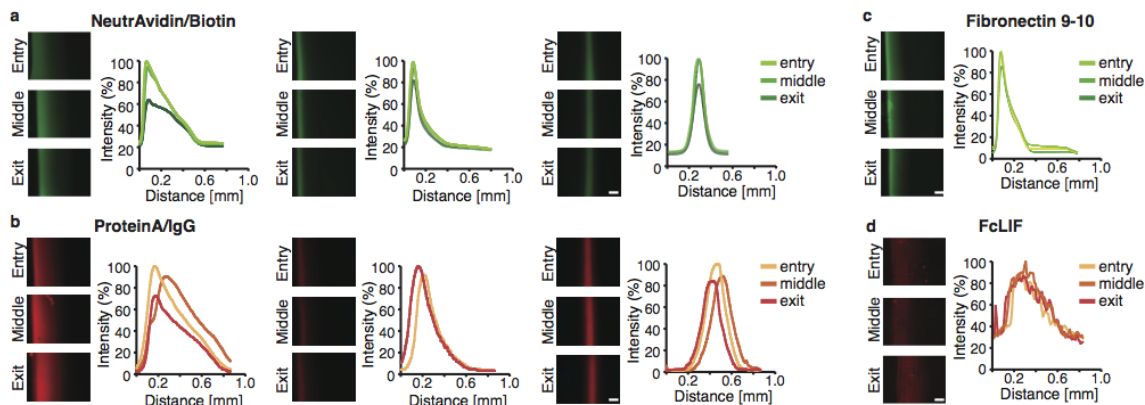
Figure 3.3 - HFF-based patterning of more complex gradient profiles. a, Micrographs and intensity profile plots of FITC-BSA-biotin on NeutrAvidin-functionalized PEG hydrogels. Linear, exponential and Gaussian gradient profiles were obtained. **b**, Micrographs and intensity profile plots of DsRED-hIgG on ProteinA-functionalized hydrogels. Linear, exponential and Gaussian gradient profiles were obtained. **c**, Micrographs and intensity profile plots of a linear FITC-FN III9-10-biotin gradient on NeutrAvidin-functionalized gels. **d**, Micrographs and intensity profile plots of a linear DsRED-FcLIF gradient on ProteinA-functionalized gels.

Patterning of overlapping protein gradient arrays

Taking advantage of an orthogonal protein capture scheme, we next aimed at generating arrays of orthogonally overlapping gradients using a two-step patterning process (Figure 3.4c). To this end, the microfluidic device (Appendix A, Figure S3) was further augmented to enable accurate orthogonal alignment of the PDMS chip to the previous pattern.

A first set of four parallel gradients of fluorescent-BSA-biotin was patterned as described above (Appendix A, Table S3). The PDMS chip was then turned by 90° for a second patterning step of parallel gradients of fluorescent-hIgG (Appendix A, Table S4). Stitched fluorescent micrographs of the resulting overlapping gradient arrays on a hydrogel are depicted in Figure 3.4d. Quantification of fluorescent intensities show a linear profile for both single and overlapping gradients (Figure 3.4e).

For this scheme to yield orthogonally overlapping gradient arrays of substantial larger areas, the microfluidic layout could be readily modified to enlarge the main channel. Indeed, the one-mm^2 area of the gradient intersection may be proven to be rather limited for application with pluripotent stem cells. However to implement this modification, we strongly believe that (i) the microfluidic device we devised for this purpose would need to be enlarged to allow patterning on larger coverlips (i.e. ø = 35 mm that would fit in six-well plates) bearing functionalized hydrogel and (ii) the insertion of micro-pillars to solidify the microchannels structure and avoid their deformation may be required.
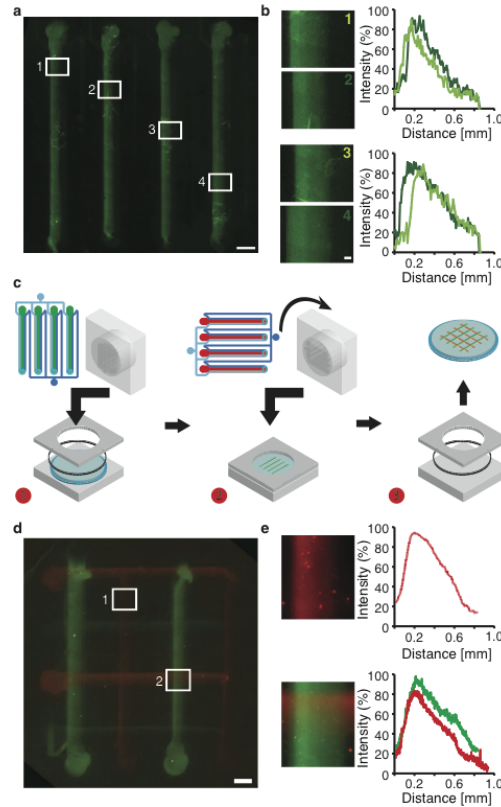
Figure 3.4 - Patterning of arrayed protein gradients. a, Stitched micrographs of four parallel Alexa488-hIgG gradients patterned on PEG gel using HFF. **b**, Micrographs showing magnification of individual gradients (white frames) and graphical representation of their respective intensity profiles (Scale bar = 100 µm). **c,** Scheme showing patterning of arrays of overlapping gradients. Step 1: The microfluidic device is assembled and a first set of four gradients is patterned. Step 2: The microfluidic device is partially disassembled with the patterned hydrogel remaining fixed to ensure good alignment. The microfluidic chip is turned by 90° and the second set of parallel gradients is patterned. Step 3: The patterned hydrogel is recovered and used for experiments. **d**, Stitched micrographs of a four-by-four gradient array of fluorescent-BSA-biotin (vertically) and fluorescent-hIgG (horizontally). (Scale bar = 900 µm) **e**, Micrographs of regions of interest of the gradient array (white frames) and graphical representation of corresponding intensity profiles.

Controlling ESC fate by tethered LIF gradients

To validate our platform, we chose to probe the effect of tethered LIF on mouse ESC self-renewal. LIF, via signal transducer and activator of transcription 3 (STAT3), is a key regulator ESC pluripotency and an essential component in maintaining ESCs in feeder-free cultures[18]. Immobilization of LIF on poly(octadecene-*alt*-maleic anhydride) substrates via a flexible PEG linker was previously shown to allow the maintenance of ESC over extended periods of time.[19]

In this study, we preferred to use a Rex1-GFP reporter mouse ESC line over the traditional Oct4-GFP reporter mouse ESC line because Rex1 is a more stringent marker for pluripotency. Moreover, the Rex1-GFP reporter mouse ESC line is coupled to a destabilized GFP that is thought to yield a more accurate readout compare to the Oct4-GFP reporter mouse ESC line which has a non-destabilized GFP (the half-life of non-destabilized GFP is rather long and

could bias our results). To facilitate ESC adhesion, PEG hydrogels were first modified with gelatin. In presence of soluble LIF, these substrates sustained efficient colony formation of self-renewing (*i.e.* Rex1 positive) ESC colonies for extended culture periods (Figure 3.5a,b), and can also be used to induce and study differentiation.

Hydrogel films were patterned by HFF to generate arrays of linear gradients of immobilized FcLIF (Figure 3.3d). We rationalized that linear FcLIF gradient would be preferable to exponential gradients, as it would enable us to resolve concentration differences in an order of magnitude (< 100 ng cm^{-2}) similar to previous reports.[19] Strikingly, colony size and morphology was strongly dependent on FcLIF concentrations; compact and round colonies were observed within regions of higher concentration, whereas they were flat and more spread at lower concentration and outside of the patterned area (Figure 3.5c and Appendix A, Figure S4a). This morphological difference suggested that ESC differentiate when not exposed to tethered FcLIF above a certain concentration. Indeed, expression of the pluripotency marker Rex1 was found to be clearly higher within regions of higher concentration compared to un-patterned areas (Figure 3.5d and Appendix A, Figure S4b,c). The distribution of GFP intensities of individual colonies (Figure 3.5e) and the colony area (Figure 3.5f) across tethered FcLIF gradients revealed a binary behavior. GFP intensities were significantly ($p < 0.001$) higher at concentrations above ca. 85 ngcm^{-2} of tethered FcLIF (Figure 3.5g). Similarly, colony areas were found to be significantly ($p < 0.001$) smaller above this threshold concentration (Figure 3.5h). Therefore, a minimal concentration of tethered FcLIF is required to sustain ESCs self-renewal on these soft PEG hydrogels. Interestingly, the threshold value of ~85 ng cm^{-2} is in good agreement with a previous report[19] in which ESC pluripotency was assessed on immobilized LIF based on the expression of the transcription factor Oct4.
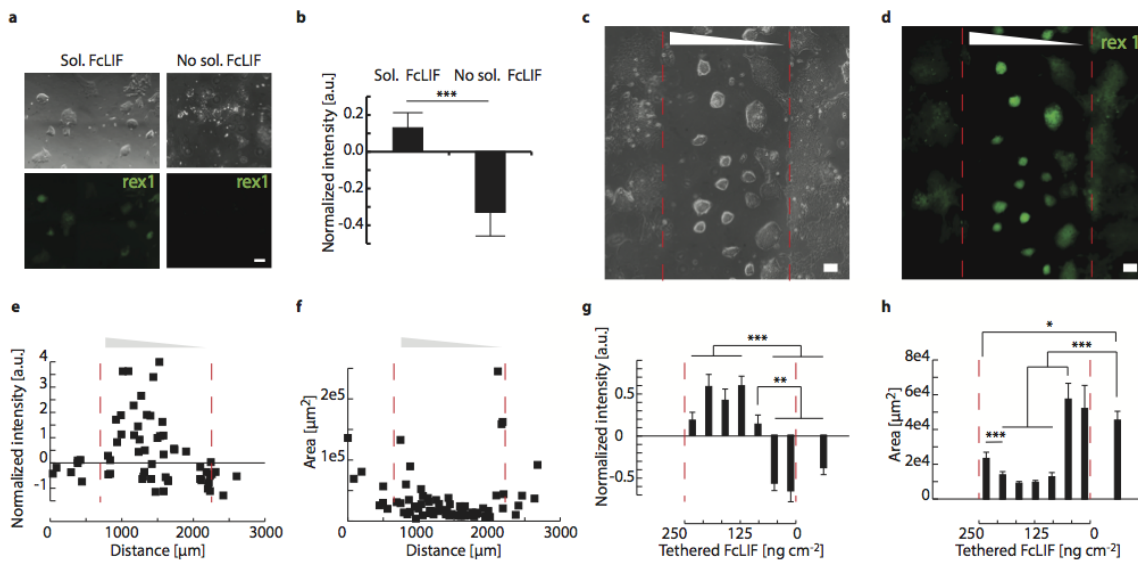
Figure 3.5 - Influence of tethered LIF gradients on ESC behavior. a, Bright-field and fluorescent micrographs of ESC cultured for 3 days on gelatin-modified PEG hydrogels in presence or absence of soluble LIF. **b,** Analysis of GFP (Rex1) signal. Normalization by standard score, average area (s.e.m.). **c,** Bright-field micrograph of ESC culture on gel displaying tethered FcLIF gradients. Dashed red lines shows pattern area. **d,** GFP signal on same area. **e,** Quantification of GFP signal (Rex1) of individual ESC colonies across a FcLIF gradient. **f,** Quantification of colony area across a FcLIF gradient. **g,** Bar plot of

GFP signal (Rex1) of individual ESC colonies across FcLIF gradients and outside of the pattern area. Normalization by standard score, average area (s.e.m.). **h**, Bar plot of colony area across FcLIF gradients and outside of the pattern area. Normalization by standard score, average area (s.e.m.). (Scale bar = 100 μm). Comparison by t-test, Bonferroni corrections for multiple comparisons. $*p<0.05$, $**p<0.005$, $***p<0.001$.

Conclusions

Here we used software-assisted hydrodynamic flow focusing to modify engineered hydrogels with graded protein patterns. Our method is amenable to generate gradients of virtually any given shape and composition. By using more sophisticated microfluidic approaches, gradient patterning could be parallelized to obtain arrays of orthogonally overlapping gradients. Because our method combines spatial patterning by microfluidics with macro-scale cell culture on biomimetic gel substrates, we believe it should be useful for studying dynamic cell behaviors such as cell migration, axonal growth and, perhaps even more excitingly, the biology of pluripotent stem cells.

Experimental section

Protein labeling. Recombinant ProteinA (BioVision) was covalently modified with a heterofunctional N-hydroxysuccinimide (NHS)–PEG–maleimide (PEG MW 3500, JenKem Technology) to facilitate covalent incorporation into a PEG hydrogel network.[16] Biotin was attached to bovine serum albumin (BSA, Invitrogen) using the NHS-EZ-link biotinylation kit (Pierce) according to the manufacturer's instruction. To visualize protein tethering on biofunctional hydrogels, BSA-biotin, human IgG (hIgG, Invitrogen) and Fc-chimeric leukemia inhibitory factor (FcLIF, generously provided by the Protein Expression Core Facility at EPF Lausanne) were fluorescently labeled with Alexa488-NHS (Invitrogen) or DsRed-NHS (Invitrogen), following the manufacturer's instructions. Fibronectin fragment 9-10 (FN III9-10, 21 kDa; generous gift from Hubbell and Martino[20]), comprising a RGD sequence and a free N-terminal Cysteine was biotinylated and fluorescently labeled. Briefly, FN III9-10 was first reduced using a tris(2-carboxyethyl) phosphine hydrochloride (TCEP) gel (Pierce) and biotinylated using EZ-link Maleimide–PEG$_2$–biotin (Pierce) following the manufacturer's instructions. The biotinylated protein was labeled with fluoresceine isothiocyanate (EZ-label FITC protein label kit, Pierce). Finally, the solution was dialyzed (Slide-A-Lyzer Mini Dialysis Unit, 10 kDa, Thermo Scientifics) against phosphate buffered saline (PBS) overnight to remove unreacted compounds.

Formation of thin biofunctional hydrogels. PEG-based hydrogels containing NeutrAvidin and/or ProteinA were cast onto round silanized (mercaptopropyltrimethoxylsilane, MPS, Falcon) glass slides or coverslips (Ø = 20 mm) as described.[16,17] Briefly, hydrogels (5% w/v) were formed via Michael-type addition by mixing two aqueous precursors containing 8arm-PEG-vinylsulfone (VS)[21] (mol. weight: 10 kDa, buffer: 0.3M triethanolamine at pH 8) and 4arm-PEG-thiol (SH) (10 kDa, NOF, Japan) at equal stoichiometry of functional groups. Crosslinking was conducted for 30 minutes at 37º Celsius. PEG-tethered NeutrAvidin or ProteinA was added to the precursor solution at a concentration of 3.36 mg mL^{-1}. To fabricate thin hydrogel films (thickness: 25 mm), the precursor solution was cast between silanized round glass coverslip and a hydrophobic (Sigmacoat, Sigma-Aldrich) glass slide. After removing the hydrophobic glass slide, covalently attached hydrogel films were extensively washed in PBS and stored at 4°C for at least eight hours before protein patterning by HFF.

Fabrication of microfluidic chips for hydrodynamic flow focusing. Standard photolithography (SU8 on silicon) and soft lithography was used to produce gradient-generating networks of microchannels as

described.[16,17] Chips were fabricated by poly(dimethylsiloxane) (PDMS) injection molding.

Microfluidic set-up and device assembly. A dedicated microfluidic device was designed and built for gradient array generation (Appendix A, Figure S3). The assembly of the microfluidic device is shown in Appendix A, Figure S1a,b. Briefly, hydrogel-coated coverslips were placed at the bottom piece of the microfluidic device. To prevent the coverslips from moving around, slight pressure was exerted onto the bottom piece using an O-ring and a PMMA coverslip holder (Appendix A, Figure S3a,b). The PDMS chip was then pressed onto the hydrogel and fixed to maintain constant sealing (Appendix A, Figure S3a, scheme 2). The assembled microfluidic device was primed with PBS using a Pasteur pipette and immersed in PBS under vacuum for 30 minutes to remove trapped air bubbles. Syringes were filled with PBS (two inlets) or protein solution (four inlets, each filled with a protein solution of interest, at 0.1 mg mL^{-1}). Finally, the syringes were mounted onto the programmable syringe pump (NEMEsys, Certoni) and Tygon tubings were connected to inlets for HFF patterning. Note that all these manipulation were performed under a culture hood to minimize risks of contaminations.

Characterization of protein patterns generated by HFF. Protein patterning was assessed by fluorescent microscopy (Leica DMI4000 or Zeiss Axio Observer). The multichannel scanning and scan reconstruction functions of the Metamorph software were used to stitch individual images to reconstruct entire gradient patterns. Intensity profiles of the fluorescent protein patterns were measured by image analysis using ImageJ.

Mouse Rex1-GFP ESC culture. A Rex1-GFP reporter mouse ESC line (generous gift from the Austin Smith, Cambridge) was used to probe maintenance of pluripotency and colony formation in response to biomolecule gradients on hydrogels. Rex1 (zfp42) is a zinc finger protein that is expressed selectively in naïve ESCs and thus a very good reporter for the *in vitro* maintenance of these cells (Austin Smith, personnel communication). ESC were expanded on gelatin-coated plastic dishes (Fluka) in DMEM (glutamax, GIBCO) medium supplemented with non-essential amino acids (0.1 mM, Invitrogen), sodium pyruvate (1 mM, Invitrogen), beta-mercaptoethanol (0.1 mM), 15% fetal bovine serum (FBS, Hyclone), 1% pen/strep, L-glutamine (0.5 mL) and leukemia inhibitory factor (LIF, 1 U mL^{-1}, Millipore).

Generation of PEG hydrogel formulations for adherent ESC culture. Biofunctional hydrogels for ESC-based assays were fabricated as mentioned above followed by immersion for one hour at 37°C in a solution containing 0.2% w/v thiolated-gelatin (Gelin-S, Glycosan Biosystems).

Quantification of tethered FcLIF concentration. ProteinA functionalized hydrogels were exposed to fluorescently tagged FcLIF (DsRED-FcLIF) solutions of defined concentrations for one hour at room temperature. The gels were washed three times for 30 minutes with PBS before imaging (Axiovert Observer, Zeiss). A standard curve was generated based on measured fluorescent intensities for each concentration.

Culture of ESC on gel-tethered FcLIF gradients. Functionalized hydrogels were prepared as described above. After HFF patterning, the patterned hydrogels were washed thoroughly with PBS and placed in a 12 well plate. 15'000 ESCs were seeded on the patterned gels in standard culture media that was depleted of soluble LIF and cultured for three days in a humidified incubator (at 37°C). Cells on arrayed gradients and controls were scanned by automated live microscopy (Axiovert Observer, Zeiss, Metamorph software). Image processing and analysis was performed using Metamorph. Non-patterned hydrogels were used for experimental controls where ESCs were culture in presence or absence of soluble LIF.

References

1   Gurdon, J. B. & Bourillot, P. Y. Morphogen gradient interpretation. *Nature* **413**, 797-803 (2001).

2   Gurdon, J. B., Harger, P., Mitchell, A. & Lemaire, P. Activin Signaling and Response to a Morphogen Gradient. *Nature* **371**, 487-492 (1994).

3   Schier, A. F. Nodal signaling in vertebrate development. *Annu Rev Cell Dev Bi* **19**, 589-621 (2003).

4   Tam, P. P. L. & Loebel, D. A. F. Gene function in mouse embryogenesis: get set for gastrulation. *Nat Rev Genet* **8**, 368-381 (2007).

5   Macri, L., Silverstein, D. & Clark, R. A. F. Growth factor binding to the pericellular matrix and its importance in tissue engineering. *Adv Drug Deliver Rev* **59**, 1366-1381 (2007).

6   Sant, S., Hancock, M. J., Donnelly, J. P., Iyer, D. & Khademhosseini, A. Biomimetic Gradient Hydrogels for Tissue Engineering. *Can J Chem Eng* **88**, 899-911 (2010).

7   Keenan, T. M. & Folch, A. Biomolecular gradients in cell culture systems. *Lab Chip* **8**, 34-57 (2008).

8   Kim, S., Kim, H. J. & Jeon, N. L. Biological applications of microfluidic gradient devices. *Integr Biol-Uk* **2**, 584-603 (2010).

9   Park, J. Y. *et al*. Differentiation of Neural Progenitor Cells in a Microfluidic Chip-Generated Cytokine Gradient. *Stem Cells* **27**, 2646-2654 (2009).

10   Moledina, F. *et al*. Predictive microfluidic control of regulatory ligand trajectories in individual pluripotent cells. *P Natl Acad Sci USA* **109**, 3264-3269 (2012).

11   Toh, Y. C. & Voldman, J. Fluid shear stress primes mouse embryonic stem cells for differentiation in a self-renewing environment via heparan sulfate proteoglycans transduction. *Faseb J* **25**, 1208-1217 (2011).

12   Toh, Y. C., Blagovic, K. & Voldman, J. Advancing stem cell research with microtechnologies: opportunities and challenges. *Integr Biol-Uk* **2**, 305-325 (2010).

13   Paguirigan, A. L. & Beebe, D. J. Microfluidics meet cell biology: bridging the gap by validation and application of microscale techniques for cell biological assays. *Bioessays* **30**, 811-821 (2008).

14   Gobaa, S. *et al*. Artificial niche microarrays for probing single stem cell fate in high throughput. *Nat Methods* **8**, 949-955 (2011).

15   Flaim, C. J., Chien, S. & Bhatia, S. N. An extracellular matrix microarray for probing cellular differentiation. *Nat Methods* **2**, 119-125 (2005).

16   Cosson, S., Kobel, S. A. & Lutolf, M. P. Capturing Complex Protein Gradients on Biomimetic Hydrogels for Cell-Based Assays. *Adv Funct Mater* **19**, 3411-3419 (2009).

17   Allazetta, S., Cosson, S. & Lutolf, M. P. Programmable microfluidic patterning of protein gradients on hydrogels. *Chem Commun* **47**, 191-193 (2011).

18   Williams, R. L. *et al*. Myeloid-Leukemia Inhibitory Factor Maintains the Developmental Potential of Embryonic Stem-Cells. *Nature* **336**, 684-687 (1988).

19   Alberti, K. *et al*. Functional immobilization of signaling proteins enables control of stem cell fate. *Nat Methods* **5**, 645-650 (2008).

20   Martino, M. M. *et al*. Controlling integrin specificity and stem cell differentiation in 2D and 3D environments through regulation of fibronectin domain stability. *Biomaterials* **30**, 1089-1097 (2009).

21   Lutolf, M. P. & Hubbell, J. A. Synthesis and physicochemical characterization of end-linked poly(ethylene glycol)-co-peptide hydrogels formed by Michael-type addition. *Biomacromolecules* **4**, 713-722 (2003).

Chapter 4

Microfluidic Synthesis of Cell-Type-Specific Artificial Extracellular Matrix Hydrogels

Microfluidic Synthesis of Cell-Type-Specific Artificial Extracellular Matrix Hydrogels[3]

Simone Allazetta, Tanja C. Hausherr and Matthias P. Lutolf

Droplet microfluidic technology is applied for the high-throughput synthesis via Michael-type addition of reactive, micron-sized poly(ethylene glycole) (PEG) hydrogels ('microgels') with precisely controlled dimension and physicochemical properties. A versatile chemical scheme is used to modify the reactive PEG microgels with tethered biomolecules to tune their bioactive properties for the bioreactor culture and manipulation of various (stem) cell types.

---
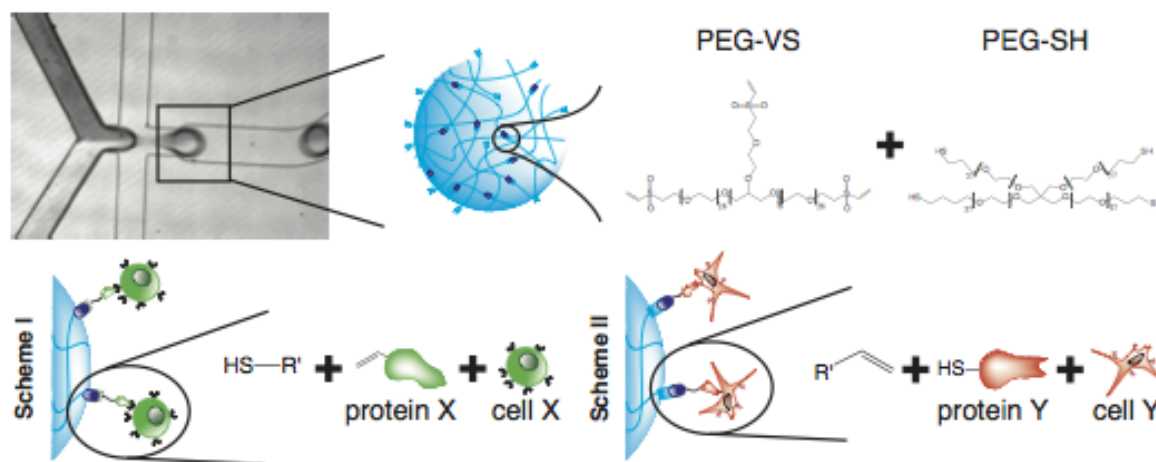
[3] This chapter is adapted with permission from Allazetta, S., Hausherr, T.C. & Lutolf, M.P., Microfluidic Synthesis of Cell-Type-Specific Artificial Extracellular Matrix Hydrogels, *Biomacromolecules* 14, 1122-1131. Copyright © 2013 American Chemical Society.

Introduction

Synthetic bioactive hydrogels such as those formed from poly(ethylene glycol) (PEG) have emerged as powerful tools to rationally manipulate cell behavior in vitro and in vivo.[1,2] Indeed, a wealth of highly selective crosslinking chemistries and well defined gel building blocks afford the fabrication of tunable gels that can mimic key properties of a cell's native extracellular matrix (ECM) in an unprecedented manner.[3] These artificial ECM (aECM) gels are used in various biomedical applications including tissue regeneration, cell culture or diagnostic platforms. A particularly promising area to exploit the full potential of aECMs is the 'ex vivo' (or in vitro) manipulation of stem cells, for example to expand stem cells to larger numbers for clinical applications by mimicking key functions of natural stem cell microenvironments (niches).[4] That is to say, stem cell function in vivo is critically influenced by signals from the stem cell niche,[5] in the absence of which most adult stem cells rapidly lose their multipotency. Thus, generating in vitro platforms that recapitulate niche signaling during cell culture can be critical for successful in vitro manipulation of stem cells.

In contrast to many 'classical' hydrogel families such as those formed from natural ECM- or plant-derived proteins or sugars (e.g. gelatin, collagen, alginate or agarose gels), thus far aECM gels have mostly been applied in stem cell culture as bulk materials; that is, their synthesis has not been widely interfaced with microtechnologies. The ability to miniaturize the size of hydrogels from the centi- or millimeter to the micrometer scale offers new perspectives to engineer tissue models and to study cell behavior in vitro.[6] For example, microscale approaches for gel synthesis such as the bottom-up assembly of microgels enable the fabrication of 3D constructs as models of native tissues, as demonstrated over the years by the Khademhosseini lab[7,8] and others.[9-11] Therefore, the goal of this work was the high-throughput generation of miniaturized aECM gels for applications in stem cell biology and biotechnology.

As a first target to apply such a platform technology, we focused on the generation of aECM microgels for the adherent culture of stem cells in bioreactors, a powerful method to generate large amounts of cells for clinical purposes.[12,13] Accordingly, such microcarriers fabricated from different materials including polystyrene, cellulose, glass or dextran have been used for several decades in the pharmaceutical industry, for example for the large-scale production of proteins or viruses.[14,15] However, despite the fact that several microcarrier families have been tested for the expansion of stem cells in bioreactors,[16-24] to the best of our knowledge, none of the existing microcarrier systems can be readily engineered to confer biochemical and biophysical properties that are reminiscent of those of native stem cell niches.

Here we combine hydrogel engineering with droplet microfluidic technology[25-27] to form aECM microgels in high-throughput. Michael-type addition chemistry was used to produce PEG microgels with modular dimension, stiffness and surface-tethered biomolecule composition. Such modularity allows tailoring microgel properties to a specific cell type and cell function of interest, for example to stimulate the robust expansion or differentiation of stem cells via display of specific niche components on the microcarrier surface.

Results and discussion

Characterization of microfluidic droplet generation

To select the most suitable system for the generation of aECM microgels, we first reproduced existing microfluidic droplet formation strategies based on a T-junction[28-30] and a flow focusing design.[31-33] Both designs were evaluated at variable geometries and flow rate ratios, which we define as the ratio of flow rates of the aqueous (discontinuous) and oil (continuous) phase (Figure 4.1). By keeping the total water flow rate constant (here: 4 µl/min; 2 µl/min for each inlet based on some of our earlier microfluidic work[34]), depending on the flow rate ratio, droplets of spherical or plug-like shape between ca. 90 and 700 µm were formed (Appendix B, Figure S1A). Droplet size decreased with increasing flow rate ratio (Figure 4.1B, C), as was expected based on published data.[31,32] Moreover, at constant flow rate ratio, droplet size increased with microchannel width. Notably, at the same flow rate ratio, droplets dimensions do not change significantly with water flow rate. The stability of the system was better for high flow rate ratios (Appendix B, Figure S2C). Taken together, in our hands, microdroplets with variable dimensions can be readily generated, consistent with earlier work.[31,32,35]

We next calculated the frequency of droplet formation defined as the ratio between the flow rate of the discontinuous phase and the volume of the droplet for a specific flow rate ratio.[36] We found a frequency range between ca. 1 Hz, for wide channels at low flow rate ratios, and 700 Hz, for narrow channels at high flow rate ratios. However, using smaller channel dimensions and higher flow rate ratios, smaller droplets have been generated at frequencies up to tens of kHz.[32] Since, in our hands, the flow focusing design allowed for better control of droplet dimensions and stability across a wide size range, as well as higher frequencies of droplets of dimensions in the range of commercially available microcarriers (100-300 µm) (Figure 4.1D and Appendix B, Figure S1B), we chose this design to generate aECM microgels.
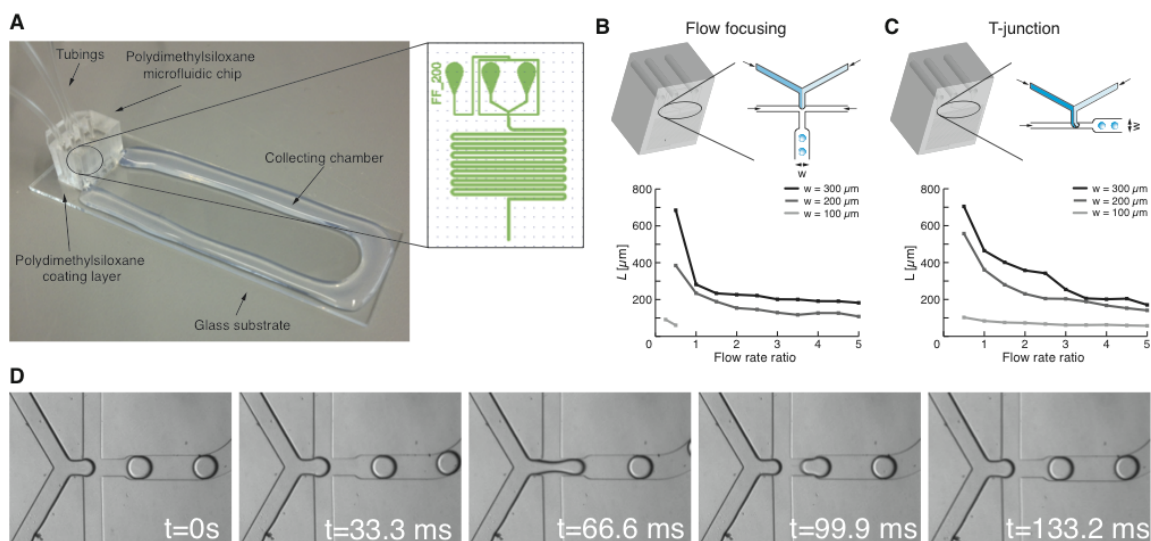
Figure 4.1 - Characterization of microfluidic droplet formation. A Experimental setup used for microgel generation. A PDMS chip was bonded on top of a glass slide and a chamber was devised to collect microbeads. The enlargement shows the microfluidic layout for the 200 µm flow-focusing design. **B,C** Flow focusing and T-junction designs used to generate microdroplets. Droplet length, L, was measured at different flow rate ratios and for different microchannels widths, w. Flow instabilities occurred in the 100

μm flow focusing design and no droplets were generated for flow rate ratio higher than 0.5. The light and dark blue colors indicate the presence of two different phases that do not mix each other under laminar flow conditions until the water stream is broken off by the organic phase. **D** Generation of a single droplet via flow focusing (200 μm channel width). The immiscible fluids form an interface at the junction; a droplet starts growing when the water stream penetrates into the main channel; the symmetric pressure gradient generated by the oil phase causes the breaking off of the droplet.[37] Frequency of droplet formation 7.5 Hz (here).

Generation of microgels with well-defined size and physicochemical properties

PEG-based microgels were generated by forming droplets composed of mixtures of equal volumes of two aqueous precursors containing reactive PEG macromers. Specifically, the mixing of vinyl sulfone (VS)-terminated 8arm-PEG in one channel and thiol (SH)-terminated 4arm-PEG in the other channel resulted in hydrogel formation by stepwise co-polymerization via Michael-type addition (Figure 4.2A).[38,39] Importantly, the laminar flow regime in the microfluidic channels avoids premature mixing and reaction of the two precursors, ensuring a precise control of the volumes mixed in each individual bead.[40-42] As a result, the size distribution of microgels that was obtained after removal of the oil phase was very narrow (Figure 4.2B).[31,42]
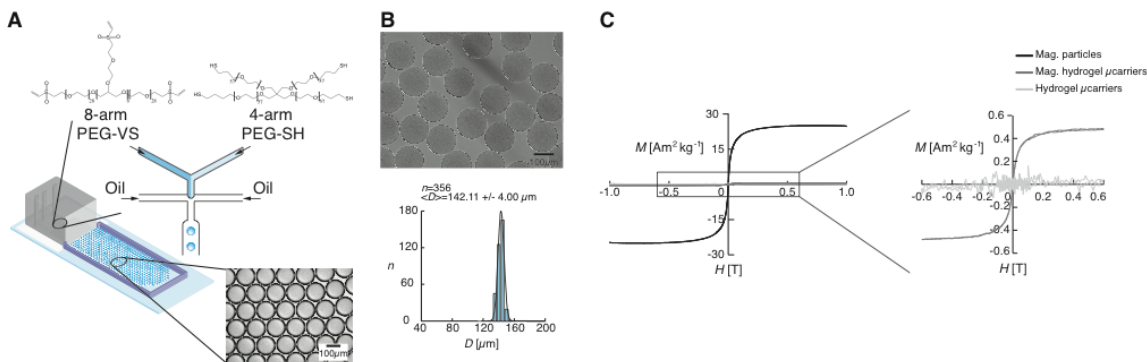
Figure 4.2 - Microfluidic synthesis of PEG hydrogel microbeads. A Microgels are generated using a flow focusing microfluidic chip. A chamber collects microgels until completion of crosslinking. **B** Transparent magnetic microgels after removal of the organic phase. Histogram in lower panels shows the size distribution of magnetic microgels. **C** Hysteresis curves (= applied magnetic field (*H*) versus the magnetization (*M*)) demonstrating microgel magnetization. Magnetic particles and microgels with and without magnetic particles were analyzed. Magnified area shows magnetization of microgels compared to negative control.

The chosen channel geometry is particularly well suited for the generation of multi-component microgels that can, for example, be obtained by loading different gel components into the precursors streams. For instance, in order to facilitate medium exchange during bioreactor cell culture, magnetic particles were loaded into one of the precursor streams to irreversibly trap them in the microgels. Vibrating sample magnetometer analysis demonstrates that the resulting microgels are indeed paramagnetic (Figure 4.2C).

Importantly, by varying the concentration of the PEG precursors between 2.5-15% (w/v), we obtain microgels with different crosslinking densities and thus physicochemical properties

such as swelling ratios (Figure 4.3A). Using the above PEG macromere formulations, gel swelling scales perfectly linear with PEG concentration (Figure 4.3B).

Atomic force microscopy was used to measure elastic moduli of microgels and bulk gels (Appendix B, Figure S2A). At a concentration of 7.5%, we found that elastic moduli of microgels and bulk gels match well, suggesting that the crosslinking reaction occurs with similar efficiencies at micro- and macro-scale. This may not be surprising as hydrogelation by stepwise co-polymerization via Michael-type addition is an efficient process.[28] Specifically, at 20% molar excess of VS-groups, we obtain Young's moduli of 28.84±4.86 kPa and 31.28±0.42 kPa for 7.5% microgels and bulk gels, respectively (Appendix B, Figure S2E). At 20% molar excess of SH-groups, we obtained elastic moduli of 28.1±5.02 kPa and 32.99±6.21 kPa for microgels and bulk gels, respectively.

Notably, microgels can also be formed from much softer PEG-co-peptide hydrogels formulations such as those crosslinked via Michael-type addition[28] (not shown) or the transglutaminase factor XIII (FXIIIa)[43] (Figure 4.3C). For instance, at a PEG concentration of 2.3% (w/v), FXIIIa-crosslinked microbeads with a modulus of ca. 750Pa were obtained. Therefore, droplet microfluidics is suitable to generate PEG-based microgels across a very wide range of crosslinking densities and mechanical properties (e.g. from hundreds of Pa up to tens of kPa in Young's modulus).
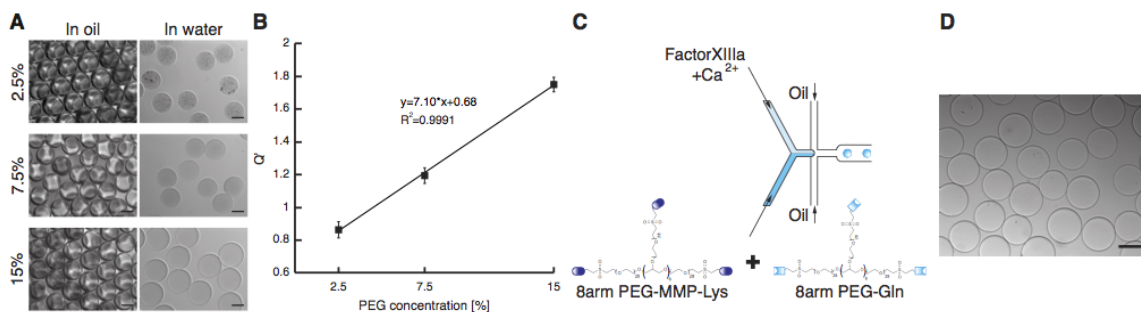
Figure 4.3 - Generation of microgels with different crosslinking density. A Micrographs showing microgels generated with a final PEG concentrations of 2.5% (w/v), 7.5% (w/v) and 15% (w/v), in the oil phase and in water. Images show how microgels swell more at higher PEG concentration. Microgels were generated with a flow rate ratio of 5 and oil flow rate of 20 µl/min. **B** Swelling ratio (Q') for hydrogel microbeads showing a perfect linear correlation between the PEG concentration and Q'. **C** Microgels formed from softer PEG-co-peptide hydrogels crosslinked via the transglutaminase factor XIII. The final PEG concentration was 2.32 % (w/v). Scale bars =100 µm.

Bioconjugation of PEG microgels via covalent coupling

Next, a bio-conjugation protocol was developed to modify the above, relatively inert microgels with biomolecules of interest (Figure 4.4). To this end, microgels were formed at slightly imbalanced stoichiometric ratio of functional groups, such that free reactive groups on bead surfaces could be used as 'chemical handles' to tether bioactive ligands. PEG precursor streams of different final concentrations were thus mixed to achieve an up to 20% molar excess of one of the reactive moieties (VS- or SH-) producing such 'activated' gel surfaces. Networks bearing free VS-groups can then be functionalized via Michael-type addition with thiolated biomolecules (Figure 4.4A), whereas SH-presenting networks are amenable for functionalization with

biomolecules bearing unsaturated groups such as vinylsulfones, maleimides, acrylates, or acrylamides. Due to its excellent specificity towards reaction with thiols, we chose maleimide groups to demonstrate the latter bioconjugation strategy (Figure 4.4B).
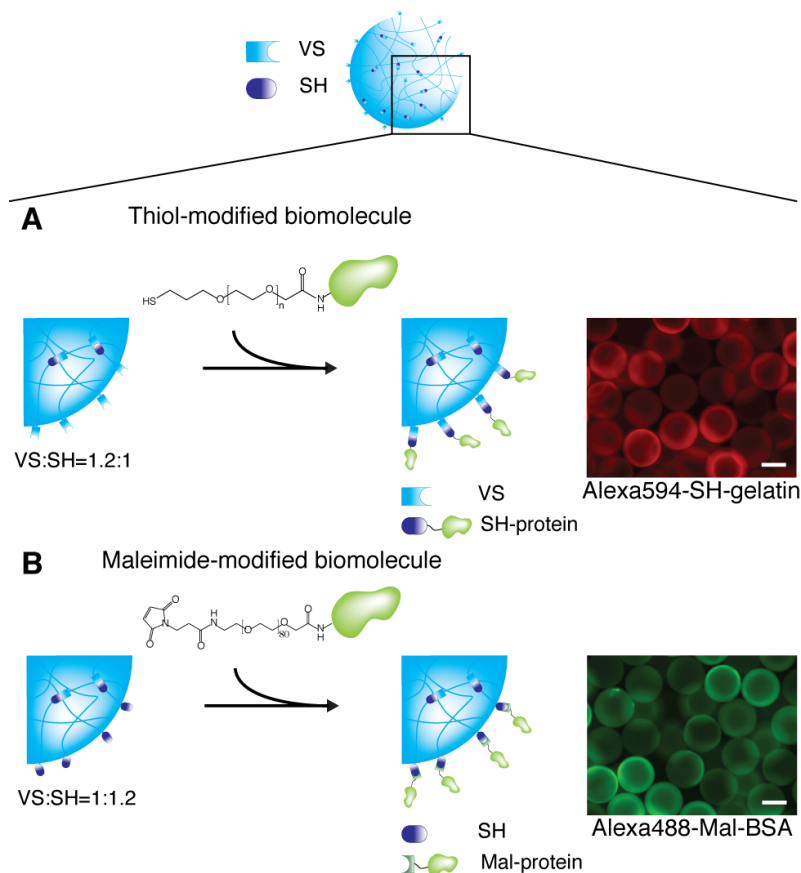
Figure 4.4 - Bioconjugation of microgels. A Microgels with molar excess of VS-groups (here: 20%) can be functionalized with thiolated biomolecules (here: fluorescent thiol-activated gelatin). **B** microgels with molar excess of SH-groups (here: 20%) can be functionalized with SH-reacting biomolecules (here: fluorescent maleimide-activated BSA). Scale bars = 100 µm. An estimation of the maximal protein amount that can be tethered to the microcarrier surface was carried out, taking into account the dry mass of the gel and the molar excess of the reactive VS- or SH-groups. Assuming a layer (or shell) of 10 nm on the surface of microcarriers that is accessible for cells to interact with, we obtain a protein surface density of ca. 3.45 nmol/cm^2 for 7.5% (w/v) microcarriers bearing a 20% molar excess of VS-groups. Similarly, at a 20% molar excess of SH-groups, 7.5% microcarriers yield a maximum of ca. 3.25 nmol/cm^2 of protein.

Bioconjugation of PEG microgels using affinity binding schemes
The versatility of the chosen two-step bioconjugation strategy allows for functionalization of PEG microgels using other strategies such as affinity-based protein capture.[34,39] This strategy could be particularly interesting for modifying microcarriers with recombinant proteins such as growth factors that are often obtained as 'chimeric' proteins containing a tag for purification (e.g. Fc tag or His-tag). For example, ProteinA or NeutrAvidin can be tethered to thiol-bearing microgels using a heterofunctional maleimide-PEG-NHS linker (Figure 4.5A,C). These microgels

efficiently capture Fc-tagged or biotinylated proteins as shown in Figure 4.5. Indeed, fluorescent intensity measurements and image analysis revealed specific binding of fluorescent model proteins (IgG and biotinylated BSA) on ProteinA- or NeutrAvidin-modified microgels (Figure 4.5B,D). Of note, a reduction of disulphide bonds by tris(2-carboxyethyl)phosphine hydrochloride does not increase the efficiency of functionalization (Appendix B, Figure S3).
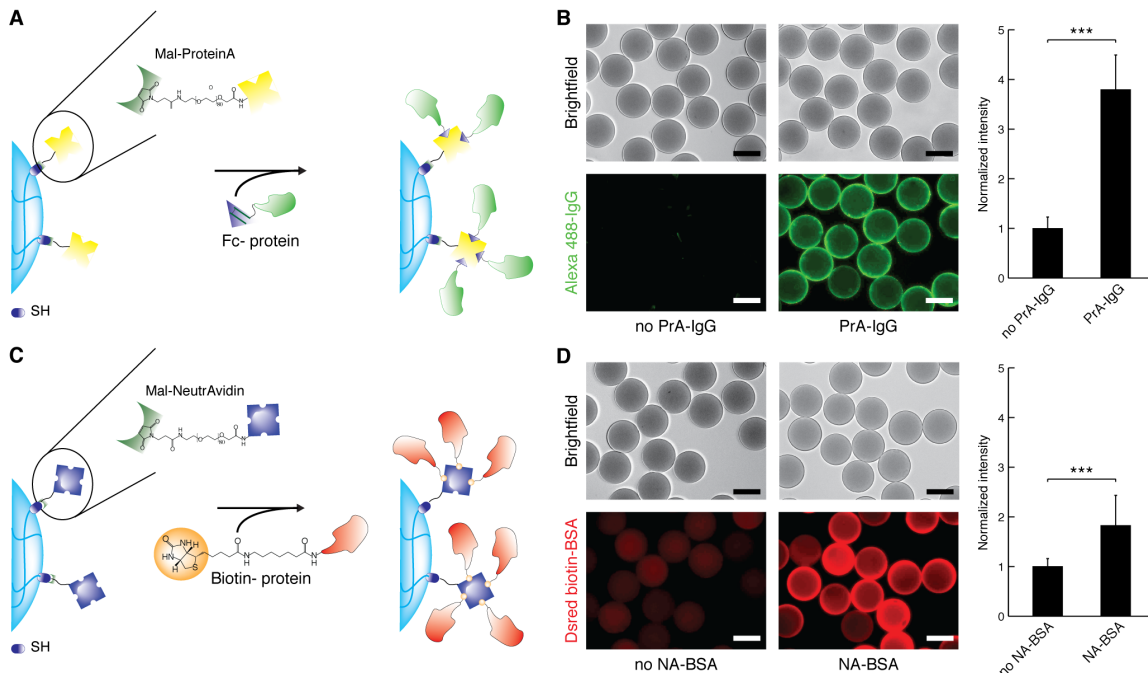
Figure 4.5 - Bioconjugation of microgels via affinitiy binding. A,C Microgels with a molar excess of SH-groups functionalized with maleimide-ProteinA or maleimide-NeutrAvidin to capture Fc- or biotin-tagged biomolecules, respectively. **B,D** Examples of microgels functionalized with ProteinA/fluorescent IgG and NeutrAvidin/fluorescent biotin-BSA. Measured fluorescence intensities were normalized to the intensity of the negative control (*i.e.* microcarriers not functionalized with ProteinA or NeutrAvidin). Quantification shows that fluorescent intensities from modified microcarriers are significantly higher. Scale bars = 100 μm.

Next, to demonstrate the possibility to modulate the surface density of biochemical factors, we functionalized ProteinA-modified microgels with different molar excess of fluorescent IgG (Figure 4.6A). Quantification of fluorescent intensities by image analysis reveals a significant increase in concentration with increasing molar excess of IgG (Figure 4.6B). Therefore, our bioconjugation strategy can be applied to control of the concentration of tethered biomolecules.
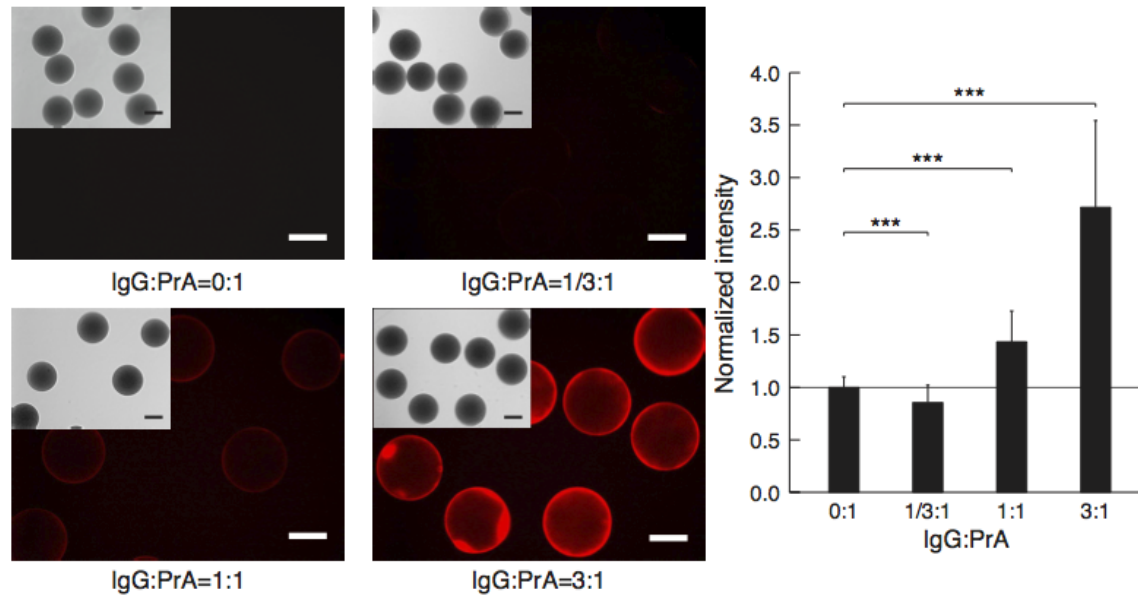
Figure 4.6 - Modulation of ligand density on microgel surface. A ProteinA-modified microgels functionalized with different amounts of Alexa546 IgG: IgG:PrA=3:1 (IgG surface density 3.25 nmol/cm^2); IgG:PrA=1:1 (IgG surface density 1.08 nmol/cm^2); IgG:PrA =1/3:1 (IgG surface density 0.36 nmol/cm^2). **B** Image-based fluorescence analysis. Microgel intensity values were normalized to the control (*i.e.* no functionalization with IgG). Functionalization with increasing amount of IgG results in a significantly higher fluorescent intensities. Scale bars = 100 μm.

Peptide or protein-functionalized PEG microgels promote stem/progenitor cell adhesion and growth

To validate our aECM microgels in bioreactor-based cell culture, selective peptide- and protein-modified formulations were tested for their ability to promote stem/progenitor cell adhesion and proliferation (Figure 4.7). To this end, VS-bearing microcarriers were functionalized with Cysteine-containing RGD peptide and used to expand C2C12 muscle progenitor cells (Figure 4.7A). Moreover, microcarriers presenting an excess of thiols were functionalized with maleimide-activated NeutrAvidin and then with biotinylated fibronectin fragment FN$_{9-10}$ for human mesenchymal stem cell (MSC) culture (Figure 4.7B). Micrographs show very good spreading and adhesion of both cell types on these bioactive PEG microgels. Compared to C2C12 cultures, a relatively low number of MSCs was observed on microgels which we attribute to the low initial cell seeding density (ca. 2800 cells/cm^2) and their slower growth rate, as very few cells were found to detach from the microgels (Figure 4.7B).
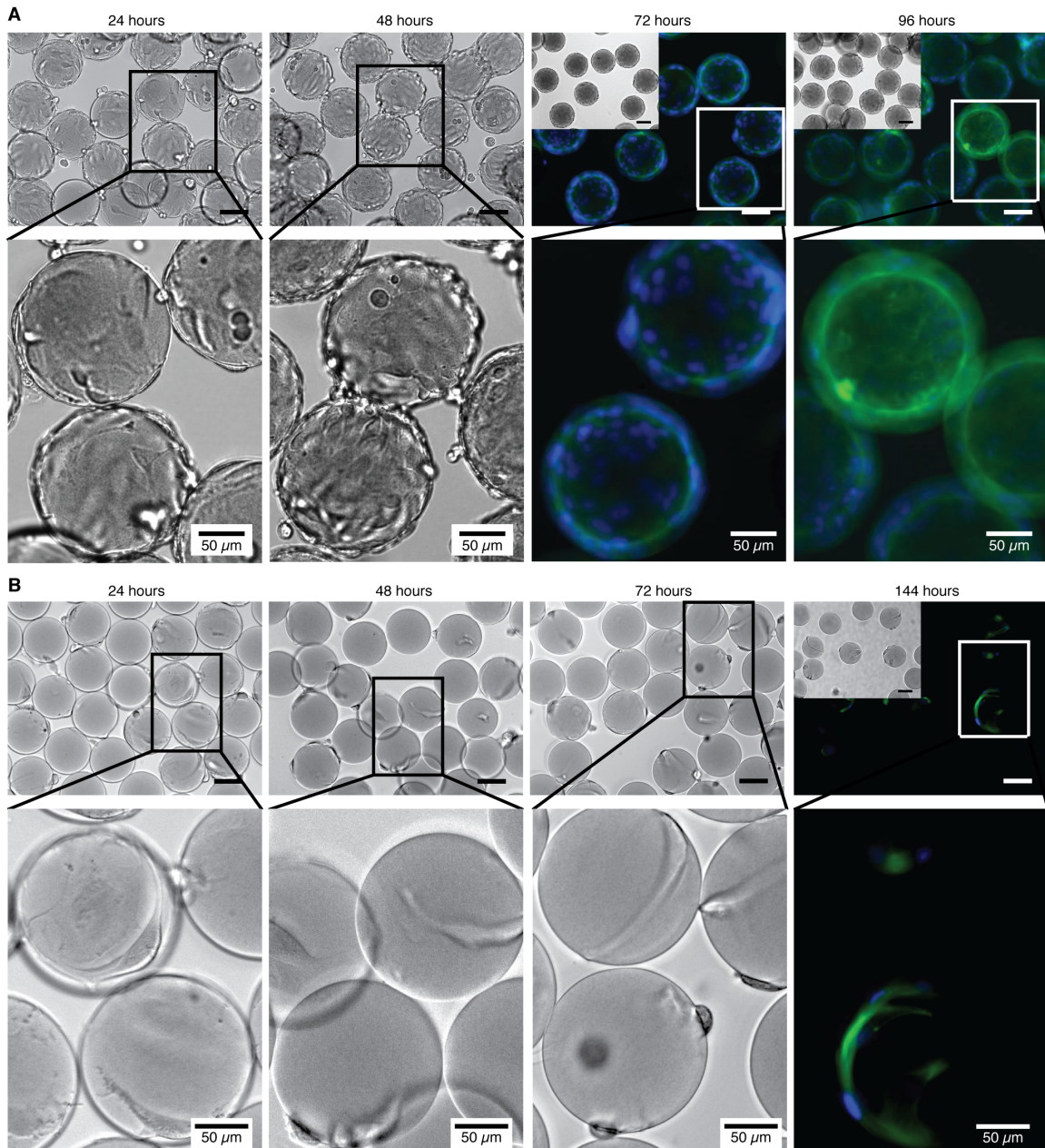
Figure 4.7 - Stem cell adhesion and growth on PEG microgels in bioreactor culture. A C2C12 cultured on RGD-functionalized microgels. **B** MSCs cultured on FN$_{9-10}$-functionalized microgels. Fluorescence micrographs depict phalloidin (cytoskeleton) and DAPI (nuclei) staining for both cell types on the last day of culture. The magnifications indicate cell spreading on microgels at different time points. Scale bars = 100 µm.

Gelatin-functionalized PEG microgels promote mouse ESC expansion

As a tractable model system to probe stem cell expansion on our aECM microgels, we used an ESC reporter line wherein GFP marks cells that express the pluripotency transcription factor Oct4. To promote efficient ESC adhesion, PEG microgels bearing excess VS-groups were modified with thiolated gelatin, a protein that is routinely used in ESC expansion culture on plastic dishes.

79

In the presence of leukemia inhibitory factor (LIF), aECM microgels promote expansion of Oct4-positive cells under bioreactor culture conditions (Figure 4.8A). Cells tended to form large clusters that often spanned over multiple carriers, a phenomenon that was previously reported.[16,17,44] Upon LIF removal, cells rapidly lost GFP expression, formed monolayers instead of larger clusters and finally detached from the carriers upon reaching confluency. Moreover, further assessment of ESC fate by flow cytometry revealed significantly less proliferation (Figure 4.8B) and lower numbers of GFP-positive cells (Figure 4.8C) in the absence of LIF. However, further functional assays are necessary to prove this point. Of note, these experiments also show that cells can be readily harvested from the microgels and used for further analyses such as flow cytometry or manipulation of cell fate in other culture formats.
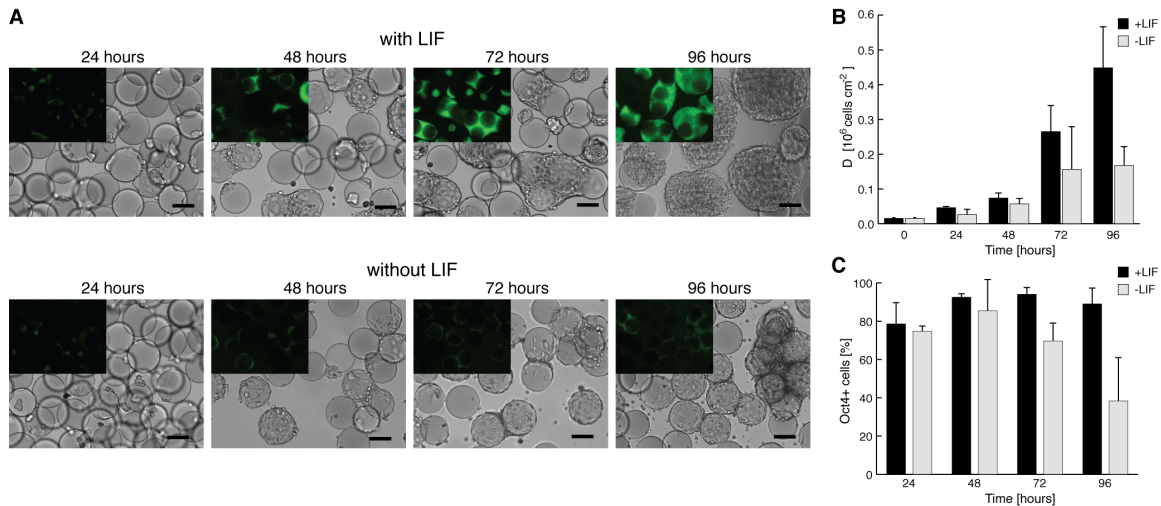
Figure 4.8 - ESC expansion on PEG microgels in bioreactor cultures. A ESC cultured on gelatin-functionalized microgels in the presence or absence of LIF. Fluorescence micrographs in the left corners indicate Oct4 expression. **B** ESC growth curves depicting cell density (*D*) for different culture periods. In presence of LIF, cells proliferate more extensively. Partial cell detachment can be observed after 4 days of culture in the absence of LIF. **C** GFP expression measured by flow cytometry. In the presence of LIF, ESCs maintain high Oct4 expression up to day 4. In the absence of LIF, Oct4 expression drops dramatically, suggesting ESC differentiation. Scale bar = 100 µm.

Conclusions

Here we demonstrate the successful application of droplet microfluidics for the reliable generation of monodisperse microgels with extremely well defined biochemical and biophysical properties. The versatility of the chosen approach allows us to combine multiple gel components and additives (such as magnetic particles) almost at will, providing the exciting opportunity to generate a huge diversity of microgels for cell manipulation and screening applications, for example to discover hydrogel formulations that allow the manipulation of difficult-to-culture cell types. Our droplet-based aECM fabrication scheme should also be useful to encapsulate cells in 3D.[26,42,45-47]

Experimental section

Materials. Poly(dimethylsiloxane) (PDMS) microfluidic chips were produced by using Sylgard 84 (Dow Corning). 4arm PEG end-functionalized with thiols (4arm-PEG-SH, 10kDa) were obtained from NOF (Japan) and dissolved in bi-distilled water. Vinylsulfone-functionalized 8arm-PEG (8arm-PEG-VS, 10kDa) was synthesized as described[38] and dissolved in triethanolamine (0.3M, pH 8). Amine-functionalized magnetic particles (size: 200nm) were supplied from Chemicell. Hexadecane and ABIL EM 90 were purchased from Sigma (USA) and Evonik Industries (Germany), respectively. Thiolated gelatin (GelinS) was purchased from Glycosan Biosystems (USA), C-RGD (Ac-GRCGRGDSPG-NH$_2$) was obtained from GL Biochem (China). Fibronectin fragment FN III$_{9-10}$ bearing a free N-terminal cysteine was a generous gift from Drs. Hubbell and Martino.[48] Maleimide-activated NeutrAvidin and recombinant ProteinA were purchased from Pierce (Switzerland) and Biovision (Switzerland), respectively. Maleimide-PEG-NHS linker (M.W. 2000Da) was obtained from JenKem Technology (USA). Biotinylation was performed using EZ-link Maleimide-PEG$_2$-biotin from Pierce (Switzerland). Human immunoglobulin (IgG) and bovine serum albumin (BSA) were purchased from Sigma (USA). AlexaFluor594 and AlexaFluor488 carboxylic acid, succinimidyl ester and AlexaFluor546 C$_5$ maleimide fluorophores were obtained from Life Technologies (USA). Tris(2-carboxyethyl)phosphine hydrochloride (TCEP) and ethyl iodoacetate were obtained from Thermo Scientific (USA) and Sigma (USA), respectively.

Fabrication of Microfluidic Chips. Clewin software was used to draw microfluidic networks for droplet generation using a T-junction and a flow focusing design composed of two microchannels for the water phase, intersected at 90° angle with the main channel for the oil phase. PDMS chips were fabricated using conventional soft lithographic techniques. 100-µm-deep channels with three different channel widths (100, 200 300 µm) were patterned on SU8 masters. Microfluidic chips were bonded on oxygen plasma-activated glass slides (Figure 4.1A).

Microgel Generation. Computer-controlled syringe pumps (neMESYS from Cetoni, Germany) were used to control flow rates. Syringes were filled with PEG solutions and hexadecane with 2% (w/v) ABIL EM surfactant used as oil phase. Tygon tubings were used to connect the syringes to the microfluidic chip inlets. Microgels were generated by loading two microfluidic channels with PEG precursors with concentrations depending on a specified molar excess of functional groups: for a 20% VS-excess, the concentrations of PEG-VS and PEG-SH were 12% (w/v) and 20% (w/v), respectively. For a 20% SH-excess we chose 8.33% (w/v) and 20% (w/v) precursors, respectively. The oil phase was removed by filtering microgels with 70µm cell strainers (BD Biosciences, USA) and extensive washing with PBS. Microgels were then swollen in PBS overnight. In order to render microgels paramagnetic, magnetic nanoparticles were mixed into the PEG-SH solution to a final concentration of 2.7 mg/ml.

Measurements of Paramagnetism. Microgels with and without trapped magnetic nanoparticles were lyophilized and fixed with silicon grease (Dow Corning, Switzerland) into gelatin caps. A MicroMag 3900 Vibrating Sample Magnetometer (Laboratory for Micro- and Nanotechnology, ETH, Zurich) was used to assess magnetic properties.

Swelling Measurements. Swelling ratios (Q') of microgel formulations were calculated as ratio between bead volume in the oil phase after droplet generation (*i.e.* before swelling) and in the water phase after swelling to equilibrium. Volumes were calculated based on the diameters of 200 microbeads per condition measured by microscopy.

Atomic Force Microscopy Measurements. Glass slides were treated with 3-mercaptopropyl-trimethoxylsilane (MPS) (Sigma-Aldrich, USA) in order to expose reactive thiol groups and covalently attach microgels to the surface of glass slides (Appendix B, Figure S2A). Measurements were carried out at 12 µm/s speed using a NanoWizard II atomic force microscope (JPK Instruments, Germany) and conical silicon nitride probes with a nominal spring constant of 0.65 N/m (CSC37, Mikromasch, Switzerland), imposing a Z-length of 6 µm. Force-distance curves were analyzed with JPK Data Processing software. The Hertz model was applied to calculate the Young's modulus, considering a Poisson's ratio of 0.5

(Appendix B, Figure S1C). Indentation forces were chosen to have a linear relationship between the indentation and the applied force. Four different forces were applied, namely 80, 100, 120 and 140nN. Young's moduli were calculated as averages of elastic moduli at different indentation forces. Each microbead and bulk gel was analyzed at three different points and measurements were carried out on 10 microbeads and 3 bulk gels.

Bioconjugation of Microgels. Protein functionalization of microgels was carried out by continuous stirring for 2 hours at 37°C using protein solutions at a concentration of up to four-fold molar excess of reactive groups. The pH of the solution was adjusted to 8 by adding 1M HEPES buffer solution at pH 9. Thiolated gelatin and BSA were fluorescently labeled with AlexaFluor594 or AlexaFluor488. In order to functionalize SH-bearing microgels, BSA was PEGylated using Maleimide-PEG-NHS. Thiolated gelatin and cysteine-containing RGD were used to functionalize VS- and SH-bearing microcarriers, respectively. Mal-NeutrAvidin, Mal-ProteinA, Alexa488-hIgG, biotin-BSA-DsRed and biotin-FN$_{9-10}$ were prepared as described.[39] After protein functionalization, microgels were filtered using 70 μm cell strainers and washed several times with PBS to remove unbound proteins. Reduction of disulphide bonds with TCEP (10mM) was performed on both Alexa488-hIgG and DsRed-BSA-biotin functionalized microcarriers to assess the effect on protein functionalization. A sulfhydryl blocking agent, ethyl iodoacetate (36 mM), was used to quench all thiol groups that did not react with maleimide, in order to reduce nonspecific binding (Figure S3A,B). A second washing step was performed at the end of the process to remove unbound proteins.

Image Analysis. Images were acquired with an inverted Olympus IX81 CellR microscope. Fluorescence measurements were performed using a Matlab script on 15 images per condition, with approximately 10 microgels each. Images were first rescaled to a normalized scale based on homogeneous imaging setup, the objects in the foreground were identified and a mask was generated based on bright-field images. A watershed function was used to automatically label beads. Finally, the average intensity per bead was calculated. Statistical t-test (type 2, number of tails 2) was performed on the samples. *** $p < 0.001$; * $p < 0.05$.

Adult Stem Cell Culture on Microgels. C2C12 (p7) and placenta-derived human MSCs (isolated and generously provided by M. Ehrbar and P. Lienemann et al.[49], Department of Obstetrics, University of Zurich Hospital, Switzerland) were cultured on tissue culture flasks in Dulbecco's Modified Eagle Medium (DMEM) with 10% Fetal Bovine Serum (FBS) or 10% Fetal Calf Serum (FCS), pen-strep (10mg/ml) and sodium pyruvate (100 mM, Gibco). After dissociation with trypsin (TripLE express, Gibco), cells were cultured on microcarriers in a suspension bioreactor (BioLevitator, Hamilton, Switzerland). During the inoculation phase, the rotation speed of the tubes was 50 rpm with an agitation period of 2 min for an entire duration of 4 hours. The agitation pause duration was set at 10 min for C2C12 cells and MSCs to minimize microcarrier 'bridging'. During cell culture, the rotation speed was increased to 80 rpm for all cell types. C2C12 (and ESC, see below) were seeded on microcarriers at a density of 14'200 cells/cm^2 (corresponding to ca. 10 cells per carrier), whereas the larger MSCs were seeded at a density of 2800 cells/cm^2 (ca. 2 cells per carrier). 6 ml of medium was used during the inoculation phase (to maximize cell-microgel contact) and 20 ml during cell culture. Medium was replaced every two days by collecting all the microcarriers on the bottom of the tube by a magnet.

Microgel-based ESC Expansion. R1 Oct4-GFP embryonic stem cells (ESC) were kindly provided by the Zandstra Laboratory (University of Toronto, Canada). ESC were cultured on 0.2% gelatin-coated Petri dishes in DMEM with 15% ESC Screened FBS (Fisher), pen-strep (10mg/ml, Invitrogen), sodium pyruvate (1 mM, Gibco), non-essential amino acids (0.1 mM, Invitrogen), beta-mercaptoethanol (0.1 mM, Life Technologies) and LIF (10^3 U/ml, Millipore). ESCs were cultured on PEG microcarriers in bioreactors as described above. Cells were counted every day by retrieving 1 ml of sample from the spinner and by passing them through a 70 μm cell strainer. Microgels were rinsed twice with PBS and trypsinized (TripLE express, Gibco) for 5 min. The resulting solution containing cells and microgels was filtered with a strainer and the cells counted using a trypan blue exclusion test. Cells were analyzed by flow cytometry using Cyan ADPS analyzer (Beckman Coulter). Data analysis was performed with FlowJo software.

References

1   Seliktar, D. Designing Cell-Compatible Hydrogels for Biomedical Applications. *Science* **336**, 1124-1128 (2012).

2   DeForest, C. A. & Anseth, K. S. Advances in Bioactive Hydrogels to Probe and Direct Cell Fate. *Annu Rev Chem Biomol* **3**, 421-444 (2012).

3   Lutolf, M. P. & Hubbell, J. A. Synthetic biomaterials as instructive extracellular microenvironments for morphogenesis in tissue engineering. *Nat Biotechnol* **23**, 47-55 (2005).

4   Lutolf, M. P. & Blau, H. M. Artificial Stem Cell Niches. *Adv Mater* **21**, 3255-3268 (2009).

5   Wagers, A. J. The Stem Cell Niche in Regenerative Medicine. *Cell Stem Cell* **10**, 362-369 (2012).

6   Gauvin, R., Parenteau-Bareil, R., Dokmeci, M. R., Merryman, W. D. & Khademhosseini, A. Hydrogels and microtechnologies for engineering the cellular microenvironment. *Wires Nanomed Nanobi* **4**, 235-246 (2012).

7   Du, Y. A., Lo, E., Ali, S. & Khademhosseini, A. Directed assembly of cell-laden microgels for fabrication of 3D tissue constructs. *Proceedings of the National Academy of Sciences of the United States of America* **105**, 9522-9527, doi:Doi 10.1073/Pnas.0801866105 (2008).

8   Khademhosseini, A., Langer, R., Borenstein, J. & Vacanti, J. P. Microscale technologies for tissue engineering and biology. *P Natl Acad Sci USA* **103**, 2480-2487 (2006).

9   Li, C. Y., Wood, D. K., Hsu, C. M. & Bhatia, S. N. DNA-templated assembly of droplet-derived PEG microtissues. *Lab Chip* **11**, 2967-2975 (2011).

10   Matsunaga, Y. T., Morimoto, Y. & Takeuchi, S. Molding Cell Beads for Rapid Construction of Macroscopic 3D Tissue Architecture. *Adv Mater* **23**, H90-H94 (2011).

11   Chen, A. A., Underhill, G. H. & Bhatia, S. N. Multiplexed, high-throughput analysis of 3D microtissue suspensions. *Integr Biol-Uk* **2**, 517-527 (2010).

12   King, J. A. & Miller, W. M. Bioreactor development for stem cell expansion and controlled differentiation. *Current Opinion in Chemical Biology* **11**, 394-398, doi:Doi 10.1016/J.Cbpa.2007.05.034 (2007).

13   Serra, M. *et al*. Process engineering of human embryonic stem cells for clinical application. *Hum Gene Ther* **22**, A56-A56 (2011).

14   Vanwezel, A. L. Growth of Cell-Strains and Primary Cells on Micro-Carriers in Homogeneous Culture. *Nature* **216**, 64-& (1967).

15   Reuveny, S. in *Large-Scale Mammalian Cell Culture Technology*   (ed A.S. Lubiniecki) 271–341 (Marcel Dekker, Inc., 1990).

16   Fok, E. Y. L. & Zandstra, P. W. Shear-controlled single-step mouse embryonic stem cell expansion and embryoid body-based differentiation. *Stem Cells* **23**, 1333-1342 (2005).

17   Abranches, E., Bekman, E., Henrique, D. & Cabral, J. M. S. Expansion of mouse embryonic stem cells on microcarriers. *Biotechnol Bioeng* **96**, 1211-1221 (2007).

18   Fernandes, A. M. *et al*. Mouse embryonic stem cell expansion in a microcarrier-based stirred culture system. *J Biotechnol* **132**, 227-236 (2007).

19   Yang, Y., Rossi, F. M. V. & Putnins, E. E. Ex vivo expansion of rat bone marrow mesenchymal stromal cells on microcarrier beads in spin culture. *Biomaterials* **28**, 3110-3120 (2007).

20   Oh, S. K. W. *et al*. Long-term microcarrier suspension cultures of human embryonic stem cells. *Stem Cell Res* **2**, 219-230 (2009).

21   Serra, M. *et al*. Stirred bioreactors for the expansion of adult pancreatic stem cells. *Annals of Anatomy-Anatomischer Anzeiger* **191**, 104-115, (2009).

22   Eibes, G. *et al*. Maximizing the ex vivo expansion of human mesenchymal stem cells using a microcarrier-based stirred culture system. *J Biotechnol* **146**, 194-197 (2010).

23   Chen, A. K. L., Chen, X. L., Choo, A. B. H., Reuveny, S. & Oh, S. K. W. Critical microcarrier properties affecting the expansion of undifferentiated human embryonic stem cells. *Stem Cell Res* **7**, 97-111 (2011).

24   Zweigerdt, R., Olmer, R., Singh, H., Haverich, A. & Martin, U. Scalable expansion of human pluripotent stem cells in suspension culture. *Nat Protoc* **6**, 689-700 (2011).

25   Theberge, A. B. *et al*. Microdroplets in Microfluidics: An Evolving Platform for Discoveries in Chemistry and Biology. *Angew Chem Int Edit* **49**, 5846-5868 (2010).

26   Velasco, D., Tumarkin, E. & Kumacheva, E. Microfluidic Encapsulation of Cells in Polymer Microgels. *Small* **8**, 1633-1642 (2012).

27   Seemann, R., Brinkmann, M., Pfohl, T. & Herminghaus, S. Droplet based microfluidics. *Reports on Progress in Physics* **75**

28   Thorsen, T., Roberts, R. W., Arnold, F. H. & Quake, S. R. Dynamic pattern formation in a vesicle-generating microfluidic device. *Physical Review Letters* **86**, 4163-4166 (2001).

29   Nisisako, T., Torii, T. & Higuchi, T. Droplet formation in a microchannel network. *Lab Chip* **2**, 24-26 (2002).

30   Xu, J. H., Luo, G. S., Li, S. W. & Chen, G. G. Shear force induced monodisperse droplet formation in a microfluidic device by controlling wetting properties. *Lab Chip* **6**, 131-136 (2006).

31   Tan, Y. C., Cristini, V. & Lee, A. P. Monodispersed microfluidic droplet generation by shear focusing microfluidic device. *Sensor Actuat B-Chem* **114**, 350-356 (2006).

32   Yobas, L., Martens, S., Ong, W. L. & Ranganathan, N. High-performance flow-focusing geometry for spontaneous generation of monodispersed droplets. *Lab Chip* **6**, 1073-1079 (2006).

33   Seo, M., Paquet, C., Nie, Z. H., Xu, S. Q. & Kumacheva, E. Microfluidic consecutive flow-focusing droplet generators. *Soft Matter* **3**, 986-992 (2007).

34   Allazetta, S., Cosson, S. & Lutolf, M. P. Programmable microfluidic patterning of protein gradients on hydrogels. *Chem Commun* **47**, 191-193 (2011).

35   Li, W. *et al*. Simultaneous generation of droplets with different dimensions in parallel integrated microfluidic droplet generators. *Soft Matter* **4**, 258-262 (2008).

36   Trivedi, V. *et al*. Microfluidic Encapsulation of Cells in Alginate Capsules for High Throughput Screening. *Embc: 2009 Annual International Conference of the Ieee Engineering in Medicine and Biology Society, Vols 1-20*, 7037-7040 (2009).

37   Teh, S. Y., Lin, R., Hung, L. H. & Lee, A. P. Droplet microfluidics. *Lab Chip* **8**, 198-220 (2008).

38   Lutolf, M. P. & Hubbell, J. A. Synthesis and physicochemical characterization of end-linked poly(ethylene glycol)-co-peptide hydrogels formed by Michael-type addition. *Biomacromolecules* **4**, 713-722 (2003).

39   Cosson, S., Kobel, S. A. & Lutolf, M. P. Capturing Complex Protein Gradients on Biomimetic Hydrogels for Cell-Based Assays. *Adv Funct Mater* **19**, 3411-3419 (2009).

40   Kim, J. W., Utada, A. S., Fernandez-Nieves, A., Hu, Z. B. & Weitz, D. A. Fabrication of monodisperse gel shells and functional microgels in microfluidic devices. *Angew Chem Int Edit* **46**, 1819-1822 (2007).

41   Duncanson, W. J. *et al*. Microfluidic synthesis of advanced microparticles for encapsulation and controlled release. *Lab Chip* **12**, 2135-2145 (2012).

42   Rossow, T. *et al*. Controlled Synthesis of Cell-Laden Microgels by Radical-Free Gelation in Droplet Microfluidics. *J Am Chem Soc* **134**, 4983-4989 (2012).

43   Ehrbar, M. *et al*. Biomolecular hydrogels formed and degraded via site-specific enzymatic reactions. *Biomacromolecules* **8**, 3000-3007 (2007).

44   Alfred, R. *et al*. Efficient Suspension Bioreactor Expansion of Murine Embryonic Stem Cells on Microcarriers in Serum-Free Medium. *Biotechnol Progr* **27**, 811-823 (2011).

45   Kumachev, A. *et al*. High-throughput generation of hydrogel microbeads with varying elasticity for cell encapsulation. *Biomaterials* **32**, 1477-1483 (2011).

46   Tumarkin, E. *et al*. High-throughput combinatorial cell co-culture using microfluidics. *Integr Biol-Uk* **3**, 653-662 (2011).

47   Tan, W. H. & Takeuchi, S. Monodisperse alginate hydrogel microbeads for cell encapsulation. *Adv Mater* **19**, 2696-+ (2007).

48   Martino, M. M. *et al*. Controlling integrin specificity and stem cell differentiation in 2D and 3D environments through regulation of fibronectin domain stability. *Biomaterials* **30**, 1089-1097 (2009).

49   Semenov, O. V. *et al*. Multipotent mesenchymal stem cells from human placenta: critical parameters for isolation and maintenance of stemness after isolation. *Am J Obstet Gynecol* **202** (2010).

Chapter 5

Engineering a Compositional Landscape of Synthetic Bioactive Microgels

Engineering a Compositional Landscape of Synthetic Bioactive Microgels

Simone Allazetta, Andrea Negro and Matthias P. Lutolf

Synthetic hydrogels are the most rapidly growing class of biomaterials and have numerous applications in biology, biotechnology and medicine. As each application may call for a chemically and physically distinct gel type, a key challenge is to identify optimal gel formulations efficiently. Current approaches for hydrogel development are complicated or expensive. We present a strategy based on automated droplet microfluidics to rapidly synthesize, process and screen a continuous landscape of poly(ethylene glycol) (PEG)-based microgels with fluorescently encoded physical and chemical compositions. Computer-controlled programming of syringe pumps allowed us to generate, in a single experiment, up to 100 combinatorial populations of microgels with varying elasticities and bioactive ligand concentrations. Thousands of compositionally distinct microgels were then analyzed by looking at the intensity levels of two fluorescence moieties incorporated within the hydrogel network. We believe that this novel platform should facilitate the discovery of new extracellular matrix compositions and it will help to gain new insights into the effect of biophysical and biochemical microenvironmental perturbations on cell behavior.
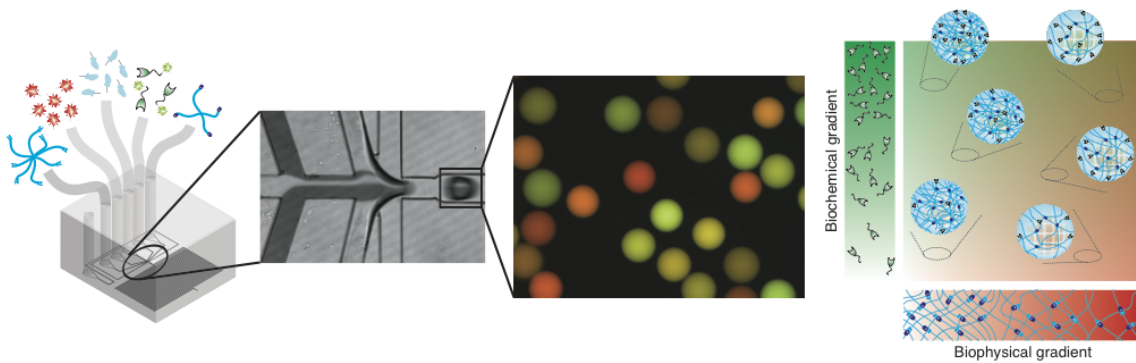
Introduction

The high water content, tissue-like physicochemical properties and ability to change their volume in response to external stimuli have made hydrogels perhaps the fastest growing class of biomaterials.[1] The diversity of hydrogel applications in various fields calls for formulations with markedly distinct physicochemical properties. Even within one field of application, no 'one-size-fits-all' type of hydrogel can be used. For example, in cell biology or tissue engineering, a targeted cell type might require a hydrogel substrate that matches the physical characteristics of its tissue of origin[2,3], as well as a biomolecular composition of its tissue-specific extracellular matrix (ECM). In this case, hydrogel stiffnesses comprising several orders of magnitude, from a few tens of Pa (*i.e.* neural tissues) up to Megapascals (*i.e.* bone tissue) and a wide biochemical parameter space needs to be covered, depending on the particular cell type. However, thus far, synthetic hydrogels have largely been synthesized manually, one-by-one, using trial-and-error approaches. This empirical approach severely limits the parameter space that can be covered in a reasonable timescale and, as such, the potential of hydrogels for various applications remains largely untapped.

We reasoned that the microfluidic technology might be amenable to speed up the discovery of hydrogel formulations for applications in the life sciences. In particular, droplet-based microfluidic technology has been widely used for the generation of several microgel families for cell biology and tissue engineering.[4-9] Previous work has shown that microgels can be formulated with variable physical properties such as stiffness[10] or bioactivity[6,11,12]. However, this approach has never been used to systematically generate a larger diversity of micron-scale hydrogels with modular physico-chemical properties.

We have previously reported a microfluidic platform for the reliable synthesis of artificial extracellular matrix hydrogels.[4] To do so, we exploited the modular nature of the poly(ethylene) glycol (PEG) chemistry, which permits the formation of microgels with tunable mechanical properties by simply changing the mass content, while simultaneously tethering bioactive ligands. Here, we adopted this technology for the high-throughput generation of a large diversity of hydrogel formulations having combinatorial biophysical and biochemical properties. Our concept is based on the fabrication of a library of reactive, fluorescently tagged hydrogel building blocks (Figure 5.1a) that can be combinatorially mixed through microfluidics, in liquid form and at the correct stoichiometric ratio (Figure 5.1b), in order to generate cross-linked microgels that span a huge parameter space. As depicted in Figure 5.1b, microfluidics can be used for highly precise modulation of microgel composition by dynamic adjustment of the flow rates of individual gel building blocks.

Hence, first, we showed the formation of microgels with varying elasticities in a wide biological range of elastic moduli, spanning from 10kPa up to 100kPa, as demonstrated by atomic force microscopy (AFM) measurements. The microfluidic platform was then modified to allow for the modulation of the concentration of a peptide, while keeping the microgels elasticity constant. Finally, we combined the two technologies for the precise synthesis of microgels with different elasticities and bioligand concentrations in a combinatorial fashion. The linearity of the system allows for a nearly perfect correlation between the values of the microgel fluorescence intensities

and each environmental condition. Fine control over the flows through computer programming allowed us to generate up to 100 populations of compositionally distinct combinatorial microgels with different elasticities and bioactive ligand concentrations in a single experiment. Finally, we demonstrated the possibility to apply this technology for the investigation of the effect of microenvironmental perturbations on biological processes, such as, for instance, cell proliferation and TGF-ß-induced epithelial-to-mesenchymal transition (EMT).
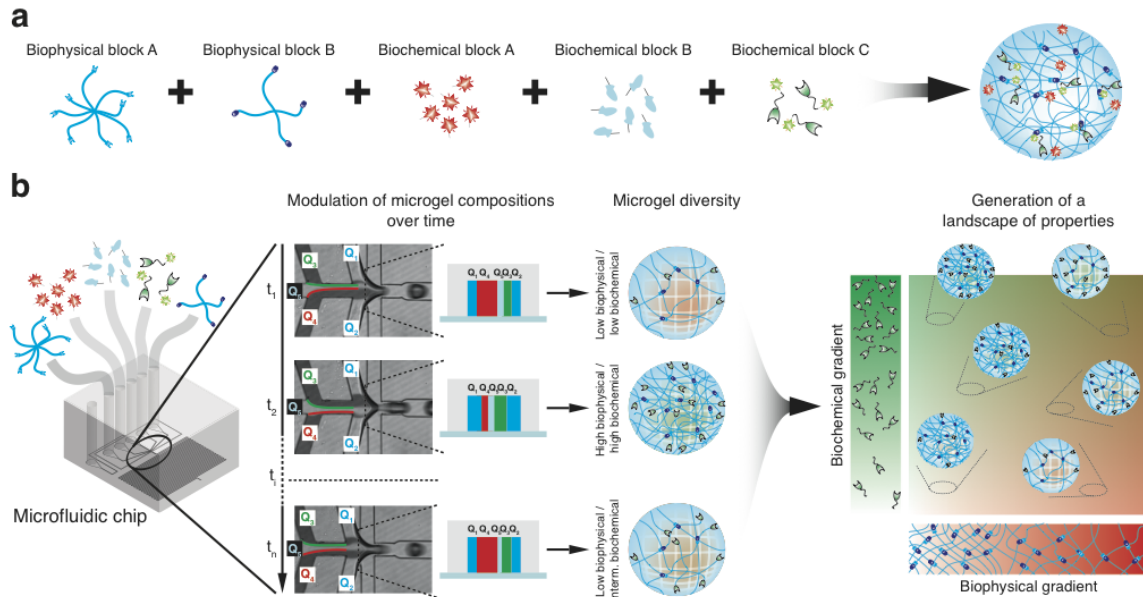
Figure 5.1 - Microfluidic generation of a compositional landscape of bioactive microgels. a, Different biophysical and biochemical blocks co-polymerize to form a microgel. Fluorescently tagged biochemical block A was used to encode for the amount of biophysical blocks A and B, in an inversely proportional way (*i.e.* higher amount of biochemical block A relates to lower content of biophysical blocks A and B). **b**, Microfluidics can be used to efficiently manipulate all the liquid gel components. Precise and automated modulation of the flows over time allows us to selectively change the amount of each different building block being incorporated within the microgel. Therefore, at any time a different microgel can be created with different biophysical and biochemical properties. For instance, at time t_1 low flow rates of biophysical blocks A and B (Q_1 and Q_2, respectively) and, simultaneously, high flow rate of biochemical block A (Q_4) and low flow rate of biochemical block B (Q_3) will lead to a microgel with low biophysical and low biochemical components. On the contrary, at time t_2 high flow rate of biophysical blocks A and B, low flow rate of biochemical block A and high flow rate of biochemical block B will lead to a microgel with high biophysical and high biochemical components. Therefore, at each time point, a different combination of flows will result in the formation of microgel with defined physico-chemical properties. Thus, fine tuning of the flows permits the generation of a continuous landscape of hydrogels with combinatorial biophysical and biochemical gradients properties.

Results

### Programmable synthesis of microgels with variable stiffness

Substrate elasticity acts as an important biophysical regulator in many biological processes.[2,13,14] Microfluidic modulation of microgel elasticity was here achieved by selectively varying the PEG content. Channels were patterned into a polydimethylsiloxane chip from a silicon master and then

bonded on top of a hydrophobic substrate. The generation of microgels with different elasticities was performed by the insertion of a central channel in the flow-focusing microfluidic design reported in [4]. The two lateral microchannels were perfused with 8arm-PEG-VS and 4arm-PEG-SH, whereas the central one was perfused with a solution of thiol-reactive maleimide Alexa660 fluorophore (Mal-Alexa660), selected for its excellent photostability. Stepwise co-polymerization via Michael-type addition of the two PEG precursors with the Mal-Alexa660 resulted in the formation of fluorescent microgels[4,15] (Figure 5.2a).

The precise microfluidic control of the three flows permitted the generation of microgels with various PEG concentrations and fluorescence intensities. Decreasing the flow rate of the fluorophore (Q_3) and simultaneously increasing both PEG precursor flow rates (Q_1 and Q_2) led to microgels with higher PEG content and lower fluorescence intensity (Figure 5.2b).

As a proof of principle, we then produced, in four independent experiments, fluorescent microgels at four different PEG concentrations, namely 2.5, 5, 7.5 and 10% (v/w) (Appendix C, Table S1). A 20% molar excess of thiol groups was used to ensure efficient incorporation of the fluorophore in the hydrogel network, as verified by a release assay (Appendix C, Figure S1). Image-based analysis was employed to compute the intensity level of the microgels and showed a linear correlation between the PEG concentration and fluorescence intensity (Figure 5.2c, red curve). In order to correlate the PEG content to the microgel elasticity, we performed atomic force microscopy (AFM) measurements on the four different microgels populations. Elastic moduli ranging from 9.98 +/- 1.20 kPa for 2.5% microgels to 99.42 +/- 4.39 kPa for 10% microgels were obtained (Figure 5.2c, black curve), which agrees well with AFM measurements performed on bulk hydrogel (Appendix C, Figure S2c). Importantly, a linear correlation was obtained between the PEG concentration and gel elasticity, covering a biologically relevant stiffness range.[2,3] The linear correlation between PEG content and fluorescence intensity (Figure 5.2c) as well gel elasticity, resulted in a linear relationship between fluorescent intensity and microgel elasticity (Figure 5.2d). Thus, microgels with distinct mechanical properties can be reliably distinguished by the specific level of fluorescent intensity.

In a next step, computer-controlled modulation of the three flows allowed for the formation of microgel populations with different elasticity on the same microfluidic chip (Movie S1). To achieve this, the same flow rates were used to serially dilute *on chip* the PEG streams with the fluorescent moiety at the same PEG and fluorophore concentrations used before (2.5, 5, 7.5 and 10%) (Appendix C, Table S2). The resulting mixed population of microgels is shown in Figure 5.2e. Fluorescence microscopy followed by image analysis allowed the fluorescence intensity and the individual microbead diameter of the entire population to be measured. Using a hierarchical clustering method, the four microgel populations nicely separated based on their intensity and diameter; the latter increased due to an increase in swelling at higher PEG concentration.[4,16] The least fluorescent microgels had the largest diameter and vice versa (Figure 5.2f).
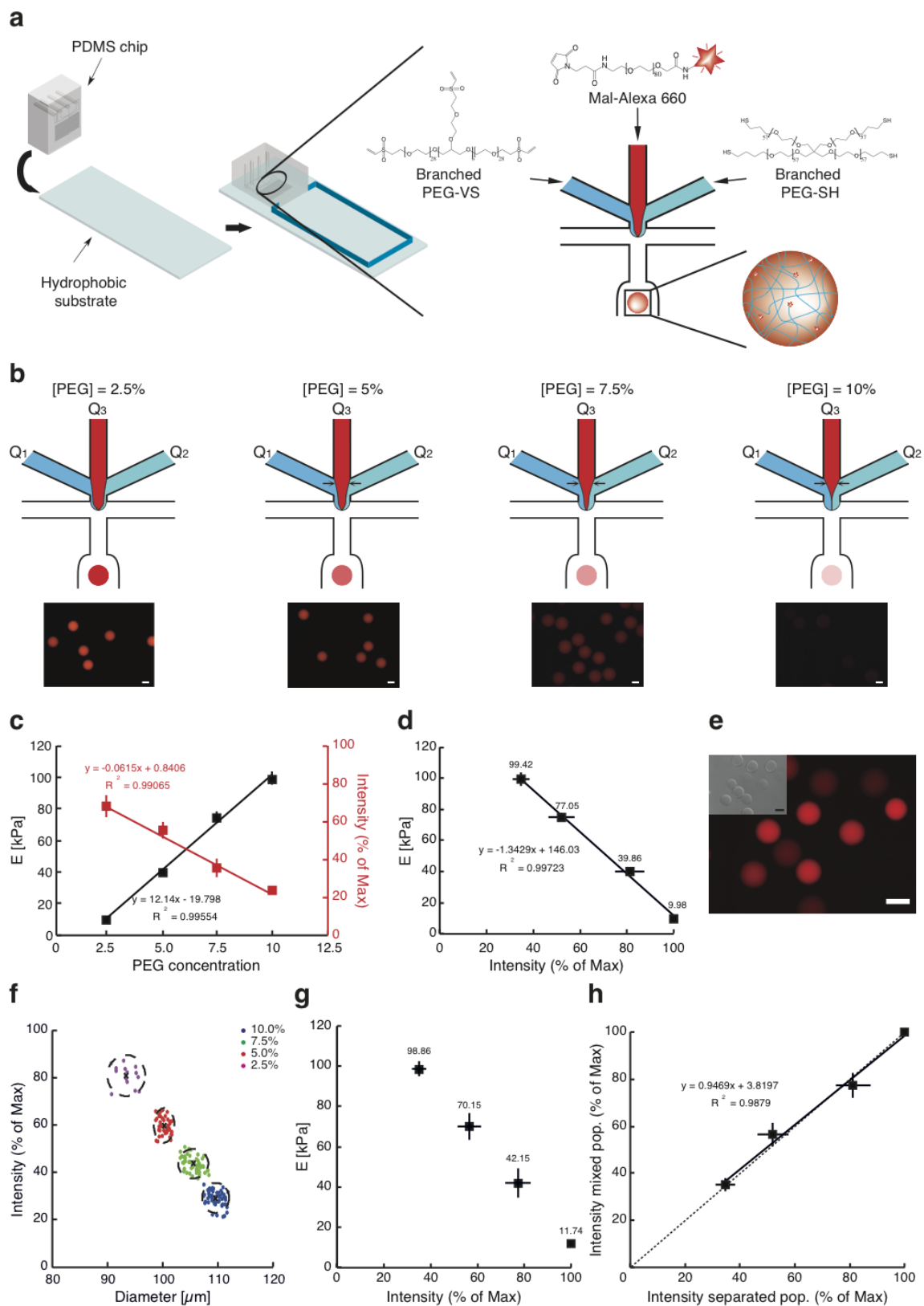
Figure 5.2 - Microfluidic generation of varying stiffness microgels. a, Schematic displaying the microfluidic chip used for the generation of microgels with varying elasticities: three inlets are depicted for

flowing the two PEG components and the Mal-Alexa660. *On chip* mixing of all the components leads to the polymerization of fluorescent microgels. **b**, Four distinct microgel populations were generated separately at variable PEG contents: 2.5% (w/v), 5% (w/v), 7.5% (w/v) and 10% (w/v). The flow rate of the fluorophore (Q_3) was decreased and, simultaneously, both PEG precursors flow rates (Q_1 and Q_2) were increased, resulting in microgels with higher PEG content and lower fluorescence intensity. The micrographs show decreasing red fluorescent intensity for microgels with increased PEG content. **c**, Atomic force microscopy was employed to measure the microgel elastic moduli and image-based analysis for the microgel intensity: both microgel elastic moduli and intensity show a linear trend with PEG content. **d**, Linear correlation between the microgel intensity and the elastic modulus. **e**, Mixed populations of microgels generated by computer-controlled programming of the flows: different fluorescence intensities encode for the different microgel elasticities. **f**, Hierarchical clustering shows four microgel populations distinct in their fluorescent intensity and diameter. The intensity correlated well with the microgel diameter (i.e. with the microgel swelling): the higher the fluorescence, the lower the microgel diameters. **g**, Based on the intensity level of the four microgel populations, generated separately previously, we linearly correlated the fluorescent intensity of the mixed microgels population with the elastic modulus. **h**, Correlation between the intensity of four separated populations and the intensity of four populations obtained by clustering within a pool of mixed microgels. Good correlation was found, as represented by close proximity of the interpolation line with the bisecting line. Scale bars 100 μm.

The previous experimental relationship between the elastic modulus and the intensity of four independently generated microgel populations was used as calibration curve. Therefore, an average intensity was calculated per each microgel population at a specific PEG content, and the elastic modulus was extrapolated from the calibration curve (Figure 5.2g). We found that the elasticity of the four mixed microgel populations was in good agreement with the values measured from the four microgel populations in the calibration curve. To verify it, the fluorescence intensity of each of the four independently generated populations was plotted against the fluorescence intensity of each microgel population within the mixed pool (Figure 5.2h). A good correlation was found in comparison to the bisecting line, demonstrating the solidity of the system. Furthermore, the clustering method was validated for its ability to measure the intensity of a pool of mixed microgels. Therefore, four separated populations were mixed together and image-based analysis was used to cluster, within the pool, four populations and to measure the intensity of each one. The intensity of four separated microgels was then compared to the intensity of four populations measured by image-based analysis. Almost no difference could be appreciated, as represented by close proximity of the interpolation line with the bisecting line (Appendix C, Figure S3).

These data show the possibility to generate microgels with different mechanical properties by modulating the flow streams in a microfluidic device. Moreover, microgel elasticity can be linearly encoded by the intensity of a fluorescent moiety incorporated in the gel. Furthermore, computer-controlled modulation of the flows allows the generation of a population of mixed microgels with varying elasticities and fluorescent intensities. Image-based analysis can be performed to separate the microgel populations based on the intensity levels that can be reliably used to estimate their elasticity, due to the linearity of the system.

**Programmable synthesis of microgels having variable bioactivity**

Many cellular processes are governed by signaling cues that act in a highly concentration-dependent manner.[17-20] Hence, the formation of microgels displaying variable biomolecular contents would be of utmost interest.

As a model, a peptide, containing the cell-adhesion binding motif, RGD, and a cysteine, was rendered fluorescent by functionalization with an Alexa488 moiety (Alexa488-Cys-RGD). The thiol groups of the cysteine reacted with the vinyl sulfone groups of the PEG, resulting in the incorporation of the fluorescent peptide within the gel network.

In order to generate microgels with variable bioactivity but equal elasticity, the addition of another channel in the previous microfluidic design is needed. Thus, the two middle streams were perfused with buffer and Alexa488-Cys-RGD, respectively. The reaction between thiol groups of Cys-RGD and vinyl sulfone groups (in 20% excess) on the PEG was expected to result in microgels bearing fluorescent RGD (Figure 5.3a). Decreasing the protein stream (Q_4) and simultaneously increasing the buffer flow rate (Q_3) while keeping the two PEG precursors (Q_1 and Q_2) constant, should result in the formation of microgels with decreasing fluorescence intensity. Hence, the amount of fluorophore would be indicative of the amount of peptide within the microgels (Figure 5.3b). The buffer was used to uncouple the peptide concentration and the microgel elasticity: it allowed modulating the peptide flow rate without diluting the PEG components, resulting in microgels with the same PEG content.

Next, we modulated the flows over time in order to generate combinatorial microgel populations in a single experiment. Similar to the *on chip* modulation of microgel stiffness described above, automated modulation of the flows allowed the formation of a mixed population of microgels possessing different RGD concentrations (Figure 5.3c). We generated fluorescent microgels at specific flow conditions (Appendix C, Table S3) to get 5% microgels at four RGD concentrations (0.08, 0.06, 0.04 and 0.02 mg/ml). Fluorescence intensity and microgel diameter were determined through image-based analysis, and clustering of the data shows four populations with different fluorescence intensity but equal diameter (Figure 5.3d). Elastic moduli were measured by AFM to verify that the microgels were characterized by the same elasticity. Microgels containing 5% (w/v) PEG content, but at different amounts of Alexa488-Cys-RGD, were analyzed and compared with microgels that had the same PEG content but no bioactive ligand. A statistically non-significant difference between the two populations was measured (Figure 5.3e).

To precisely correlate the microgel intensity with the actual peptide concentration retained within the microgels, the incorporation efficiency was determined. Therefore, gels containing increasing amounts of fluorescent peptide were analyzed for the fluorescence of the peptide released. Figure 5.3f shows the mass of peptide non-incorporated in comparison with the total theoretical RGD mass in the gels. More peptide was released when more peptide was conjugated in the gel, following a linear trend. Nevertheless, the percentage of RGD released was constant and statistically non significant (around 2.5%) throughout all the conditions (Figure 5.3g). Therefore, the experimental correlation between microgel intensity and peptide concentration could be well fitted with a linear interpolation (Figure 5.3h). Taken together, these data show that we were able to generate microgels having different concentrations of bioactive ligand yet equal elasticity. Moreover, the efficient peptide incorporation allows for linearly correlating the microgel intensity with the peptide concentration.
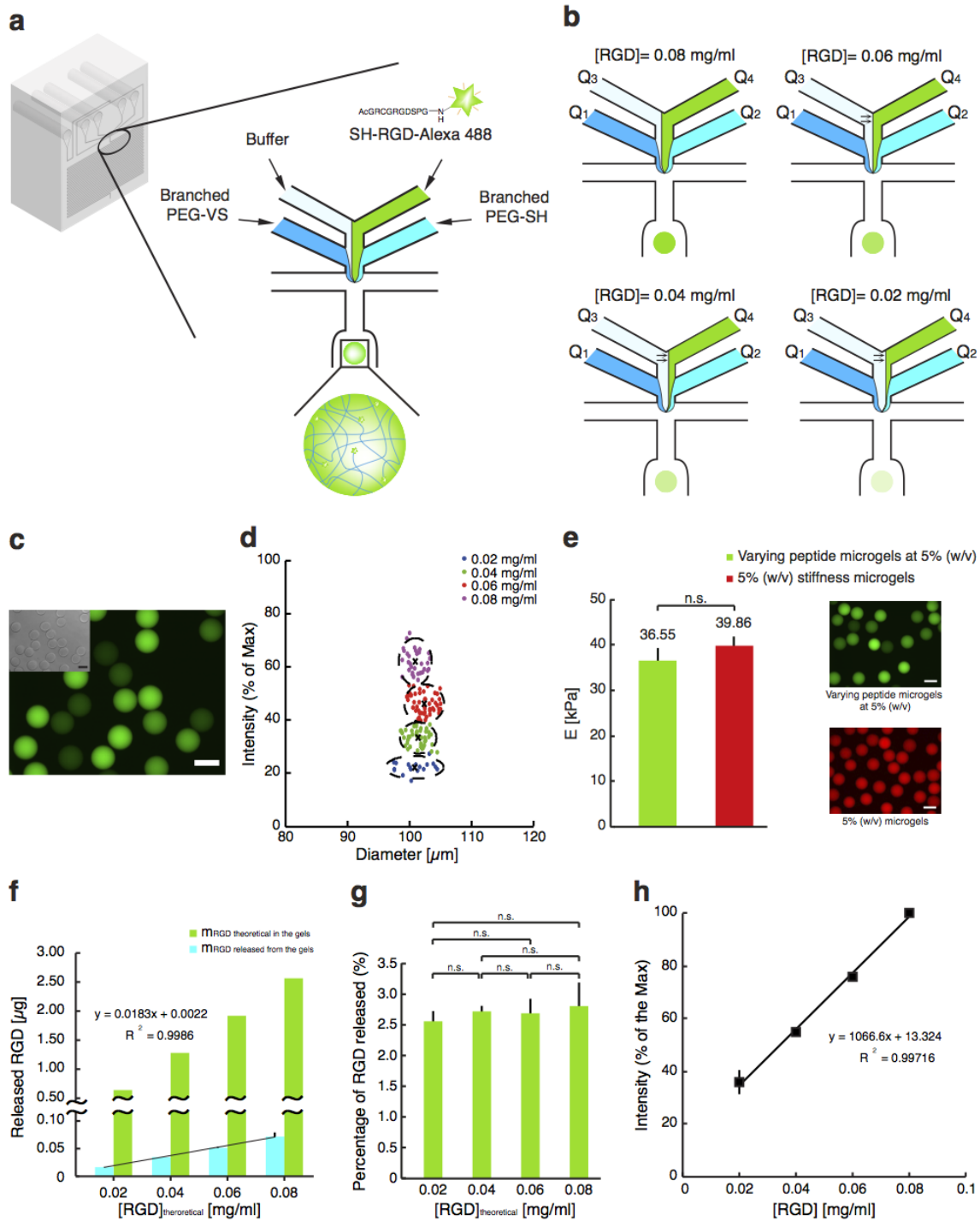
Figure 5.3 - Microfluidic generation of microgels with varying biochemical ligand concentrations. a, Schematic displaying the microfluidic chip used for the generation of microgels with different bioligand concentrations: four inlets are depicted for flowing the two PEG components, the buffer and Alexa488-Cys-RGD. *On chip* mixing of all the components leads to the polymerization of fluorescent microgels, containing specific concentrations of the fluorescent bioactive ligand. **b**, Four distinct microgel populations were generated, by computer-controlled modulation of the flows, at four distinct RGD concentrations: 0.02 (mg/ml), 0.04 (mg/ml), 0.06 (mg/ml) and 0.08 (mg/ml). Microgels with 5% (w/v) PEG content were

generated. The flow rates of both PEG precursors (Q_1 and Q_2) were kept constant to assure the formation of microgels with the same elasticity. Microgels with increasing RGD content were formed by increasing the flow rate of the fluorescent bioactive ligand (Q_4) and simultaneously decreasing the flow rate of the buffer (Q_3), resulting in microgels with higher fluorescent intensity. **c**, The micrograph shows the mixed populations of microgels generated by computer-controlled programming of the flows: different fluorescence intensities encode for the different bioligand concentrations within the microgels. **d**, Hierarchical clustering shows four microgel populations distinct in their fluorescent intensity but having the same diameter. With the same PEG content, microgels undergo swelling to the same degree, resulting in microgels with the same diameter. Higher bioligand concentration resulted in higher fluorescence intensity. **e**, Atomic force microscopy measurements show no significant difference in the elastic modulus of microgels with variable bioactivity at 5% (w/v) PEG content compared to that of microgels with homogeneous bioactivity at the same PEG content. **f**, Release assay performed on 5% (w/v) PEG content hydrogels with an increasing concentration of fluorescent peptide. The green bars represent the theoretical mass in µg of RGD within the gel, and the light blue bars the mass in µg of RGD released in the supernatant. As expected, the mass of RGD released linearly increased for increasing RGD final concentration within the gel. **g**, Percentage of RGD released at increasing RGD concentrations within the gel: in all conditions the percent of release is around 2.5% and there is no significant difference between all the conditions. **h**, The experimental relationship between the microgels intensity and the peptide concentration shows therefore a linear trend. Scale bars 100 µm.

Combinatorial generation of a compositional landscape of bioactive microgels

To generate microgels with modular elasticity and bioactivity, we designed a new microfluidic chip with two downside channels for PEG supply and three upside channels for the stiffness-encoding fluorophore, the buffer and the fluorescent peptide (Figure 5.4a). Incorporation of both fluorescent components was achieved without any molar excess of reactive group, therefore without preferential binding affinity of one of the two reacting moieties. Hence, the modulation of the flows would lead to the formation of combinatorial microgel environments with distinct stiffness and protein content, each of them specifically encoded by different intensity levels of one of the two fluorophores.
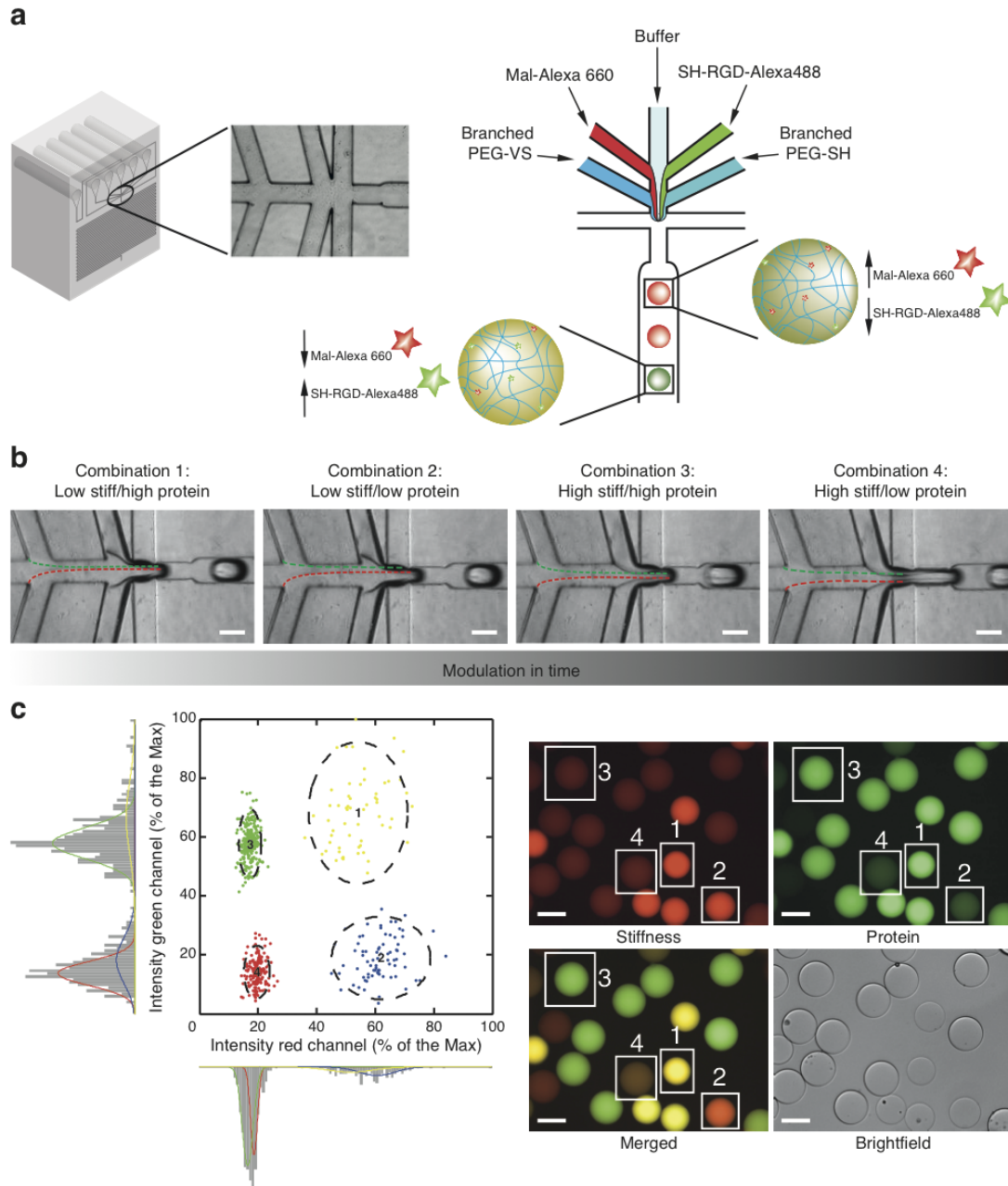
Figure 5.4 - Microfluidic generation of combinatorial microgels. **a**, Schematic displaying the microfluidic chip used for the generation of combinatorial microgels: six inlets are used to flow the two PEG components, the maleimide-conjugated fluorophore, the buffer and the fluorescent thiolated bioligand. *On chip* co-polymerization of all the components will lead to fluorescent microgels with different levels of both fluorophores. **b**, Computer-controlled modulation of the flows allows the *on-chip* formation of combinatorial microgels. Four distinct combinations were targeted. The micrographs show how the stream flows change over time in each condition. The PEG streams (bottom channels) are wider, and the maleimide fluorophore stream, marked with a red line, is simultaneously narrower when stiffer microgels are generated (combination 3 and 4). The stream of the bioligand, marked with a green line, is wider when microgels with higher peptide content are generated (combination 1 and 3). **c**, Scatter plot representing the intensities of the red and the green fluorophores of the four populations. Hierarchical clustering was employed to distinguish the four populations, containing different amounts of the fluorophores. The

histograms show the Gaussian distribution of the intensity for each population in each channel. The fluorescent micrographs help to visualize the four microgel populations. Scale bars 100 μm.

As a proof of principle, four combinatorial microenvironments were generated at flow conditions summarized in the Table S4 of the Appendix C. 2.5% (w/v) and 10% (w/v) were selected as PEG contents and 0.08 mg/ml and 0.02 mg/ml as peptide concentrations. Figure 5.4b shows the formation of the combinatorial microgels for each combination. The stream widths were modulated in time by adjusting the flow conditions to obtain each specific microgel population (Movie S3-S4, Appendix C, Table S4). For instance, microgels with low stiffness and high peptide content (*i.e.* combination 1) were generated by using a higher red fluorophore flow rate, higher peptide flow rate and lower PEG flow rates, whereas microgels with high stiffness and low peptide content (*i.e.* combination 4), were formed by imposing a low red fluorophore flow rate, low peptide flow rate and high PEG flow rates. Image-based analysis and clustering revealed the presence of four distinct combinatorial microgel populations, which were characterized by high and low stiffnesses (*i.e.* low and high red fluorescence, respectively) and by high and low peptide concentrations (*i.e.* high and low green fluorescence, respectively). The scatter plot represents each microgel as a dot with a specific value of green and red intensities in the red-green intensity plane (Figure 5.4c). The soft microgels, characterized by high red fluorescence, show higher fluorescence variability in both channels, as demonstrated by a greater population scattering as well as a wider gaussian distribution, which is reported on the side of the scatter plot. The increased variability can be attributed to the less efficient incorporation of both fluorophores at lower PEG content, in which less active groups are available for binding. A release assay performed on combinatorial gels (Appendix C, Figure S4) demonstrated a higher percent of release of both fluorophores at lower PEG concentration (*i.e.* combination 1 and 2), accompanied by higher standard deviation. However, at equal PEG content, the percent of both fluorophores release is constant, independent on the PEG concentration, in accordance to the data shown in Figure 5.3g. In addition, we looked at the fluorescent intensity as a function of microgel diameter, which is directly correlated with the microgel elasticity, as previously demonstrated in Figure 5.2f. The scatter plot in Figure 5.5a shows a decreasing red fluorescence of microgels with higher diameter, *i.e.* higher swelling ratio and, therefore, higher elasticity. On the contrary, the green intensity was not correlated with the microgel diameter, as shown in Figure 5.3d, resulting in 4 distinct populations in the green-diameter plane.

To prove the versatility of our technology in producing diverse combinatorial microgel populations, the flows were programmed to generate sixteen distinct populations (Appendix C, Table S5, Figure S5). Going further, flow programming was employed to generate a continuous landscape of up to one hundred different microenvironments, targeting ten elasticities having PEG content between 2.5% (w/v) and 10% (w/v) and ten RGD concentrations in the range between 0.02 mg/ml and 0.08 mg/ml (flow conditions in the Table S6 of the Appendix C). Figure S6 of Appendix C shows the distribution of the intensities of both channels for four and one hundred combinatorial microgel populations. The latter condition was characterized by homogenous distribution of the intensities, preventing clear distinction of populations in the red-green intensity plane. The relationship between fluorescence intensity and diameter (Figure 5.5c) showed no correlation for the green fluorescence and the microgel size. However, decreasing red

intensity with increasing diameter suggested the generation of multiple elasticities within the microgel populations. The data were also displayed as 3D surfaces and as heat maps for all the combinatorial conditions tested (Figure 5.5b-d, Appendix C, Figure S5c).
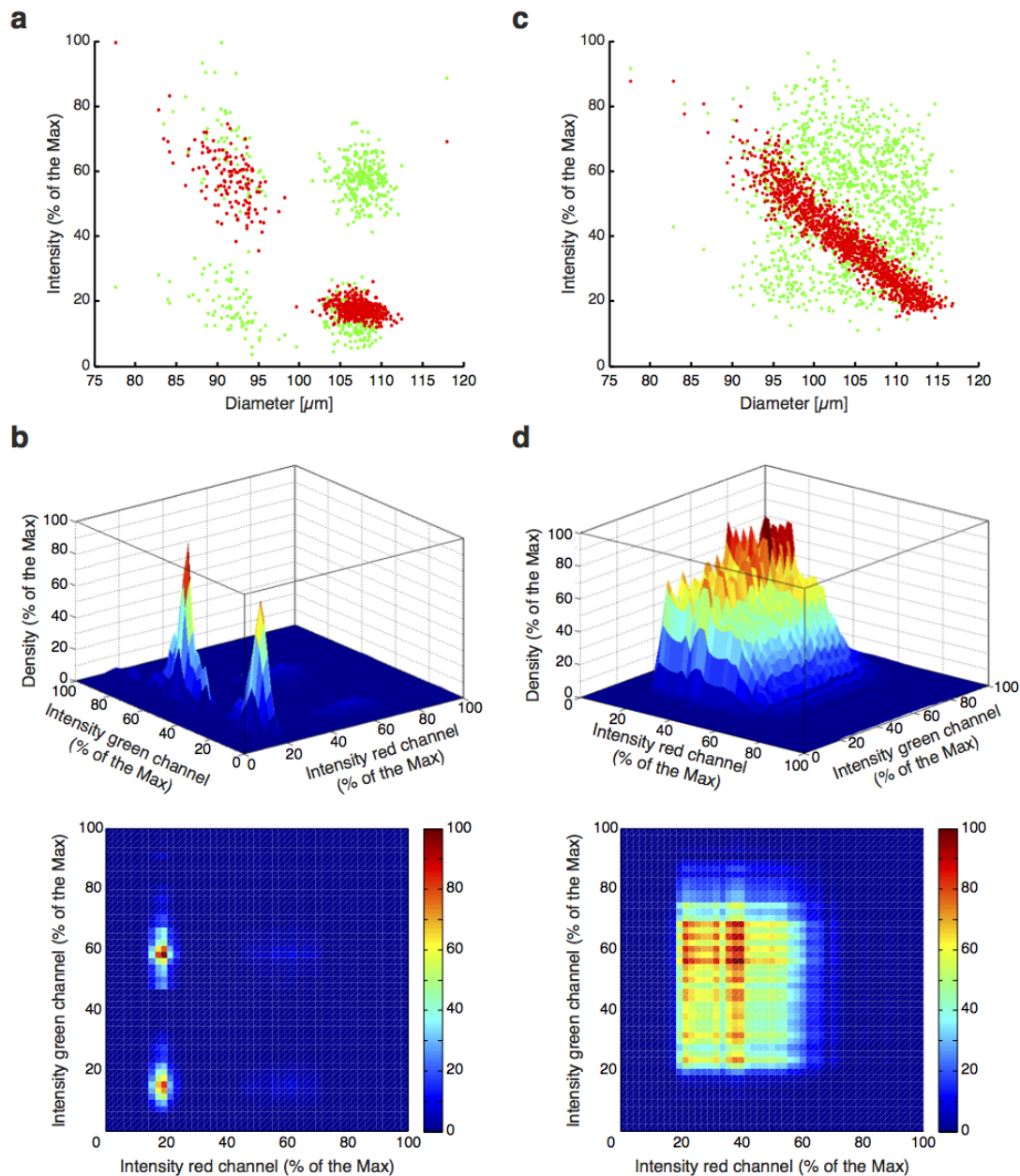
Figure 5.5 - Scatter and density plot of a library of combinatorial microgels. a, Scatter plot showing the intensity of both fluorophores as a function of the microgel diameter for four distinct populations. The diameter reflects the swelling ratio of the microgels. Softer beads, characterized by higher red fluorescence, are smaller on average than stiffer beads, characterized by lower red fluorescence. The green fluorescence is scattered in four separated regions of the intensity-diameter plot, showing no correlation between the peptide content (*i.e.* the green fluorescence) and the microgels size. **b,** Density plot showing four distinct populations as a 3D surface (top) or a heat map (bottom). **c,** Scatter plot showing the intensity values of both fluorophores as a function of the microgel diameter for one hundred populations. The intensity of the

red fluorophore is decreasing as the diameter increases, whereas the green intensity covers a wide range of values for both parameters and thus shows no correlation with diameter. **d**, Density plot showing a continuous landscape of microgel properties, represented as a 3D surface (top) or a heat map (bottom).

To verify whether a change in the fluorescence intensity correlates to an actual change of the microgels properties, we tested for the variation in the intensity measurements ascribed to the microscope imaging. Hence, we confined the microgels within microwells and we imaged them every minute for 10 minutes. The intensity values of 15 independent beads containing the highest RGD concentration (0.08 mg/ml) were tracked by using the same illumination settings (Appendix C, Figure S7). A percentage error in the intensity level of around 2% was calculated for all the beads, suggesting that the imaging does not significantly affect the intensity measurements.

Biological assays on combinatorial microgels

To prove that our technology permits cell culturing to investigate biological responses to different microenvironmental conditions, combinatorial microgels were used to support cell adhesion and proliferation on their surface. To perform this analysis, the biological readout of interest must be detectable by fluorescence. To show how this technology can be adopted for biological assays, we looked at cell proliferation and epithelial-to-mesenchymal transition (EMT).

In case of cell proliferation, the number of cells can be estimated by looking at the intensity of the DAPI signal, which stains the nuclei. Normal murine mammary gland (NMuMG) cells were cultured in suspension on four combinatorial microgel populations, generated at flow conditions summarized in the Table S7 of the Appendix C: 2.5% (w/v) and 10% (w/v) were chosen as PEG contents and 1.08 mg/ml and 0.54 mg/ml as RGD peptide concentrations, to support adequate cell adhesion. Images were acquired in multiple fluorescent channels, upon staining cell nuclei with DAPI on different days. A proliferation trend could be detected comparing the DAPI signal at day 1 to day 7, showing a higher intensity at later time points (Figure 5.6a).

The system also allows the expression of any specific biological markers of interest to be investigated. To prove this, we looked at TGF-ß-induced epithelial-to-mesenchymal transition.[21,22] Cells were cultured in presence or absence of TGF-ß on combinatorial microgels with the same mechanical and biochemical properties as before. After 2 days of treatment, cells were stained with DAPI. As expected, a decrease in the DAPI signal was observed due to fewer cells remaining adherent on the microgels after treatment with TGF-ß, which is commonly known to have an anti-mitogenic effect.[23] Furthermore, immunostaining was performed to detect the expression of an epithelial marker, E-cadherin, and a mesenchymal marker, vimentin. Next, images were acquired in all the four fluorescent channels (Figure 5.6b). Normal epithelial morphology could be seen in absence of TGF-ß and independent of the microgel property. However, when treated with TGF-ß, cells changed their morphology depending on the microgel property. In accordance with the literature,[24-26] cells maintained an epithelial-like round shape on soft microgel (characterized by high red intensity), while being more elongated on stiff microgels (characterized by low red intensity), which suggests a mesenchymal phenotype.

These examples show the ability to perform biological assays on combinatorial microgels and to observe the expression of specific markers of interest through traditional immunostaining techniques.
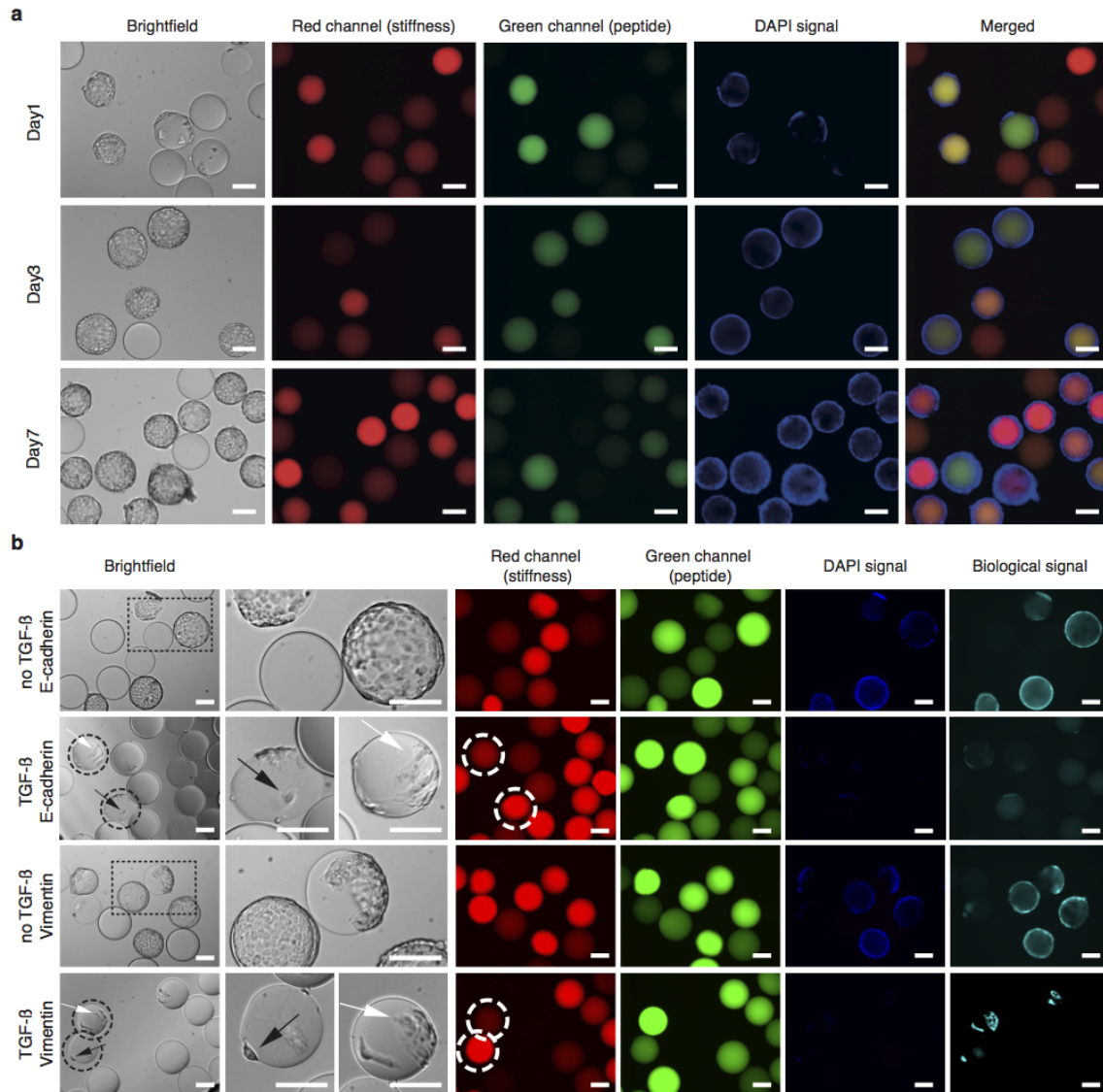
Figure 5.6 – Biological assays on combinatorial microgels. **a**, NMuMG cells cultured on four combinatorial microgels for up to 7 days. Cell nuclei were stained with DAPI as a marker for proliferation at different days of culture. Fluorescent images were acquired in the red channel, which encoded for microgel elasticity, in the green channel, encoding for the RGD concentration, and in the blue one, for the DAPI signal. **b**, Micrographs showing combinatorial microgels, supporting NMuMG cells adhesion in presence or absence of TGF-ß. Cells nuclei were stained with DAPI, and immunostaining was performed for E-cadherin and vimentin. Enlargements from the brightfield images show cell monolayers in absence of TGF-ß. On the other hand, in presence of TGF-ß, cells maintained a round morphology (black arrows) when cultured on soft microgels (characterized by high red fluorescence), whereas cells were more elongated (white arrows) on stiff microgels (characterized by low red fluorescence). Scale bar 100 μm.

Discussion

Synthetic hydrogels have quickly become increasingly important for various biomedical applications, such as drug delivery, diagnostic and tissue engineering. To cover this broad spectrum of applications, biomaterials must be incredibly diverse. Therefore, there has been an urgent need to precisely synthesize hydrogels with specific physico-chemical properties. Unfortunately, discovering new hydrogel formulations is a trial-and-error process in which many conditions must be tested in a combinatorial fashion. Microarray technologies have been developed to screen thousands of combinations of polymers or hydrogels. However, the cost of using these technologies, as well as the difficulty in manipulating their final products, prevents them from reaching their full potential for high-throughput screening applications.

Here, we present a powerful microfluidic platform to generate combinatorial microgels with varying elasticity, biochemical ligands or both. A programmable approach was employed to sequentially dilute the biophysical gel building blocks with fluorescent moieties *on chip* by changing the flow rates in an automated fashion. Through this approach, microgels with varying elasticity were synthesized and distinguished based on the intensity of a fluorophore. Atomic force microscopy analysis showed a linear correlation between the intensity and the stiffness of the microgels, with elastic moduli spanning in a range of cell physiology relevance[2] (from 10kPa up to 100 kPa). Furthermore, the programmable approach was implemented for the generation of microgels with varying biochemical ligand concentrations. As a model protein, we chose Alexa488-functionalized cell adhesion-promoting thiolated-RGD peptide. The versatile chemistry allows the functionalization of any growth factor or morphogen of interest for selective incorporation within the network. Due to the extremely efficient binding affinity, the linear correlation between microgel intensity and ligand concentration was highly reliable and suggested tight control over the microgel composition. Combining the two approaches permitted the generation of microgels with specific elasticities and protein concentrations in a combinatorial fashion. The encoding approach was adopted to track the elasticity and ligand concentration of each microgel population in the red-green fluorescence plane. Fine modulation of the microfluidic flows allowed a continuous landscape of one hundred microgel combinations to be formed, each bearing specific physico-chemical properties.

Finally, we proved the possibility to culture cells on combinatorial microgels and to track the fluorescence of specific markers of interest over days. For instance, cell proliferation could be studied by looking at the DAPI signal, and epithelial-to-mesenchymal transition could be investigated by relating the expression of epithelial or mesenchymal markers, such as E-cadherin or vimentin, to the microgel properties. However, the fluorescent signal generated by cells adherent to a 3D surface requires the acquisition of stacks by confocal imaging to reliably quantify the signal. Unfortunately, confocal imaging is time-consuming and incompatible with high-throughput analysis. Flow or mass cytometry represent attractive alternatives for quantifying the signal, and the ease of microgel manipulation and distribution makes them appealing to be used with these technologies,[6,11,27] paving the way towards new and more powerful methods of performing screens. Therefore, in the next chapter, we tailored the microfluidic technology to generate microgels with a compatible size for flow cytometry-based analysis.

We strongly believe that our novel platform has an unprecedented potential for screening of multifactorial microenvironments in many biological systems, such as in the stem cell field [18,28-30], cancer biology [24,25,31] and mechanobiology [3,32]. In fact, cells could be easily cultured on the surface of [4] or inside the microgels [5-7], allowing the effect of microenvironmental perturbations on the expression of genes of interest to be investigated in both 2D and 3D settings.

Furthermore, the versatility of the technology readily permits the generation of 'on-demand' microgels with desired properties. For instance, a combinatorial library of two growth factors of interest could be generated by replacing the stiffness fluorophore with another bioactive component. In addition, the simple insertion of multiple microchannels in the microfluidic design allows multi-component combinatorial libraries of cells microenvironments to be generated. These libraries could then be used to study the effect of substrate elasticity and multiple growth factors on cell behavior in a high-throughput fashion.

Experimental section

Chip Fabrication. For the generation of microgels with varying elasticities the two upside lateral microchannels were designed forming 45° with the oil channels, whereas for the generation of microgels with different protein concentration as well as combinatorial microgels the two downside and upside lateral channels were designed respectively forming 30° and 60° angles with the oil channels. The height of the channels was 100 μm and the width of the upstream channels was 75 μm. All the different microfluidic devices were fabricated as already explained in [4]. Briefly, PDMS chips (Sylgard 84, Dow Corning) were fabricated from SU8-patterned silicon masters using conventional soft lithography and, subsequently, bonded on oxygen plasma-activated hydrophobic substrates and baked at 80°C overnight.

Microfluidic Synthesis of Combinatorial Microgels. The microfluidic chip was connected through flexibile Tygon tubings to Socochim syringes (Switzerland), previously filled with PEG solutions, maleimide-Alexa660 solution, fluorescent peptide solution, triethanolamine buffer (0.3M, pH8) and hexadecane (Sigma, U.S.A.) with 2% (w/v) ABIL EM surfactant (Evonik, Germany) as oil phase. Four-arm PEG end-functionalized with thiols (4-arm-PEG-SH, 10kDa) (NOF, Japan) was reconstituted in bidistilled water and vinylsulfone-functionalized eight-arm-PEG (8-arm-PEG-VS, 10kDa) (NOF, Japan) in triethanolamine buffer. Depending on the targeted molar excess of functional groups, the syringes were filled with PEG solutions at different concentrations: the concentration of PEG-SH for all conditions was 20% (w/v), whereas the concentration of the PEG-VS was 8.33% (w/v), 10% (w/v) and 12% (w/v) for a 20% SH-excess, for no excess of any functional group and for a 20% VS-excess, respectively. Microgels washing procedure followed the protocol reported in [4].

Syringe Pump Programming. Programmable syringe-pumps (neMESYS, Cetoni, Germany) were used to control the flow rates of the different components. The flow profile mode of the software was used for setting each syringe flow for 5 minutes at rate conditions summarized, for each experimental condition, in the Supplementary tables of Appendix C. The sum of the flow rates of the three streams was maintained constant to 5 μl/min, while simultaneously changing them independently. The oil phase flow rate was set at 10 μl/min, allowing the formation of microgels, before swelling, with the same diameter, around 100 μm.

Chemical Release Assays. Maleimide-Alexa660 (Lifetechnologies, U.S.A.) and CRGDLF(Lys)-FITC (GenScript, U.S.A.) were used for the release assays. They were both reconstituted in water at desired concentration immediately before use. 10μl gels were casted in IBIDI μ-chambers at the same conditions used for the generation of microgels with varying stiffness or different bioligand concentrations. 50 μl of PBS was added and collected after 24h for measuring the fluorescence at 660 nm (for the maleimide-

Alexa660 moiety) and at 488nm (for the FITC-peptide) by means of a spectrophotometer (Tecan, U.S.A.). Total mass of RGD released from the gels was then calculated based on calibration curve measurements.

Peptide Fluorescent Bioconjugation. Ac-GRCGRGDSPG-NH$_2$ (GL Biochem, China) and N-hydroxysuccinimide (NHS) ester-Alexa488 fluorophore (Lifetechnologies, U.S.A.) were reconstituted in water, mixed together with 10% molar excess of peptide. The pH of the solution was adjusted to 7.4 by adding PBS 10x and the components were let react for 1 hour. The unreacted succinimidyl groups were subsequently cleaved with TRIS buffer at pH 7 for 30 min.

Atomic Force Microscopy Measurements. Microgels and bulk gels were immobilized onto glass substrates by following the protocol in [4]. All measurements were carried out using a NanoWizard II atomic force microscope (JPK Instruments, Germany) and performed in PBS. Conical silicon cantilevers with a Cr/Au backside coating (CSC37/Cr-Au, MikroMasch, U.S.A.) and a nominal average spring constant of 0.3 N/m were used to indent the samples, applying an indentation force of 100 nN. Force-distance curves were analyzed with JPK Data Processing software (Appendix C, Figure S2b), applying the Hertz model to calculate the Young's modulus (Poisson's ratio considered 0.5). Each microbead and bulk gel were analyzed by indenting three different points and measurements were performed on 20 beads and 3 gels per condition.

Image Acquisition and Analysis. Images were acquired using an inverted Olympus IX81 CellR microscope equipped with a Hamamatsu camera. All the illumination settings were kept constant during the acquisition of all the images and different parameters were chosen to minimize the cross-talk between the two channels: time of exposure of 200ms and 1ms, 100% and 70% lamp intensity and binning 1 were used during the acquisition of the far red channel (ex. 650/13) and the green channel (ex. 485/20), respectively. Multiple images were acquired in order to generate a numerous (ca. 200) beads population for enhancing the significance of the experiments. Each image was taken in different wavelengths, brightfield, far red (660nm) and/or green fluorescence (488nm), and stored in the same folder, assigning an increasing index and a code for the wavelength in a 16-bit codification. Matlab (Mathworks, Natick, U.S.A.) script was developed for image analysis and subsequent data clustering. After loading of the images, the intensity of the red and the green channels were summed to enhance the contrast between the beads and the background and a watershed-based routine was used to create a binary mask, discriminating each bead from the background. Beads diameter and intensity in both channels were then measured for each bead. All the experiments were repeated independently three times and the intensity shows the average value of three independent repetitions of a sample of around 200 beads.

Hierarchical Clustering. A Matlab script was also developed for the data hierarchical clustering was performed based on the expected number of stiffness and/or protein concentration classes. Linkage function was used to measure the relative distance between the data and the cluster function was adopted for the classification. Data were represented as a scatter plot where each bead was represented by a dot with a specific value of intensity. Combinatorial microgels were represented as a scatter plot in the stiffness (red intensity)-protein (green intensity) plane where different colors encode for distinct beads populations. For each bead population the intensity distribution for both channels was represented by an ellipse in the plane and by a gaussian projected along each axis.

Cell Culture on Combinatorial Microgels. Normal murine mammary (NMuMG) cells were generously provided by Prof. Christofori, Department of Biomedicine, University of Basel, Switzerland. They were cultured on tissue culture flasks in Dulbecco's Modified Eagle Medium (DMEM) with 10% Fetal Bovine Serum (FBS), pen-strep (10mg/ml). After dissociation with trypsin (TripLE express, Gibco), cells were cultured on combinatorial microgels in a suspension bioreactor (BioLevitator, Hamilton, Switzerland). During the inoculation phase, the rotation speed of the tubes was 50 rpm with an agitation period of 2 min for an entire duration of 4 hours. The agitation pause duration was set at 10 min to minimize microcarrier 'bridging'. During cell culture, the rotation speed was increased to 80 rpm for all cell types. Cells were seeded on microcarriers at a density of 14'200 cells/cm^2 (corresponding to ca. 10 cells per carrier). 6 ml of

medium was used during the inoculation phase (to maximize cell-microgel contact) and 20 ml during cell culture.

Immunostaining. Fixation with paraformaldehyde (PFA) (4%, 10 min) was followed by membrane permeabilization with a solution of TritonX 0.2% in PBS for 5 min. Incubation with a goat serum blocking solution for 2 hours was followed by overnight incubation with a monoclonal mouse antibody to E-cadherin or vimentin (1:100, Sigma, USA). After extensive washing, primary antibodies were stained by anti-mouse (1:500) Alexa546-labeled secondary antibodies (Lifetechnologies, USA) for 2 hours. DAPI (1:1000) was then added for 15 min.

Microwell Fabrication. The microwells were fabricated following the protocol in [33]. Thin PEG hydrogel films, formed by 10kDa PEG precursors with either thiol (TH) or vinylsulfone (VS) reactive groups, were cast at the bottom of four-well plates (Nunc). A topologically structured silicone stamp with micro pillars of 450 um in diameter and 100 um in height, custom-made by microfabrication, was used to soft-emboss the partially cross-linked hydrogel film. Subsequent to embossing, microwell arrays were de-molded, washed with PBS and UV-sterilized.

References:

1   Celiz, A. D. *et al*. Materials for stem cell factories of the future. *Nat Mater* **13**, 570-579 (2014).

2   Engler, A. J., Sen, S., Sweeney, H. L. & Discher, D. E. Matrix elasticity directs stem cell lineage specification. *Cell* **126**, 677-689 (2006).

3   Discher, D. E., Janmey, P. & Wang, Y. L. Tissue cells feel and respond to the stiffness of their substrate. *Science* **310**, 1139-1143 (2005).

4   Allazetta, S., Hausherr, T. C. & Lutolf, M. P. Microfluidic Synthesis of Cell-Type-Specific Artificial Extracellular Matrix Hydrogels. *Biomacromolecules* **14**, 1122-1131 (2013).

5   Headen, D. M., Aubry, G., Lu, H. & Garcia, A. J. Microfluidic-Based Generation of Size-Controlled, Biofunctionalized Synthetic Polymer Microgels for Cell Encapsulation. *Adv Mater* (2014).

6   Tumarkin, E. *et al*. High-throughput combinatorial cell co-culture using microfluidics. *Integr Biol-Uk* **3**, 653-662 (2011).

7   Rossow, T. *et al*. Controlled synthesis of cell-laden microgels by radical-free gelation in droplet microfluidics. *Journal of the American Chemical Society* **134**, 4983-4989 (2012).

8   Velasco, D., Tumarkin, E. & Kumacheva, E. Microfluidic encapsulation of cells in polymer microgels. *Small* **8**, 1633-1642 (2012).

9   Tan, W. H. & Takeuchi, S. Monodisperse alginate hydrogel microbeads for cell encapsulation. *Adv Mater* **19**, 2696-+ (2007).

10   Kumachev, A. *et al*. High-throughput generation of hydrogel microbeads with varying elasticity for cell encapsulation. *Biomaterials* **32**, 1477-1483 (2011).

11   Li, C. Y., Wood, D. K., Huang, J. H. & Bhatia, S. N. Flow-based pipeline for systematic modulation and analysis of 3D tumor microenvironments. *Lab Chip* **13**, 1969-1978 (2013).

12   Eydelnant, I. A., Li, B. B. & Wheeler, A. R. Microgels on-demand. *Nat Commun* **5** (2014).

13   Gilbert, P. M. *et al*. Substrate Elasticity Regulates Skeletal Muscle Stem Cell Self-Renewal in Culture. *Science* **329**, 1078-1081 (2010).

14   Chaudhuri, O. *et al*. Extracellular matrix stiffness and composition jointly regulate the induction of malignant phenotypes in mammary epithelium. *Nat Mater* **13**, 970-978 (2014).

15   Allazetta, S., Cosson, S. & Lutolf, M. P. Programmable microfluidic patterning of protein gradients on hydrogels. *Chem Commun* **47**, 191-193 (2011).

16   Lutolf, M. P. & Hubbell, J. A. Synthesis and physicochemical characterization of end-linked poly(ethylene glycol)-co-peptide hydrogels formed by Michael-type addition. *Biomacromolecules* **4**, 713-722 (2003).

17   Ashe, H. L. & Briscoe, J. The interpretation of morphogen gradients. *Development* **133**, 385-394 (2006).

18   Lutolf, M. P., Gilbert, P. M. & Blau, H. M. Designing materials to direct stem-cell fate. *Nature* **462**, 433-441 (2009).

19   Keenan, T. M. & Folch, A. Biomolecular gradients in cell culture systems. *Lab Chip* **8**, 34-57 (2008).

20   Mosiewicz, K. A. *et al*. In situ cell manipulation through enzymatic hydrogel photopatterning. *Nat Mater* **12**, 1071-1077 (2013).

21   Xu, J., Lamouille, S. & Derynck, R. TGF-beta-induced epithelial to mesenchymal transition. *Cell Res* **19**, 156-172 (2009).

22   Zavadil, J. & Bottinger, E. P. TGF-beta and epithelial-to-mesenchymal transitions. *Oncogene* **24**, 5764-5774 (2005).

23   Heldin, C. H., Miyazono, K. & ten Dijke, P. TGF-beta signalling from cell membrane to nucleus through SMAD proteins. *Nature* **390**, 465-471 (1997).

24   Lee, K. *et al*. Matrix compliance regulates Rac1b localization, NADPH oxidase assembly, and epithelial-mesenchymal transition. *Mol Biol Cell* **23**, 4097-4108 (2012).

25   Nelson, C. M., Khauv, D., Bissell, M. J. & Radisky, D. C. Change in cell shape is required for matrix metalloproteinase-induced epithelial-mesenchymal transition of mammary epithelial cells. *J Cell Biochem* **105**, 25-33 (2008).

26   Gomez, E. W., Chen, Q. K., Gjorevski, N. & Nelson, C. M. Tissue geometry patterns epithelial-mesenchymal transition via intercellular mechanotransduction. *J Cell Biochem* **110**, 44-51 (2010).

27   Cho, C. F., Azad, B. B., Luyt, L. G. & Lewis, J. D. High-Throughput Screening of One-Bead-One-Compound Peptide Libraries Using Intact Cells. *Acs Comb Sci* **15**, 393-400 (2013).

28   Ranga, A. *et al*. 3D niche microarrays for systems-level analyses of cell fate. *Nat Commun* **5**, 4324 (2014).

29   Watt, F. M. & Huck, W. T. S. Role of the extracellular matrix in regulating stem cell fate. *Nat Rev Mol Cell Bio* **14**, 467-473 (2013).

30   Ankam, S., Teo, B. K. K., Kukumberg, M. & Yim, E. K. F. High throughput screening to investigate the interaction of stem cells with their extracellular microenvironment. *Organogenesis* **9**, 128-142 (2013).

31   Leight, J. L., Wozniak, M. A., Chen, S., Lynch, M. L. & Chen, C. S. Matrix rigidity regulates a switch between TGF-beta 1-induced apoptosis and epithelial-mesenchymal transition. *Mol Biol Cell* **23**, 781-791 (2012).

32   Eyckmans, J., Boudou, T., Yu, X. & Chen, C. S. A Hitchhiker's Guide to Mechanobiology. *Dev Cell* **21**, 35-47 (2011).

33   Gobaa, S. *et al*. Artificial niche microarrays for probing single stem cell fate in high throughput. *Nat Methods* **8**, 949-955 (2011).

Chapter 6

High-throughput Analysis of Combinatorial Microgels

High-throughput Analysis of Combinatorial Microgels

Simone Allazetta, Lucas Delannoy and Matthias P. Lutolf

The ease of manipulation of microgels holds the promise to interface them with high-throughput analysis techniques, such as flow cytometry. Here, multiple microfluidic splitting junctions were designed to generate poly(ethylene glycol) (PEG)-based microgels with a diameter smaller than 30 µm, compatible with cytometry-based analysis. Finally, we proved microgels with combinatorial physico-chemical properties have the ability to support cell adhesion.
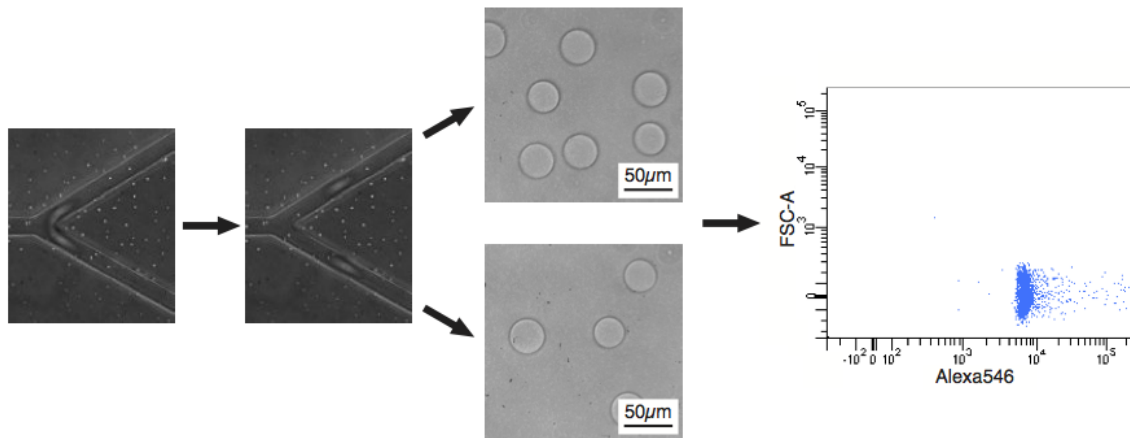
Introduction

High-throughput screening of multifactorial microenvironments allows cell behavior to be investigated more systematically in the stem cell field[1-4] and cancer biology,[5-7] as well as mechanobiology.[8,9] Since an intricate interplay of biophysical and biochemical cues governs many biological processes, *in vitro* platforms able to decouple the effects of the individual factors would be invaluable to address many fundamental biological questions.

The creation of various combinatorial microenvironment libraries requires a high degree of automation and miniaturization. Both qualities have been sufficiently progressed in cellular microarrays;[10,11] however, in the approach, cells cannot easily be manipulated for further analysis or exposed to certain chemical stimuli. Furthermore, these technologies can rarely be interfaced with high-throughput analysis approaches, such as flow or mass cytometry and rely on time-consuming image-based analysis techniques.

Droplet-based microfluidics has been used to create miniaturized gels that serve as either two or three-dimensional tools to study stem cell expansion and differentiation [12,13], growth and viability.[14-17] The ease of microgel manipulation make them very attractive tools to perform high-throughput screenings in an unprecedented manner, without employing expensive and complicated robotic equipment. Despite a few interesting examples[17-19], microgel technology has not yet been widely adopted in combination with high-throughput analysis approaches. This may be due to technical limitations impeding the use of big particles, such as microgels, with technologies developed specifically for small objects, such as cells. To address this issue, researchers have developed sorters capable of analyzing objects with dimensions ranging from 20 μm to 1500 μm. Unfortunately, the potential of these technologies is still not yet comparable to traditional flow cytometers that permit the simultaneous analysis of multiple fluorescent channels. However, using the majority of the available cytometry-based high-throughput techniques would require microgels with a size compatible with the fluidics of the machines, usually ranging from 10 μm up to 40 μm.

Droplet-based microfluidic technology permits strict control over the droplet size by modulating either the channel dimensions or relative flow rates.[20] However, excessive reduction of the microchannel size may lead to flow instabilities, which dramatically affect the microgel formation. On the other hand, increasing the flow rate of the discontinuous phase leads to a reduction of the droplet size until a lower size limit is reached.[21]

Here, we modified the microfluidic platform, which was developed in [12] for a stable generation of PEG-based microgels, with one or more Y-junctions to allow symmetric microgel splitting into smaller microgel daughters. We successfully generated microgels that have a size compatible with the majority of available high-throughput technologies (*i.e.* in a range from 25 and 40 μm). Flow cytometry analysis was performed on fluorescently labeled microgels and showed a clear separation from the negative control. Subsequently, we generated a library of four distinct combinatorial hydrogel microenvironments with various physico-chemical properties, encoded by the expression of fluorescent markers. Finally, we were able to show adhesion of mammalian cells on the surface of these microgels. We envision that the integration of microgels having combinatorial properties with high-throughput flow or mass cytometry analysis will significantly impact basic and applied cell biology, potentially unveiling the influence of exogenous signaling cues on cell behavior in both 2D and 3D.

Results and discussion

Microfluidic splitting of microgels

The microfluidic production of small, PEG-based microbeads followed the protocol reported in [12]. Microgels were formed by the copolymerization of multibranched PEG precursors, which were previously functionalized with vinyl sulfone (VS-) and thiols (SH-) functional groups. The microfluidic chip previously reported in Chapter 4 was redesigned to contain a mixing serpentine and a splitting junction. Figure 6.1a shows the different components of the microfluidic design. At the first junction, the two gel components form microgels upon breakup by the oil phase (1). Then, microgels pass through a serpentine where the gel components are homogeneously mixed (2), and subsequently pass through a channel restriction that accelerates the microgels (3) before being symmetrically split in a Y-junction (4). Two down-stream serpentines (5) allow the microgels to be collected into two separate reservoirs.

The characterization of microgel dimensions was performed with different channel dimensions. 50µm-high microchannels were patterned with two different widths of the upstream channels, 75 µm and 50 µm (named 75/50 and 50/50). Monodisperse microgels were generated in both conditions, as reported by the dimensional distribution in Figure 6.1b. The effect of various flow rate ratios (defined as the ratio between the flow rate of the oil phase and the flow rate of the water phase) was also investigated for different designs (Figure 6.1c). As previously reported[12,22,23], increasing the flow rate ratio or reducing the channel dimensions could decrease the microgel dimensions. Microgel diameters of 53.73 +/- 1.78 µm and 47.18 +/- 1.73 µm were measured at a flow rate ratio of 6 for channels 75µm- and 50µm-wide, respectively. Theoretical microbead dimensions are also reported for microfluidic designs with the same dimensions but without a splitting junction. When the volumes are not split by a Y-junction, the theoretical diameters are expected to be larger by a factor of 1.2 than when split.

To generate two homogeneous microgel populations upon splitting, two requirements need to be met. First, just after the Y-junction, the resistance of the two downstream serpentines has to be exactly equal to prevent asymmetric splitting of the microgels. Second, the gel components need to be mixed properly before the microgels are split. In fact, an inefficient mixing of the gel components would hinder correct polymerization and result in microgels with different mechanical properties and swelling ratios.[12] Therefore, right after formation, the microdroplets flow in a serpentine where multiple winding channels fold the fluid, allowing for a better mixing of the gel components. Microgels from the two separate outlets were then collected, and their dimensions were analyzed separately (Figure 6.1d). A non-significant difference in diameter was measured from microgels collected in outlet 1 compared to those in outlet 2, suggesting that mixing and microgel polymerization occurred properly.

However, most available high-throughput screening technologies, such as flow or mass cytometers, usually have an upper limit of 40 µm for objects being analyzed. Therefore, we implement a second splitting branch in the microfluidic device, which should allow the microgel dimensions to be reduced by a factor of 0.8 and be below the upper limit of detection (Figure 6.1e).

Thus, microgels were generated using microfluidic devices with the same height, 50µm, and upstream channel dimensions, 75 µm and 50 µm, as before (Figure 6.1f). The dimensional distributions show the formation of monodisperse microgels in both cases. Diameters were

measured at different flow rate ratios, showing smaller microgels than the ones generated with one single split. Moreover, the diameters agreed with the theoretical reduction factor of 0.8. The implementation of a microfluidic device containing two splitting junctions and having a height and upstream channels of 50 µm allowed us to generate microgels with an average diameter of 33.05 +/- 1.29 µm and 34.00 +/- 2.03 µm at flow rate ratios of 5 and 6, respectively. Therefore, this condition was selected to generate microgels for further analysis by high-throughput machines.
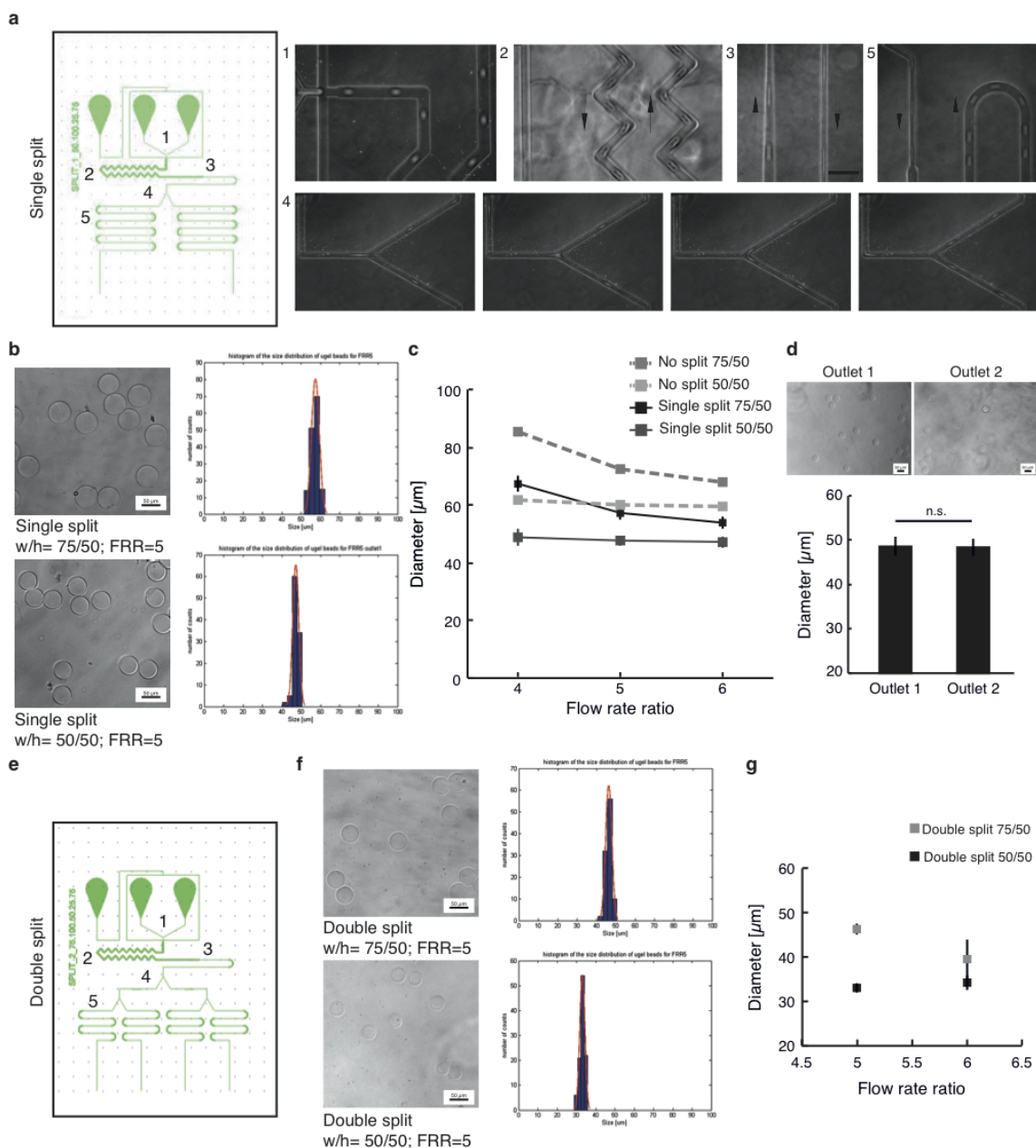
**Figure 6.1 – Generation of small microgels by microfluidic splitting. a**, Design of the microfluidic chip used to generate small microgels. The micrographs show the different parts of the layout: an initial junction where the two PEG components mix together and the microgels are formed (1), a serpentine for the correct homogenization of the two PEG components (2), a restriction to increase the microgel velocity (3), a

splitting junction with equal flow resistance where the two smaller daughter microgels are generated (4) and a final serpentine, which is connected to the chip outlets and decreases the microgel velocity (5). The sequential images reported in the panel 4 show the different phases of microgel splitting in two smaller daughter microgels. The arrows show the flow directions. **b**, Micrographs showing microgels formed by using microfluidic chips with one splitting Y-junction, with a height (h) of 50 µm and a width (w) of the upstream channels of 75 µm or 50 µm. The histograms on the side show the monodispersity of the microgels. The flow rate ratio (FRR) used was 5. **c**, Dimensional characterization of microgels generated at different flow rate ratios, by using chips with different microchannel sizes. Dashed lines interpolate the theoretical microgel diameters in the case of a microfluidic chip with the same dimensions but without a Y-junction. **d**, Diameters of microgels collected by two separate outlets of a 50µm-high microfluidic chip with an upstream channel dimension of 50 µm (flow rate ratio of 5). Micrographs show the microgels collected from the outlet 1 and 2. **e**, Design of a microfluidic chip with a second splitting branch. **f**, Micrographs and dimensional distribution of microgels formed by using microfluidic chips with two splitting Y-junctions, with a height (h) of 50 µm and with a width (w) of the upstream channels of 75 µm or 50 µm. **g**, Diameters of microgels generated with a double splitting design at different flow rate ratios and with different microchannel dimensions.

Flow cytometry analysis of microgels

To verify the feasibility of flow cytometer-based analysis, microgels were generated with a 50µm height, 50µm width and a double split microfluidic design. A maleimide-activated Alexa546 moiety was co-polymerized within the gel network to render the microgels fluorescent (Figure 6.2a). An unstained microgel population was generated as negative control. To confirm microgel size, the average diameter was measured with an image-based cytometer. Figure 6.2b shows a homogeneous microgel size distribution that has an average diameter of 24 µm, which is smaller than expected (around 34 µm) and likely suggests a partial deformation of the microgels during analysis.
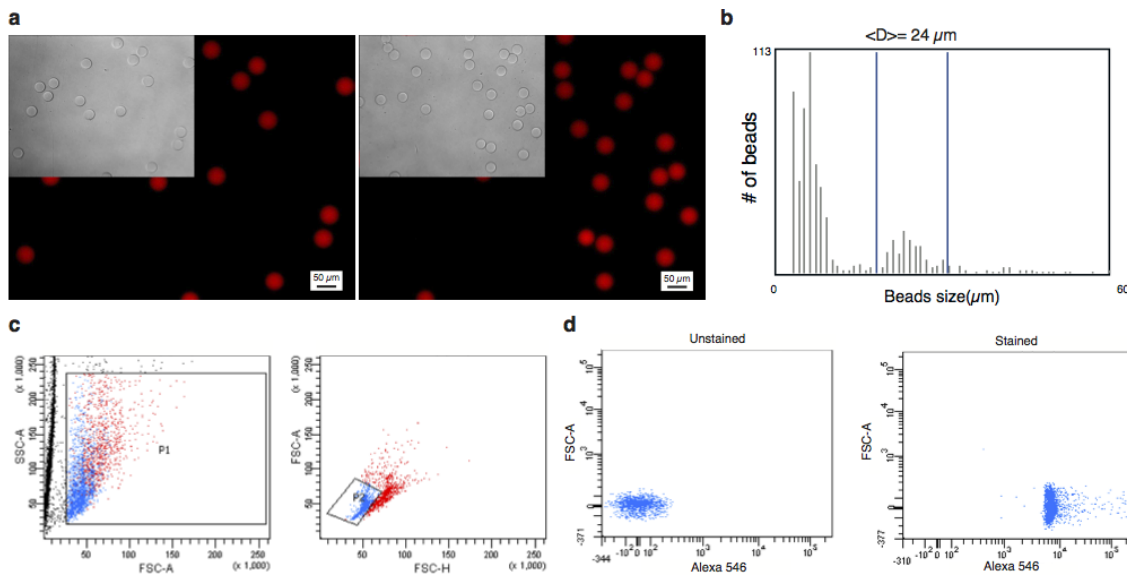
Figure 7.2 – Flow cytometry-based analysis of fluorescent microgels. a, Micrographs showing Alexa546-loaded microgels generated with a double split microfluidic chip with 50µm-high and 50µm-wide channels. **b**, Microgel dimensions analyzed by an image-based cytometer. The analysis gave an

average microgel size of 24 µm. **c**, Flow cytometry analysis performed on small microgels, reporting the dot plot relative to the forward scatter (FSC) versus the side scatter (SSC). A dot plot showing the height and the area of the forward scatter signal (FSC-H and FSC-A) was used to discard the doublets (marked in red) from the singlets (in light blue). **d**, Fluorescent signal from the unstained and the stained sample of single microgels.

Microgels were analyzed with a flow cytometer (Figure 6.3c-d). The forward scatter signal shows a microgel population with high homogeneity of size; however, the population presents a spread signal in the side scatter channel, indicative of a low grade of granularity. Analyzing the height versus the area of the forward scatter signal shows the presence of two populations of microgels, one larger (marked in red in Figure 6.2c) than the other (marked in light blue in Figure 6.2c). This suggests the presence of doublets, which is also demonstrated by the higher forward scatter area of the red-marked population. Doublets can frequently occur by PEG microgels sticking to each other. Analysis performed on single microgels showed a striking difference in fluorescent signal between the stained microgels and the unstained sample (Figure 6.2d). Taken together, these results show the possibility to interface the microgel technology with high-throughput flow cytometry-based analysis.

Generation of combinatorial microgels for high-throughput analysis
The addition of splitting branches into the microfluidic design presented in Figure 5.4a, would permit the generation of combinatorial microgels that have a size compatible with high-throughput screening analysis.
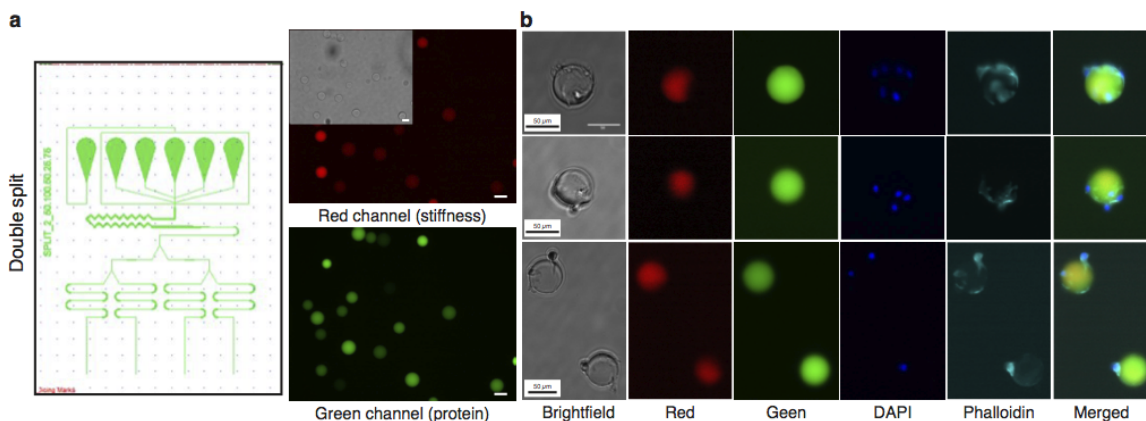
Figure 7.3 – Cell adhesion on small combinatorial microgels. a, Design of the microfluidic chip used to generate small combinatorial microgels with a double splitting branch. The micrographs show four combinatorial microgel populations, characterized by two levels of intensity both in the red and green channel. **b**, Random examples of fibroblasts growing on combinatorial microgels. The brightfield micrographs show cell morphology on microgels with different physico-chemical properties. The red and green fluorescence encode for the microgel stiffness and the RGD content, respectively. Cells nuclei and actin filaments were stained with DAPI and Alexa555-conjugated phalloidin, respectively.

A double split design was integrated into the microfluidic design, and four distinct combinatorial PEG formulations were generated by programming the flows according to the Table S4 in Appendix C. Maleimide-Alexa660 defined the microgel stiffness, whereas Alexa488 moiety encoded the different concentrations of thiolated-RGD, which provided cell adhesion. Two stiffness conditions, relative to 2.5% (w/v) and 10% (w/v) PEG contents, and two RGD concentrations, 1mM and 1.2mM, were targeted (Figure 6.3a). Microgels have different sizes, which reflects a different swelling ratio based on the PEG content (as reported in Chapter 5).[12] Therefore, to best run a cytometry-based analysis, the dimensions of the beads after swelling should be taken into account. In this case, the average bead diameter was around 38 μm.

To prove the potential application of the technology, fibroblasts were seeded on microgels and cultured in suspension for 48 hours. Brightfield images in Figure 6.3b show cell morphology on microgels with different elasticities and various RGD concentrations, as found in the red and green fluorescent pictures, respectively. Staining with DAPI was performed to show cell nuclei, whereas cell spreading was assessed in the different conditions by phalloidin staining, which highlights actin filaments.

Conclusions

The ease of microgel manipulation makes them very attractive tools to perform high-throughput screenings in an unprecedented manner, without requiring expensive and complicated robotic equipment. Therefore, interfacing them with technologies such as flow or mass cytometry would pave the way for novel methods of cellular screening. Here, we adopt a microfluidic platform for the stable generation of PEG-based microgels that have a size compatible with the majority of the high-throughput techniques available. To achieve this, splitting branches were introduced into the microfluidic design to allow the symmetric formation of smaller daughter microgels. Then, we proved the possibility to adopt flow cytometry for the analysis of microgels, capable of supporting cell adhesion. We envision that cytometry-based high-throughput analysis of microgels would resolve the issues related to an image-based analysis, such as time-consuming imaging and intricate computational data analysis. Therefore, it would be possible to analyze the activation of specific genes of interest based on the microenvironmental physico-chemical conditions, shedding light on some biological processes in stem cell and cancer biology.

Experimental section

Materials. Poly(dimethylsiloxane) (PDMS) microfluidic chips were produced by using Sylgard 84 (Dow Corning). 4arm PEG end-functionalized with thiols (4arm-PEG-SH, 10kDa) were obtained from NOF (Japan) and dissolved in bi-distilled water. Vinylsulfone-functionalized 8arm-PEG (8arm-PEG-VS, 10kDa) was synthesized as described[24] and dissolved in triethanolamine (0.3M, pH 8). Hexadecane and ABIL EM 90 were purchased from Sigma (USA) and Evonik Industries (Germany), respectively. Maleimide-conjugate AlexaFluor546 C_5 and Alexa660 and Alexa488-NHS fluorophores were obtained from Life Technologies (USA).

Design and Fabrication of Microfluidic Chips. Clewin software was used to draw microfluidic networks for droplet generation using a flow focusing design composed of two microchannels for the water phase, intersected at 90° angle with the main channel for the oil phase. 50-μm-deep channels with two different

channel widths of the upstream part (75, 50 μm) were patterned on SU8 masters. The microfluidic chips were designed to have a 100μm-wide serpentine with winding sections at 60° angle. Symmetric Y-junctions were designed forming a 60° angle. In case of single split the width was 25 μm; in case of double split the first Y-junction was designed with a width of 50 μm and the second one with a width of 25 μm. Before each splitting junction, channel restrictions were designed: in case of single split, from 100 μm down to 25 μm; in case of double split, from 100μm down to 50 μm and then down to 25 μm. A final serpentine with a width of 75 μm connects the channels with the outlets of the chip (Figure 6.1a-e). PDMS chips were fabricated using conventional soft lithographic techniques and then bonded on oxygen plasma-activated glass slides, coated with a thin film of PDMS. Upon overnight thermal treatment, separated collecting chambers were generated in correspondence of each outlet.

Microgel Generation. Syringes were filled with PEG solutions and hexadecane with 2% (w/v) ABIL EM surfactant used as oil phase. Tygon tubings were used to connect the syringes to the microfluidic chip inlets. Microgels were generated by loading two microfluidic channels with PEG-VS at a concentration of 8.33% (w/v) and PEG-SH at a concentration of 20% (w/v), in order to have a 20% SH-excess. Equal volumes of precursors were mixed to obtain microgels with 5% (w/v) PEG content. To fluorescently label the microgels, maleimide-conjugated AlexaFluor546 was previously mixed in the PEG-SH solution in order to get a final concentration of the fluorophore of around 0.56 μg/ml. Combinatorial microgels were instead generated by flowing PEG-VS at a concentration of 10% (w/v) and PEG-SH at a concentration of 20% (w/v), resulting in microgels without molar excess of any reactive group. Maleimide-conjugated Alexa660 fluorophore and Alexa488-conjugated thiolated-RGD were supplied at initial concentrations of 2 μg/ml and 2 mg/ml, respectively. As buffer we used triethanolamine buffer (0.3M, pH8). Computer-controlled syringe pumps (neMESYS from Cetoni, Germany) were used to control flow rates, as reported in Table S7, in Appendix C.

Washing of Microgels. The oil phase was removed by filtering microgels with pre-hydrated 20μm cell strainers (Sysmex Digitana, Switzerland) and by extensive washing with PBS. The filters were connected to a vacuum generator to facilitate the removal of the liquid phase. Microgels were then swollen in PBS overnight.

Peptide fluorescent bioconjugation. Ac-GRCGRGDSPG-NH$_2$ (GL Biochem, China) and N-hydroxysuccinimide (NHS) ester-Alexa488 fluorophore (Lifetechnologies, U.S.A.) were reconstituted in water, mixed together with 10% molar excess of peptide. The pH of the solution was adjusted to 7.4 by adding PBS 10x and the components were let react for 1 hour. The unreacted succinimidyl groups were subsequently cleaved with TRIS buffer at pH 7 for 30 min.

Flow cytometry. FACS AriaII, equipped with a 130μm nozzle, was used to analyze the microgels. Before running through the cytometer, the beads were passed through a 40μm strainer (BD, Sigma) to prevent nozzle clogging. A green laser (561nm) with a filter 585/15 was used to analyze the microgel fluorescence.

Cell Culture on Microgels. Fibroblasts were cultured on tissue culture flasks in Dulbecco's Modified Eagle Medium (DMEM) with 10% Fetal Bovine Serum (FBS) and pen-strep (10mg/ml). After dissociation with trypsin (TripLE express, Gibco), cells were cultured on microcarriers in a suspension bioreactor (BioLevitator, Hamilton, Switzerland), following the conditions reported in [12].

Staining and Imaging. For staining, cells were first fixed in 5% PFA for 10 min, permeabilized for 5 min by TritonX (0.2% solution in PBS) and then stained with Alexa555 phalloidin (Invitrogen, USA) and DAPI (Sigma, USA), at a dilution 1:200 and 1:1000, respectively. Images were acquired with an inverted Olympus IX81 CellR microscope in four different fluorescent channels: Cy5 filter (time of exposure 200ms) was used to acquire the stiffness-encoding fluorophore; FITC filter (time of exposure 1ms) to acquire the signal from the RGD peptide; DAPI and Cy3 filters (time of exposure 20ms) were used for the acquisition of the signal from cell nuclei and phalloidin, respectively.

References

1   Lutolf, M. P., Gilbert, P. M. & Blau, H. M. Designing materials to direct stem-cell fate. *Nature* **462**, 433-441 (2009).

2   Ranga, A. & Lutolf, M. P. High-throughput approaches for the analysis of extrinsic regulators of stem cell fate. *Curr Opin Cell Biol* **24**, 236-244 (2012).

3   Watt, F. M. & Huck, W. T. S. Role of the extracellular matrix in regulating stem cell fate. *Nat Rev Mol Cell Bio* **14**, 467-473 (2013).

4   Ankam, S., Teo, B. K. K., Kukumberg, M. & Yim, E. K. F. High throughput screening to investigate the interaction of stem cells with their extracellular microenvironment. *Organogenesis* **9**, 128-142 (2013).

5   Nelson, C. M., Khauv, D., Bissell, M. J. & Radisky, D. C. Change in cell shape is required for matrix metalloproteinase-induced epithelial-mesenchymal transition of mammary epithelial cells. *J Cell Biochem* **105**, 25-33 (2008).

6   Lee, K. *et al*. Matrix compliance regulates Rac1b localization, NADPH oxidase assembly, and epithelial-mesenchymal transition. *Mol Biol Cell* **23**, 4097-4108 (2012).

7   Leight, J. L., Wozniak, M. A., Chen, S., Lynch, M. L. & Chen, C. S. Matrix rigidity regulates a switch between TGF-beta 1-induced apoptosis and epithelial-mesenchymal transition. *Mol Biol Cell* **23**, 781-791 (2012).

8   Eyckmans, J., Boudou, T., Yu, X. & Chen, C. S. A Hitchhiker's Guide to Mechanobiology. *Dev Cell* **21**, 35-47 (2011).

9   Discher, D. E., Janmey, P. & Wang, Y. L. Tissue cells feel and respond to the stiffness of their substrate. *Science* **310**, 1139-1143 (2005).

10   Gobaa, S. *et al*. Artificial niche microarrays for probing single stem cell fate in high throughput. *Nat Methods* **8**, 949-955 (2011).

11   Flaim, C. J., Chien, S. & Bhatia, S. N. An extracellular matrix microarray for probing cellular differentiation. *Nat Methods* **2**, 119-125 (2005).

12   Allazetta, S., Hausherr, T. C. & Lutolf, M. P. Microfluidic Synthesis of Cell-Type-Specific Artificial Extracellular Matrix Hydrogels. *Biomacromolecules* **14**, 1122-1131 (2013).

13   Headen, D. M., Aubry, G., Lu, H. & Garcia, A. J. Microfluidic-Based Generation of Size-Controlled, Biofunctionalized Synthetic Polymer Microgels for Cell Encapsulation. *Adv Mater* (2014).

14   Rossow, T. *et al*. Controlled synthesis of cell-laden microgels by radical-free gelation in droplet microfluidics. *Journal of the American Chemical Society* **134**, 4983-4989 (2012).

15   Velasco, D., Tumarkin, E. & Kumacheva, E. Microfluidic encapsulation of cells in polymer microgels. *Small* **8**, 1633-1642 (2012).

16   Tan, W. H. & Takeuchi, S. Monodisperse alginate hydrogel microbeads for cell encapsulation. *Adv Mater* **19**, 2696-+ (2007).

17   Tumarkin, E. *et al*. High-throughput combinatorial cell co-culture using microfluidics. *Integr Biol-Uk* **3**, 653-662 (2011).

18   Cho, C. F., Azad, B. B., Luyt, L. G. & Lewis, J. D. High-Throughput Screening of One-Bead-One-Compound Peptide Libraries Using Intact Cells. *Acs Comb Sci* **15**, 393-400 (2013).

19   Li, C. Y., Wood, D. K., Huang, J. H. & Bhatia, S. N. Flow-based pipeline for systematic modulation and analysis of 3D tumor microenvironments. *Lab Chip* **13**, 1969-1978 (2013).

20   Seemann, R., Brinkmann, M., Pfohl, T. & Herminghaus, S. Droplet based microfluidics. *Rep Prog Phys* **75** (2012).

21   Anna, S. L., Bontoux, N. & Stone, H. A. Formation of dispersions using "flow focusing" in microchannels. *Appl Phys Lett* **82**, 364-366 (2003).

22   Tan, Y. C., Cristini, V. & Lee, A. P. Monodispersed microfluidic droplet generation by shear focusing microfluidic device. *Sensor Actuat B-Chem* **114**, 350-356 (2006).

23   Yobas, L., Martens, S., Ong, W. L. & Ranganathan, N. High-performance flow-focusing geometry for spontaneous generation of monodispersed droplets. *Lab Chip* **6**, 1073-1079 (2006).

24   Lutolf, M. P. & Hubbell, J. A. Synthesis and physicochemical characterization of end-linked poly(ethylene glycol)-co-peptide hydrogels formed by Michael-type addition. *Biomacromolecules* **4**, 713-722 (2003).

Chapter 7

3D Cell-instructive Microgels with Tailor-made Physico-chemical Properties

3D Cell-instructive Microgels with Tailor-made Physico-chemical Properties

Simone Allazetta, Samantha Zerbib and Matthias P. Lutolf

Manuscript in preparation

A microfluidic in vitro cell encapsulation platform for systematically testing the effects of microenvironmental parameters on cell fate in 3D was developed. Multiple cell types including primary fibroblasts, mouse embryonic stem cells and cancer cells were incorporated in enzymatically cross-linked poly(ethylene glycol) (PEG)-based microgels having defined and tunable biophysical and biochemical properties. Furthermore, different approaches to prevent cell 'escape' from the microcapsules were explored and shown to substantially enhance the potential of this technology. Finally, co-encapsulation of microgels within non-degradable gels allowed us to study cell viability, proliferation and morphology in different microenvironmental conditions up to 21 days in culture.
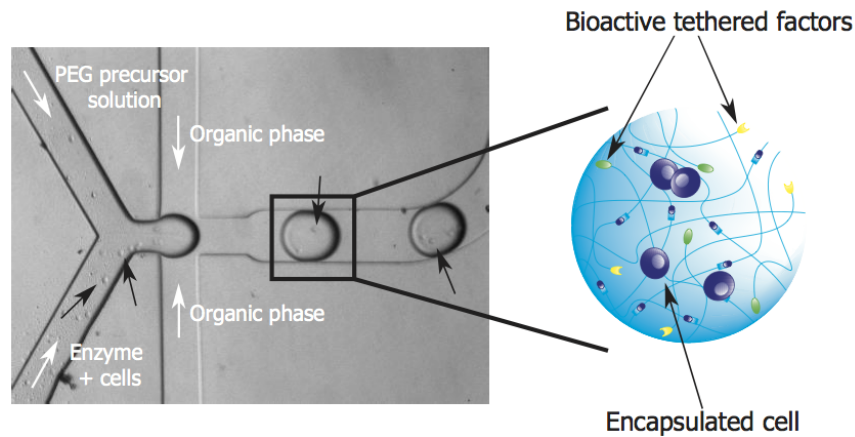
Introduction

Encapsulation of mammalian cells in 3D matrices has gained great importance as a cell culture model for tissue engineering and regenerative medicine applications. Furthermore, cell confinement within small capsules has been widely used in cell-based transplantation assays; the compartmentalization could prevent the entry of antibodies and immune cells into the capsule yet permit the release of cell products.[1-3]

It is widely recognized that a 3D cell biology approach has the potential to mimic the physiology of the native cellular microenvironment more faithfully than traditional two-dimensional (2D) techniques.[4-6] In mammalian tissues, multiple cell types interact with each other and the extracellular matrix (ECM) through complex crosstalk. Several *in vitro* methods have been reported that recapitulate these intricate cellular and molecular interactions to some extent. An example is the microgel-based technology, which combines the precision of microfluidics with the versatility of hydrogel chemistry and offers the unique opportunity to compartmentalize cells into monodisperse and physico-chemically defined matrices. Through compartmentalization, cell activity in response to the microenvironment can be accurately and independently observed. Additionally, fine control over the matrix degradability and the mechanical and biochemical gel properties is critical to recreate reliable *in vitro* 3D platforms to study cell behavior.[7]

Many types of synthetic and natural biopolymers have been used for microfluidic cell encapsulation, such as PEG[8,9], polyglycerol[10], self assembling peptides[11], collagen[12,13], agarose[14,15], alginate[16] and hyaluronic acid[17]. Although some of these platforms can modify microcapsule biophysical or biochemical properties, there are no examples of microgels displaying tunable mechanical, biochemical and biodegradability properties at the same time.

Here, we tailor the microfluidic platform developed for the generation of cell microcarriers [18] to cell encapsulation in hydrogel microcapsules produced through an enzymatically cross-linked PEG-based hydrogel. This system allows attachment of bioactive building blocks and mild crosslinking without the generation of cell-damaging free radicals.[19] Notably, by modifying the amino acid sequences conjugated to the PEG macromers, the system allows matrices to be produced with varying levels of degradability.

We show the successful microfluidic cell encapsulation of multiple mammalian cell types, such as fibroblasts, mouse embryonic stem cells and cancer cells. We first characterized the cell encapsulation then optimized its efficiency by developing a protocol that increased it to 60%, thus significantly reducing the number of empty beads. Unfortunately, using the technology for long-term cell culture applications was undermined by cell escape from the microcapsules after a few days of culture. We found the escape kinetics to be dependent on both the microgel properties and the cell type. Therefore, we explored preventing cell escape by coating the microcapsules with biomolecules such as poly-L-lysine and by double-encapsulation into non-degradable gel matrices. The latter method allowed us to study cell proliferation, viability and cell morphology in different microenvironmental conditions after up to 21 days of culture.

Results and discussion

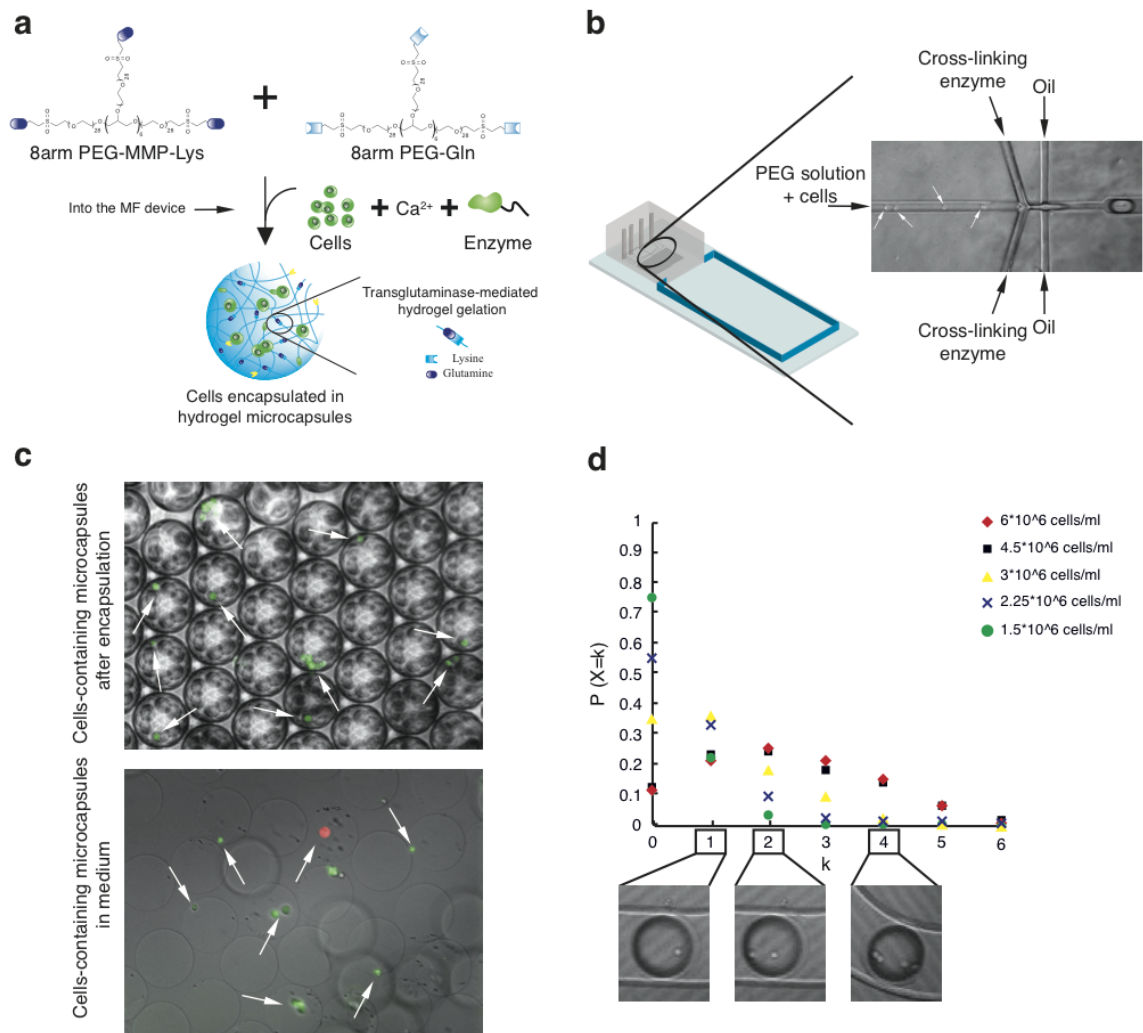**Microfluidic cell encapsulation in hydrogel microcapsules**

An enzymatically cross-linked PEG hydrogel matrix was used for cell encapsulation in microcapsules. Multiarm PEG-VS macromers were modified to display the FactorXIIIa substrates, as previously shown[19]. One precursor was functionalized with the native glutamine acceptor peptide (NQEQVSPL) and the other one with the lysine donor peptide (FKGG). Furthermore, the gel was made cell-degradable by inserting the cell protease (MMP)-sensitive amino acid sequence GPQGIWGQ into the lysine-modified PEG macromer. This would render the gel also degradable to dissociation reagents like trypsin, giving the advantage of being able to retrieve the encapsulated cells for further analysis such as flow cytometry and PCR. Non-degradable gels could be also generated by adding the amino acid sequence GDQGIAGF, which is not cleavable by cell proteases (Appendix D, Figure S1a). To promote cell adhesion, the integrin-binding peptide RGD was incorporated within the gel network by chemically linking it to the lysine substrate peptide (H-FKGGRGDSPG-NH$_2$).

Modifying the PEG concentration resulted in the polymerization of gels with different elasticity in a range from 300 Pa up to 3000 Pa, measured by rheology (Appendix D, Figure S1b). In this work we mainly used degradable gels in a stiffness range between 500 Pa and 1000 Pa, which corresponded to a PEG concentration between 2.12% (w/v) and 2.52% (w/v). Mixing the PEG solution, cells, a calcium buffer and the enzyme solution in the microfluidic chip leads to a transglutaminase-mediated gelation of a cell-laden microgel (Figure 7.1a).

A four-inlet microfluidic flow focusing design was used for cell encapsulation experiments. The PEG solution was mixed with cells and injected in the middle stream, while the FactorXIIIa solution containing calcium buffer was injected symmetrically from the two side channels. Mineral oil supplemented with 2% surfactant came from the side channels and contributed to the formation of cell-laden microgels (Figure 7.1b). GFP-transfected fibroblasts were used for a first encapsulation trial. Figure 7.1c shows cell-containing microcapsules right after encapsulation in the oil phase and after washing in cell medium. PI staining (red cells) showed high cell viability right after the encapsulation process (around 90%). Modifying the initial cell concentration gives fine control over the number of cells per droplet. Cell encapsulation follows a Poisson-like distribution equation [20,21]:

$$P(x) = e^{-\lambda} * \frac{\lambda^x}{x!}$$

where P(x) is the probability to find x number of cells within a beads, and λ is the average number of cells per droplet. We found large agreement between the measured encapsulation distribution at different cell concentrations ($6*10^6$, $4.5*10^6$, $3*10^6$, $2.25*10^6$ and $1.5*10^6$ cells/ml) and the theoretical Poisson distribution. The maximum number of cells encapsulated shifted from 0 up to 2 by increasing the cell concentration, in accordance with [20]. For example, the probability to find 2 cells per bead was around 0.25 at a cell concentration of $6*10^6$ cells/ml, while the probability was almost 0 at a cell concentration of $1.5*10^6$ cells/ml, where 75% of beads were empty (Figure 7.1d). Although cell encapsulation is a stochastic process, these data show the possibility to control the number of cells encapsulated by tuning the cell concentration.

Figure 7.1 - Microfluidic set-up for cell encapsulation in hydrogel microcapsules. a, Multiarm PEG precursors were chemically modified to contain a lysine and a glutamine as substrates for the enzymatic reaction of the transglutaminase FactorXIIIa enzyme. In order to render the gel cell-degradable, an amino acid sequence, named as MMP and selectively recognized by cell proteases, was incorporated within the lysine PEG precursor. Mixing the PEG macromers with cells, calcium-rich buffer and the crosslinking enzyme within a microfluidic device will generate a cell-laden microgel. **b**, Schematic showing the microfluidic device used for cell encapsulation in hydrogel microbeads: three channels were used for flowing the suppliers. The two downstream channels were used to flow the cross-linking enzyme solution, while the middle one flowed the PEG premix solution and cells. **c**, Micrographs showing GFP fibroblast-laden microcapsules in the oil phase right after encapsulation (on the top) and after washing in the medium phase (on the bottom). The red staining (PI) indicates dead cells. White arrows point the encapsulated cells. **d**, Cell distribution at different concentrations: P(X=k) stands for the probability to find a number *k* of cells in a microbead, as shown in the small micrographs on the bottom. The maximum of the distribution shifted towards higher cell numbers at increasing cell concentrations, whereas for low cell concentrations the probability to find empty beads was around 0.75.

Optimization of cell encapsulation efficiency

Microfluidic cell encapsulation in hydrogel microbeads is highly affected by cell sedimentation in the syringes caused by density differences between the cells and growth medium (1.1 g/ml and 1 g/ml, respectively) and resulting in a dramatic reduction in cell encapsulation efficiency.[21] Figure 7.2a shows micrographs of the microfluidic channels during a cell encapsulation experiment at different time points. A dramatic decrease in the number of cells flowing can be noticed after only 15 min and even more strikingly after 30 min, compared with the number of cells at time 0. Overall, cell encapsulation efficiency was around 20%, due to the high number of empty microbeads generated after 1 hour (Figure 7.2b). C2C12 muscle progenitor cells were used for the encapsulation experiments.

As previously shown, the average number of cells encapsulated per bead follows a Poisson-like distribution, and the number can be finely controlled by modifying the cell concentration. Therefore, to maximize the cell encapsulation efficiency, a high cell concentration of around $8*10^{\wedge 6}$ cells/ml was used throughout all the experiments. However, after around 30 min the statistical distribution would dramatically shift towards empty beads, regardless of the cell concentration (data not shown). A possible solution to increase the encapsulation efficiency was to match the cell medium density to the cell density by adding an appropriate amount of a commercially available density matching solution called Optiprep. Different concentrations were tested, and the cells were counted as they passed through a channel section at different time points: 0, 30 and 60 min (Figure 7.2c-d). Even at time 0 min, fewer cells were counted in the absence of Optiprep compared to all conditions in which Optiprep was used, suggesting the cell sedimentation is an issue from the beginning of the experiment. The number of cells counted follows a biphasic behavior, with a maximum around 16 µl of Optiprep for 100 µl of cell medium (Figure 7.2c). Low amounts of Optiprep (0% and 8%) do not prevent cell sedimentation, and high concentrations (32%) instead produce the opposite effect of "sedimentation" in the upper part of the syringe, as confirmed by the cell number normalized to the number of cells at time 0 min (Figure 7.2d). An Optiprep concentration of 24% showed the highest cell percentage after 60 min. However, since the cell number at both the beginning and 30 min was higher with 16% Optiprep concentration, this condition was chosen for further experiments, in accordance with published results.[21] It should be emphasized that the optimal Optiprep concentration is cell type-dependent. For example, encapsulation of the cancer cell line MDA-MB231 or of embryonic stem cells required 20% volume of Optiprep to achieve optimal encapsulation efficiency. Additionally, the presence of cell clusters would cause faster cell sedimentation and thus affected cell encapsulation efficiency. Although the tendency to form aggregates is cell-type dependent (for instance, epithelial-like cells tend to cluster more than mesenchymal-like cells), the trypsinization time can be optimized to increase the number of single cells in suspension. Longer exposure times (8 min) to trypsin resulted in fewer cell aggregates and, therefore, a higher efficiency of single-cell encapsulation compared to short trypsinization times (3 min) that increased the number of cell aggregates being encapsulated and reduced the encapsulation efficiency. Therefore, combining a long trypsinization time with the optimal Optiprep concentration provided the highest encapsulation efficiency, around 60% (Figure 7.2e).
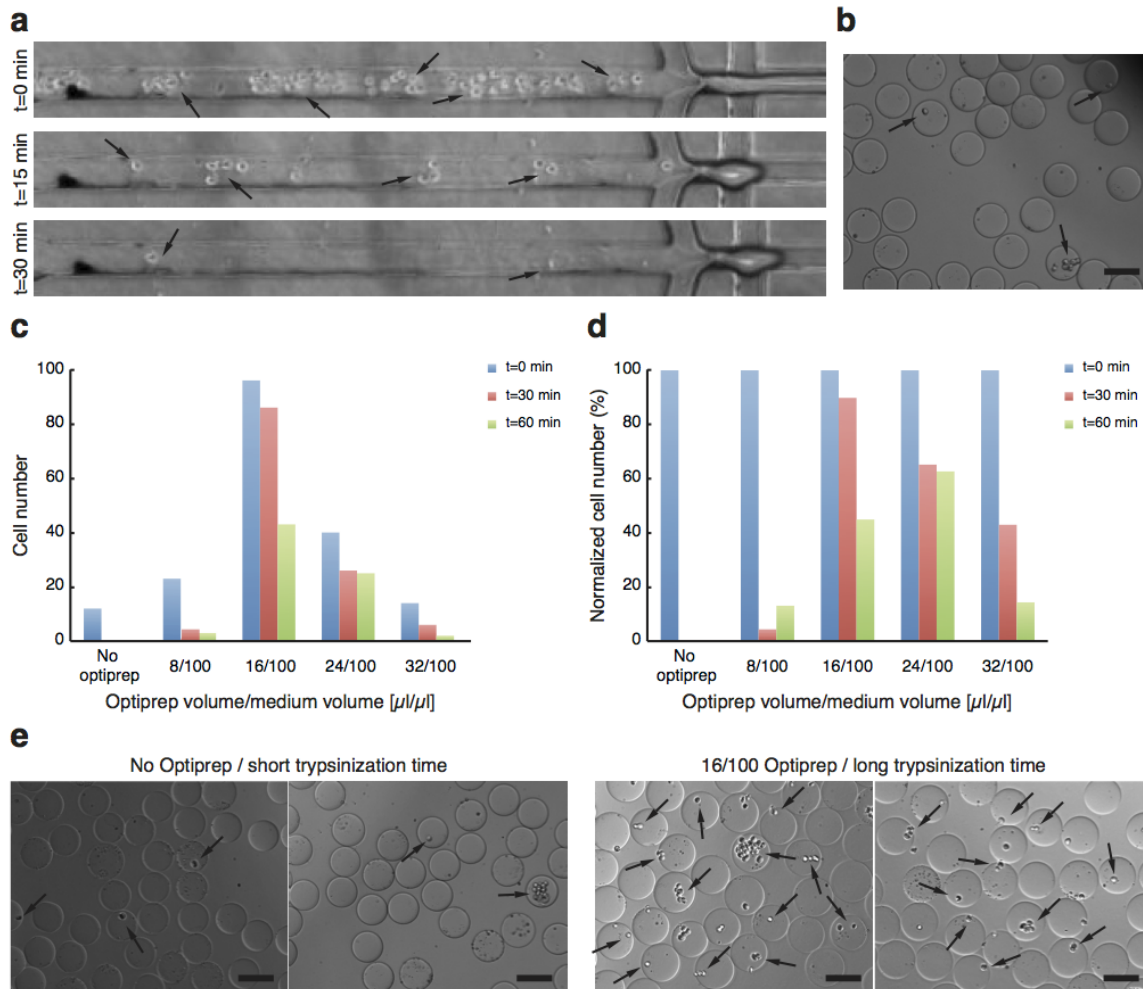
Figure 7.2 - Optimization of cell encapsulation efficiency. **a**, Micrographs showing the cell distribution in the microfluidic channels at different time points. A dramatic decrease in the number of cells being encapsulated was noticed after 15 min and so more after 30 min of production compared with the number of cells in the channels at time 0 min. This effect was seen to be from cell sedimentation in the syringe over time (the cell concentration was $3*10^6$ cells/ml). **b**, Micrograph showing cell-laden microbeads generated after 1 hour: very few cells can be found encapsulated with an efficiency around 20% (cell density used $3*10^6$ cells/ml). **c**, Cell counted in the channels at different time points (0, 30 and 60 min) at various concentrations of Optiprep. Cell number distribution follows a bimodal distribution around 16% Optiprep concentration. Too low or too high concentrations (0%, 8% and 32%, respectively) did not prevent cell sedimentation from the beginning of the experiment onward. **d**, Normalization of the cell number to the number of cells at time 0 showed the lowest decrease after 60 min with 24% Optiprep concentration. However, 16% Optiprep concentration was chosen for further experiments because it gave the highest cell number at time 0 min and 30 min. **e**, Effect of the trypsinization time on the cell encapsulation efficiency: longer trypsinization (8 min) with the addition of 16% Optiprep prevented cell clusters and increased the number of cells encapsulated (right) compared to short trypsinization time (3 min) with no Optiprep (left). Cell encapsulation efficiency was increased up to 60%. Black arrows indicate encapsulated cells. Scale bars 100μm.

Cell escape from hydrogel microcapsules and prevention by poly-L-lysine coating

Cell encapsulation within microcapsules of a diameter ranging from 80 to 150 μm led to the escape of the majority of cells after few days of culture, with cell-type dependent dynamics.[13,22-24] Oct4 GFP mouse embryonic stem (mES) cells were selected for their poor motility, and their escape was monitored by time lapse imaging (Figure 7.3a). We found that the cells were already exiting the capsules after 20 hours of culture (black arrows indicate cell escaping), and after escaping, cell colonies attached to the tissue culture plate and started to grow, keeping their Oct4 expression.

One possible solution to prevent cell escape, reported previously [22,24,25], involves exposing alginate beads (negatively charged) to a poly-L-lysine (PLL) solution (positively charged), resulting in the formation of a barrier layer around the microbeads that would retain the cells inside. However, in order to electrostatically bind the PLL to the microbeads, negative charges must be present on their surface. Due to rapid alginate polymerization within the microchannels, hyaluronic acid (HA) was mixed within the PEG solution to give negative charges able to bind the PLL. In particular, we chose HA with a high molecular weight (M.W. 15000-30000 Da) to ensure its entanglement within the PEG microgel network. HA concentrations of 1 mg/ml and 2mg/ml were tested in the hybrid system and led to microbeads with a more granular texture (Figure 7.3b).

FITC-labeled PLL was used to assess the microbead coating. Microgels with 1 mg/ml HA or without HA were exposed for different times (10min and 30min) to a 0.5 mg/ml FITC-PLL solution, and the intensity was then measured (Figure 7.3c). Strong fluorescence intensity was measured in the case of HA-containing microbeads exposed to PLL compared to the negative control, suggesting that a molecule layer was captured on the microgel surface. No significant difference was noticed between 10min and 30 min exposure to PLL, whereas on the negative control (no HA) no signal was detected, suggesting that no superficial unspecific adsorption occurred (Figure 7.3d).

Then, we tested the stability of the PLL layer under cell culture conditions for up to 14 days. A dramatic drop in the PLL intensity was noticed after 1 day of culture for both exposure times, but then no significant decrease was measured until 14 days for any of the two conditions, suggesting that the PLL coating was stable over time (Figure 7.3e). A significant difference was found between the HA-modified microgels in culture condition and the microgels without HA (Appendix D, Figure S2a,b).
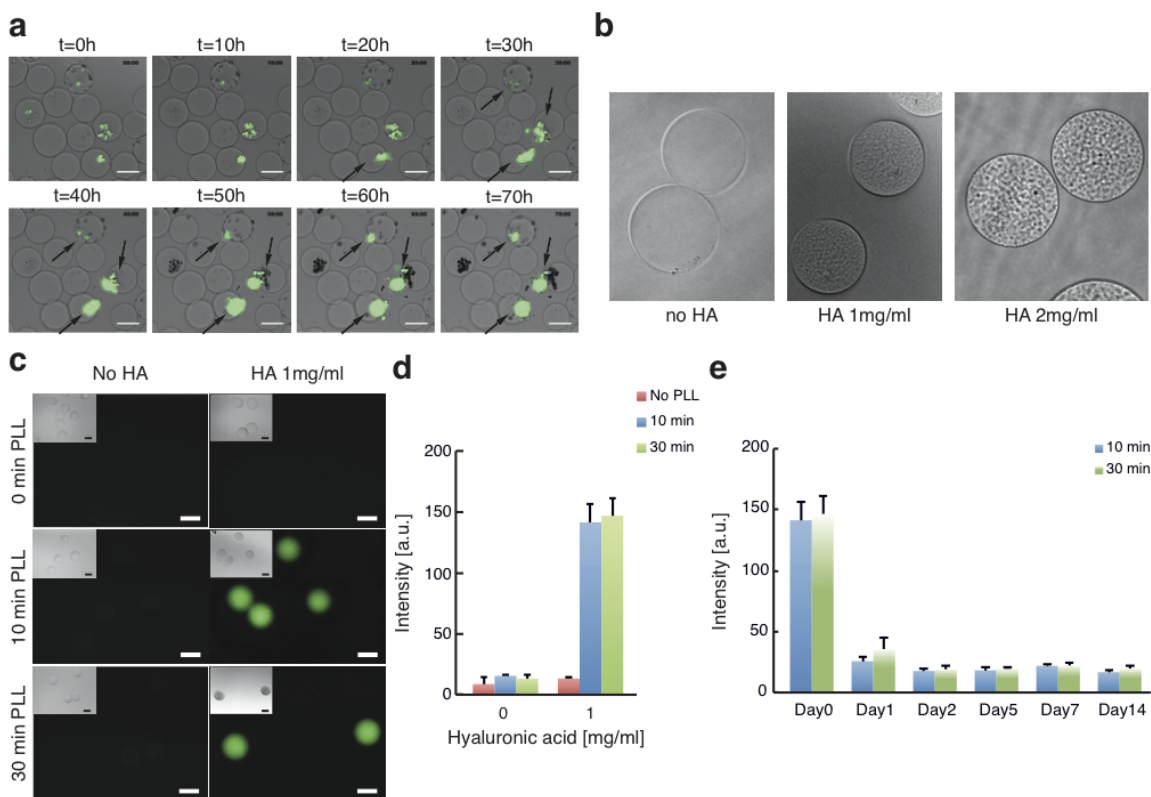
Figure 7.3 – Cell escape from gel microcapsules and poly-L-lysine coating of hybrid PEG-HA microbeads. a, Time lapse showing mouse embryonic stem cells escaping from PEG microcapsules. Cells tended to escape after just 20 hours of incubation (black arrows indicate cells escaping). After escaping, cell colonies would attach to the tissue culture plate and proliferate, keeping their Oct4-GFP expression (represented by the green fluorescence). **b**, Micrographs showing the morphology of microbeads with different HA concentrations: 0 mg/ml, 1 mg/ml and 2 mg/ml. The beads appeared more granular at increasing HA concentration within the PEG network. **c**, Fluorescent images showing microbeads after different incubation times with FITC-labeled PLL: in the absence of HA within the PEG network, no fluorescence could be measured, whereas a signal could be detected in the presence of HA after 10 and 30 min of PLL exposure. **d**, Intensity measurements of microbeads with and without HA exposed to PLL for different times on day0: no significant difference was detected from microbeads exposed for 30 min compared to 10 min. **e**, Fluorescence intensity of PLL-coated microbeads in long-term cell culture condition: the intensity significantly dropped from day0 to day1 and then remained constant for up to 14 days. Scale bars = 100 μm.

Therefore, we were able to successfully generate negatively charged microbeads and coat them with a PLL layer. To investigate cell escape in this system, we chose the MDB-MA-231 cancer cell line, which is known to be highly motile. Cell escape and viability were monitored when PEG microbeads containing 1 mg/ml HA were coated with small molecular weight PLL (in the range of 15-30 kDa). Cells exited from the non-coated microbeads, while almost no cells were found outside the microbeads that had been exposed to PLL for 1min and 10min (Figure 7.4a). Microgels were isolated from the culture plate and exposed to Trypsin for 5 min to retrieve the cells. Then, flow cytometry was performed after staining the dead cells with PI. This analysis revealed a dramatic decrease in cell viability to 10% and 1% after 3 days of culture, when

microbeads were exposed to PLL for 1 min and 10 min, respectively. On the contrary, cells in the non-coated microbeads maintained viability above 80% after 3 days of culture (Figure 7.4b). This suggested that exposure to soluble PLL was highly toxic and led to massive cell death, consistent with previous reports.[26,27]
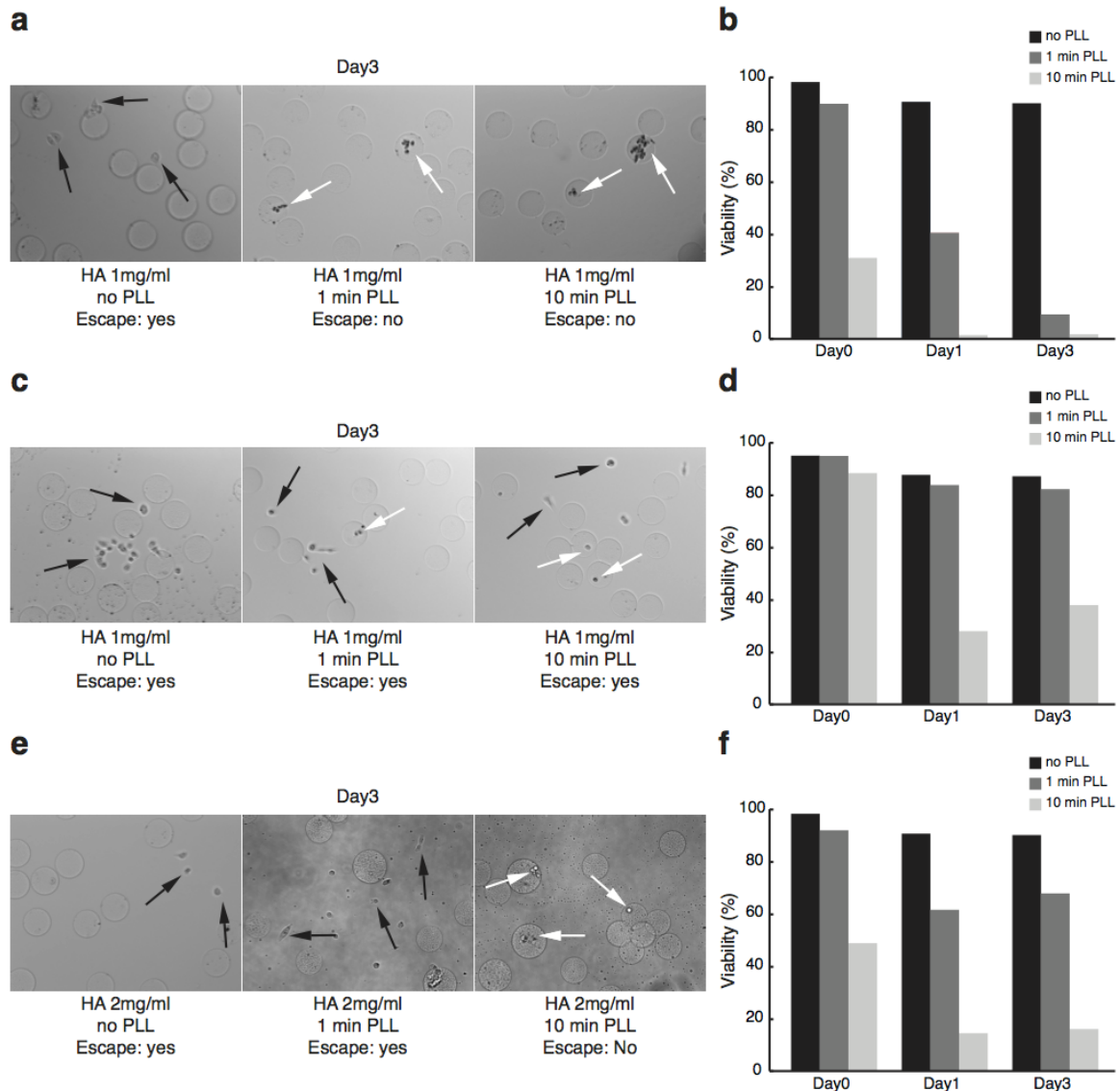
Figure 7.4 - Cell escape and viability within PLL-coated microcapsules. a, Micrographs showing cell escape at day 3 from PEG-HA microgels: cells did not escape when the microbeads were treated with PLL (MW 15-30 kDa) for 1 min and 10 min. **b**, Cell viability at different days of culture in the three tested conditions: a significant drop occurred when microbeads were treated with PLL. **c**, Micrographs showing cell escape from microgels treated with high molecular weight PLL (MW 150-300 kDa): cell escaped from the beads in all the conditions. **d**, Histogram showing good cell viability (greater than 80%) in the case of beads non-treated or treated for 1 min with PLL. PLL incubation for 10 min caused a drop in cell viability around 40% and did not prevent cell escape. **e**, Micrographs showing cell escape from PEG microbeads containing 2mg/ml HA and treated with high molecular weight PLL ((MW 150-300 kDa): cells did not escape in the case of 10 min treatment with PLL. **f**, Cell viability dropped down to 20% in the case of treatment for 10 min, while in the other conditions cell viability was always greater than 60%, even after 3

days. Black arrows indicate the cells escaping and attaching on the tissue culture flask; white arrows show the cells encapsulated in the microgels.

To prevent PLL diffusion inside the microbeads, we employed higher molecular weight PLL (in a range of 150-300 kDa). Microbeads were again exposed to the PLL solution for 1 min or 10 min, and cell escape was noticed in all the conditions (Figure 7.4c). Flow cytometry analysis revealed high viability after 3 days of culture (greater than 80%) for both the cells encapsulated in the non-coated beads and the beads exposed for 1 min. However, 10 min PLL exposure led to more than 60% cell death (Figure 7.4d).

These data suggested that high molecular weight PLL diffuses less and cell death was prevented by shortening the incubation time (1 min); however, cell escape was not avoided. Therefore, in order to increase the surface layer of PLL, the HA concentration was increased up to 2 mg/ml. PLL with high molecular weight was used for different incubation times. Cell escape occurred as before with the non-coated and the 1min-treated microbeads but not with the 10min-treated microbeads (Figure 7.4e). Unfortunately, when exposed to PLL for 10 min, cell viability after 3 days of culture was drastically low (below 20%), while 1 min incubation resulted in 60% cell viability. Higher HA concentrations inside the microbeads were not possible to test, due to the high viscosity of the HA-PEG solution that hindered microgel formation.

In conclusion, PLL coating did not prevent cell escape but rather caused a dramatic drop in cell viability, contrary to previous reports in which other negatively charged biopolymers were used.[22,24,25] In the case of alginate, the reaction kinetics of functionalization with charged molecules, such as PLL or chitosan, is rapid and leads to the formation of a thick complex onto the surface, acting as a physical barrier.[25] This is due to the higher molarity of negative charges present on the surface of alginate gels (around 20 times more) compared to the PEG-HA hybrid matrices. Furthermore, the gel architecture in the two cases is markedly different. Alginate is less permissive to the diffusion of big molecules, particularly for short incubation times [24], while PEG is more porous to big molecules, as demonstrated by PLL penetration through gel disk sections (Appendix D, Figure S2c).

Cell-laden microgels encapsulated in thin gel layers
In order to prevent cell escape, cell-laden microgels were co-encapsulated within a 200µm-thick film of non-degradable Michael-type addition gel, formed by co-polymerization of multi-branched PEG-VS and PEG-SH precursors (Figure 7.5a). Specifically, the gel cannot be degraded by cell proteases, and the architecture of the gel macromolecules allows for higher stiffness and much smaller mesh size compared to the enzyme-mediated cross-linked gel. Therefore, this kind of matrix prevents cell migration via both ameboidal, i.e. a crawling-like movement through the matrix pores, and mesenchymal, i.e. involving an active cellular proteolytic degradation of the ECM barriers, mechanisms.[28] However, since the outer gel layer is not degradable, retrieving the cells for further high-throughput analysis methods, such as flow cytometry or PCR, could be not performed, limiting the analysis to imaging.

Thin gels containing cell-laden microgels were therefore cast onto a coverslip and transferred to culture conditions. In order to investigate cell escape and cell morphology after

long-term cell culture, the MDA MB-231 cell line was again encapsulated into microcapsules with elasticities of 500 and 1000 Pa and in the presence of RGD. No cell escape was noticed, and cell viability was investigated by performing live-dead staining at different time points for up to 15 days (Figure 7.5b). To assess the effect of the outer gel layer stiffness, two PEG concentrations were used, 5% (w/v) and 10% (w/v), corresponding to an elastic modulus of around 40kPa and 100kPa, respectively (data not shown).

Cell viability dropped dramatically after 1 day of culture in microgels of both elasticities when co-encapsulated in stiffer gels (10% (w/v)). In this time, these gels tended to swell more,[18] thus exerting compressive forces on the cell-laden microgels and ultimately causing a drop in the cell viability, as also reported by [29,30]; however, no further significant cell viability drop was detected after 15 days of culture. Independent of the microgel stiffness, cell viability was on average lower when stiffer gels were used for the co-encapsulation.
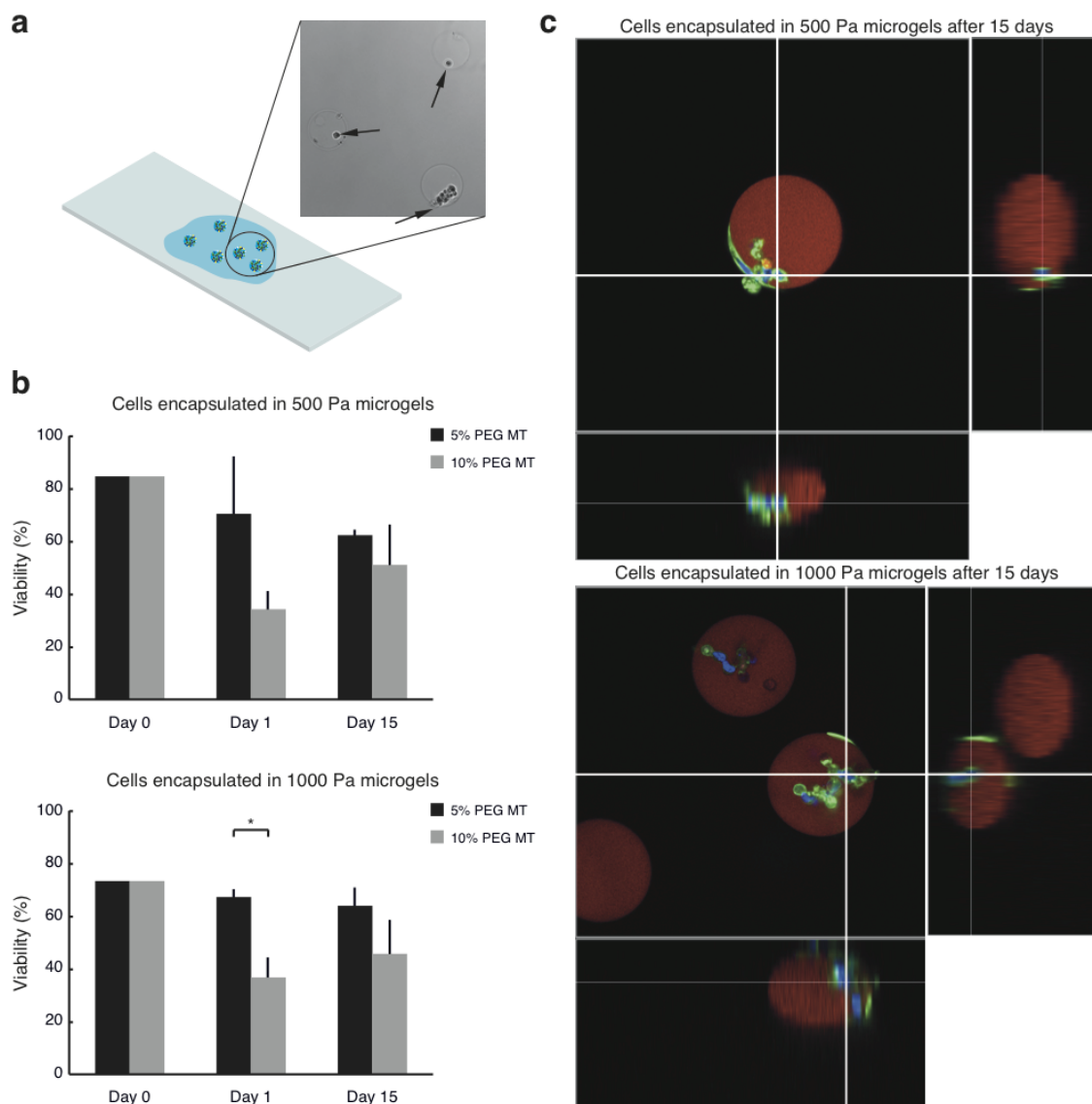
Figure 7.5 - Cell escape prevention by co-encapsulation in thin gel layers. a, Schematic of the encapsulation of cell-laden microgels in thin hydrogel layers, casted on top of glass coverslips. **b**, Viability

of cells encapsulated in microgels of different elasticities (500 Pa and 1000 Pa) and then co-encapsulated in non-degradable gels with various PEG contents (5% (w/v) and 10% (w/v)) and thus different stiffness. Cell viability was assessed by live-dead staining, analyzing around 20 beads per condition. **c**, Confocal images of cell-laden microgels loaded with fluorescent RGD and co-encapsulated in PEG thin gel layers after 15 days of culture. Cell actin filaments and nuclei were stained with phalloidin (green) and DAPI, respectively. The examples report microgels encapsulated in 5% (w/v) PEG outer gel.

To improve the visualization of the cell position within the microcapsules, we used a fluorescent (Alexa546) version of the RGD adhesion peptide. Confocal images of various cell-laden microgels were acquired up to 21 days in culture to investigate cell morphology and cell escape. Phalloidin and DAPI stainings were performed to decorate the cell actin filaments and nuclei, respectively (representative images in Figure 7.5c, more images in Appendix D, Figure S3). From the confocal images, cells could be found inside the microbeads, even though at times some protrusions were found in between the two gel layers, suggesting a partial cell escape in 10% of the cases. This might be due to the highly motile cell type used and the low matrix stiffness that allows for cell movement after long-term culture. No evident difference in cell morphology was noticed between cells encapsulated in microgels with different elasticities.

This example demonstrates that the co-encapsulation could help prevent cell escape, even though more matrix optimization is needed to study long-term biological mechanisms. Furthermore, the possibility to tune the elasticity and, therefore, the swelling of the outer gel layer might open up new avenues in studying cellular mechanotransduction. For example, the influence of difference compression forces on cell viability, proliferation and stem cell fate decisions can be explored.

Co-encapsulation of cell-laden microgels in hydrogel microbeads

Based on the previous results, we developed a microfluidic strategy to generate a physical barrier to prevent cell escape from microgels, thus allowing stem cell proliferation in microgels with different physico-chemical properties to be studied. Therefore, co-encapsulation of a cell-laden microgel into another microbead was carried out to confine the microgels within a secondary physical shell. Cell-laden microgels were generated as previously explained and later re-injected into a 150μm-deep microfluidic chip, allowing for the co-encapsulation of a bead-in-a-bead.

Medium with cell-laden microgels was injected into the middle stream of the microfluidic chip, while the PEG-VS and PEG-SH macromers came from the lateral channels (Figure 7.6a). We encapsulated Oct4 GFP mES cells into factorXIIIa microgels and ran them through the second microfluidic chip. We were able to successfully co-encapsulate cell-containing microgels into a bigger non-degradable bead (Figure 7.6b). The co-encapsulation process follows a Poisson statistical distribution that causes the formation of non-degradable beads trapping a different number of cell-containing microgels. In the insets of Figure 7.6b, beads containing 0, 1 or 2 microgels are shown. The co-encapsulation efficiency was around 10% due to microbeads sedimentation in the syringe. Therefore, 16% Optiprep was added to the microgel-containing medium solution to increase the co-encapsulation efficiency up to 40% (data not shown) as was done for the initial cell-containing microgel.

To test whether this approach prevented cell escape, we studied mES proliferation within microgels with different elasticities, 500 Pa and 1000 Pa. Since mES cells do not need adhesion ligands for their survival in an undifferentiated state, the microgels were not functionalized with the RGD peptide; however, they were cultured in medium supplemented with LIF. The outer PEG layer was produced to have a final gel dry mass of 5% (w/v), corresponding to a stiffness of around 40 kPa. No cell escaped the microgels up to 4 days of culture, and when a cell colony was found close to the microgel edge, cells tended to deform the matrix but could not escape. Figure 7.6c shows some examples of mES cell colonies confined within the microgels with different elasticities at various days of culture.
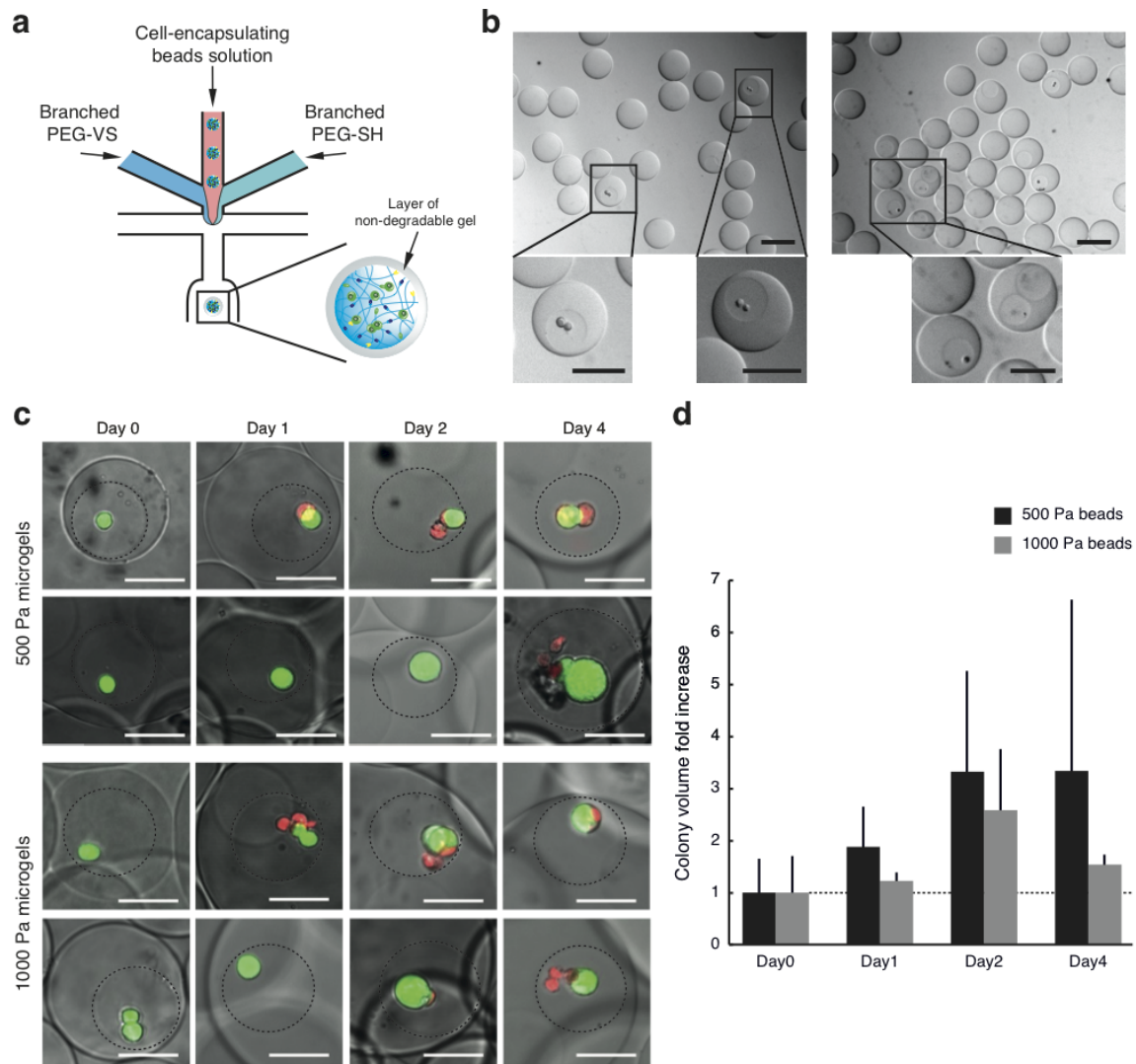
Figure 7.6 – Cell-laden microgels co-encapsulation within non-degradable gel microbeads. **a**, Schematic of the microfluidic approach used for co-encapsulation of a bead-in-a-bead: medium containing cell-laden microgels was injected from the central channel, and the non-degradable Michael-type-addition multibranched PEG-VS and PEG-SH gel precursors were injected from the side channels. **b**, Micrographs showing mES cells-laden microgels co-encapsulated in a non-degradable gel shell. The insets show microbeads containing 0, 1 or 2 microgels. **c**, Micrographs showing the growth of mES cells encapsulated in soft (500 Pa) and stiff (1000 Pa) microgels at different time points. Green represents the Oct4 expression

of the mES colonies, and the red signal stains for the dead cells. More cell death was observed after 4 days of culture in 1000 Pa microgels. The dashed lines draw the edges of the cell-laden microgels. **d**, Quantification of the proliferation of mES cells encapsulated in microgels with different elasticity and co-encapsulated in 5% (w/v) non-degradable beads: slower proliferation trend and higher cell death at day 4 was measured for cells in stiff microgels. Scale bars = 100μm.

Quantification of cell proliferation was performed by measuring the average volume of around 10 cell colonies per condition at different days of culture with confocal microscopy. Cells were stained with PI (red signal) to distinguish dead cells from those expressing Oct4 (GFP positive). Non-significant difference was measured in the colony volume fold increase between the soft and the stiff condition. Compared to day 0, a 3-fold increase was measured at day 4 in the soft (500 Pa) microgels, whereas a 2.5-fold increase was measured at day 3 in stiff (1000 Pa) microgels. In the latter condition, higher cell death was observed at day 4, resulting in a drop in the cell proliferation (Figure 7.6d). This slow proliferation trend might be attributed to the stiffness of the outer bead (much higher than the microgels stiffness) that may limit cell growth and viability through compression. Additional studies could take into account the effect of the outer layer stiffness on cell growth potential.

Microfluidic co-encapsulation strategy represents an elegant solution to prevent cell escape, thus allowing the observation of cell behavior in microcapsules bearing varying physico-chemical properties. However, the non-degradable gel layer prohibits cell retrieval for further analysis such as flow cytometry or PCR, therefore limiting the high-throughput potential of the technology, requiring intense and laborious three-dimensional confocal microscopy. Engineering the outer gel layer to render it selectively degradable to specific proteases may represent a valuable alternative for the full exploitation of the high-throughput potential of the technology.

Conclusions

This work shows the successful implementation of the microfluidic technologies, developed for the generation of microgels with combinatorial biophysical and biochemical properties, for the encapsulation of cells in gel microcapsules. FactorXIIIa enzyme-mediated gel polymerization was adopted for the cell encapsulation under mild conditions and allowed the elasticity, biodegradability and the biochemical properties of the matrix to be modified. We showed the possibility to control the encapsulation efficiency of multiple cell types, such as fibroblasts, mouse embryonic stem cells and cancer cells. However, cell escape significantly limited the potential of the technology for long-term cell culture studies. In this work, we explored some possibilities to prevent cell escape by either engineering a chemical or a physical barrier to cell movement. Co-encapsulation of microbeads within a non-degradable gel would prevent cell escape, yet limiting the possibility to retrieve the cells for further biological analysis. Therefore, engineering a gel layer with a peptide sequence selectively degradable by pre-defined dissociation reagents, as opposed to cells, would allow for cell retrieval for further analysis.[31] By adopting the microfluidic platform previously explained, combinatorial modulation of microgel biophysical and biochemical properties would help elucidate the effects of microenvironmental perturbations on cell behavior in 3D.

Experimental section

Materials. Poly(dimethylsiloxane) (PDMS) microfluidic chips were produced by using Sylgard 84 (Dow Corning). 4arm PEG end-functionalized with thiols (4arm-PEG-SH, 10kDa) was obtained from NOF (Japan) and dissolved in bi-distilled water. Vinylsulfone-functionalized 8arm-PEG (8arm-PEG-VS, 10kDa and 40kDa) were synthesized as described in [32] and in [19], respectively and dissolved in triethanolamine (0.3M, pH 7.4). The FactorXIIIa substrates peptides Ac-FKGGGPQGIWGQ-ERCG-NH$_2$ (named TG-MMP-Lys, M.W. 1717.9 g/mol) and H-NQEQVSPL-ERCG-NH2 (named TG-Gln, M.W. 1358.5 g/mol) and the RGD peptides, H-FKGGRGDSPG-NH$_2$ (named TG-RGD-Lys, M.W. 1018.07 g/mol) and H-NQEQVSPLRGDSPQRCG-NH$_2$ (named TG-RGD-NQ, M.W. 1871.03 g/mol) were purchased from GL Biochem (China). FactorXIIIa enzyme was purchased from the Veterinary Service of EPFL (Switzerland) and subsequently activated following the protocol in [19]. Hyaluronic acid from rooster comb was purchased from Sigma (USA). Mineral oil and Optiprep were purchased from Sigma (USA); ABIL EM 90 form Evonik Industries (Germany). Poly-L-lysine hydrobromide (M.W. 15000-30000Da and M.W. 150000-300000Da) and FITC-labeled Poly-L-lysine (M.W. 15000-30000Da) were purchased form Sigma (USA). AlexaFluor546 carboxylic acid, succinimidyl ester fluorophore was obtained from Life Technologies (USA).

Fabrication of Microfluidic Chips. Clewin software was used to draw microfluidic networks for droplet generation using a flow focusing design composed of three microchannels for the water phase, intersected at 90° angle with the main channel for the oil phase. PDMS chips were fabricated using conventional soft lithographic techniques. 100-µm-deep or 150-µm-deep (for the co-encapsulation experiments) channels with a width of 200 µm were patterned on SU8 masters. Microfluidic chips were bonded by oxygen plasma on glass slides coated with a thin PDMS layer.

PEG-peptide Conjugation. TG-MMP-Lys and TG-NQ peptides were let reacting with 8arms-PEG-VS (M.W. 40 kDa) macromers (1.2 molar SH- excess over the VS- groups) in 0.3 M triethanolamine (pH 8) for 2 hours at 37°C. After dialyzation in ultrapure water to remove unbound peptides, the products were lyophilized to obtain white powder.

Microgel Generation. Computer-controlled syringe pumps (neMESYS from Cetoni, Germany) were used to control the flow rates and Tygon tubings to connect the syringes to the microfluidic chip inlets. Microgels were generated loading one channel with a premix solution of PEG precursors, 8arm-PEG-MMP-Lys and 8arm-PEG-Gln, at 10% (w/v) concentration, and cells at various concentrations. HA and RGD peptide were also loaded with the gel solution, at specific initial concentrations to get a final amount of 1 or 2 mg/ml and 50 µM, respectively. The side channels were loaded with buffer (50 mM solution of TRIS and CaCl$_2$, pH 7.4), and with activated factorXIIIa (final concentration in the gel of 20 u/ml). As continuous phase we used mineral oil with 2% (w/v) ABIL EM surfactant. All the experiments were performed in sterile conditions by filling the syringes under hood and by confining the microfluidic chip within a sterile polystyrene box (Thermo Scientific, USA) modified with a hole to allow for the connection of the tubings to the chip. The oil phase was removed by filtering microgels with 70µm cell strainers (BD Biosciences, USA) and by extensive washing with PBS. Cell-laden microgels were then cultured in medium under 37°C and 5% CO$_2$ conditions.

Michael-type Addition Gel Formation. Synthesis of the non-degradable PEG gel was previously reported in [18,33] and PEG-VS was reconstituted in triethanolamine (TEA) at pH 7.4. No molar excess of functional groups was targeted and the concentrations of PEG-VS and PEG-SH were 5% (w/v) and 10% (w/v), respectively. Therefore, a final concentration of 5% (w/v) could be achieved by mixing equal volumes of the two PEG precursors and the cell-laden microgels-containing medium. The precursor concentrations were doubled in case of obtaining a gel with 10% (w/v) final concentration.

Microgel Co-encapsulation in Non-degradable Gels. Cell-laden microgels were first concentrated and resuspended in cell medium. For the microfluidic co-encapsulation, syringes were filled with equal volumes of cell-laden microgels and the two PEG precursors at the desired concentrations and run through

a second microfluidic chip having a height of 150 µm. For the casting of the thin gels, a glass slide was first treated to expose free thiols groups [18] and a drop of 30 µl of microgel-containing non-degradable gel was casted. A thin Sigmacote-treated coverslip was put on top of the drop in order to generate a thin gel layer. After polymerization (5min), the coverslip was removed and the gel attached to the glass slide transferred in medium.

Poly-L-lysine Microgels Coating. Microgels were incubated for different time in 0.5 mg/ml PLL solution. After incubation, the gels were washed extensively in PBS by using 70 µm strainers and resuspended either in PBS or in cell medium.

Gel Dissociation. Gel microbeads or disks were first washed with PBS to remove cell medium and then exposed to 1X Tryple Express (Life Technologies, USA) solution for 5 min and 20 min, respectively. Gels containing hyaluronic acid were dissociated for 30 min. After dissociation, cells were collected and resuspended in medium.

Rheology Measurements. 50µl gel disks were made and allowed to swell in PBS overnight. Swollen hydrogel disks of 1mm thickness were placed between the two plates of a Bohlin CV 120 rheometer and compressed up to 80% of their original thickness. Measurements were conducted in constant strain (5%) mode and in a frequency range between 0.1 and 10 Hz. Storage modulus (G') was plotted as a function of PEG content for both degradable and non-degradable gels.

Protein Labeling. NQ-conjugated RGD peptide (H-NQEQVSPLRGDSPERCG-NH$_2$, M.W. 1871.03 g/mol) was covalently modified with a heterofunctional N-hydroxysuccinimide (NHS)–Alexa546 fluorescent moiety (Invitrogen, USA). In order to avoid a cross-reaction of the fluorophore with the NH$_2$- groups present in the lysine amino acid of the K-RGD peptide, NQ-modified RGD was used for the fluorescent labeling. A molar excess of 7 moles of peptide per moles of fluorophore was used. The reaction was carried out at room temperature for one hour with the addition of a volume of PBS 10X equal to one tenth of the total volume in order to have a pH of 7.4. TRIS buffer (pH 7.5) was added for 30 min at the end of the reaction to quench the unreacted NHS- groups.

Image Analysis. Images were acquired with an inverted Olympus IX81 CellR microscope. In order to assess the cell encapsulation efficiency, 300 frames movies (frequency of acquisition of 30 Hz) were acquired at different time points and the cells were manually counted. Fluorescence measurements were performed using a Matlab script on 15 images per condition, with approximately 10 microgels each. Images were first rescaled to a normalized scale based on homogeneous imaging setup, the objects in the foreground were identified and a mask was generated based on bright-field images. A watershed function was used to automatically label beads. Finally, the average intensity per bead was calculated. Statistical t-test (type 2, number of tails 2) was performed on the samples. *** $p < 0.001$; * $p < 0.05$.

Staining and Confocal Microscopy. A cell viability assay was performed staining live cells with calcein AM (green, pre-dilution in DMSO 1:80 and dilution in PBS 1:660) and dead cells with ethidium iodide (red, dilution in PBS 1:1000). For confocal images cells were first fixed in 5% PFA for 10 min, permeabilized for 5 min by TritonX (0.2% solution in PBS) and then stained with Alexa488 phalloidin (Invitrogen, USA) and DAPI (Sigma, USA). Confocal images were acquired with an upright point-scanning confocal microscope (Zeiss, 710 LSM) equipped with a 405 nm diode laser (30 mW) and with W N-Achroplan ×20/0.5 or EC Plan-Neofluar ×10/0.30 objectives. IZ-stacks were recorded acquiring images every 5µm. Images were then processed with Imaris.

Cell Culture. R1 Oct4-GFP embryonic stem cells (ESC) were kindly provided by the Zandstra Laboratory (University of Toronto, Canada). ESC were cultured on 0.2% gelatin-coated Petri dishes in DMEM with 15% ESC Screened FBS (Fisher), pen-strep (10mg/ml, Invitrogen), sodium pyruvate (1 mM, Gibco), non-essential amino acids (0.1 mM, Invitrogen), beta-mercaptoethanol (0.1 mM, Life Technologies) and LIF (10^3 U/ml, Millipore). MDB-MA-231 cell line was kindly provided by the Brisken Laboratory (École Polytechnique Fédérale de Lausanne). GFP transfected fibroblasts and MDB-MA-231 cell line were cultured on tissue culture flasks in Dulbecco's Modified Eagle Medium (DMEM) with 10% Fetal Bovine Serum (FBS) and pen-strep (10mg/ml). After dissociation with trypsin (TripLE express, Gibco), cells were

re-suspended in 20% Optiprep-containing medium solution and mixed with the PEG premix in the syringe at desired concentrations. Cell-laden microbeads were cultured in suspension bioreactor (BioLevitator, Hamilton, Switzerland) for different days. During the inoculation phase, the rotation speed of the tubes was 50 rpm with an agitation period of 2 min for an entire duration of 4 hours. The agitation pause duration was set at 10 min for C2C12 cells and cancer cells to minimize microcarrier 'bridging'. During cell culture, the rotation speed was increased to 80 rpm for all cell types. 6 ml of medium was used during the inoculation phase (to maximize cell-microgel contact) and 20 ml during cell culture. Medium was replaced every two days. In order to assess cell escape, instead, cell-laden microbeads were transferred on tissue-culture plastic plates.

Flow cytometry analysis. Cells were analyzed by flow cytometry using Cyan ADPS analyzer (Beckman Coulter). Data analysis was performed with FlowJo software.

References

1   Panda, P. *et al*. Stop-flow lithography to generate cell-laden microgel particles. *Lab Chip* **8**, 1056-1061 (2008).

2   Yeh, J. *et al*. Micromolding of shape-controlled, harvestable cell-laden hydrogels. *Biomaterials* **27**, 5391-5398 (2006).

3   Sakai, S. *et al*. Cell-enclosing gelatin-based microcapsule production for tissue engineering using a microfluidic flow-focusing system. *Biomicrofluidics* **5** (2011).

4   Yamada, K. M. & Cukierman, E. Modeling tissue morphogenesis and cancer in 3D. *Cell* **130**, 601-610 (2007).

5   Barrila, J. *et al*. Organotypic 3D cell culture models: using the rotating wall vessel to study host-pathogen interactions. *Nat Rev Microbiol* **8**, 791-801 (2010).

6   Pampaloni, F., Reynaud, E. G. & Stelzer, E. H. K. The third dimension bridges the gap between cell culture and live tissue. *Nat Rev Mol Cell Bio* **8**, 839-845 (2007).

7   Velasco, D., Tumarkin, E. & Kumacheva, E. Microfluidic Encapsulation of Cells in Polymer Microgels. *Small* **8**, 1633-1642 (2012).

8   Headen, D. M., Aubry, G., Lu, H. & Garcia, A. J. Microfluidic-Based Generation of Size-Controlled, Biofunctionalized Synthetic Polymer Microgels for Cell Encapsulation. *Adv Mater* **26**, 3003-3008 (2014).

9   Li, C. Y., Wood, D. K., Huang, J. H. & Bhatia, S. N. Flow-based pipeline for systematic modulation and analysis of 3D tumor microenvironments. *Lab Chip* **13**, 1969-1978 (2013).

10   Rossow, T. *et al*. Controlled Synthesis of Cell-Laden Microgels by Radical-Free Gelation in Droplet Microfluidics. *J Am Chem Soc* **134**, 4983-4989 (2012).

11   Tsuda, Y., Morimoto, Y. & Takeuchi, S. Monodisperse Cell-Encapsulating Peptide Microgel Beads for 3D Cell Culture. *Langmuir* **26**, 2645-2649 (2010).

12   Matsunaga, Y. T., Morimoto, Y. & Takeuchi, S. Molding Cell Beads for Rapid Construction of Macroscopic 3D Tissue Architecture. *Adv Mater* **23**, H90-H94 (2011).

13   Ma, S. H. *et al*. Monodisperse collagen-gelatin beads as potential platforms for 3D cell culturing. *J Mater Chem B* **1**, 5128-5136 (2013).

14   Tumarkin, E. *et al*. High-throughput combinatorial cell co-culture using microfluidics. *Integr Biol-Uk* **3**, 653-662 (2011).

15   Kumachev, A. *et al.* High-throughput generation of hydrogel microbeads with varying elasticity for cell encapsulation. *Biomaterials* **32**, 1477-1483 (2011).

16   Morimoto, Y., Tan, W. H., Tsuda, Y. & Takeuchi, S. Monodisperse semi-permeable microcapsules for continuous observation of cells. *Lab Chip* **9**, 2217-2223 (2009).

17   Jia, X. Q. *et al.* Hyaluronic acid-based microgels and microgel networks for vocal fold regeneration. *Biomacromolecules* **7**, 3336-3344 (2006).

18   Allazetta, S., Hausherr, T. C. & Lutolf, M. P. Microfluidic Synthesis of Cell-Type-Specific Artificial Extracellular Matrix Hydrogels. *Biomacromolecules* **14**, 1122-1131 (2013).

19   Ehrbar, M. *et al.* Enzymatic formation of modular cell-instructive fibrin analogs for tissue engineering. *Biomaterials* **28**, 3856-3866 (2007).

20   Clausell-Tormos, J. *et al.* Droplet-based microfluidic platforms for the encapsulation and screening of mammalian cells and multicellular organisms (vol 15, pg 427, 2008). *Chem Biol* **15**, 875-875 (2008).

21   Mazutis, L. *et al.* Single-cell analysis and sorting using droplet-based microfluidics. *Nat Protoc* **8**, 870-891 (2013).

22   Horiguchi, I., Chowdhury, M. M., Sakai, Y. & Tabata, Y. Proliferation, Morphology, and Pluripotency of Mouse Induced Pluripotent Stem Cells in Three Different Types of Alginate Beads for Mass Production. *Biotechnol Progr* **30**, 896-904 (2014).

23   Maguire, T., Novik, E., Schloss, R. & Yarmush, M. Alginate-PLL microencapsulation: Effect on the differentiation of embryonic stem cells into hepatocytes. *Biotechnol Bioeng* **93**, 581-591 (2006).

24   Tabata, Y., Horiguchi, I., Lutolf, M. P. & Sakai, Y. Development of bioactive hydrogel capsules for the 3D expansion of pluripotent stem cells in bioreactors. *Biomater Sci-Uk* **2**, 176-183 (2014).

25   Krasaekoopt, W., Bhandari, B. & Deeth, H. The influence of coating materials on some properties of alginate beads and survivability of microencapsulated probiotic bacteria. *Int Dairy J* **14**, 737-743 (2004).

26   Morgan, D. M. L., Larvin, V. L. & Pearson, J. D. Biochemical-Characterization of Polycation-Induced Cyto-Toxicity to Human Vascular Endothelial-Cells. *J Cell Sci* **94**, 553-559 (1989).

27   Fischer, D., Li, Y. X., Ahlemeyer, B., Krieglstein, J. & Kissel, T. In vitro cytotoxicity testing of polycations: influence of polymer structure on cell viability and hemolysis. *Biomaterials* **24**, 1121-1131 (2003).

28   Ridley, A. J. *et al.* Cell migration: Integrating signals from front to back. *Science* **302**, 1704-1709 (2003).

29   Takamatsu, H. & Rubinsky, B. Viability of deformed cells. *Cryobiology* **39**, 243-251 (1999).

30   Gawlitta, D. *et al.* The relative contributions of compression and hypoxia to development of muscle tissue damage: An In vitro study. *Ann Biomed Eng* **35**, 273-284 (2007).

31   Geraths, C. *et al.* Synthesis and characterization of a stimulus-responsive L-ornithine-degrading hydrogel. *J Control Release* **165**, 38-43 (2013).

32   Lutolf, M. P. & Hubbell, J. A. Synthesis and physicochemical characterization of end-linked poly(ethylene glycol)-co-peptide hydrogels formed by Michael-type addition. *Biomacromolecules* **4**, 713-722, doi:Doi 10.1021/Bm025744e (2003).

33   Allazetta, S., Cosson, S. & Lutolf, M. P. Programmable microfluidic patterning of protein gradients on hydrogels. *Chem Commun* **47**, 191-193 (2011).

General Discussion and Outlook

In this thesis, novel microfluidic technologies were established to recapitulate some of the complex biophysical and biochemical interactions present within the native stem cell microenvironment. Compared to existing microscale technologies, this work developed versatile tools displaying the capability to: (i) pattern the surface of a biomimetic hydrogel with user-defined biomolecule gradients; (ii) probe the morphogen-dose effect on pluripotent stem cells; (iii) generate microgels with well-defined dimensional and biochemical properties allowing the culture of multiple stem cell types in bioreactor-based cultures; (iv) modulate microgel elasticity and biochemical ligand concentration in a combinatorial fashion, generating a continuous landscape of microenvironmental conditions; (v) interface the microgels with high-throughput screening analysis; (vi) encapsulate mammalian cells within microcapsules of varying physico-chemical properties.

In a first approach, we developed a microfluidic technology to display gradients of Fc- or biotin-tagged biomolecules on the surface of ProteinA- or NeutrAvidin-functionalized hydrogels. Computer-controlled hydrodynamic flow focusing allowed for the generation of user-defined graded profiles of nearly any type of shape, such as linear, exponential and gaussian. Modulation of the flow parameters afforded fine control over the patterning resolution and composition. By using more sophisticated microfluidic approaches, gradient patterning could be parallelized to obtain arrays of orthogonally overlapping gradients, allowing for probing *in vitro* the effect of multiple biomolecule gradients on cell behavior. Furthermore, this method combines spatial patterning by microfluidics with macro-scale cell culture on biomimetic gel substrates, rendering it suitable for a broad range of multiple cell-based assays, such as cell migration, axonal growth and the biology of pluripotent stem cells. Therefore, the platform was used to assess an optimal concentration of tethered leukemia inhibitor factor (LIF) supporting mouse embryonic stem cell self-renewal.

Next, built on the previous system, we established a novel approach able to simultaneously control biophysical and biochemical cues, for studying the effect of multiple microenvironmental factors on stem cell behavior. Therefore, we combined droplet-based microfluidics and synthetic hydrogels for the reliable generation of monodisperse microgels with extremely well defined biochemical and biophysical properties. For the first time, we were able to precisely tune the microgel biochemical properties. The versatility of the chosen approach allowed us to functionalize the microgels with single or multiple proteins or peptides of interest and to combine additives (such as magnetic particles), rendering the microgels suitable for suspension culture of multiple stem cell types.

Since in most cases a combination of many microenvironmental cues jointly regulate stem cell behavior, we developed a microfluidic platform to generate combinatorial microgels with varying elasticity, biochemical ligands or both. A programmable approach was employed to sequentially dilute *on chip* the biophysical gel building blocks with fluorescent moieties, changing the stream flow rates in an automated fashion. Therefore, microgels with varying elasticity were synthesized and distinguished based on the intensity of a fluorescent molecule.

Microgels with elastic moduli spanning in a range of cell physiological relevance (from 10kPa up to 100 kPa) were generated, as demonstrated by atomic force microscopy analysis. Furthermore, the same programmable approach was implemented for the generation of microgels with varying concentrations of a fluorescently tagged RGD peptide. Owing to the efficient binding affinity, we could rely on a linear correlation between microgel intensity and its physico-chemical properties, suggesting a high control over the microgel composition. The combination of the two technologies allowed for the generation of microgels with modular elasticities and protein concentrations, at the same time. Fine modulation of the microfluidic flows allowed for the formation of a continuous landscape of hundred combinations of microgels, each bearing specific physico-chemical properties, encoded by specific values of fluorescent intensity.

Although we proved the capability of combinatorial microgels to support cell adhesion and proliferation, the technology relied upon an image-based readout analysis, not suitable for high-throughput screenings. Fully exploiting the potential of the developed technology would require interfacing the microgels with high-throughput analysis technologies, such as flow cytometry. The ease of manipulation and the high-throughput generation via droplet-based microfluidics make the microgels ideal candidates for screening the enormous diversity of stem cell microenvironments in high-throughput. Therefore, we developed a microfluidic chip able to generate combinatorial microgels with a size compatible to flow cytometry-based analysis.

This work presents also the possibility to successfully implement the microgel technology for cell encapsulation within microcapsules with defined biophysical and biochemical properties. At this purpose, factorXIIIa enzyme was used to mediate the polymerization of PEG-based hydrogels, enabling the cell encapsulation under mild conditions and, for the first time, the modulation of the microcapsule elasticity, biodegradability and the biochemical properties. In this thesis, we showed the possibility to control the encapsulation efficiency of multiple cell types, such as fibroblasts, mouse embryonic stem cells and cancer cells. Since cell escape significantly limited the potential of the technology for long-term cell culture studies, we explored some possibilities to prevent it by either engineering a chemical or a physical barrier. Co-encapsulation of microbeads within a non-degradable gel would partially prevent cell escape, yet limiting the possibility to retrieve the cells for further biological analysis.

Taken all these achievements together, we envision that, in the future, the combinatorial microgel platform in combination with suitable high-throughput screening analysis methods will provide new insights in the influence of the microenvironment in stem cell or cancer biology. Furthermore, combinatorial modulation of the microcapsule properties would pave the way towards the investigation, in a 3D context, of cell behavior under different microenvironmental stimuli.

Suggested improvements for the combinatorial microgel platform

The combinatorial microgel platform can be used as a novel system which may help dissect the mechanisms and principles governing the microenvironmental regulation of stem cell fate. However, the potential of the technology is hindered so far by the complex image-based analysis required. Imaging of cell-coated or cell-laden microgels requires the acquisition of Z-stacks to capture the cell signal from the entire 3D surface of the bead. Standard light microscopy would be, therefore, insufficient for a reliable detection of the signal. In fact, 'light leakage' from the different focal planes would compromise the analysis, causing an overestimation of the actual fluorescent signal. Moreover, although the PEG is translucent, fluorescent lasers have different optical paths at different wavelengths, i.e. the detection of certain objects at focal planes far from the objectives would be different from the one of objects closer to the objective. To overcome these limitations, adoption of confocal or spinning disc confocal microscopy would be necessary, which would, on the other hand, extend the acquisition times to durations incompatible with high-throughput analysis. Furthermore, the computational analysis used for measuring microgel intensity should be adapted for processing 3D stack images, as well as for better clustering the distinct discrete microgel populations.

With these limitations in mind and motivated by the ease in microgel manipulation, we decided to tailor our technology to existing high-throughput analysis techniques, such as flow cytometry, suitable for reliably analyzing the intensity of 3D objects.

Many biological processes are influenced by very low substrate elasticity, usually below 1kPa.[1] Microgels within this range of elasticity were successfully generated with a PEG content of around 1.5% (w/v). However, the incorporation of the red encoding fluorophore at this concentration was not very efficient, due to the lack of chemical binding groups (in our case SH-groups) able to link the maleimide moieties of the fluorophore. Hence, correlation between the fluorescent intensity and the elastic modulus was not linear any more.

To prevent this problem, chemical pre-coupling of the PEG-SH precursor with the maleimide-activated fluorophore could be performed, by targeting a few percent of the total reactive groups available. Successful preliminary investigation was carried out, showing microgels with different elasticities, different swelling ratios and different fluorescent intensities. In this case, the bead size would be directly proportional to fluorophore intensity. Hence, we envision that this strategy would allow for preventing any non-linearity of the system at low PEG concentrations, reliably correlating fluorescence intensity to microgel elasticity in a broader range of mechanical properties.

In order to increase the technology potential, a future enhancement could take into account the modification of the microfluidic design to allow for the modulation of more than two microgel properties. Therefore, the insertion of other microfluidic channels would enable the generation of 'on-demand' multi-components microgels, for instance, suitable for studying simultaneously the effect of the substrate elasticity and multiple growth factors on cell behavior.

Suggested improvements for the 3D cell encapsulation technology

Cell compartmentalization in microcapsules offers a unique tool for easily observing single cell behavior in regards to their microenvironment. Modulation of the physico-chemical properties of the microcapsules holds the promise to carry out high-throughput screening of 3D matrixes supporting specific cell functions.

However, this technology presents some limitations, especially concerning the control over the number of cells encapsulated per bead. As reported in the last chapter of this thesis, cell distribution follows a stochastic Poisson-like distribution. Further enhancements of this technology should implement some microfluidic strategy to achieve higher control over the number of cells encapsulated. For instance, tuning the channel aspect ratio have been shown to evenly space the cells while travelling in the microchannels, enabling a very well-ordered single cell encapsulation.[2] Another interesting approach used Dean forces in curved microchannels to spatially arrange the position of cells and obtain controlled encapsulation.[3]

However, the major bottleneck of this technology is represented by the cell escape. At the short distance range of a microcapsule, cells tend to leave from their confinement with a kinetic dependent on the cell type and on the matrix degradability and stiffness.

Although this thesis investigated some biochemical and physical strategies to overcome this limitation, other approaches should be examined to ameliorate the performances of the technology. An elegant solution would be to microfluidically generate double emulsions, such as water-in-oil-in-water emulsions, therefore microfluidically generate an additional layer, acting as cell physical barrier. Such approach has been already used for industrial applications, drug delivery[4,5] and for rapid formation of stem cell spheroids[6], also in combination with flow cytometry.[7] Based on these approaches, in this thesis co-encapsulation of cell-laden microbeads in non-degradable microcapsules was demonstrated. However, designing a selectively degradable outer matrix would be of great benefit to retrieve the cells for further analysis. One interesting example has been demonstrated in[8] where they used proteases from tobacco etch virus (TEV). The integration into the gel network of a specific amino acid sequence selectively recognized by such proteases could be elegantly adopted for a selective degradation of different bead layers.

Furthermore, we could also imagine employing the platform for 3D cell co-culture models. In fact, modeling the *in vivo* cellular microenvironment typically involves co-culturing of different types of cells in a three-dimensional matrix. For instance, cell-cell interactions between cancer and stromal cells play a key role in tumor growth and invasion.[9-11] Hence, the microfluidic platform presented in this thesis could be potentially used to generate cell-laden microgels, simultaneously supporting cell aggregation and attachment on their surface, for studying the interactions of multiple cell types. Finally, microfluidic co-encapsulation of a bead within another bead could be also implemented for the generation of modular microsystems, suitable for engineering various biological models of cell co-culturing.

Envisioned applications of the combinatorial microgel platform

The combinatorial microgel platform, developed in this thesis, enables the high-throughput generation of microgels, acting as cellular microenvironments with precisely controlled physico-chemical properties. Owing to their easy manipulation and the possibility to precisely modulate their size, microgels can be interfaced with cytometry-based analysis technologies, paving the way towards an unprecedented manner of performing high-throughput screenings.

Most of the high-throughput biomaterials research conducted has been limited to the assessment of the interactions between stem cells and material surfaces, based on microscopy automation, which allows cell behavior on these surfaces to be evaluated only in a relative high throughput manner.[12] Despite some interesting examples of screening cytotoxic drugs[13,14] or antibiotics[15], by combining droplet microfluidic technology with high-throughput techniques, there are no evidences in literature about the investigation of the effects of microenvironmental perturbations on cell behavior.

We envision that our platform could be used for microgel-based high-throughput screenings, in combination with robotic handling and with cytometry-based analysis techniques (Figure 1). The unique possibility to use these microgels, both as 3D matrixes and as 2D substrates, having multiple physico-chemical properties, would allow the influence of combinatorial exogenous signaling cues on cell behavior to be unveiled both in 2D and in 3D context. Furthermore, manipulation of microgels into single wells of a microtiter plate would additionally allow for screening the effects of different soluble compounds, such as growth factors or drugs. Hence, multiple combinations of various microenvironmental factors and soluble cues could be screened simultaneously. Subsequent cytometry-based analysis would enable the assessment of the expression of specific biomarkers of interest in regards to precisely defined culture conditions.
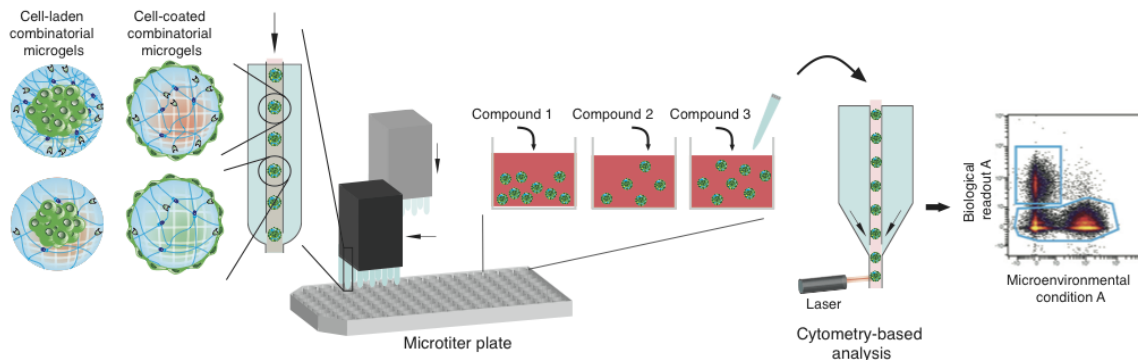
Figure 1 - Microgel-based high-throughput screening. Schematic of the integration of the microgel-based technology with high-throughput screening platforms. Cell-laden or cell-coated combinatorial microgels can be easily handled and dispensed by robotic equipment in wells of a microtiter plate. Multiple soluble factors, such as drugs or growth factors, can be added at several concentrations, for high-throughput screening of multiple exogenous signaling cues on cell behavior. Microgels can be then analyzed by means of cytometry-based analysis, such as flow or mass cytometry, to correlate the expression of biological markers of interest to specific microenvironmental culture conditions.

This platform could find several applications in basic or applied biology, for new drug discovery and toxicology tests, with a strong impact in the stem cell or cancer field. Envisioning these kinds of applications, a suitable readout analysis method, able to capture multiple channels simultaneously, appears crucial. Polychromatic flow cytometry-based approaches could be adopted. However, increasing the number of microenvironmental properties and cellular readouts analyzed would require strategies alternative to a fluorescence-based approach, limited by an overlapping of the fluorophore optical spectra. At this purpose, mass cytometry, a novel technique coupling flow cytometry and mass spectrometry, would be a valuable option. This technology, in fact, has been recently developed to overcome the compensation issues related to a fluorescence-based analysis and to significantly increase the number of biomarkers being interrogated.[16,17] The technique relies on labeling multiple biomarkers with unique metal isotopes, increasing the analysis up to 70-100 parameters, in shorter times. A preliminary successful analysis of microgels by means of a mass cytometer has been achieved in this thesis. We strongly believe that designing combinations of isotopes to selectively encode for the different microgel properties would enable the investigation of complex microenvironment-mediated biological phenomena that cannot be studied anyhow else.

References

1   Gomez, E. W., Chen, Q. K., Gjorevski, N. & Nelson, C. M. Tissue Geometry Patterns Epithelial-Mesenchymal Transition Via Intercellular Mechanotransduction. *J Cell Biochem* **110**, 44-51 (2010).

2   Edd, J. F. *et al*. Controlled encapsulation of single-cells into monodisperse picolitre drops. *Lab Chip* **8**, 1262-1264 (2008).

3   Kemna, E. W. M. *et al*. High-yield cell ordering and deterministic cell-in-droplet encapsulation using Dean flow in a curved microchannel. *Lab Chip* **12**, 2881-2887 (2012).

4   Engel, R. H., Riggi, S. J. & Fahrenba.Mj. Insulin - Intestinal Absorption as Water-in-Oil-in-Water Emulsions. *Nature* **219**, 856-& (1968).

5   Gresham, P. A., Barnett, M., Smith, S. V. & Schneide.R. Use of a Sustained-Release Multiple Emulsion to Extend Period of Radioprotection Conferred by Cysteamine. *Nature* **234**, 149-& (1971).

6   Chan, H. F. *et al*. Rapid formation of multicellular spheroids in double-emulsion droplets with controllable microenvironment. *Sci Rep-Uk* **3** (2013).

7   Yan, J. *et al*. Monodisperse Water-in-Oil-in-Water (W/O/W) Double Emulsion Droplets as Uniform Compartments for High-Throughput Analysis via Flow Cytometry. *Micromachines-Basel* **4**, 402-413 (2013).

8   Kapust, R. B. *et al*. Tobacco etch virus protease: mechanism of autolysis and rational design of stable mutants with wild-type catalytic proficiency. *Protein Engineering* **14**, 993-1000 (2001).

9   Kalluri, R. & Zeisberg, M. Fibroblasts in cancer. *Nature reviews*. *Cancer* **6**, 392-401 (2006).

10   Littlepage, L. E., Egeblad, M. & Werb, Z. Coevolution of cancer and stromal cellular responses. *Cancer cell* **7**, 499-500 (2005).

11   Bissell, M. J. & Radisky, D. Putting tumours in context. *Nature reviews. Cancer* **1**, 46-54 (2001).

12   Mei, Y., Goldberg, M. & Anderson, D. The development of high-throughput screening approaches for stem cell engineering. *Curr Opin Chem Biol* **11**, 388-393 (2007).

13   Brouzes, E. *et al*. Droplet microfluidic technology for single-cell high-throughput screening. *P Natl Acad Sci USA* **106**, 14195-14200 (2009).

14   Theberge, A. B. *et al*. Microfluidic platform for combinatorial synthesis in picolitre droplets. *Lab Chip* **12**, 1320-1326 (2012).

15   Churski, K. *et al*. Rapid screening of antibiotic toxicity in an automated microdroplet system. *Lab Chip* **12**, 1629-1637 (2012).

16   Bodenmiller, B. *et al*. Multiplexed mass cytometry profiling of cellular states perturbed by small-molecule regulators. *Nat Biotechnol* **30**, 858-U889 (2012).

17   Bendall, S. C., Nolan, G. P., Roederer, M. & Chattopadhyay, P. K. A deep profiler's guide to cytometry. *Trends Immunol* **33**, 323-332 (2012).

Appendix A

Supplementary Information: Patterning of Cell-instructive Hydrogels by Hydrodynamic Flow Focusing

Characterization of longitudinal stability of patterned gradients[4]
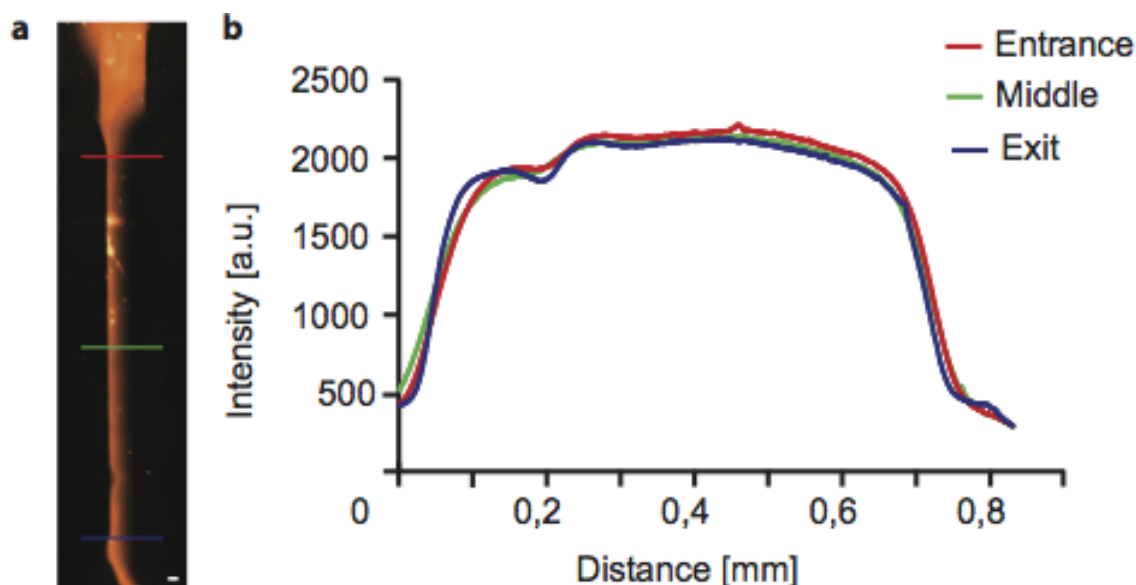
Figure S1 - Characterization of longitudinal stability of patterned gradients. a, Stitched fluorescent micrographs of a stripe pattern by HFF on hydrogel. (Scale bar = 200 µm) **b**, Graphical representation of the intensity profile measured at, respectively, the entrance (red line), the mid section (green line) and the end (blue line) of patterned stripe shown in **a**.

Complex generation of biologically relevant protein gradients
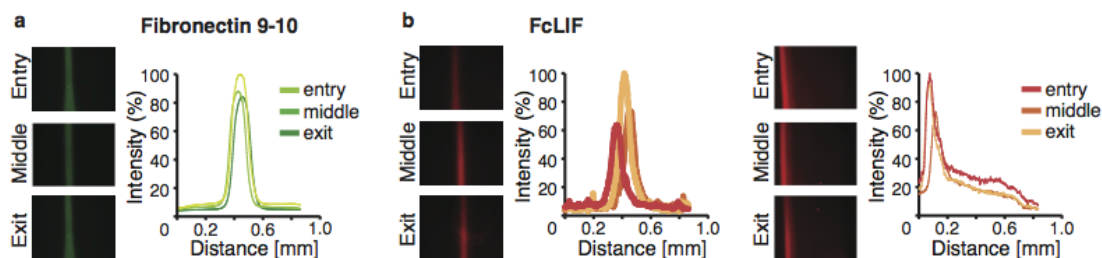
Figure S2 - HFF-based patterning of more complex gradient profiles for biologically relevant proteins. a, Micrographs and intensity profile plots of FITC-FNIII9-10-biotin on NeutrAvidin-functionalized PEG hydrogels. Gaussian gradient profiles were obtained. **b**, Micrographs and intensity profile plots of DsRED-FcLIF on ProteinA-functionalized PEG hydrogels. Exponential and Gaussian gradient profiles were obtained.

---

[4] This appendix is adapted with permission from Cosson, S., Allazetta, S. & Lutolf, M.P., Patterning of Cell-Instructive Hydrogels by Hydrodynamic Flow Focusing, *Lab on a Chip* 13, 2099-2105. Copyright © 2013 Royal Society of Chemistry.
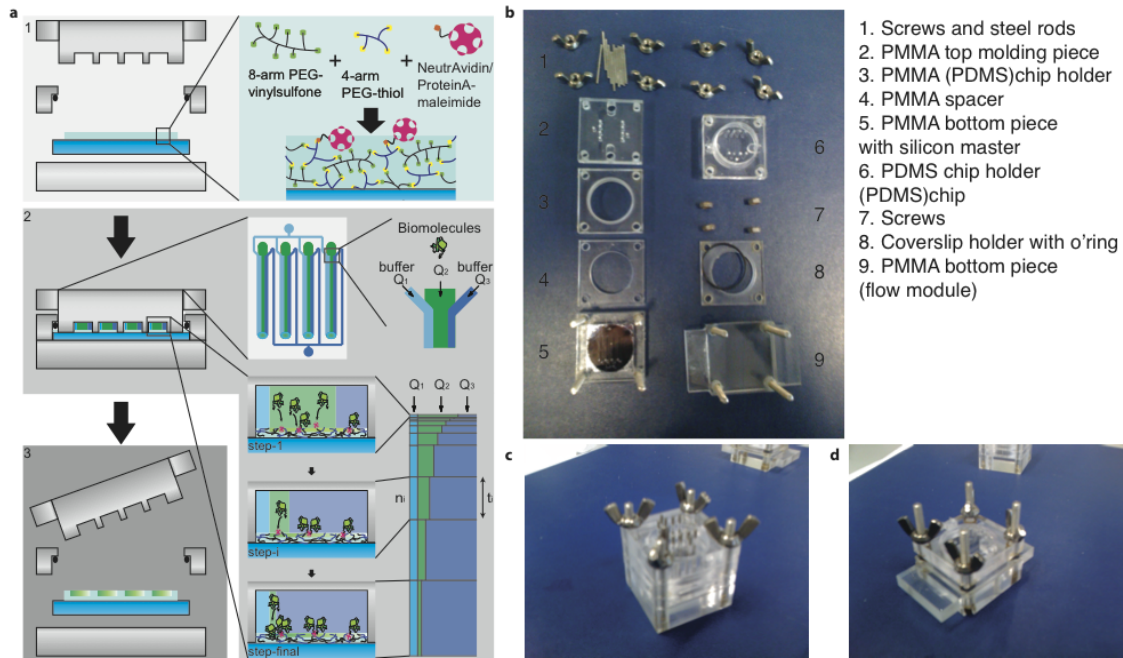
Figure S3 - Modular microfluidic device assembly for injection molding and microfluidics patterning of four parallel biomolecular gradients on hydrogel. a, Microfluidic patterning of four parallel gradients. *Step 1.* The device was assembled onto hydrogels functionalized with NeutrAvidin and/or ProteinA, casted on round coverslips (right box). These hydrogels are then placed onto the bottom piece. An O-ring and a coverslip holder are tightened to prevent the hydrogel to slide. The PDMS chip enclosed in the holder is pressed onto the construct and tightened to ensure proper sealing of the microchannels. *Step 2.* The microfluidic layout comprises four parallel flow focusing units and it was used to pattern linear gradients of proteins by hydrodynamic flow focusing. Control of the buffer (Q_1 and Q_3) and protein solution (Q_2) flow rates enables to sequentially reduce, in several steps (n_i), the protein stream width (green) from right-to-left. NeutrAvidin and/or ProteinA grafted to the hydrogel readily capture (black arrows) tagged proteins from solution. The duration of individual steps (t_i) dictates the amount of protein being locally captured on the hydrogel surface. *Step 3.* The device can be disassembled and the patterned coverslip can be recovered for further imaging and cell experiments. **b**, Molding module (left) and microfluidic module (right) with different pieces required for PDMS molding. The different pieces required for microfluidics are depicted and labelled. **c**, Assembled module for PDMS injection molding. **d**, Assembled microfluidic device.
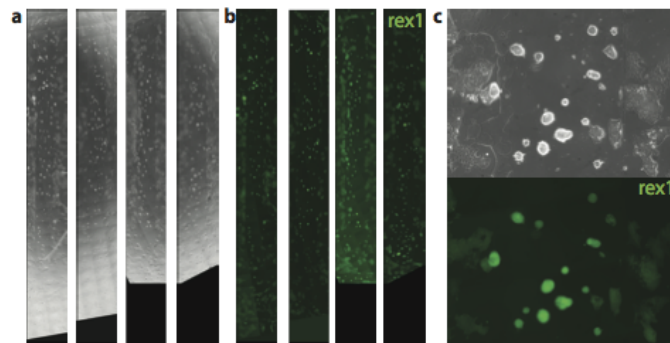
Figure S4 - ESCs cultured on tethered FcLIF gradients. a-b, Stitched brightfield (a) and fluorescent (b) micrographs of ESCs cultured on tethered FcLIF gradients. **c**, Brightfield and fluorescent images of ESCs culture on adherent hydrogel in presence of soluble FcLIF.

Summary of programming parameters

NeutrAvidin/BSA-biotin												
	5 steps				10 steps				20 steps			
step	time [s]	Q1 [µl/min]	Q2 [µl/min]	Q3 [µl/min]	time [s]	Q1 [µl/min]	Q2 [µl/min]	Q3 [µl/min]	time [s]	Q1 [µl/min]	Q2 [µl/min]	Q3 [µl/min]
1	0.1	12	10	3	0.2	12	10	3	0.1	12	10	3
2	54	14	8	3	22.8	13	9	3	10.8	12.5	9.5	3
3	60	16	6	3	24.6	14	8	3	10.8	13	9	3
4	144.6	18	4	3	25.2	15	7	3	11.4	13.5	8.5	3
5	941.4	20	2	3	25.8	16	6	3	12	14	8	3
6					39	17	5	3	12	14.5	7.5	3
7					59.4	18	4	3	12	15	7	3
8					87.6	19	3	3	11.4	15.5	6.5	3
9					128.4	20	2	3	12	16	6	3
10					787.2	21	1	3	13.8	16.5	5.5	3
11									18.6	17	5	3
12									23.4	17.5	4.5	3
13									27.6	18	4	3
14									31.8	18.5	3.5	3
15									39.6	19	3	3
16									49.8	19.5	2.5	3
17									58.8	20	2	3
18									64.2	20.5	1.5	3
19									82.8	21	1	3
20									697.2	21.5	0.5	3

Table S1 – Program parameters for linear gradient patterning/effect of discrete step number

NeutrAvidin/BSA-biotin										
		linear 10 µl/min			linear 15 µl/min			linear 20 µl/min		
step	time [s]	Q1 [µl/min]	Q2 [µl/min]	Q3 [µl/min]	Q1 [µl/min]	Q2 [µl/min]	Q3 [µl/min]	Q1 [µl/min]	Q2 [µl/min]	Q3 [µl/min]
1	0.2	12	10	3	7	15	3	2	20	3
2	22.8	13	9	3	8.5	13.5	3	4	18	3
3	24.6	14	8	3	10	12	3	6	16	3
4	25.2	15	7	3	11.5	10.5	3	8	14	3
5	25.8	16	6	3	13	9	3	10	12	3
6	39	17	5	3	14.5	7.5	3	12	10	3
7	59.4	18	4	3	16	6	3	14	8	3
8	87.6	19	3	3	17.5	4.5	3	16	6	3
9	128.4	20	2	3	19	3	3	18	4	3
10	787.2	21	1	3	20.5	1.5	3	20	2	3

Table S2 - Program parameters for linear gradient patterning/ effect of flow rate

NeutrAvidin/BSA-biotin

		Exponential				Gaussian		
step	time [s]	Q1 [µl/min]	Q2 [µl/min]	Q3 [µl/min]	time [s]	Q1 [µl/min]	Q2 [µl/min]	Q3 [µl/min]
1	0.1	12	10	3	0.1	7.5	10	7.5
2	0.6	13	9	3	0.6	8	9	8
3	0.6	14	8	3	1.8	8.5	8	8.5
4	0.6	15	7	3	4.8	9	7	9
5	2.4	16	6	3	10.8	9.5	6	9.5
6	5.4	17	5	3	21.6	10	5	10
7	11.4	18	4	3	37.2	10.5	4	10.5
8	25.2	19	3	3	68.4	11	3	11
9	57	20	2	3	175.2	11.5	2	11.5
10	1096.8	21	1	3	879.6	12	1	12

Table S3 - Program parameters for complex gradient patterning

Protein A/IgG

	linear				exponential				Gaussian			
step	time [s]	Q1 [µl/min]	Q2 [µl/min]	Q3 [µl/min]	time [s]	Q1 [µl/min]	Q2 [µl/min]	Q3 [µl/min]	time [s]	Q1 [µl/min]	Q2 [µl/min]	Q3 [µl/min]
1	0.2	12	10	3	3.6	7	15	3	0	5	15	5
2	27	13	9	3	2.4	8.5	13.5	3	0.6	5.75	13.5	5.75
3	39	14	8	3	3	10	12	3	0	6.5	12	6.5
4	72	15	7	3	6	11.5	10.5	3	1.8	7.25	10.5	7.25
5	71.4	16	6	3	9.6	13	9	3	6.6	8	9	8
6	82.2	17	5	3	16.2	14.5	7.5	3	17.4	8.75	7.5	8.75
7	105.6	18	4	3	42	16	6	3	54	9.5	6	9.5
8	130.2	19	3	3	96.6	17.5	4.5	3	140	10.25	4.5	10.25
9	225	20	2	3	182.4	19	3	3	268.2	11	3	11
10	447.6	21	1	3	838.2	20.5	1.5	3	701.4	11.75	1.5	11.75

Table S4 - Program parameters for gradient patterning

160
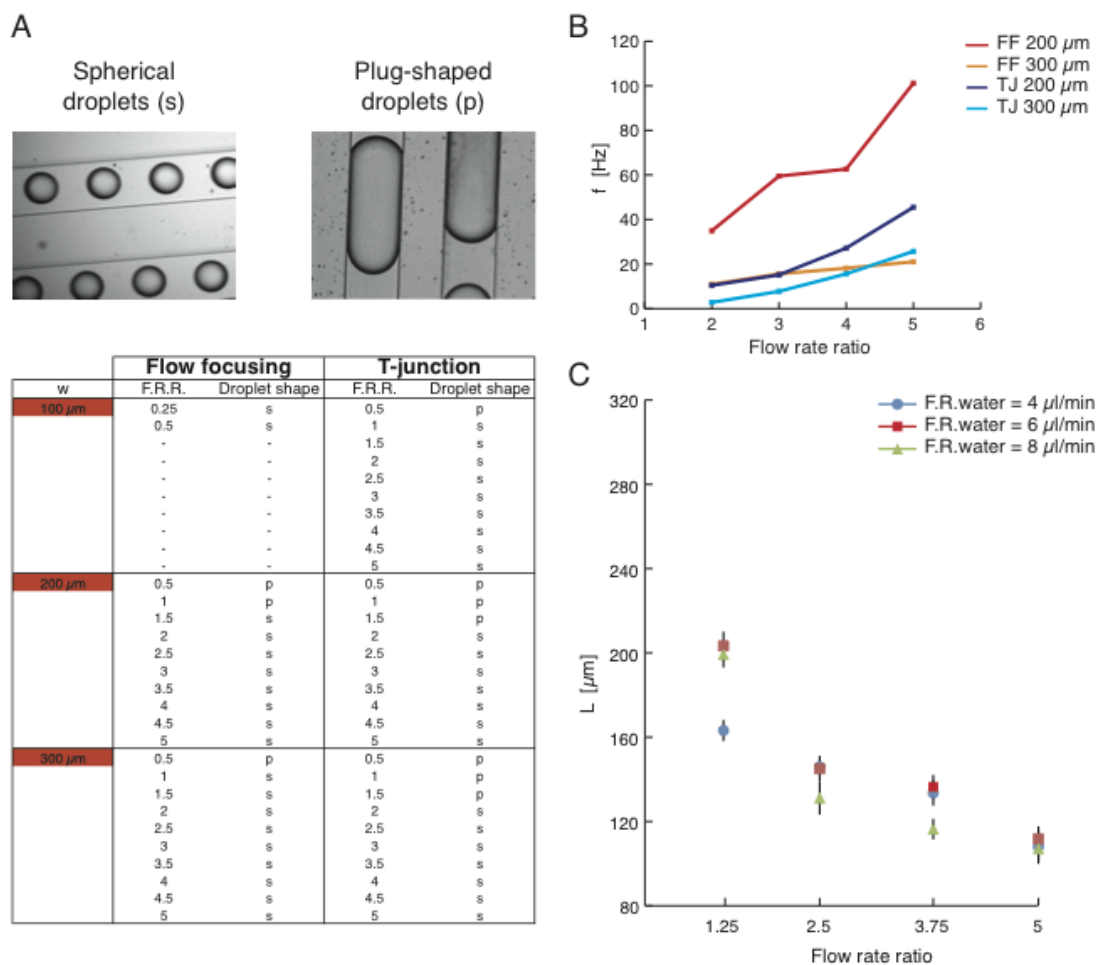
Appendix B

Supplementary Information: Microfluidic Synthesis of Cell-Type-Specific Artificial Extracellular Matrix Hydrogels

Characterization of the droplet frequency generation [5]

w	Flow focusing		T-junction	
	F.R.R.	Droplet shape	F.R.R.	Droplet shape
100 µm	0.25	s	0.5	p
	0.5	s	1	s
	-	-	1.5	s
	-	-	2	s
	-	-	2.5	s
	-	-	3	s
	-	-	3.5	s
	-	-	4	s
	-	-	4.5	s
	-	-	5	s
200 µm	0.5	p	0.5	p
	1	p	1	p
	1.5	s	1.5	p
	2	s	2	s
	2.5	s	2.5	s
	3	s	3	s
	3.5	s	3.5	s
	4	s	4	s
	4.5	s	4.5	s
	5	s	5	s
300 µm	0.5	p	0.5	p
	1	s	1	p
	1.5	s	1.5	p
	2	s	2	s
	2.5	s	2.5	s
	3	s	3	s
	3.5	s	3.5	s
	4	s	4	s
	4.5	s	4.5	s
	5	s	5	s

Figure S1. Droplet frequency generation. A. Depending on the flow rate ratio between the continuous and the discontinuous phase droplets can have two different shapes, plug-like or spherical. The table reports the droplets shapes for different values of flow rate ratios and for the microchannel geometries tested. *p* and *s* stand for plug-like shape and spherical, respectively. **B.** The graph shows the relationship between the flow rate ratio and the frequency (*f*) of droplets generation for different microchannel designs. The frequency was calculated as the ratio between flow rate of the discontinuous phase and the volume of the droplet generated. Flow focusing design with 200 µm-wide microchannel shows the highest frequency generation, compared to the other designs. The bigger is the microchannel width and the lower is the frequency, due to the higher droplets dimensions. Microfluidic designs with 100 µm-wide microchannels were not included because the droplets formation was just stable for few flow rate ratio values, hence not allowing for a systematic comparison. **C.** Microdroplet dimensions at different flow rate ratios with different water flow rates (4 µl/min, 6 µl/min and 8 µl/min). By keeping the same flow rate ratio, independently from the water flow rate used, microdroplets have a similar length. Furthermore, by increasing the flow rate ratio, microdroplet formation appears more stable, as revealed by a lower

difference in droplet size at different water flow rates. 200 µm flow focusing design was used for the characterization
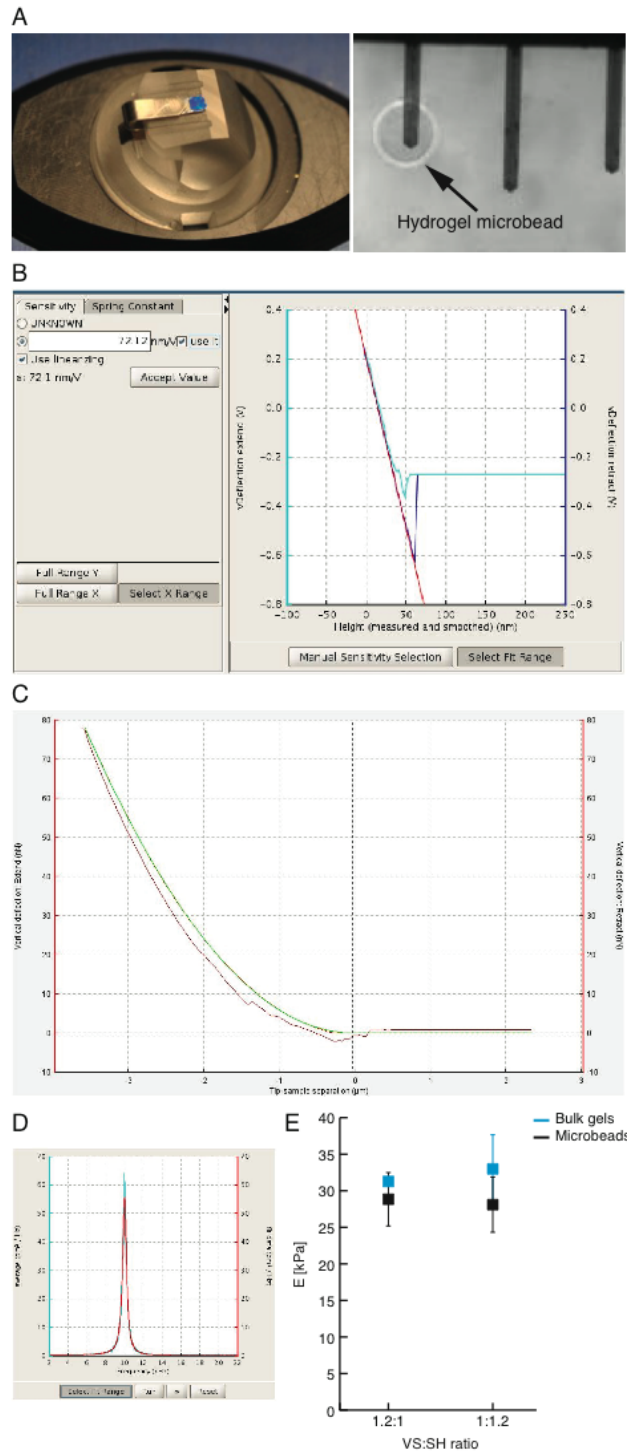
Figure S2. Mechanical characterization of PEG hydrogels by atomic force microscopy (AFM). A The cantilever was fixed on the holder of the AFM and the tip was positioned on top of the hydrogel microbead, covalently coupled to an MPS-treated glass slide, to avoid movements during the measurements. **B** The sensitivity of the cantilever was measured by performing a force curve in contact with the hard surface of a

glass slide and by software-automated fitting of the linear part of the retracted curve. **C** Force curve showing the relationship between the vertical deflection of the cantilever and the tip-sample separation. The fitting of the force curve with the Hertz model (green line) allows the calculation of the elastic modulus. **D** Example of fitting of the resonant peak performed to calibrate the spring constant of the cantilever. The thermal noise method was used: the cantilever was retracted from the surface and, by fitting the resonance spectrum, the software calculated the spring constant value from the resonance frequency. **E** AFM measurements of the elastic moduli of microgels and bulk gels at a PEG concentration of 7.5% (w/v), with 20% molar excess of either VS- or SH- groups. The results show a good matching of mechanical properties of microgels and bulk gels, suggesting that the crosslinking reaction is occurring similarly in the two cases.
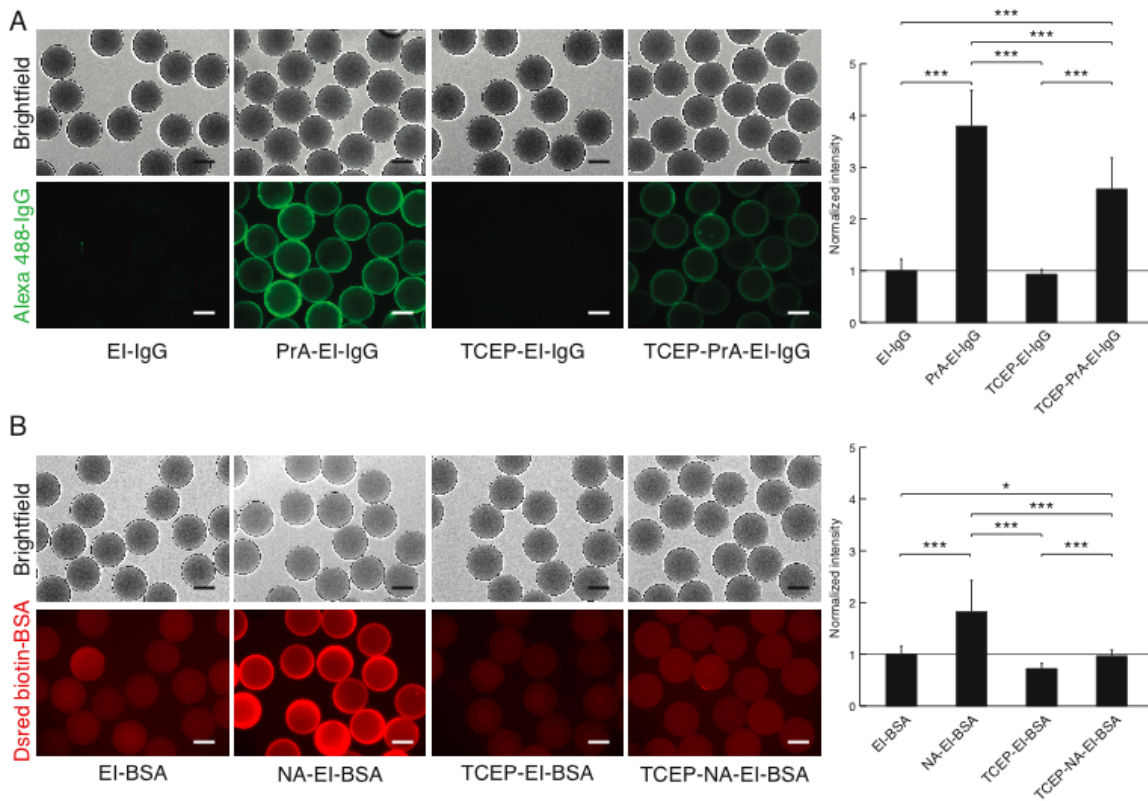
Figure S3. Microgel bioconjugation. A-B) Microcarriers bearing a molar excess of thiols were functionalized with maleimide-activated ProteinA (A) or maleimide-activated NeutrAvidin (B) and then with fluorescent humanIgG or with fluorescent biotin-bovine serum albumin (BSA), respectively. Image-based fluorescence intensity measurements are reported in the charts for all the conditions tested. In order to improve the binding efficiency, microcarriers were previously treated with tris(2-carboxyethyl)phoshine hydrochloride (TCEP) to reduce disulphide bonds and, after functionalization with the capturing agent, treated with ethyl iodoacetate (EI) to quench the thiols groups not reacting with the capturing agents. Fluorescence intensity was normalized to the negative control (i.e. microgels without ProteinA or without NeutrAvidin) in order to show the relative increase. Interestingly, in both binding schemes, TCEP treatment significantly reduced the microgel intensity, compared to the negative controls (PrA-EI-IgG/NA-EI-BSA condition versus TCEP-PrA-EI-IgG/TCEP-NA-Ei-BSA condition). Traces of TCEP still remaining after washing might partially denature the protein, resulting in lower protein binding. Furthermore, functionalization with BSA showed a partial non-specific binding (not seen in the case of IgG functionalization), as revealed by the higher intensity value of the negative control, although the difference in intensity for the functionalized microgels remains significant (EI-BSA condition versus NA-EI-BSA condition).

Appendix C

Supplementary Information: Engineering a
Compositional Landscape of Synthetic
Bioactive Microgels
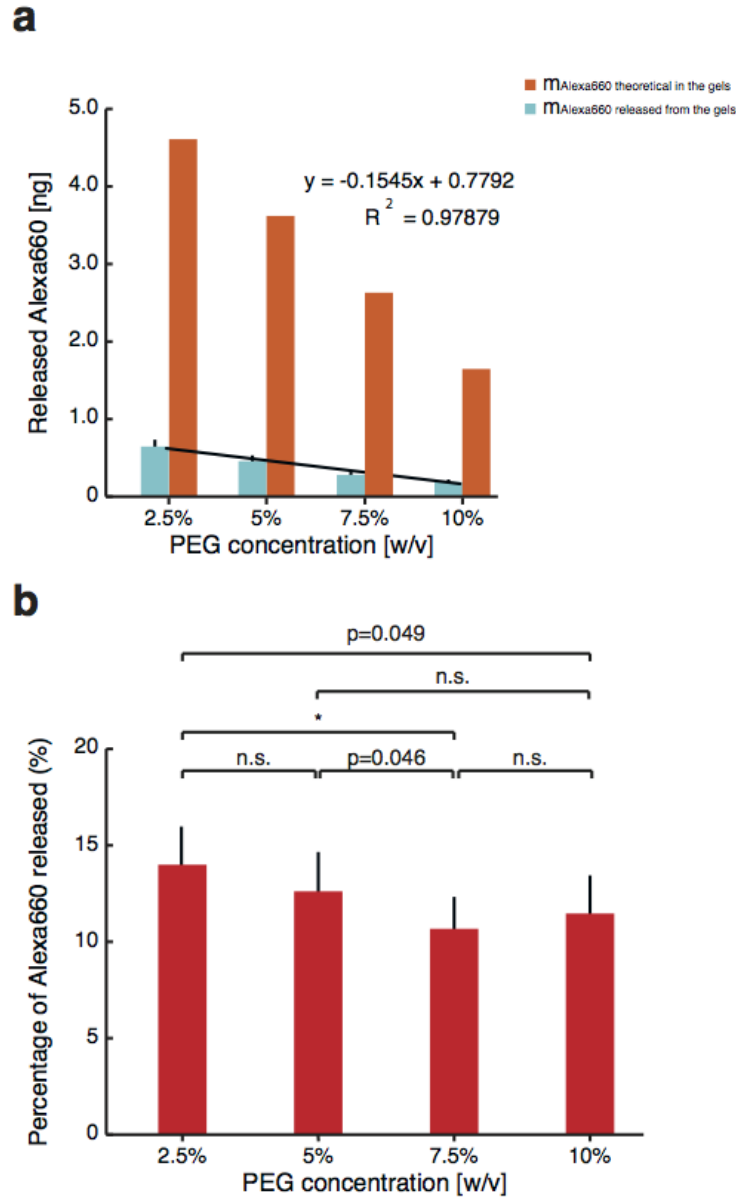
Figure S1. Release of maleimide fluorophore Alexa 660 from gels at different PEG concentrations. a Chart showing the mass of maleimide-Alexa660 released from gels at different PEG concentrations: 2.5% (w/v), 5% (w/v), 7.5% (w/v) and 10% (w/v). The gel formation followed the same conditions employed for the generation of the microgels, with the incorporation of increasing concentrations of fluorophore for decreasing PEG contents. The red bars represent the theoretical mass in ng of fluorophore incorporated within the gel and the light blue bars the mass in ng of fluorophore released: as expected, increasing the PEG concentration (*i.e.* decreasing the fluorophore concentration) led to a linear decrease in the amount of fluorophore released. **b**, The percentage of fluorophore released from the gel is in all the conditions lower than 15%. By comparing all the conditions among each other, we measured a significant release at lower PEG contents (2.5% (w/v) and 5% (w/v)), if compared with the conditions at higher PEG concentrations (7.5% (w/v) and 10% (w/v)), suggesting a lower binding efficiency when less reactive groups are available for binding.
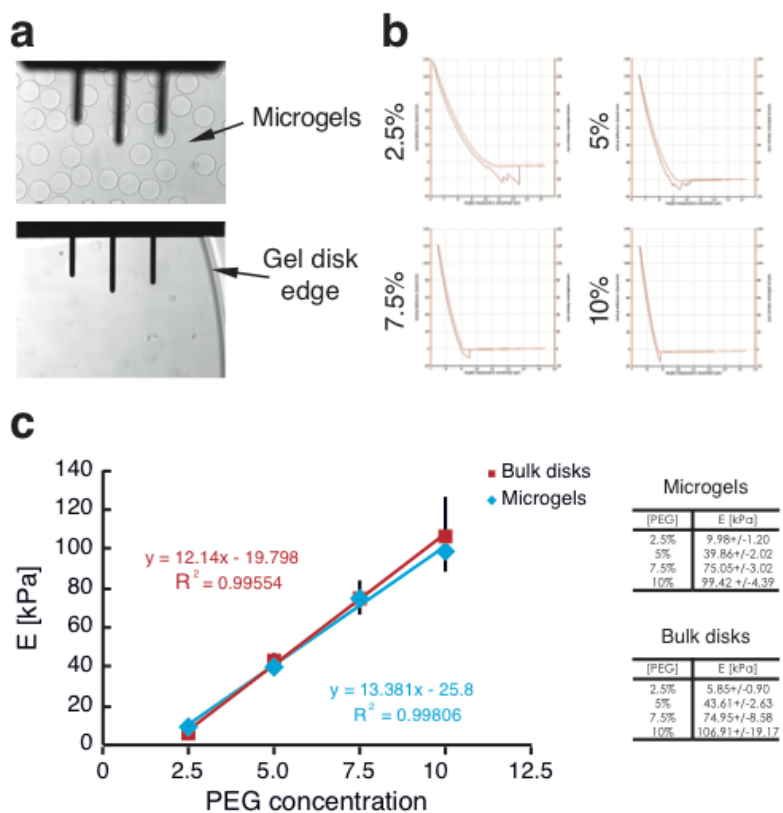
Figure S2. Atomic force microscopy measurements on hydrogel disks and microgels. a, Micrographs showing the microgels and the hydrogel disks on the atomic force microscopy apparatus. During the measurements, the cantilevers are moved on top of the sample and the indentations are performed. **b**, Typical force-indentation curves for microgels at different PEG contents: 2.5% (w/v), 5% (w/v), 7.5% (w/v) and 10% (w/v). The slope of the indentation curve becomes more steep, i.e. higher elastic modulus, for increasing PEG content. **c**, Graph reporting the elastic moduli of hydrogel disks and microgels at various PEG contents by using atomic force microscopy, showing a good match between the two sets of data. The tables report the actual values of the elastic moduli measured for both gel compositions in all the conditions.
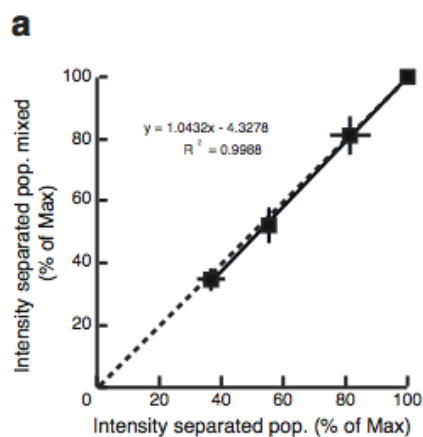
Figure S3. Validation of the clustering method for measuring the microgels intensity. a, The intensity from separated microgels were compared to the intensity obtained by clustering the intensity levels of the

four separated populations mixed together. The interpolation line lies in close proximity of the bisecting line, showing the solidity of the clustering method to extract the intensity levels of different microgel populations.
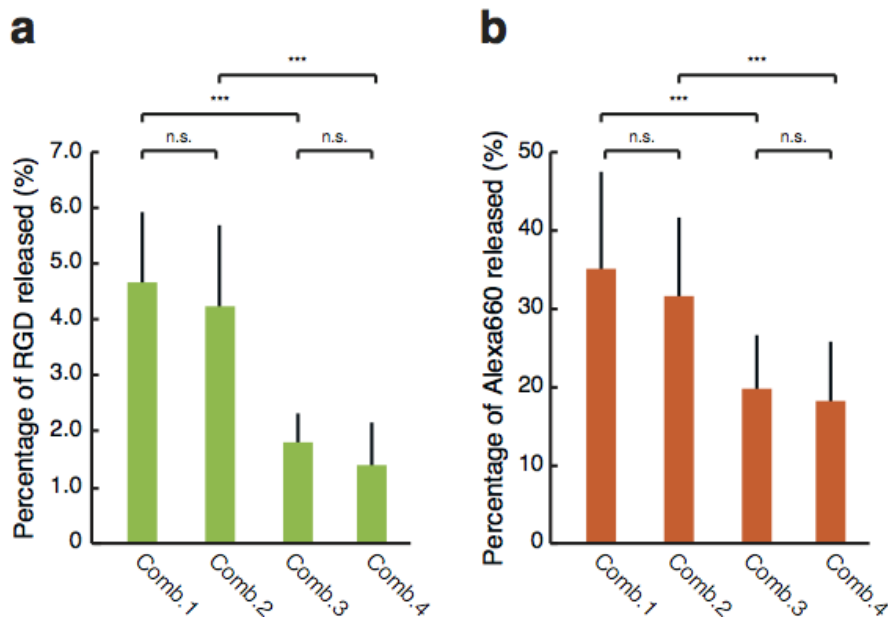
Figure S4. Fluorophore release assay performed on combinatorial hydrogels. Gels were casted following the same conditions used for the generation of four combinatorial microgels populations: low stiffness/high protein (2.5% (w/v) PEG content and 0.08 mg/ml RGD concentration) (combination 1), low stiffness/low protein (2.5% (w/v) PEG content and 0.02 mg/ml RGD concentration) (combination 2), high stiffness/high protein (10% (w/v) PEG content and 0.08 mg/ml RGD concentration) (combination 3) and high stiffness/low protein (10% (w/v) PEG content and 0.02 mg/ml RGD concentration) (combination 4). **a**, The release of FITC-labeled RGD was expressed as a percentage of the amount incorporated within the gel. As expected, a significantly higher percentage of release, less than 5%, was measured at the low PEG content, when compared with the high PEG content, less than 2%, for both high and low RGD concentrations, in good accordance with the data reported in Figure S1b. However, when comparing the release at the same PEG content, independently on the RGD concentration, no significant release was measured, in accordance with the data in Figure 5.3g. The higher standard deviation measured at low PEG concentration reflects the lower binding affinity at this condition, where less active groups are available for binding. **b**, The release of maleimide Alexa660 follows the same trend as for the FITC-labeled RGD. However, in this case the percentage of release is less than 40% for the low PEG content gels (combination 1 and 2) and less than 20% for the high PEG content gels (combination 3 and 4). In both cases the release is higher than the one measured for gels at different PEG concentrations in Figure S1b. This can be due to the chemical competition between the SH- groups of the RGD peptide and the maleimide- groups of the red fluorophore for binding within the gel: being the RGD peptide more concentrated than the red fluorophore (at minimum RGD concentration 20 µg/ml versus 0.461 µg/ml at maximum red fluorophore concentration), the former will be linked preferentially within the gel network, resulting into a lower release.
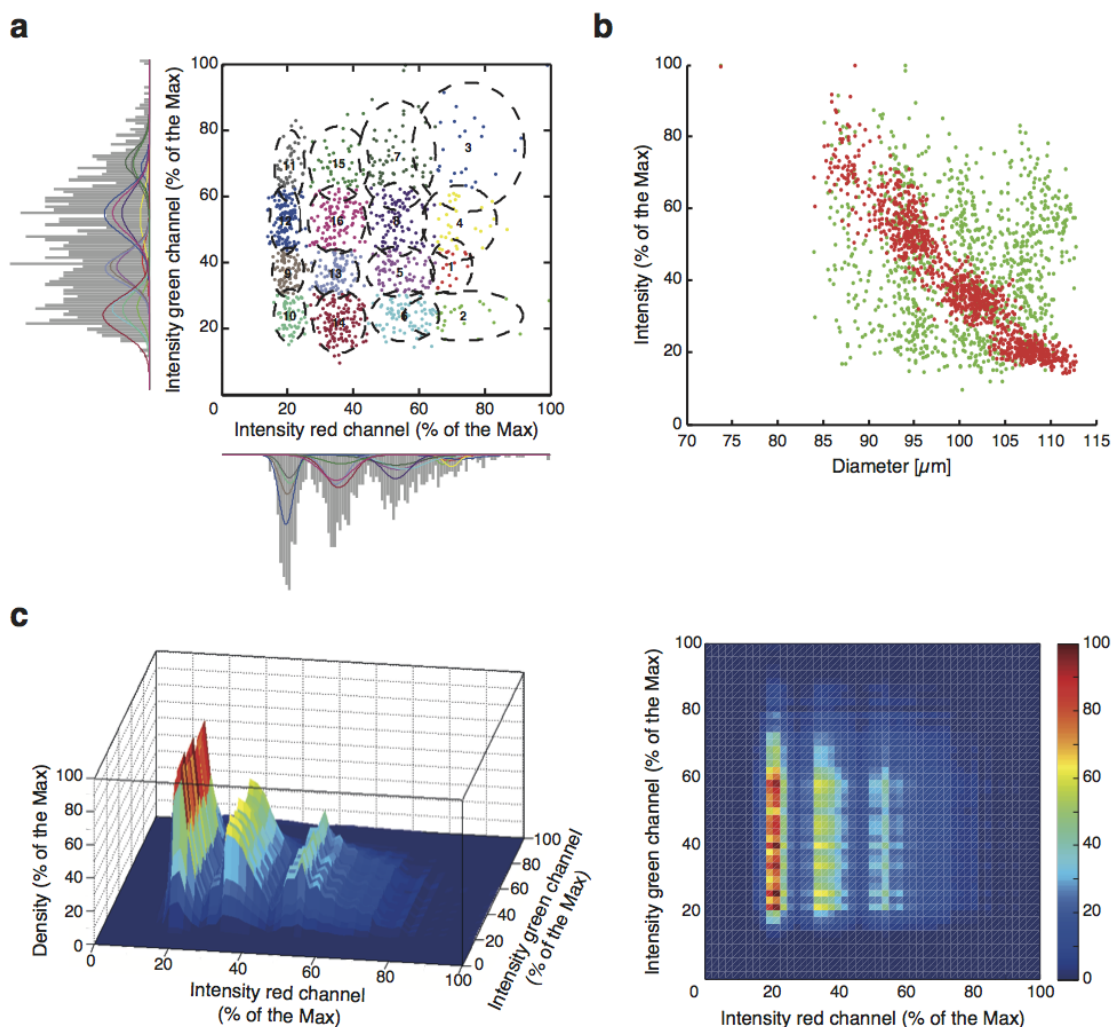
Figure S5. Generation of sixteen combinatorial microgels populations. a, Sixteen combinatorial microgel populations were generated by computer-controlled modulation of the flows, targeting four PEG content (10% (w/v), 7.5% (w/v), 5% (w/v) and 2.5% (w/v)) and four RGD concentrations (0.08 mg/ml, 0.06 mg/ml, 0.04 mg/ml and 0.02 mg/ml). The scatter plot represents sixteen microgel populations, after hierarchical clustering. On the side of each axis Gaussian curves represent the distribution of each population for both channels. The high red microgel population (i.e. microgels with low PEG content) shows higher variability, due to the lower binding efficiency at that PEG content. **b,** Scatter plot showing the relationship between the fluorescent intensity of both channels as a function of the microgel diameter. Four microgel populations can be distinguished in the red channel, where lower red intensity corresponds to higher microgels diameter. On the contrary, in the green channel no correlation with the diameter can be seen. **c,** Density plots as 3D surface and as a heat map show the distribution of the intensity of both fluorescent channels, for sixteen combinatorial microgel populations. The light blue intensity relative to the high red populations reflects the spreading of these populations.
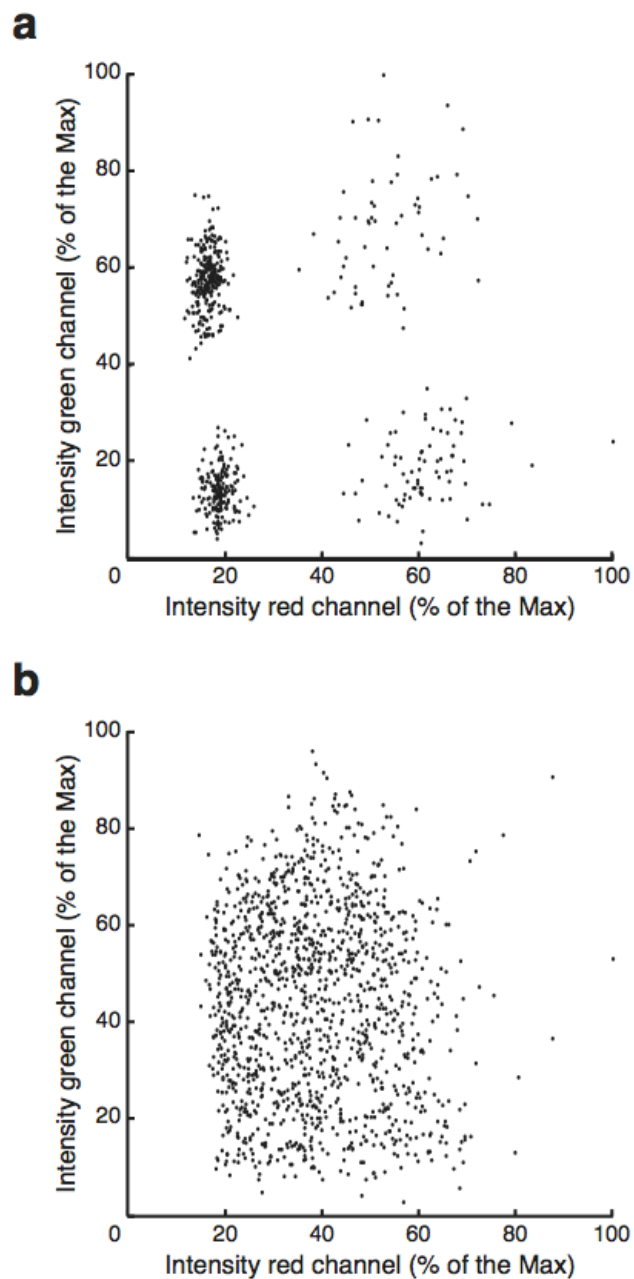
Figure S6. Scatter plot of the intensity of both fluorescent channels for combinatorial microgels populations. a, Scatter plot showing the distribution of the red intensity and the green intensity for four combinatorial microgel populations. **b**, Scatter plot showing the distribution of the intensity of both channels for one hundred combinatorial microgel populations: no clear distinction into discrete populations can be performed.
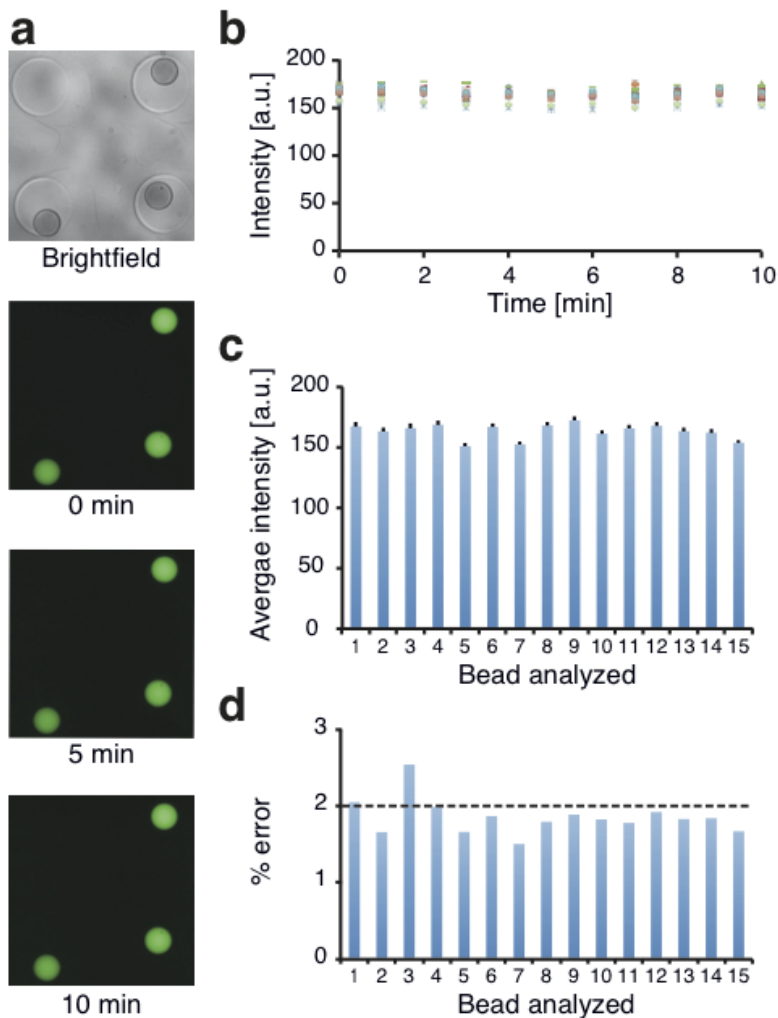
Figure S7. Tracking the microgels intensity over time. a, Microwells were fabricated to confine fifteen microgels and to allow the tracking of their fluorescent intensity over time. Microgels were formed with high RGD concentration (0.08 mg/ml) and at high PEG content (10% (w/v)) to minimize the fluorophore release. Micrographs show the microgels confined within microwells and their fluorescence intensity at 0min, 5min and 10 min. **b,** Fluorescent images were acquired every minute for 10 minutes for each of the 15 microgels. **c,** The average intensity over all the measurements was calculated for each microgels. The variation in the average intensity measured for each beads can be ascribed to microfluidic perturbations of the flows during the microgels generation. **d,** The percent error for the fluorescence intensity was lower than 2% for almost all the microgels, suggesting a negligible effect of the microscopy on the microgels intensity.

Summary of programming parameters

[PEG] [w/v]	PEG VS [μl/min]	PEG SH [μl/min]	Mal-Alexa660 [μl/min]
2.5%	0.44	0.44	4.12
5%	0.88	0.88	3.24
7.5%	1.32	1.32	2.35
10%	1.76	1.76	1.47

Table S1. Flow rate conditions to generate combinatorial microgels with varying elasticities. Here, four distinct PEG concentrations (i.e. four different stiffnesses) were targeted: 2.5% (w/v), 5% (w/v), 7.5% (w/v) and 10% (w/v).

[PEG] [w/v]	$C_{Alexa660}$ [μg/ml]
2.5%	0.461
5%	0.362
7.5%	0.263
10%	0.165

Table S2. Relationship between the PEG concentration and the maleimide-conjugated Alexa660 final concentration in the gel. The less concentrated the PEG, the higher the fluorophore concentration.

[RGD] [mg/ml]	PEG VS [μl/min]	PEG SH [μl/min]	RGD-Alexa488 [μl/min]	Buffer [μl/min]
0.02	0.88	0.88	0.50	2.74
0.04	0.88	0.88	1.00	2.24
0.06	0.88	0.88	1.50	1.74
0.08	0.88	0.88	2.00	1.24

Table S3. Flow rate conditions to generate combinatorial microgels with different RGD peptide concentrations. Here, four distinct peptide final concentrations in the gel were targeted: 0.02 (mg/ml), 0.04 (mg/ml), 0.06 (mg/ml) and 0.08 (mg/ml). The flow rates used for the two PEG precursors will lead to the formation of a 5% (w/v) gel.

	[PEG] [w/v]	[RGD] [mg/ml]	PEG VS [μl/min]	PEG SH [μl/min]	Mal-Alexa660 [μl/min]	RGD-Alexa488 [μl/min]	Buffer [μl/min]
Comb.1	2.5%	0.08	0.44	0.44	2.31	0.40	1.41
Comb.2	2.5%	0.02	0.44	0.44	2.31	0.10	1.71
Comb.3	10%	0.08	1.76	1.76	0.82	0.40	0.25
Comb.4	10%	0.02	1.76	1.76	0.82	0.10	0.55

Table S4. Flow programming to generate 4 combinatorial microgels populations with varying elasticity and different bioligand concentrations. Four populations were targeted: two stiffness conditions (10% and 2.5%) and two protein concentrations (0.02 mg/ml and 0.08 mg/ml). The mal-Alexa660 final concentration was kept consistent with the experiments performed for the generation of varying stiffness microgels.

	[PEG] [w/v]	[RGD] [mg/ml]	PEG VS [μl/min]	PEG SH [μl/min]	Mal-Alexa660 [μl/min]	RGD-Alexa488 [μl/min]	Buffer [μl/min]
Comb.1	2.5%	0.08	0.44	0.44	2.31	0.40	1.41
Comb.2	2.5%	0.06	0.44	0.44	2.31	0.30	1.51
Comb.3	2.5%	0.04	0.44	1.76	2.31	0.20	1.61
Comb.4	2.5%	0.02	0.44	1.76	2.31	0.10	1.71
Comb.5	5%	0.08	0.88	0.88	1.81	0.40	1.03
Comb.6	5%	0.06	0.88	0.88	1.81	0.30	1.13
Comb.7	5%	0.04	0.88	0.88	1.81	0.20	1.23
Comb.8	5%	0.02	0.88	0.88	1.81	0.10	1.33
Comb.9	7.5%	0.08	1.32	1.32	1.32	0.40	0.64
Comb.10	7.5%	0.06	1.32	1.32	1.32	0.30	0.74
Comb.11	7.5%	0.04	1.32	1.32	1.32	0.20	0.84
Comb.12	7.5%	0.02	1.32	1.32	1.32	0.10	0.94
Comb.13	10%	0.08	1.76	1.76	0.82	0.40	0.25
Comb.14	10%	0.06	1.76	1.76	0.82	0.30	0.35
Comb.15	10%	0.04	1.76	1.76	0.82	0.20	0.45
Comb.16	10%	0.02	1.76	1.76	0.82	0.10	0.55

Table S5. Flow programming to generate 16 combinatorial microgels with varying elasticity and different bioligand concentrations. Sixteen populations were targeted: four stiffness conditions (10%, 7.5%, 5% and 2.5%) and four protein concentrations (0.02 mg/ml, 0.04 mg/ml, 0.06 mg/ml and 0.08 mg/ml). As previously specified, the mal-Alexa660 final concentration was kept consistent with the experiments performed for the generation of varying stiffness microgels.

	[PEG] [w/v]	[RGD] [mg/ml]	PEG VS [µl/min]	PEG SH [µl/min]	Mal-Alexa660 [µl/min]	RGD-Alexa488 [µl/min]	Buffer [µl/min]
Comb.1	2.5%	0.080	0.44	0.44	2.31	0.40	1.41
Comb.2	2.5%	0.073	0.44	0.44	2.31	0.37	1.45
Comb.3	2.5%	0.067	0.44	0.44	2.31	0.33	1.48
Comb.4	2.5%	0.060	0.44	0.44	2.31	0.30	1.51
Comb.5	2.5%	0.053	0.44	0.44	2.31	0.27	1.55
Comb.6	2.5%	0.047	0.44	0.44	2.31	0.23	1.58
Comb.7	2.5%	0.040	0.44	0.44	2.31	0.20	1.61
Comb.8	2.5%	0.033	0.44	0.44	2.31	0.17	1.65
Comb.9	2.5%	0.027	0.44	0.44	2.31	0.13	1.68
Comb.10	2.5%	0.020	0.44	0.44	2.31	0.10	1.71
Comb.11	3.33%	0.080	0.59	0.59	2.14	0.40	1.28
Comb.12	3.33%	0.073	0.59	0.59	2.14	0.37	1.32
Comb.13	3.33%	0.067	0.59	0.59	2.14	0.33	1.35
Comb.14	3.33%	0.060	0.59	0.59	2.14	0.30	1.38
Comb.15	3.33%	0.053	0.59	0.59	2.14	0.27	1.42
Comb.16	3.33%	0.047	0.59	0.59	2.14	0.23	1.45
Comb.17	3.33%	0.040	0.59	0.59	2.14	0.20	1.48
Comb.18	3.33%	0.033	0.59	0.59	2.14	0.17	1.52
Comb.19	3.33%	0.027	0.59	0.59	2.14	0.13	1.55
Comb.20	3.33%	0.020	0.59	0.59	2.14	0.10	1.58
Comb.21	4.17%	0.080	0.74	0.74	1.98	0.40	1.15
Comb.22	4.17%	0.073	0.74	0.74	1.98	0.37	1.19
Comb.23	4.17%	0.067	0.74	0.74	1.98	0.33	1.22
Comb.24	4.17%	0.060	0.74	0.74	1.98	0.30	1.25
Comb.25	4.17%	0.053	0.74	0.74	1.98	0.27	1.29
Comb.26	4.17%	0.047	0.74	0.74	1.98	0.23	1.32
Comb.27	4.17%	0.040	0.74	0.74	1.98	0.20	1.35
Comb.28	4.17%	0.033	0.74	0.74	1.98	0.17	1.39
Comb.29	4.17%	0.027	0.74	0.74	1.98	0.13	1.42
Comb.30	4.17%	0.020	0.74	0.74	1.98	0.10	1.45
Comb.31	5%	0.080	0.88	0.88	1.81	0.40	1.02
Comb.32	5%	0.073	0.88	0.88	1.81	0.37	1.06
Comb.33	5%	0.067	0.88	0.88	1.81	0.33	1.09
Comb.34	5%	0.060	0.88	0.88	1.81	0.30	1.12
Comb.35	5%	0.053	0.88	0.88	1.81	0.27	1.16
Comb.36	5%	0.047	0.88	0.88	1.81	0.23	1.19
Comb.37	5%	0.040	0.88	0.88	1.81	0.20	1.22
Comb.38	5%	0.033	0.88	0.88	1.81	0.17	1.26
Comb.39	5%	0.027	0.88	0.88	1.81	0.13	1.29
Comb.40	5%	0.020	0.88	0.88	1.81	0.10	1.32
Comb.41	5.83%	0.080	1.03	1.03	1.65	0.40	0.90
Comb.42	5.83%	0.073	1.03	1.03	1.65	0.37	0.93
Comb.43	5.83%	0.067	1.03	1.03	1.65	0.33	0.96
Comb.44	5.83%	0.060	1.03	1.03	1.65	0.30	1.00
Comb.45	5.83%	0.053	1.03	1.03	1.65	0.27	1.03
Comb.46	5.83%	0.047	1.03	1.03	1.65	0.23	1.06
Comb.47	5.83%	0.040	1.03	1.03	1.65	0.20	1.10
Comb.48	5.83%	0.033	1.03	1.03	1.65	0.17	1.13
Comb.49	5.83%	0.027	1.03	1.03	1.65	0.13	1.16
Comb.50	5.83%	0.020	1.03	1.03	1.65	0.10	1.20

Comb.51	6.67%	0.080	1.18	1.18	1.48	0.40	0.76
Comb.52	6.67%	0.073	1.18	1.18	1.48	0.37	0.80
Comb.53	6.67%	0.067	1.18	1.18	1.48	0.33	0.83
Comb.54	6.67%	0.060	1.18	1.18	1.48	0.30	0.86
Comb.55	6.67%	0.053	1.18	1.18	1.48	0.27	0.90
Comb.56	6.67%	0.047	1.18	1.18	1.48	0.23	0.93
Comb.57	6.67%	0.040	1.18	1.18	1.48	0.20	0.96
Comb.58	6.67%	0.033	1.18	1.18	1.48	0.17	1.00
Comb.59	6.67%	0.027	1.18	1.18	1.48	0.13	1.03
Comb.60	6.67%	0.020	1.18	1.18	1.48	0.10	1.06
Comb.61	7.5%	0.080	1.32	1.32	1.32	0.40	0.63
Comb.62	7.5%	0.073	1.32	1.32	1.32	0.37	0.67
Comb.63	7.5%	0.067	1.32	1.32	1.32	0.33	0.70
Comb.64	7.5%	0.060	1.32	1.32	1.32	0.30	0.73
Comb.65	7.5%	0.053	1.32	1.32	1.32	0.27	0.77
Comb.66	7.5%	0.047	1.32	1.32	1.32	0.23	0.80
Comb.67	7.5%	0.040	1.32	1.32	1.32	0.20	0.83
Comb.68	7.5%	0.033	1.32	1.32	1.32	0.17	0.87
Comb.69	7.5%	0.027	1.32	1.32	1.32	0.13	0.90
Comb.70	7.5%	0.020	1.32	1.32	1.32	0.10	0.93
Comb.71	8.33%	0.080	1.47	1.47	1.15	0.40	0.51
Comb.72	8.33%	0.073	1.47	1.47	1.15	0.37	0.54
Comb.73	8.33%	0.067	1.47	1.47	1.15	0.33	0.57
Comb.74	8.33%	0.060	1.47	1.47	1.15	0.30	0.61
Comb.75	8.33%	0.053	1.47	1.47	1.15	0.27	0.64
Comb.76	8.33%	0.047	1.47	1.47	1.15	0.23	0.67
Comb.77	8.33%	0.040	1.47	1.47	1.15	0.20	0.71
Comb.78	8.33%	0.033	1.47	1.47	1.15	0.17	0.74
Comb.79	8.33%	0.027	1.47	1.47	1.15	0.13	0.77
Comb.80	8.33%	0.020	1.47	1.47	1.15	0.10	0.81
Comb.81	9.17%	0.080	1.62	1.62	0.99	0.40	0.37
Comb.82	9.17%	0.073	1.62	1.62	0.99	0.37	0.41
Comb.83	9.17%	0.067	1.62	1.62	0.99	0.33	0.44
Comb.84	9.17%	0.060	1.62	1.62	0.99	0.30	0.47
Comb.85	9.17%	0.053	1.62	1.62	0.99	0.27	0.51
Comb.86	9.17%	0.047	1.62	1.62	0.99	0.23	0.54
Comb.87	9.17%	0.040	1.62	1.62	0.99	0.20	0.57
Comb.88	9.17%	0.033	1.62	1.62	0.99	0.17	0.61
Comb.89	9.17%	0.027	1.62	1.62	0.99	0.13	0.64
Comb.90	9.17%	0.020	1.62	1.62	0.99	0.10	0.67
Comb.91	10%	0.080	1.76	1.76	0.82	0.40	0.25
Comb.92	10%	0.073	1.76	1.76	0.82	0.37	0.28
Comb.93	10%	0.067	1.76	1.76	0.82	0.33	0.31
Comb.94	10%	0.060	1.76	1.76	0.82	0.30	0.35
Comb.95	10%	0.053	1.76	1.76	0.82	0.27	0.38
Comb.96	10%	0.047	1.76	1.76	0.82	0.23	0.41
Comb.97	10%	0.040	1.76	1.76	0.82	0.20	0.45
Comb.98	10%	0.033	1.76	1.76	0.82	0.17	0.48
Comb.99	10%	0.027	1.76	1.76	0.82	0.13	0.51
Comb.100	10%	0.020	1.76	1.76	0.82	0.10	0.55

Table S6. Flow programming to generate 100 combinatorial microgels with varying elasticity and different bioligand concentrations. One hundred populations were targeted: ten stiffness conditions (2.5%, 3.33%, 4.17%, 5%, 5.83%, 6.67%, 7.5%, 8.33%, 9.17% and 10%) and four protein concentrations (0.020 mg/ml, 0.027 mg/ml, 0.033 mg/ml, 0.040 mg/ml, 0.047 mg/ml, 0.053 mg/ml, 0.060 mg/ml, 0.067 mg/ml, 0.0073 mg/ml and 0.080 mg/ml). As previously specified, the mal-Alexa660 final concentration was kept consistent with the experiments performed for the generation of varying stiffness microgels.

	[PEG] [w/v]	[RGD] [mg/ml]	PEG VS [µl/min]	PEG SH [µl/min]	Mal-Alexa660 [µl/min]	RGD-Alexa488 [µl/min]	Buffer [µl/min]
Comb.1	2.5%	1.08	0.42	0.42	0.46	1.08	2.62
Comb.2	2.5%	0.54	0.42	0.42	0.46	0.54	3.16
Comb.3	10%	1.08	1.67	1.67	0.16	1.08	0.96
Comb.4	10%	0.54	1.67	1.67	0.16	0.54	0.42

Table S7. Flow programming to generate 4 combinatorial microgels with varying elasticity and different bioligand concentrations, for supporting NMuMG cells adhesion. Four populations were targeted: two stiffness conditions (10% and 2.5%) and two protein concentrations (0.54 mg/ml and 1.08 mg/ml). The initial concentration of the red fluorophore and the fluorescent RGD were 5 µg/ml and 5mg/ml, respectively. The mal-Alexa660 final concentration was kept consistent with the experiments performed for the generation of varying stiffness microgels.
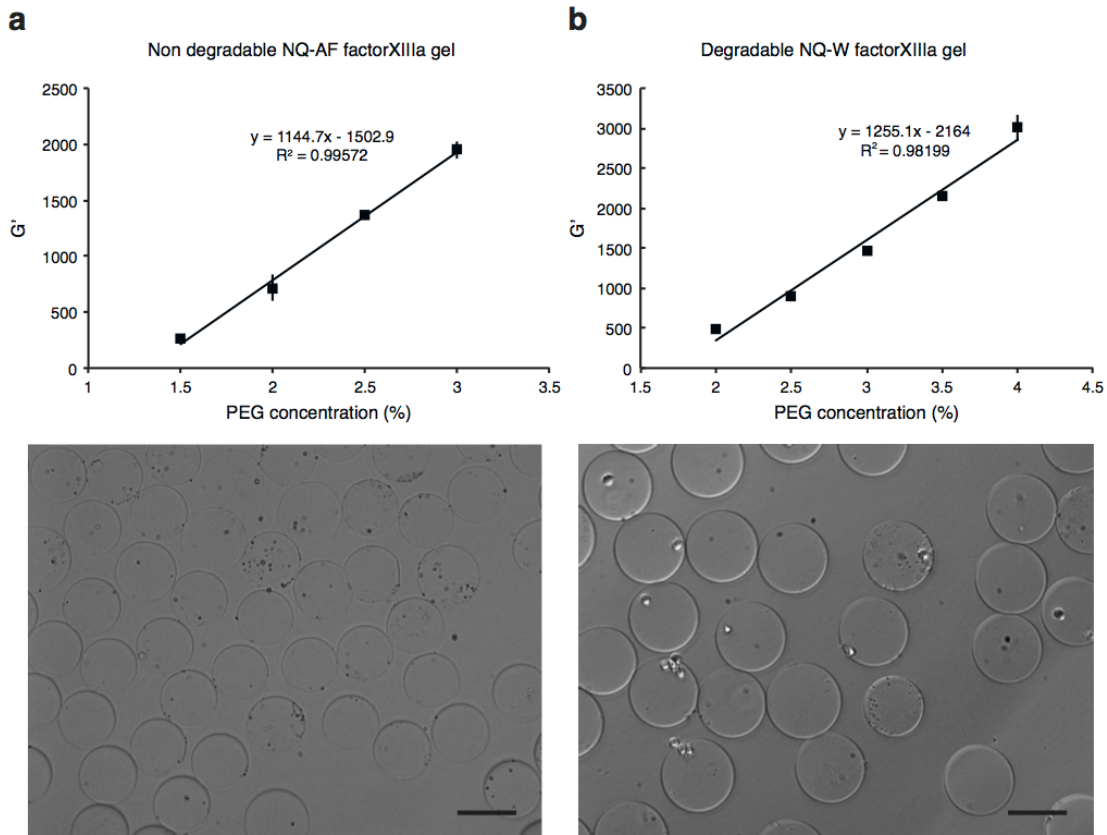
Appendix D

Supplementary Information: 3D Cell-instructive Microgels with Tailor-made Physico-chemical Properties

Figure S1 – Mechanical properties of enzymatically cross-linked gels. a, Rheological measurements performed on non-degradable gel disks. The lysine-containing PEG precursor was modified inserting the peptide sequence, GDQGIAGF (termed as AF). Non-degradable microgels were generated microfluidically (bottom panel). **b**, Rheological measurements performed on degradable gel disks, where the MMP-sensitive sequence, Ac-FKGGGPQGIWGQ-ERCG-NH$_2$ (termed as W) was added to the lysine-containing PEG precursor. The micrograph shows cell-containing degradable beads (bottom panel). In both cases a linear relationship between PEG concentration and shear modulus was found in a range spanning from around 300 Pa up to 3000 Pa. Scale bar 100μm.
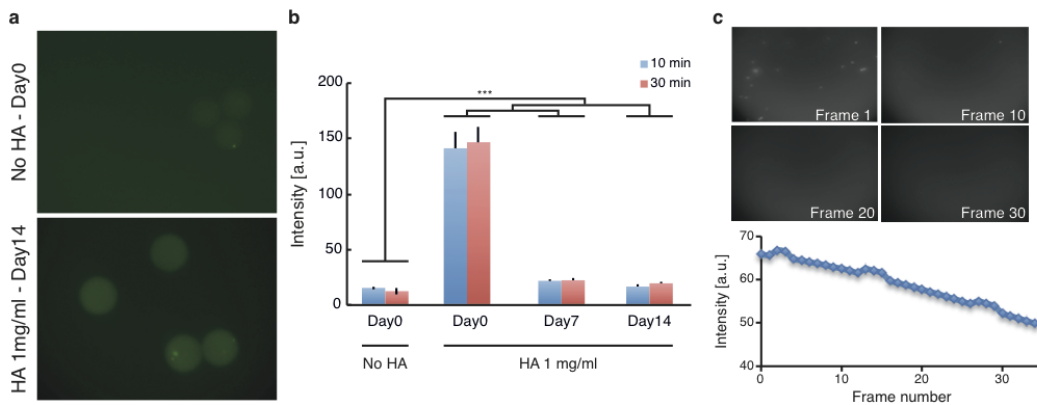
Figure S2 – PLL coating of microgels and penetration within gel sections. a, Fluorescent intensity of microbeads without (top panel) or with (bottom panel) hyaluronic acid, after incubation with PLL, at day 0 and at day 14 in cell culture condition, respectively. High background was present in the negative control.

b, Histograms showing the fluorescent intensity of microgels with and without hyaluronic acid and exposed for 10 min or 30 min to PLL solution. In presence of HA the intensity was always significantly higher compared to the negative control. **c**, Fluorescent micrographs of different sections of a cell-containing gel disk exposed for 10 min to PLL solution: the frame 1, i.e. the surface of the gel, shows higher intensity that linearly decreases until the frame 30, showing the diffusion of the PLL within PEG gels, as shown by the intensity profile (bottom panel). The bright spots in the frame number 1 represent cells that died upon PLL exposure: less cell death was noticed at higher distances from the surface of gel.
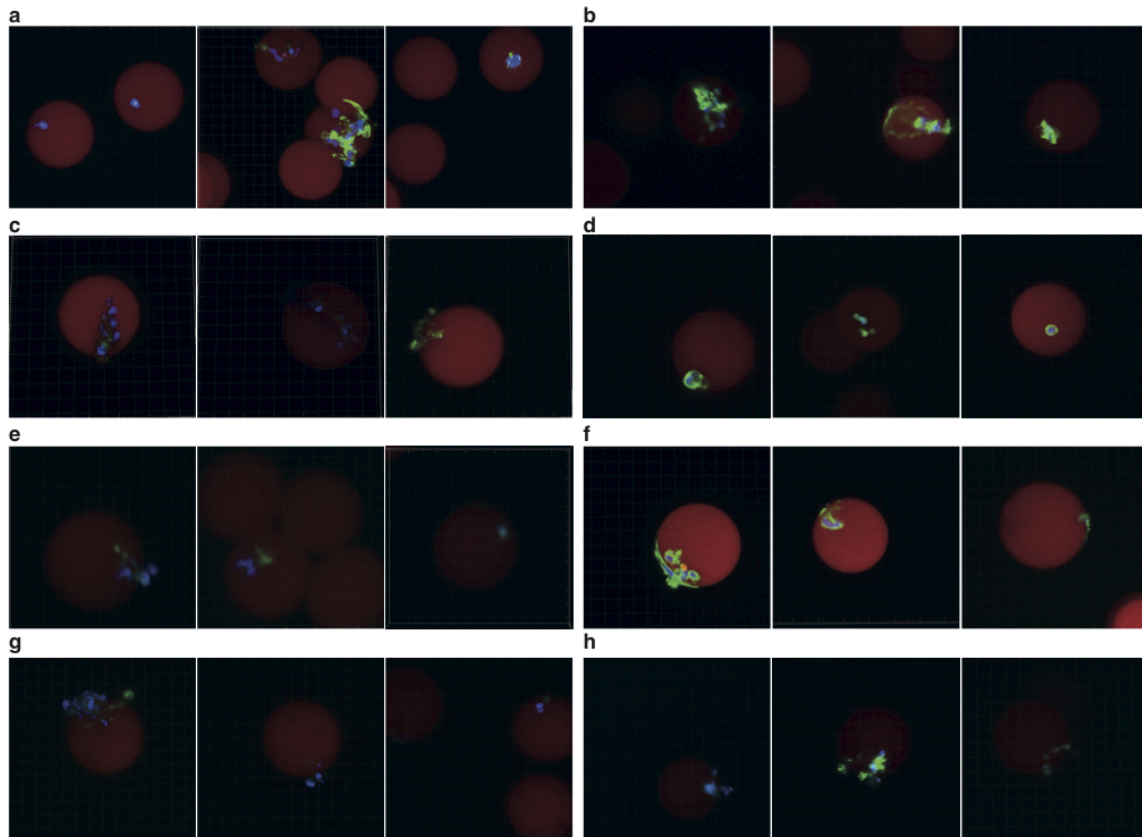
Figure S3 – Morphology of cells after long-term encapsulation in microcapsules with varying mechanical properties. MDA-MB-231 cells were encapsulated in hydrogel microbeads that were co-encapsulated in thin hydrogel disks with different PEG contents (5% (w/v) and 10% (w/v)). **a-b**, Morphology of cells encapsulated in 1kPa microgels, co-encapsulated into 5% gel disks, after 15 days (a) and 21 days (b) of culture. **c-d**, Morphology of cells encapsulated in 1kPa microgels, co-encapsulated into 10% gel disks, after 15 days (c) and 21 days (d) of culture. **e-f**, Morphology of cells encapsulated in 500 Pa microgels, co-encapsulated into 5% gel disks, after 15 days (e) and 21 days (f) of culture. **g-h**, Morphology of cells encapsulated in 500 Pa microgels, co-encapsulated into 10% gel disks, after 15 days (g) and 21 days (h) of culture. Red: Alexa546-functionalized RGD; Blue: DAPI staining for cell nuclei; Green: Phalloidin staining for actin filaments.

Simone Allazetta

Av. d'Echallens 41
1004, Lausanne
simone.allazetta@gmail.com
Mobile +41 78 843 39 36

25 November 1985
Single
Italian
Valid B Permit

EDUCATION

2010-2014 **Ph.D. in Stem Cell Bioengineering** at École Polytechnique Fédérale de Lausanne (EPFL)
Project title: Microfluidic Engineering of Artificial Stem Cell Niches
(thesis proposed for the "Professor René Wassermann" award)

2004-2009 **Master of Science in Bioengineering**, Polytechnic University of Turin (Italy)
- Major in Biomechanical and Biomaterial Engineering (with honors)
- Minor in Biomedical Engineering
- Project Double Master Degree (Alta Scuola Politecnica)

2007-2009 **Diploma Alta Scuola Politecnica** at Polytechnic University of Turin (Italy) and Polytechnic University of Milan (Italy)
Project title: Robotics-assisted surgery with renewed and enhanced technology for orthopedic surgery

PROFES5IONAL EXPERIENCES

2010-2014 **Research Assistant** at École Polytechnique Fédérale de Lausanne (EPFL)

2010-2012 **Technical Consultant**, Hamilton Company (Bonaduz, Switzerland) and École Polytechnique Fédérale de Lausanne (EPFL)

2007-2012 **Tutor**, École Polytechnique Fédérale de Lausanne (EPFL) and Polytechnic University of Turin

PUBLICATIONS

Allazetta S., Lutolf M.P., *Stem Cell Niche Engineering Through Droplet Microfluidics,* in submission, 2014

Allazetta S., Negro A., Lutolf M.P., *Precise Microfluidic Synthesis of Combinatorial Microgels with Varying Mechanical and Biochemical Properties,* in submission, 2014

Allazetta S., Zerbib S., Lutolf M.P., *Biophysical Modulation of Synthetic Hydrogel Microcapsules for Three-dimensional Cell Culture Applications,* in submission, 2014

Allazetta S., Hausherr T., Lutolf M.P., *Microfluidic Synthesis of Cell-Type-Specific Artificial Extracellular Matrix Hydrogels,* Biomacromolecules, 2013

Cosson S., **Allazetta S**.*, Lutolf M.P., *Patterning of Cell-Instructive Hydrogels by Hydrodynamic Flow Focusing*, Lab on a Chip, 2013 (***co-first author**)

Allazetta S., Cosson S., Lutolf M.P., *Programmable Microfluidic Patterning of Protein Gradients on Hydrogels*, Chemical Communications, 2011

INTERNATIONAL CONFERENCES

Allazetta S., Lutolf M.P., *Biomechanical and Biochemical Modulation of Cellular Microniches Using Droplet-based Microfluidics,* (oral presentation), Gordon Research Conference, Boston (USA), 2014

Allazetta S., Lutolf M.P., *Droplet-based microfluidic generation of microcarriers for stem cell manipulation* (oral presentation), Materials Research Society, San Francisco (USA), 2012